Developing an Automated Nitrous Acid (HONO) Platform to Detect Emerging Pollutants in a Commercial and Domestic Environment

Melodie Lao

A thesis submitted to the Faculty of Graduate Studies in partial fulfillment of the requirements for the degree of

Master of Science

Graduate Program in Chemistry

York University

Toronto, Ontario

April 2022

Abstract

Nitrous acid (HONO) is an emerging household pollutant linked to adverse health effects and an important contributor to the indoor hydroxyl radical (OH) budget. Both play an essential role in indoor oxidation chemistry as HONO can readily photolyze to form OH under low light conditions, and OH can react with volatile organic compounds to generate secondary pollutants. There are growing reports of higher levels of HONO indoors than outdoors, reaching up to 100 parts per billion (ppb) from direct combustion emissions. Studies involving indoor surface chemistry have observed HONO background levels of ~5 ppb in various indoor environments likely derived from heterogenous secondary processes, but dominant mechanisms controlling indoor HONO levels remain unclear due to the limited number of high time resolution measurements available.

To minimize any measurement uncertainty calibration sources are required to maintain accuracy and repeatability. Historically, HONO has been a challenging compound to generate at atmospherically relevant mixing ratios, but also has several well-documented sources that are instrument artifacts. This work presents a simple calibration source that reaches low HONO mixing ratios of a few parts per trillion (ppb) and up to tens of ppb using a nitrite-coated reaction device with the addition of humid air and/or hydrochloric acid (HCl) from a permeation device. The source can be easily assembled to generate stable HONO mixing ratios (relative standard error, RSE $\leq$ 2 %) within 2 hours. The source was subjected to field transport simulations to find output concentrations varying $\leq$ 10 % under ideal conditions to prove its robustness in generating a reproducible output. The calibration source has high HONO purity (> 90 %) and tunability for sub-ppbv mixing ratios that can be reached with reasonable dilution flows. The design of the source makes it highly versatile for field and lab experiments, in addition to being utilized for all state-of-the-art instrumentations to identify systematic bias and interferences present in HONO measurements.

To understand the impact of HONO on the indoor oxidative capacity, new instrument advances are required, in addition to a calibration source, to perform time-resolved measurements in various indoor facilities. Existing instruments have been primarily designed to measure outdoor HONO. Their transition to survey indoor environments come with several challenges such as specialized operators of expensive research-grade equipment, lack of mobility to survey various indoor atmospheres, hazardous components/solutions, and instrumental interferences. To overcome these

challenges, an automated HONO platform (a component of a total reactive nitrogen instrument that senses three chemical fractions of gaseous species) was built to perform modulated measurements of NO_x and HONO. It is specifically designed to be suitable for conducting indoor air quality surveys and to study the chemistry of indoor air. A series of experiments were performed to characterize and validate the real-time detection of NO_x (NO + NO_2) and HONO with a time response of 1 minute. Preliminary measurements of the instrument were made to demonstrate proof of concept. The design, control, and data processing of the instrument are intended to be made open source to encourage the atmospheric chemistry community to replicate and perform widespread measurements of indoor facilities.

Lastly, the developed HONO platform was deployed in a commercial kitchen located in a university residence for three weeks during the KOCENA (Kitchen Organic Carbon, Emissions, Nitrogen, and Aerosol) campaign. Cooking and sensor-controlled ventilation provided optimal exhaust rates based on standard requirements for heat and smoke control. The high ventilation in the kitchen effectively removed pollutants emitted directly from high-volume cooking activities with gas appliances. The removal of direct emissions was so rapid (< 20 minutes) that the majority of HONO emitted from cooking combustion processes were excluded during the data processing, in contrast to the hours-long decay profiles observed for direct emissions in private residences. Daytime and nighttime measurements of NO, NO_2, and HONO were compared based on the ventilation initiation and kitchen operation hours. The outdoor transportation of NO_x was found to contribute to early morning elevated levels and NO_2 likely controlled the production of HONO in this space. Heterogenous processes played a vital role in the temporal behavior of HONO with NO_2 as its precursor. A simple model involving sources and sinks of HONO was constructed to compare against the kitchen measurements of HONO. The predicted HONO levels were estimated by the concentration of HONO produced by NO_2 surface uptake and its loss by HONO photolysis. The model suggested that heterogenous HONO formation, with reactive uptake coefficients consistent with the literature, contributed substantially to the observed daytime levels of HONO. Our results also show that equilibrium partitioning of HONO from surfaces is likely maintaining levels of HONO in the absence of direct cooking emissions a strong outdoor to indoor transport of NO_2. This HONO reservoir is likely located on the kitchen surfaces with deposited nitrite that can desorb as HONO. Calculations of OH production rate by HONO photolysis confirm that the commercial kitchen act as a persistent OH source due to its 24-hour lighting. This means that

HONO photolysis may be an important driver in indoor oxidation chemistry in commercial kitchen environments with low photon levels and consistent lighting. Overall, two new instruments were built to improve the accuracy and detection of HONO indoors and provided proof-of-function in a commercial facility. The design and program of these instruments will be open source to encourage scientists to perform more time-resolved measurements of HONO in various indoor facilities that have yet to be explored or published.

Acknowledgements

I thank my graduate supervisor, Trevor VandenBoer, for mentoring my development as a scientist and allowing me to explore, learn, and gain many skills under your guidance.

I thank Leigh Crilley for being an outstanding teammate and postdoc. Your guidance, expertise, and advice always gave me confidence in tackling problems.

I thank my committee members, Cora Young and Rob McLaren, for their feedback and support during my graduate studies.

Cheers to all my VDB and CJY research colleagues! I wish you all the best in your research and endeavors. Big shout-out to Leyla, Alessia, Lisa, Teles, Andrea, Shira, Fahim, and Stephen for all the wonderful conversations and support!

Table of Contents

List of Figures

List of Tables

List of Symbols and Abbreviations

±	plus-minus
λ	wavelength
≥	greater than or equal to
≤	less than or equal to
◦C	degree Celsius
%	percent
τ	response time
“	inch
ads	adsorbed
AER	air exchange rate
ADE	acid displacement efficiency
Al	aluminum
AVG	average
cc	cubic centimeter
CIMS	chemical ionization mass spectrometer
cm	centimeter
CRDS	cavity ring down spectroscopy
ft	feet
h	hour
HCl	hydrochloric acid
HNO_3	nitric acid
HVAC	heating, ventilation, and air conditioning
HONO	nitrous acid
IC-CD	ion chromatography-conductivity detection
i.d.	inner diameter
L	liter
LPM	liter per minute

M	meter
MFC	mass flow controller
min	minute
mg	milligram
mL	milliliter
mm	millimeter
molec cm^{-3}	molecules per cubic centimeters
m/z	mass-to-charge ratio
n	number of experiments
N/A	not applicable
nm	nanometer
N_2	molecular nitrogen
N_2O_5	dinitrogen pentoxide
NaCl	sodium chloride
NaOH	sodium hydroxide
Na_2CO_3	sodium carbonate
$NaNO_2$	sodium nitrite
NH_3	ammonia
NH_x	ammonia and amides
NO	nitrogen oxide
NO_2	nitrogen dioxide
NO_2^-	nitrite
NO_x	nitrogen oxides (NO_2 + NO)
NO_x^*	nitrogen oxides (NO, NO_2, and NO_y species)
NO_x analyzer	chemiluminescence analyzer that measures NO_x
O	singlet oxygen
O_2	oxygen
O_3	ozone

OH	hydroxyl radical
o.d.	outer diameter
PD	permeation devices
PFA	perfluoroalkoxy alkane
pH	scale of acidity, $-\log(H^+)$
PID	proportional-integral-differential
ppb	parts per billion
ppbv	parts per billion by volume
ppm	parts per million
ppmv	parts per million by volume
ppt	parts per trillion
pptv	parts per trillion by volume
PTFE	polytetrafluoroethylene
s	second
sccm	standard cubic centimeter per minute
SD	standard deviation
SLPM	standard liter per minute
Temp	temperature
tN_r	total reactive nitrogen
RH	relative humidity
RSD	relative standard deviation
RSE	relative standard error
UV	ultraviolet
V	volts
VIS	visible
VOC	volatile organic compounds
ZA	zero air

Other projects undertaken during MSc

I had the pleasure of contributing to multiple projects outside of this thesis involving:

1. building automated precipitation samplers (co-author),
2. analyzing ozone passive samplers in collaboration with a New Home Air Quality Study (NHAQS) with Health Canada,
3. collaboration with Dr. Tara Kahan in analyzing near-source hypochlorous acid (HOCl) emissions from cleaning a residential bathroom (co-first author),
4. and analyzing various cleaning product emissions with cost-effective sensors (co-author).

CHAPTER One:

Importance of studying oxides of nitrogen ($NO_x = NO + NO_x$) and nitrous acid (HONO) indoors

Author Contributions:

ML wrote and TCV edited this work.

1.1 Why we care about indoor air chemistry

Research in indoor air chemistry is a relatively new field with increasing interest and growth on the chemical and physical transformations in an indoor environment (Ault et al., 2020; Nazaroff and Weschler, 2020). New indoor facilities have evolved by increasing their energy efficiency measures to have increasingly airtight buildings with reduced ventilation rates, which results in elevated concentrations of indoor pollutants (Weschler, 2009). We have better understanding of the driving sources of pollution and air quality in the outdoor environment and its associated health impacts, but we do not understand inhalation exposure and chemistry within many indoor environments (e.g. offices, houses, schools, etc.). Developing new regulations to continually improve our indoor air quality with new buildings can benefit human health and sustainability because we spend 90 % of our lives indoors (Klepeis et al., 2001; Leech et al., 2002). The chemistry of indoor air is difficult to assess and model because they have unique properties that depend on the location, building design, and reactive species therein that can undergo complex heterogenous and multiphase reactions. Indoor pollutants such as gases and particulate matter can be produced, removed, or transformed by indoor processes involving direct emissions, indoor-outdoor air exchange, and surface deposition (Abbatt and Wang, 2020). Indoor pollutants can be directly emitted from furnishings, building materials, and common household and personal care products (Farmer et al., 2019; Weschler and Carslaw, 2018). Outdoor transportation of air pollutants indoors can occur by natural (opening windows and doors) and mechanical ventilation (heating, ventilation, and air conditioning; HVAC), as well as infiltration through the building envelope (Carslaw, 2007; Waring and Wells, 2015). Indoor environments differ vastly from outdoors because there are less extreme temperature fluctuations, less direct and lower energy sunlight photons and no rain, larger surface-area-to-volume ratios, and a large impact from human occupancy. Human behavior and activities (e.g., cooking, cleaning, and smoking) can strongly

influence the emissions and temporal profiles of indoor pollutants (Collins et al., 2018; Farmer et al., 2019; Li et al., 2020; Wang et al., 2020b; Weschler and Carslaw, 2018; Wisthaler and Weschler, 2010).

1.2 Pollutants of interest, oxides of nitrogen (NO_x = NO + NO_2) and nitrous acid (HONO)

Oxides of nitrogen (NO_x = NO + NO_2) and nitrous acid (HONO) are well known and emerging gaseous pollutants that are associated with adverse health effects and respiratory disease (Gligorovski, 2016; Jarvis et al., 2005; Salonen et al., 2019). Mixing ratios of NO_x and HONO can typically be found higher indoors than outdoors, with reported levels ranging up to 400 parts per billion (ppb) of NO and NO_2, and up to 100 ppb of HONO. Their sources can be outdoor pollution transported indoors and high-temperature combustion processes like cooking with gas appliances, smoking, lighting candles, and fireplaces (Bartolomei et al., 2015; Collins et al., 2018; Dennekamp et al., 2001; Lee et al., 2002; Mullen et al., 2016; Singer et al., 2017; Zhou et al., 2018). These pollutants play an essential role in oxidant cycling as both sources and sinks indoors, especially in areas with sunlight where NO_2 can photolyze to form O_3 (Kowal et al., 2017) and HONO photolyzes to form OH (Gómez Alvarez et al., 2013; Kowal et al., 2017; Zhou et al., 2018). In the presence of O_3, NO will rapidly react to form NO_2 which can contribute to the oxidant cycle as a HONO precursor (Zhou et al., 2019). Historically, indoor research has focused on the concentrations of O_3 and its contribution to indoor oxidative capacity (Nazaroff and Weschler, 2022; Weschler and Shields, 1996; Wisthaler and Weschler, 2010). However, residential studies have observed indoor environments with low O_3 of a few ppb (Nazaroff and Weschler, 2022; Zhou et al., 2019), suggesting that the hydroxyl radical (OH) may be the most important oxidant that drives indoor chemistry in these spaces. A key contributor and source of OH is HONO photolysis, which can generate OH at low photon energies (≤ 405 nm) with a maximum absorption at 354 nm (R1).

$$\mathbf{HONO_{(g)} \xrightarrow{h\nu} OH + NO_{(g)}} \qquad \mathbf{(R1)}$$

Indoor levels of OH radicals are likely to be underestimated by current approaches because they are short-lived species with a lifetime of < 1 second (s), making it difficult to measure directly. Previously, the ozonolysis of alkenes was suggested to be the main chemical pathway leading to indoor OH formation, resulting in an estimated indoor range of 10^4 – 10^5 molecules cm^{-3} (Weschler

and Shields, 1996). As a result, indoor OH has previously been predicted to be lower by an order of magnitude compared to outdoor concentrations (~10^6 molecules cm^{-3}), but a recent report in a classroom observed 1.8 x 10^6 molecules cm^{-3} OH which is comparable to outdoor OH in urban regions (Carslaw, 2007; Gómez Alvarez et al., 2013). Gómez Alvarez et al. (2013) reported the correlation between OH concentration and linked its production to HONO photolysis, highlighting the importance of HONO as an essential radical source. Following this discovery, chamber experiments were performed with varying light intensities commonly found indoors and direct HONO emissions from a burning candle to confirm OH formation of 10^6 – 10^7 molecules cm^{-3} (Bartolomei et al., 2015). In addition, artificial lighting with lower photon energy than sunlight (i.e., halogen, incandescent, and fluorescent tubing) have since been shown capable of photolyzing HONO (Kowal et al., 2017). In order to accurately predict indoor OH concentrations and improve indoor oxidation in models, we must understand the formation processes of HONO and its potential as an OH precursor in many indoor environments with widely varying uses.

1.3 Indoor HONO chemistry

Indoor HONO sources include direct emissions from combustion processes and heterogenous reactions of its precursor NO_2 on indoor surfaces (R2). Multiple studies have reported high levels of HONO indoors, where the highest mixing ratios are observed directly emitted from gas appliances and other combustion processes (Bartolomei et al., 2015; Collins et al., 2018; Jarvis et al., 2005; Leaderer et al., 1999; Lee et al., 2002; Park et al., 2008; Zhou et al., 2018). Average background levels of HONO in the absence of combustion emissions are typically reported to be ~5 ppb indoors (Brauer et al., 1990; Collins et al., 2018; Gómez Alvarez et al., 2013; Jarvis et al., 2005; Lee et al., 2002; Zhou et al., 2018), and are thought to be likely sourced from heterogeneous surface reactions. Surface chemistry can significantly influence the temporal behaviour of indoor pollutants like NO_2 and HONO because indoor environments have higher surface-to-volume ratios of ~3 $m^{-1,}$ which is hundreds of times higher than outdoors (0.01 m^{-1}) (Abbatt and Wang, 2020; Ault et al., 2020; Manuja et al., 2019; Wang et al., 2020b). The reactive uptake of NO_2 to indoor surfaces is an important sink and precursor to the heterogenous formation of HONO in areas with low photon levels and away from sunlight (Collins et al., 2018; Finlayson-Pitts et al., 2003; Kowal et al., 2017). There are uncertainties in fully understanding the heterogenous formation of HONO, but one well-described mechanism is NO_2 hydrolysis (R2) (Finlayson-Pitts et al., 2003). Gaseous

NO_2 can interact with a thin film of water on indoor surfaces to form gas-phase HONO and adsorbed nitric acid (HNO_3) (Finlayson-Pitts et al., 2003).

$$\mathbf{2\ NO_{2(g)} + H_2O_{(ads)} \xrightarrow{surface} HONO_{(g)} + HNO_{3(ads)}} \quad \textbf{(R2)}$$

Laboratory studies have proposed heterogenous HONO formation is first order in NO_2, and water is essential in converting NO_2 to HONO (Finlayson-Pitts et al., 2003; Pitts et al., 1984; Sakamaki et al., 1983; Svensson et al., 1987). The reaction of NO_2 hydrolysis is relatively linear in water vapour concentrations below ~65 % relative humidity (RH) (Finlayson-Pitts et al., 2003). Further lab investigations have stated that HONO formed on surfaces does not remain adsorbed, partitioning into gas-phase readily as HONO (Collins et al., 2018; Finlayson-pitts, 2009; Finlayson-Pitts et al., 2003; Spicer et al., 1993; Wainman et al., 2001; Wang et al., 2020b). However, those lab surfaces were highly acidified under the given experimental conditions, which would promote HONO partitioning. Steady levels of HONO have been observed in the nocturnal outdoor atmosphere, which suggested HONO surface deposition as a potential loss process under atmospherically-relevant conditions (Collins et al., 2018; Lee et al., 2002; Spicer et al., 1993; Stutz et al., 2004; VandenBoer et al., 2013). The partitioning of HONO outdoors and indoors has been found to be dependent on surface reactivity or pH and can be displaced from formed nitrite salts by common atmospheric acids or other sources of H_3O^+ (VandenBoer et al., 2015; Wang et al., 2020a). Spicer et al., (1993) proposed that nitrite on surfaces acts as a reservoir of gas-phase HONO, suggesting an equilibrium process is present indoors (R3).

$$\mathbf{HONO_{(surface)} \leftrightharpoons HONO_{(g)}} \quad \textbf{(R3)}$$

Wainman et al. (2001) suggested Henry's law equilibrium can explain the slow release of gas-phase HONO from nitrite/HONO sorbed to surfaces in the presence of a thin film of water, such that indoor levels were not entirely dependent on NO_2 surface uptake. Recent studies by Collin et al. (2018) and Wang et al. (2020a) have produced models that include active sources and sink processes happening simultaneously in residencies. To match observations and temporal features, these studies proposed the presence of a large HONO reservoir as the most likely mechanism sustaining the stable levels observed after performing multiple enhanced ventilation experiments where indoor HONO levels quickly recovered from the rapid ventilation-driven dilution (both

natural and mechanical) in the residency. During these experiments Wang et al. (2020a) measured a response time of the indoor surfaces on the order of ~1 minute.

1.3.1 Indoor parameters and influences on HONO chemistry

Indoor environments are constantly evolving. Over the years, there have been continuous changes in building material, design, and furnishings, which provide many varied surfaces for multiphase chemistry (Weschler, 2009). There are different indoor spaces, from hidden and dark areas filled with grime to open and sunlit areas. Indoor factors such as lighting, RH, surface material, and surface chemical composition can influence the behaviour of HONO. Various types of indoor lighting can decompose photolabile HONO. This is possible in areas with artificial lighting and sunlight passing through windows, even when the windows attenuate photon energies to those shorter than ~330 nm (Kowal et al., 2017). Recently, photochemical reactions of painted surfaces containing titanium oxide have been identified as sources of NO_2 and HONO when illuminated by indoor light sources (Gandolfo et al., 2015; Monge et al., 2010; Schwartz-Narbonne et al., 2019).

Indoor temperatures and relative humidity are more stable with fewer fluctuations than outdoor weather. Variations in indoor temperature and RH can exist, particularly when close to heat and water sources such as the kitchen and bathroom. Higher temperatures are known to enhance emissions of HONO during combustion processes, and the heterogenous production of HONO is codependent on RH (Finlayson-Pitts et al., 2003; Wainman et al., 2001). Indoor surfaces act as an interface for heterogenous reactions and surface materials that readily sorb water can be key contributors to building HONO reservoirs indoors (Wainman et al., 2001). Surfaces that have been identified to lead to heterogenous HONO formation include concrete, glass, soil, mineral dust, carpets, and painted walls coated with photocatalytic paint (Ammann et al., 1998; Finlayson-Pitts et al., 2003; Gandolfo et al., 2020; Grosjean, 1985; Kirchstetter et al., 1996; Schwartz-Narbonne et al., 2019; Stemmler et al., 2006; Wainman et al., 2001). The chemical characteristics of surfaces like pH can increase or decrease the extent of HONO partitioning and depends on the type of activity (i.e., cooking and cleaning). When cooking with gas appliances, combustion processes directly emit NO_2, which can then deposit onto surfaces to form HONO (Collins et al., 2018; Wang et al., 2020b). Cleaning products can increase the basicity or acidity of surfaces, shifting the HONO gas-surface equilibrium (Wang et al., 2020a, Wang et al., 2020b). For example, Wang et al. (2020b) cleaned indoor surfaces on to which HONO had been previously deposited from gas stove

emissions, using vinegar to observe strong partitioning of HONO to the gas phase due to increasing surface acidity and possibly acid displacement reactions. These indoor factors create a wide range of potential chemistries that could affect levels of HONO indoors since there is still a lack of understanding on how surface area, surface wetness, air exchange rates, and temperature interact with chemical production and loss mechanisms. The variability in indoor environments and its evolving nature as trends change for furnishing and used building materials change, makes indoor HONO chemistry challenging and will require consistent monitoring and research progress for the foreseeable future. These chemical processes require further investigation in order to be understood at a molecular level in adsorption/desorption chemistry and aqueous thin-film chemistry. Previous studies have focused on changes in gas-phase composition, and future research should expand their perspective to molecular views of surface properties and interactions. Most pressing are advancements in indoor instrumentation that can be used to perform widespread measurements, which are accessible to a large community of industry and academic professionals for future deployment in various indoor facilities to understand how indoor factors can affect indoor air quality.

1.4 The current state of indoor instrumentation

This thesis presents the development of two new instruments, a portable calibration source to provide stable and pure HONO for all instruments and an automated platform that performs time-resolved measurements of NO_x and HONO suitable for indoor environments.

1.4.1 HONO calibration sources

Gas-phase HONO is a challenging compound to measure and results in several instrument artifacts. Positive artifacts can occur in instrument inlet lines from heterogenous formation of HONO on wet surfaces (Kleffmann and Wiesen, 2008; Zhou et al., 2002) and negative artifacts result in wall losses from the reactive nature of HONO (Pinto et al., 2014). Calibration sources are used to reduce measurement uncertainty and maintain accuracy and precision for HONO-detecting instruments. Past intercomparison studies have shown a large discrepancy between various instrument methods in detecting HONO. Authors have reported that HONO mixing ratios in their instruments have systematic variations even though they provided similar temporal trends (Cheng et al., 2013; Crilley et al., 2019; Pinto et al., 2014; Stutz et al., 2010). These measured differences are challenging to identify and could originate from the instruments being externally calibrated

with different calibration techniques that have assumptions that result in poor agreement with each other. Thus, the motivation for developing a new portable gaseous HONO calibration unit that is compatible with all instruments and analytical techniques could help prevent systematic bias and help identify interferences between various instruments. An ideal calibration source should be simple in operation and generate stable and pure mixing ratios of HONO at an atmospherically relevant range.

Previous calibration sources have utilised acid displacement from solutions containing nitrite or from solid sodium nitrite ($NaNO_2$), with the reactant acids including sulfuric acid, hydrochloric acid (HCl), and oxalic acid, in addition to sublimation of NH_4NO_2 (Braman and de la Cantera, 1986; Febo et al., 1995; Taira and Kanda, 1990; Večeřa and Dasgupta, 1991). However, these sources can result in low HONO purity with the formation of other nitrogen oxides. The most commonly used calibration source was presented by Febo et al. (1995), utilizing acid displacement between gas-phase hydrochloric acid and $NaNO_2$ powder to generate continuous levels of HONO (R4).

$$\mathbf{NaNO_{2(s)} + HCl_{(g)} \rightarrow HONO_{(g)} + NaCl_{(s)}} \quad \textbf{(R4)}$$

This calibration source requires a gas-tight vessel of HCl solution housed in a thermostatic bath which can be difficult to use and travel to field sites. Additional challenges in utilizing this source includes the fact that it makes high HONO mixing ratios up to 20 ppm, requiring a large dilution to reach atmospherically relevant mixing ratios. Outdoor measurements of HONO are typically ≤1 ppb (Vandenboer et al., 2013b), while average indoor levels of HONO are ~ 5 ppb and increase up to 100 ppb from combustion cooking processes (Collins et al., 2018; Zhou et al., 2018) so the production of high calibration mixing ratios in parts per million (ppm) is unnecessary. High quantities of HONO production in calibration sources can also lead to autodissociation of HONO (R5), resulting in the production of nitrogen oxide impurities such as NO and NO_2 (Febo et al., 1995; Neuman et al., 2016), and ClNO in the presence of HCl at ppmv levels (Gingerysty and Osthoff, 2020).

$$\mathbf{HONO_{(g)} + HONO_{(ads)} \rightarrow NO_{(g)} + NO_{2(g)} + H_2O} \quad \textbf{(R5)}$$

The variability in HONO output is reduced by continuously mixing powered $NaNO_2$ to maintain equilibrium between the adsorbed HONO and carrier gas flowing over the salt bed to minimize

the production of NO_x. Plus, a Teflon filter is required to prevent the physical loss of suspended $NaNO_2$ crystals and the degradation of powered $NaNO_2$ can limit the lifetime of the source, which results in unstable HONO production rates (Febo et al., 1995; Gingerysty and Osthoff, 2020). While there have been recent adaptations of this source in HCl (immersing thin-wall Teflon tubing in concentrated HCl, high-concentration HCl cylinders, and HCl permeation devices) and dispersed $NaNO_2$ in tubing (McGrath et al., 2019; Roberts et al., 2010; VandenBoer et al., 2015; Zhou et al., 2018), the calibration output suffers from sensitivity to vibration causing changes in HONO output and limiting the calibration accuracy (Zhou et al., 2018). Most modified calibration sources require up to a day to stabilize, must be continuously operated, and be stationary (i.e. vibration isolated) to preserve stable HONO output. These challenges in previous calibration sources highlight the need for a new development of a portable and easy to assemble calibration source that can generate pure and stable quantities of HONO.

1.4.2 Indoor instruments to detect NO_x and HONO

To understand the driving processes of indoor HONO formation, we require real-time and accurate measurements of both HONO and NO_2, along with other observations of indoor air and surface composition that can affect the chemical production and loss pathways relative to air exchange. There are limited studies that report simultaneous indoor measurements of NO, NO_2, and HONO together. Past studies have focused on the indoor emissions of NO and NO_2 due to their association with adverse health effects because they arise from major anthropogenic sources (e.g. transported vehicle exhaust, space heaters, gas appliances, and water heaters) (Breysse et al., 2005; Diette et al., 2007; Hu and Zhao, 2020; Mullen et al., 2016). Most previous indoor studies measuring NO_2 are now known to be biased high because of quantitative HONO interferences in NO_2 passive samplers or detection by molybdenum (Mo) catalyst chemiluminescence analyzers (Spicer et al., 1994, Spicer et al., 2001; Zhou et al., 2018). Passive samplers for NO_2 collection are coated with triethanolamine but can also react with HONO to produce the nitrite reaction product (Spicer et al., 1994, Spicer et al., 2001), while Mo-catalysts in chemiluminescence analyzers can convert HONO and other NO_y species to NO, resulting in another quantitative measurement bias in NO_2 (Dunlea et al., 2007; Joseph and Spicer, 1978; Spicer et al., 1994; Villena et al., 2012). The recent residential study by Zhou et al. (2018) observed that HONO represented a significant fraction of NO_2 measurements, as an artifact in their NO_2* measured by chemiluminescence. The authors concluded that previously reported measurements of NO_2 could have an overestimation by up to a

factor of 3 due to HONO interference. This recent discovery means we require more measurements of in-situ indoor environments to accurately characterize the absolute and relative levels of NO, NO_2, and HONO, further improving indoor chemical models and the role of HONO as an oxidant precursor.

The current state of the science instruments to detect HONO were developed for outdoor research and includes: the long path absorption photometer (LOPAP) (Heland et al., 2001; Reed et al., 2016; Ren et al., 2010), differential absorption optical spectroscopy (DOAS) (Perner and Platt, 1980; Wojtal et al., 2011) and chemical ionization mass spectroscopy (CIMS) (Collins et al., 2018; Roberts et al., 2010; Vandenboer et al., 2013a; Wang et al., 2020a). Transitioning these instruments for indoor research can be challenging when performing door-to-door measurements in multiple facilities because they are costly to operate and require time to assemble due to its bulkiness. In addition, it may discourage occupants from allowing scientists to analyze their indoor environment due to space requirements and instrument hazards. The LOPAP contains toxic dyes and strong acids, DOAS requires a long optical pathway with a high intensity light source operated at dangerous UV wavelengths, and CIMS has a radioactive ion source which could generate toxic reagent ions to measure HONO (e.g. CH_3I for I- chemistry is a known DNA intercalator). These three instruments require a specialized operator who regularly ensures measurements are accurate, which may hinder the lifestyle of the occupants. There are safer options available such as denuders or collection by scrubbing into liquid solutions, but these approaches require extraction and offline analysis by techniques like ion chromatography with conductivity detection, which are time-consuming and labor intensive (Place et al., 2018; VandenBoer et al., 2014, 2015; Večeřa et al., 1991). Real-time detection is preferable because it provides the capacity to investigate the formation and fate of HONO that occurs on timescales on the order of minutes. This is impossible when relying on a collection medium which can be saturated or integrates observations over long collection periods of hours to days. Consequently, new instrumentation that is compatible with the practical requirements of measuring indoors is needed to accurately identify direct emissions and chemical sources of HONO indoors, with safety and automation paramount when working in occupied indoor environments like domestic residences that include pets and children.

1.5 Thesis objectives

The goal of this thesis was to develop advanced instrumentation that generates a pure and robust HONO calibration source and automated HONO platform that can perform time-resolved measurements of NO_x and HONO. The design of these instruments has (or will be) presented on an open-sourced platform for the atmospheric research community to easily replicate and to promote new techniques in capable of making accurate and precise near realtime measurements of NO, NO_2, and HONO. Lastly, the deployment of the automated HONO platform in a commercial kitchen was performed to provide proof-of-concept instrument performance and also investigate how indoor activities in a commercial facility influence the temporal behaviors of HONO and its formation processes.

These following three thesis chapters address key aspects of these research questions.

Chapter 2:

Can we develop a new calibration source that can generate stable and high-purity HONO outputs at atmospherically relevant mixing ratios and solve the challenges of past calibration sources? Can the calibration source be easily assembled for field work and does the HONO quantity change when simulating vibrations and movement from travelling for field work? Is this calibration source compatible with the current state-of-the-art instrumentation to measure HONO in the atmospheric research community?

Chapter 3:

Can a new automated instrument detect real-time changes of emerging indoor pollutants (NO_x and HONO) accurately and is this design suitable for indoor air quality applications? Can this new HONO platform be used in indoor and outdoor environments?

Chapter 4:

Will the newly developed platform successfully detect measurements of NO, NO_2, and HONO in a commercial kitchen facility? Can we utilize these novel field observations to understand their chemical transformations and fate in a commercial setting with higher ventilation and varied cooking and cleaning activities compared to past domestic observations? Can we represent these

field measurements of HONO in a simple model of known processes of sources and sinks, as well as impacts on potential oxidant production?

1.6 References

Abbatt, J. P. D. and Wang, C.: The atmospheric chemistry of indoor environments, Environ. Sci. Process. Impacts, 22(1), 25–48, doi:10.1039/c9em00386j, 2020.

Ammann, M., Kalberer, M., Jost, D. T., Tobler, L., Rössler, E., Piguet, D., Gäggeler, H. W. and Baltensperger, U.: Heterogeneous production of nitrous acid on soot in polluted air masses, Nature, 395(6698), 157–160, doi:10.1038/25965, 1998.

Ault, A. P., Grassian, V. H., Carslaw, N., Collins, D. B., Destaillats, H., Donaldson, D. J., Farmer, D. K., Jimenez, J. L., McNeill, V. F., Morrison, G. C., O'Brien, R. E., Shiraiwa, M., Vance, M. E., Wells, J. R. and Xiong, W.: Indoor Surface Chemistry: Developing a Molecular Picture of Reactions on Indoor Interfaces, Chem, 6, 1–16, doi:10.1016/j.chempr.2020.08.023, 2020.

Bartolomei, V., Gomez Alvarez, E., Wittmer, J., Tlili, S., Strekowski, R., Temime-Roussel, B., Quivet, E., Wortham, H., Zetzsch, C., Kleffmann, J. and Gligorovski, S.: Combustion processes as a source of high levels of indoor hydroxyl radicals through the photolysis of nitrous acid, Environ. Sci. Technol., doi:10.1021/acs.est.5b01905, 2015.

Brauer, M., Ryan, P. B., Suh, H. H., Koutrakls, P. and Spengler, J. D.: Measurements of Nitrous Acid inside Two Research Houses, Environ. Sci. Technol., 24(10), 1521–1527, doi:10.1021/es00080a011, 1990.

Breysse, P. N., Buckley, T. J., Williams, D., Beck, C. M., Jo, S. J., Merriman, B., Kanchanaraksa, S., Swartz, L. J., Callahan, K. A., Butz, A. M., Rand, C. S., Diette, G. B., Krishnan, J. A., Moseley, A. M., Curtin-Brosnan, J., Durkin, N. B. and Eggleston, P. A.: Indoor exposures to air pollutants and allergens in the homes of asthmatic children in inner-city Baltimore, Environ. Res., 98(2), 167–176, doi:10.1016/j.envres.2004.07.018, 2005.

Carslaw, N.: A new detailed chemical model for indoor air pollution, Atmos. Environ., 41(6), 1164–1179, doi:10.1016/j.atmosenv.2006.09.038, 2007.

Collins, D. B., Hems, R. F., Zhou, S., Wang, C., Grignon, E., Alavy, M., Siegel, J. A. and Abbatt, J. P. D.: Evidence for Gas-Surface Equilibrium Control of Indoor Nitrous Acid, Environ. Sci. Technol., 52(21), 12419–12427, doi:10.1021/acs.est.8b04512, 2018.

Dennekamp, M., Howarth, S., Dick, C. A. J., Cherrie, J. W., Donaldson, K. and Seaton, A.: Ultrafine particles and nitrogen oxides generated by gas and electric cooking, Occup. Environ. Med., 58(8), 511–516, doi:10.1136/oem.58.8.511, 2001.

Diette, G. B., Hansel, N. N., Buckley, T. J., Brosnan, J. C., Eggleston, P. A., Matsui, E. C., McCormack, M. C., Williams, D. L. and Breysse, P. N.: Home indoor pollutant exposures among inner-city children with and without asthma, Environ. Health Perspect., 115(11), 1665–1669, doi:10.1289/ehp.10088, 2007.

Dunlea, E. J., Herndon, S. C., Nelson, D. D., Volkamer, R. M., San Martini, F., Sheehy, P. M., Zahniser, M. S., Shorter, J. H., Wormhoudt, J. C., Lamb, B. K., Allwine, E. J., Gaffney, J. S., Marley, N. A., Grutter, M., Marquez, C., Blanco, S., Cardenas, B., Retama, A., Yillegas, C. R. R., Kolb, C. E., Molina, L. T. and Molina, M. J.: Evaluation of nitrogen dioxide chemiluminescence monitors in a polluted urban environment, Atmos. Chem. Phys., 7(10), 2691–2704, doi:10.5194/acp-7-2691-2007, 2007.

Farmer, D. K., Vance, M. E., Abbatt, J. P. D., Abeleira, A., Alves, M. R., Arata, C., Boedicker, E., Bourne, S., Cardoso-Saldaña, F., Corsi, R., Decarlo, P. F., Goldstein, A. H., Grassian, V. H., Hildebrandt Ruiz, L., Jimenez, J. L., Kahan, T. F., Katz, E. F., Mattila, J. M., Nazaroff, W. W., Novoselac, A., O'Brien, R. E., Or, V. W., Patel, S., Sankhyan, S., Stevens, P. S., Tian, Y., Wade, M., Wang, C., Zhou, S. and Zhou, Y.: Overview of HOMEChem: House Observations of Microbial and Environmental Chemistry, Environ. Sci. Process. Impacts, 21(8), 1280–1300, doi:10.1039/c9em00228f, 2019.

Finlayson-pitts, B. J.: Reactions at surfaces in the atmosphere: integration of experiments and theory as necessary (but not necessarily sufficient) for predicting the physical chemistry of aerosols, Phys. Chem. Chem. Phys., 11(36), 7760–7779, doi:10.1039/b906540g, 2009.

Finlayson-Pitts, B. J., Wingen, L. M., Sumner, A. L., Syomin, D. and Ramazan, K. A.: The heterogeneous hydrolysis of NO2 in laboratory systems and in outdoor and indoor atmospheres: An integrated mechanism, Phys. Chem. Chem. Phys., 5(2), 223–242, doi:10.1039/b208564j, 2003.

Gandolfo, A., Bartolomei, V., Gomez Alvarez, E., Tlili, S., Gligorovski, S., Kleffmann, J. and Wortham, H.: The effectiveness of indoor photocatalytic paints on NOx and HONO levels, Appl. Catal. B Environ., doi:10.1016/j.apcatb.2014.11.011, 2015.

Gandolfo, A., Bartolomei, V., Truffier-Boutry, D., Temime-Roussel, B., Brochard, G., Bergé, V., Wortham, H. and Gligorovski, S.: The impact of photocatalytic paint porosity on indoor NOx and HONO levels, Phys. Chem. Chem. Phys., doi:10.1039/c9cp05477d, 2020.

Gligorovski, S.: Nitrous acid (HONO): An emerging indoor pollutant, J. Photochem. Photobiol. A Chem., 314, 1–5, doi:10.1016/j.jphotochem.2015.06.008, 2016.

Gómez Alvarez, E., Amedro, D., Afif, C., Gligorovski, S., Schoemaecker, C., Fittschen, C., Doussin, J.-F. and Wortham, H.: Unexpectedly high indoor hydroxyl radical concentrations associated with nitrous acid, Proc. Natl. Acad. Sci., 110(33), 13294–13299, doi:10.1073/pnas.1309171110, 2013.

Grosjean, D.: Wall Loss of Gaseous Pollutants in Outdoor Teflon Chambers, Environ. Sci. Technol., 19(11), 1059–1065, doi:10.1021/es00141a006, 1985.

Heland, J., Kleffmann, J., Kurtenbach, R. and Wiesen, P.: A new instrument to measure gaseous nitrous acid (HONO) in the atmosphere, Environ. Sci. Technol., 35(15), 3207–3212, doi:10.1021/es000303t, 2001.

Hu, Y. and Zhao, B.: Relationship between indoor and outdoor NO2: A review, Build. Environ., 180(2), 106909, doi:10.1016/j.buildenv.2020.106909, 2020.

Jarvis, D. L., Leaderer, B. P., Chinn, S. and Burney, P. G.: Indoor nitrous acid and respiratory symptoms and lung function in adults, Thorax, 60(6), 474–479, doi:10.1136/thx.2004.032177, 2005.

Joseph, D. W. and Spicer, C. W.: Chemiluminescence Method for Atmospheric Monitoring of Nitric Acid and Nitrogen Oxides, Anal. Chem., 50(9), 1400–1403, doi:10.1021/ac50031a054, 1978.

Kirchstetter, T. W., Harley, R. A. and Littlejohn, D.: Measurement of nitrous acid in motor vehicle exhaust, Environ. Sci. Technol., 30(9), 2843–2849, doi:10.1021/es960135y, 1996.

Klepeis, N. E., Nelson, W. C., Ott, W. R., Robinson, J. P., Tsang, A. M., Switzer, P., Behar, J. V., Hern, S. C. and Engelmann, W. H.: The National Human Activity Pattern Survey (NHAPS): A resource for assessing exposure to environmental pollutants, J. Expo. Anal. Environ. Epidemiol., 11(3), 231–252, doi:10.1038/sj.jea.7500165, 2001.

Kowal, S. F., Allen, S. R. and Kahan, T. F.: Wavelength-Resolved Photon Fluxes of Indoor Light Sources: Implications for HOx Production, Environ. Sci. Technol., 51(18), 10423–10430, doi:10.1021/acs.est.7b02015, 2017.

Leaderer, B. P., Naeher, L., Jankun, T., Balenger, K., Holford, T. R., Toth, C., Sullivan, J., Wolfson, J. M., Koutrakis, P., Environmental, S., Perspectives, H., Mar, N., Leaderer, B. P., Naeher, L., Jankun, T., Balenger, K., Holford, T. R., Toth, C., Wolfson, J. M. and Koutrakis, P.: Indoor, Outdoor, and Regional Summer and Winter Concentrations of PM10, PM2.5, SO4, 2-, H+, NH4+, NO3-, NH3, and Nitroud Acid in Homes with and without Kerosene Space Heaters, Environ. Health Perspect., 107(3), 223–231 [online] Available from: https://www.jstor.org/stable/3434513, 1999.

Lee, K., Xue, J., Geyh, A. S., Özkaynak, H., Leaderer, B. P., Weschler, C. J. and Spengler, J. D.: Nitrous acid, nitrogen dioxide, and ozone concentrations in residential environments, Environ. Health Perspect., 110(2), 145–149, doi:10.1289/ehp.02110145, 2002.

Leech, J. A., Nelson, W. C., Burnett, R. T., Aaron, S. and Raizenne, M. E.: It's about time: A comparison of Canadian and American time-activity patterns, J. Expo. Anal. Environ. Epidemiol., 12(6), 427–432, doi:10.1038/sj.jea.7500244, 2002.

Li, M., Weschler, C. J., Bekö, G., Wargocki, P., Lucic, G. and Williams, J.: Human Ammonia Emission Rates under Various Indoor Environmental Conditions, Environ. Sci. Technol., 54(9), 5419–5428, doi:10.1021/acs.est.0c00094, 2020.

Manuja, A., Ritchie, J., Buch, K., Wu, Y., Eichler, C. M. A., Little, J. C. and Marr, L. C.: Total surface area in indoor environments, Environ. Sci. Process. Impacts, 21(8), 1384–1392, doi:10.1039/c9em00157c, 2019.

McGrath, D. T., Ryan, M. D., Macinnis, J. J., Vandenboer, T. C., Young, C. J. and Katz, M. J.: Selective decontamination of the reactive air pollutant nitrous acid: Via node-linker cooperativity in a metal-organic framework, Chem. Sci., 10(21), 5576–5581, doi:10.1039/c9sc01357a, 2019.

Monge, M. E., D'Anna, B. and George, C.: Nitrogen dioxide removal and nitrous acid formation on titanium oxide surfaces-an air quality remediation process?, Phys. Chem. Chem. Phys., 12(31), 8991–8998, doi:10.1039/b925785c, 2010.

Mullen, N. A., Li, J., Russell, M. L., Spears, M., Less, B. D. and Singer, B. C.: Results of the California Healthy Homes Indoor Air Quality Study of 2011-2013: Impact of natural gas appliances on air pollutant concentrations, Indoor Air, 26(2), 231–245, doi:10.1111/ina.12190, 2016.

Nazaroff, W. W. and Weschler, C. J.: Indoor acids and bases, Indoor Air, 30(4), 559–644, doi:10.1111/ina.12670, 2020.

Nazaroff, W. W. and Weschler, C. J.: Indoor ozone: Concentrations and influencing factors, Indoor Air, 32(1), 1–21, doi:10.1111/ina.12942, 2022.

Park, S. S., Hong, J. H., Lee, J. H., Kim, Y. J., Cho, S. Y. and Kim, S. J.: Investigation of nitrous acid concentration in an indoor environment using an in-situ monitoring system, Atmos. Environ., doi:10.1016/j.atmosenv.2008.05.023, 2008.

Perner, D. and Platt, U.: Detection of nitrous acid in the atmosphere by differential optical absorption, Geophys. Res. Lett., 6(12), 917–920, doi:10.1029/GL006i012p00917, 1980.

Pitts, J. N., Sanhueza, E., Atkinson, R., Carter, W. P. L., Winer, A. M., Harris, G. W. and Plum, C. N.: An investigation of the dark formation of nitrous acid in environmental chambers, Int. J. Chem. Kinet., 16(7), 919–939, doi:10.1002/kin.550160712, 1984.

Place, B. K., Young, C. J., Ziegler, S. E., Edwards, K. A., Salehpoor, L. and VandenBoer, T. C.: Passive sampling capabilities for ultra-trace quantitation of atmospheric nitric acid (HNO 3) in remote environments, Atmos. Environ., 191(November 2017), 360–369, doi:10.1016/j.atmosenv.2018.08.030, 2018.

Reed, C., Brumby, C. A., Crilley, L. R., Kramer, L. J., Bloss, W. J., Seakins, P. W., Lee, J. D. and Carpenter, L. J.: HONO measurement by differential photolysis, Atmos. Meas. Tech., 9(6), 2483–2495, doi:10.5194/amt-9-2483-2016, 2016.

Ren, X., Gao, H., Zhou, X., Crounse, J. D., Wennberg, P. O., Browne, E. C., LaFranchi, B. W., Cohen, R. C., McKay, M., Goldstein, A. H. and Mao, J.: Measurement of atmospheric nitrous acid at Bodgett forest during BEARPEX2007, Atmos. Chem. Phys., 10(13), 6283–6294, doi:10.5194/acp-10-6283-2010, 2010.

Roberts, J. M., Veres, P., Warneke, C., Neuman, J. A., Washenfelder, R. A., Brown, S. S., Baasandorj, M., Burkholder, J. B., Burling, I. R., Johnson, T. J., Yokelson, R. J. and De Gouw, J.: Measurement of HONO, HNCO, and other inorganic acids by negative-ion proton-transfer chemical-ionization mass spectrometry (NI-PT-CIMS): Application to biomass burning emissions, Atmos. Meas. Tech., 3(4), 981–990, doi:10.5194/amt-3-981-2010, 2010.

Sakamaki, F., Hatakeyama, S. and Akimoto, H.: Formation of nitrous acid and nitric oxide in the heterogeneous dark reaction of nitrogen dioxide and water vapor in a smog chamber, Int. J. Chem. Kinet., doi:10.1002/kin.550151006, 1983.

Salonen, H., Salthammer, T. and Morawska, L.: Human exposure to NO2 in school and office indoor environments, Environ. Int., 130(March), 104887, doi:10.1016/j.envint.2019.05.081, 2019.

Schwartz-Narbonne, H., Jones, S. H. and Donaldson, D. J.: Indoor Lighting Releases Gas Phase Nitrogen Oxides from Indoor Painted Surfaces, Environ. Sci. Technol. Lett., 6(2), 92–97, doi:10.1021/acs.estlett.8b00685, 2019.

Singer, B. C., Pass, R. Z., Delp, W. W., Lorenzetti, D. M. and Maddalena, R. L.: Pollutant concentrations and emission rates from natural gas cooking burners without and with range hood exhaust in nine California homes, Build. Environ., 122(2), 215–229, doi:10.1016/j.buildenv.2017.06.021, 2017.

Spicer, C. W., Kenny, D. V., Ward, G. F. and Billick, I. H.: Transformations, Lifetimes, and Sources of NO2, HONO, and HNO3 in Indoor Environments, J. Air Waste Manage. Assoc., 43(11), 1479–1485, doi:10.1080/1073161X.1993.10467221, 1993.

Spicer, C. W., Kenny, D. V., Ward, G. F., Billick, I. H. and Leslie, N. P.: Evaluation of NO2 Measurement Methods for Indoor Air Quality Applications, Air Waste, 44(2), 163–168, doi:10.1080/1073161X.1994.10467245, 1994.

Spicer, C. W., Billick, I. H. and Yanagisawa, Y.: Nitrous Acid Interference with Passive NO2 Measurement Methods and the Impact on Indoor NO2 Data, Indoor Air, 11(3), 156–161, doi:10.1034/j.1600-0668.2001.011003156.x, 2001.

Stemmler, K., Ammann, M., Donders, C., Kleffmann, J. and George, C.: Photosensitized reduction of nitrogen dioxide on humic acid as a source of nitrous acid, Nature, 440(7081), 195–198, doi:10.1038/nature04603, 2006.

Stutz, J., Alicke, B., Ackerman, R., Geyer, A., Wang, S., White, A. B., Williams, E. J., Spicer, C. W. and Fast, J. D.: Relative humidity dependence of HONO chemistry in urban areas, J. Geophys. Res. Atmos., 109(3), doi:10.1029/2003jd004135, 2004.

Svensson, R., Ljungström, E. and Lindqvist, O.: Kinetics of the reaction between nitrogen dioxide and water vapour, Atmos. Environ., 21(7), 1529–1539, doi:10.1016/0004-6981(87)90315-5, 1987.

Vandenboer, T. C., Brown, S. S., Murphy, J. G., Keene, W. C., Young, C. J., Pszenny, A. A. P., Kim, S., Warneke, C., De Gouw, J. A., Maben, J. R., Wagner, N. L., Riedel, T. P., Thornton, J. A., Wolfe, D. E., Dubé, W. P., Öztürk, F., Brock, C. A., Grossberg, N., Lefer, B., Lerner, B., Middlebrook, A. M. and Roberts, J. M.: Understanding the role of the ground surface in HONO vertical structure: High resolution vertical profiles during NACHTT-11, J. Geophys. Res. Atmos., 118(17), 10155–10171, doi:10.1002/jgrd.50721, 2013a.

VandenBoer, T. C., Brown, S. S., Murphy, J. G., Keene, W. C., Young, C. J., Pszenny, A. A. P., Kim, S., Warneke, C., De Gouw, J. A., Maben, J. R., Wagner, N. L., Riedel, T. P., Thornton, J. A., Wolfe, D. E., Dubé, W. P., Öztürk, F., Brock, C. A., Grossberg, N., Lefer, B., Lerner, B., Middlebrook, A. M. and Roberts, J. M.: Understanding the role of the ground surface in HONO vertical structure: High resolution vertical profiles during NACHTT-11, J. Geophys. Res. Atmos., 118(17), 10155–10171, doi:10.1002/jgrd.50721, 2013.

VandenBoer, T. C., Markovic, M. Z., Sanders, J. E., Ren, X., Pusede, Browne, E. C., Cohen, R. C., Zhang, L., Thomas, J., Brune, W. H. and Murphy, J. G.: Evidence for a nitrous acid (HONO) reservoir at the ground surface in Bakersfield, CA, during CalNex 2010, J. Geophys. Res. Atmos., 119, 9093–9106, doi:10.1002/ 2013JD020971, 2014.

VandenBoer, T. C., Young, C. J., Talukdar, R. K., Markovic, M. Z., Brown, S. S., Roberts, J. M. and Murphy, J. G.: Nocturnal loss and daytime source of nitrous acid through reactive uptake and displacement, Nat. Geosci., 8(1), 55–60, doi:10.1038/ngeo2298, 2015.

Vandenboer, T. C. T. C., Brown, S. S. S. S., Murphy, J. G. J. G., Keene, W. C. W. C., Young, C. J. C. J., Pszenny, A. A. P. A. P., Kim, S., Warneke, C., De Gouw, J. A. J. A., Maben, J. R. J. R., Wagner, N. L. N. L., Riedel, T. P. T. P., Thornton, J. A. J. A., Wolfe, D. E. D. E., Dubé, W. P. W. P., Öztürk, F., Brock, C. A., Grossberg, N., Lefer, B., Lerner, B., Middlebrook, A. M. A. M. and Roberts, J. M.: Understanding the role of the ground surface in HONO vertical structure: High resolution vertical profiles during NACHTT-11, J. Geophys. Res. Atmos., 118(17), 10155–10171, doi:10.1002/jgrd.50721, 2013b.

Večeřa, Z., Dasgupta, P. K. and Večeřa, Z.: Measurement of Ambient Nitrous Acid and a Reliable Calibration Source for Gaseous Nitrous Acid, Environ. Sci. Technol., 25(2), 255–260, doi:10.1021/es00014a006, 1991.

Villena, G., Bejan, I., Kurtenbach, R., Wiesen, P. and Kleffmann, J.: Interferences of commercial NO2 instruments in the urban atmosphere and in a smog chamber, Atmos. Meas. Tech., 5(1), 149–159, doi:10.5194/amt-5-149-2012, 2012.

Wainman, T., Weschler, C. J., Lioy, P. J. and Zhang, J.: Effects of surface type and relative humidity on the production and concentration of nitrous acid in a model indoor environment, Environ. Sci. Technol., 35(11), 2200–2206, doi:10.1021/es000879i, 2001.

Wang, C., Bottorff, B., Reidy, E., Rosales, C. M. F., Collins, D. B., Novoselac, A., Farmer, D. K., Vance, M. E., Stevens, P. S. and Abbatt, J. P. D.: Cooking, Bleach Cleaning, and Air Conditioning Strongly Impact Levels of HONO in a House, Environ. Sci. Technol., 54(21), 13488–13497, doi:10.1021/acs.est.0c05356, 2020a.

Wang, C., Collins, D. B., Arata, C., Goldstein, A. H., Mattila, J. M., Farmer, D. K., Ampollini, L., DeCarlo, P. F., Novoselac, A., Vance, M. E., Nazaroff, W. W. and Abbatt, J. P. D.: Surface reservoirs dominate dynamic gas-surface partitioning of many indoor air constituents, Sci. Adv., 6(8), 1–12, doi:10.1126/sciadv.aay8973, 2020b.

Waring, M. S. and Wells, J. R.: Volatile organic compound conversion by ozone, hydroxyl radicals, and nitrate radicals in residential indoor air: Magnitudes and impact of oxidant sources, Atmos. Environ., 106, 382–391, doi:10.1016/j.atmosenv.2014.06.062., 2015.

Weschler, C. J.: Changes in indoor pollutants since the 1950s, Atmos. Environ., 43(1), 153–169, doi:10.1016/j.atmosenv.2008.09.044, 2009.

Weschler, C. J. and Carslaw, N.: Indoor Chemistry, Environ. Sci. Technol., 52(5), 2419–2428, doi:10.1021/acs.est.7b06387, 2018.

Weschler, C. J. and Shields, H. C.: Production of the hydroxyl radical in indoor air, Environ. Sci. Technol., 30(11), 3250–3258, doi:10.1021/es960032f, 1996.

Wisthaler, A. and Weschler, C. J.: Reactions of ozone with human skin lipids: Sources of carbonyls, dicarbonyls, and hydroxycarbonyls in indoor air, Proc. Natl. Acad. Sci. U. S. A., 107(15), 6568–6575, doi:10.1073/pnas.0904498106, 2010.

Wojtal, P., Halla, J. D. and McLaren, R.: Pseudo steady states of HONO measured in the nocturnal marine boundary layer: A conceptual model for HONO formation on aqueous surfaces, Atmos. Chem. Phys., 11(7), 3243–3261, doi:10.5194/acp-11-3243-2011, 2011.

Zhou, S., Young, C. J., VandenBoer, T. C., Kowal, S. F. and Kahan, T. F.: Time-Resolved Measurements of Nitric Oxide, Nitrogen Dioxide, and Nitrous Acid in an Occupied New York Home, Environ. Sci. Technol., 52(15), 8355–8364, doi:10.1021/acs.est.8b01792, 2018.

Zhou, S., Young, C. J., VandenBoer, T. C. and Kahan, T. F.: Role of location, season, occupant activity, and chemistry in indoor ozone and nitrogen oxide mixing ratios, Environ. Sci. Process. Impacts, 21, 1374–1383, doi:10.1039/c9em00129h, 2019.

Chapter Two:

A portable, robust, stable, and tunable calibration source for gas-phase nitrous acid (HONO)

M. Lao[1], L.R. Crilley[1], L. Salehpoor[1], T.C. Furlani[1], I. Bourgeois[2,3], J.A. Neuman[2,3], A.W. Rollins[2], P.R. Veres[2], R.A. Washenfelder[2], C.C. Womack[2,3], C.J. Young[1], and T.C. VandenBoer[1]

[1]Department of Chemistry, York University, Toronto, ON, Canada

[2]NOAA Chemical Sciences Laboratory, Boulder, CO, USA

[3]Cooperative Institute for Research in Environmental Sciences, University of Colorado, Boulder, CO, USA

In Press: Lao, M. et al., *Atmos. Meas. Tech.*, 13, 5873-5890, 2020, https://doi.org/10.5194/amt-13-5873-2020

Author Contributions:

TCV, CJY, and RAW conceptualized the calibration source. TCV and CJY supervised the experiments, acquired the funding, and provided the resources to support this work. TCV designed the experiments, guided the investigations, and managed the project. **ML** constructed the custom PDs under the guidance of TCF and LS. **ML** and LS built the custom permeation oven and analyzed IC-CD samples. LRC and **ML** performed the mass balance, reaction device, and purity experiments. LRC and **ML** established and validated the methodologies. IB, JAN, AWR, PRV, RAW, and CCW provided instrumental resources and performed measurements included in the stability and purity experiments. LS created the schematics and wrote the detailed description of the custom permeation oven. **ML** constructed the reaction devices, performed part or the entirety of the experiments, and prepared the manuscript with contributions from all authors. All authors participated in data analysis, as well as the review and editing of the manuscript.

Abstract

Atmospheric HONO mixing ratios in indoor and outdoor environments span a range of less than a few parts per trillion by volume (pptv) up to tens of parts per billion by volume (ppbv) in combustion plumes. Previous HONO calibration sources have utilized proton transfer acid displacement from nitrite salts or solutions, with output that ranges from tens to thousands of ppbv. Instrument calibrations have thus required large dilution flows to obtain atmospherically relevant mixing ratios. Here we present a simple universal source to reach very low HONO calibration mixing ratios using a nitrite-coated reaction device with the addition of humid air and/or HCl from a permeation device. The calibration source developed in this work can generate HONO across the atmospherically relevant range and has high purity (> 90 %), reproducibility, and tunability. Mixing ratios at the tens of pptv level are easily reached with reasonable dilution flows. The calibration source can be assembled to start producing stable HONO mixing ratios (relative standard error, RSE ≤ 2 %) within 2 h, with output concentrations varying ≤ 25 % following simulated transport or complete disassembly of the instrument and with ≤ 10 % under ideal conditions. The simplicity of this source makes it highly versatile for field and lab experiments. The platform facilitates a new level of accuracy in established instrumentation, as well as intercomparison studies to identify systematic HONO measurement bias and interferences.

2.1 Introduction

In the lower troposphere, the hydroxyl radical (OH) is the principal daytime gas-phase oxidant and will react with volatile organic compounds (VOCs) to form secondary pollutants such as ozone (O_3) and secondary organic aerosols (Spataro and Ianniello, 2014; Ye et al., 2018). Photolysis of nitrous acid (HONO) is a direct source of the hydroxyl radical (OH) (Reaction R1). Consequently, this can be a significant contributor to the integrated daily OH budget, ranging from 4 % to 56 % in urban areas (Lee et al., 2013; Volkamer et al., 2010) up to 80 % in semirural areas in the winter (Kim et al., 2014), along with additional vertical and temporal variability (Crilley et al., 2016; Young et al., 2012; Zhang et al., 2009).

$$\mathbf{HONO_{(g)} + h\nu\ (\lambda < 405\ nm) \rightarrow OH_{(g)} + NO_{(g)}} \qquad \mathbf{(R1)}$$

The reported daytime mixing ratios of ambient HONO outdoors can vary considerably for different environments, ranging from a few parts per trillion by volume (pptv) in the clean remote marine

and Arctic boundary layers (Honrath et al., 2002; Kasibhatla et al., 2018; Reed et al., 2017) to 18 parts per billion by volume (ppbv) in polluted megacities such as Milan, Los Angeles, and Beijing (Elshorbany et al., 2009; Febo et al., 1996; Harris et al., 1982; Tong et al., 2016; Zhang et al., 2019). Measurements within biomass burning plumes from forest fires have shown very high HONO levels, often up to 60 ppbv (Chai et al., 2019; Neuman et al., 2016; Veres et al., 2010b). There is a growing body of evidence that HONO concentrations can be significant in indoor environments, with levels up to 50 ppbv reported from gas stove cooking emissions (Collins et al., 2018; Gligorovski, 2016; Gómez Alvarez et al., 2012; Liu et al., 2019; Young et al., 2019; Zhou et al., 2018). There are a number of atmospheric HONO sources that have been reported: direct emissions (e.g., vehicles and biomass burning), gas-phase homogenous reaction of NO and OH, biological production in soils (Mushinski et al., 2019), and a number of heterogeneous surface reactions (Spataro and Ianniello, 2014, and references therein). Despite the importance of HONO to atmospheric photochemistry and radical budgets, the contribution of these sources to observed HONO levels is still poorly constrained, particularly during the daytime (Gall et al., 2016; Kleffmann, 2007; Lee et al., 2016; Oswald et al., 2013; Pusede et al., 2015; Sörgel et al., 2015; Tsai et al., 2018; Ye et al., 2016).

Due to the importance of HONO in our understanding of tropospheric photochemical oxidation and indoor atmospheric oxidation chemistry, accurate and precise quantitative measurements are required. However, gas-phase HONO has remained a challenging compound to measure due to several instrument artifacts and interferences. Within inlet lines, positive artifacts can occur as a result of heterogenous HONO formation on wet surfaces (Kleffmann and Wiesen, 2008; Zhou et al., 2002), while the reactive nature of HONO can also lead to negative artifacts due to wall losses (Pinto et al., 2014). Furthermore, there can be interferences from ambient components in the atmospheric matrix, such as the reduction of NO_2 by numerous compounds, as well as particulate nitrite (Kleffmann et al., 2006; Kleffmann and Wiesen, 2008; Rubio et al., 2009; Sörgel et al., 2011; VandenBoer et al., 2014). Recent intercomparison studies have shown substantial differences between various HONO measurement techniques (Cheng et al., 2013; Crilley et al., 2019; Pinto et al., 2014; Stutz et al., 2010). Crilley et al. (2019) observed that while different HONO measurement techniques agreed on the temporal trends in HONO concentrations, the reported absolute concentrations displayed systematic variation. Most studies are unable to pinpoint the exact cause of the observed divergence between instruments; it may be due to spatial

heterogeneity in ambient HONO concentration, unknown chemical interference(s), and/or differences in the accuracy and precision of calibration approaches. A portable calibration unit compatible with all instruments/techniques could assist in ruling out systematic bias and identifying interferences between instruments during intercomparison studies.

A variety of approaches have been used in the past to generate gaseous HONO standards. Most of these depend on acid displacement from a solution containing nitrite (NO_2^-) or from solid sodium nitrite ($NaNO_2$). Acids used have included sulfuric acid, hydrochloric acid, and oxalic acid, with evaporation of NH_4NO_2 also reported (Braman and de la Cantera, 1986; Febo et al., 1995; Taira and Kanda, 1990; Večeřa and Dasgupta, 1991). By far the most widely employed modern HONO calibration methods stem from the report of Febo et al. (1995), who presented a system for generating a continuous source of stable gas-phase HONO in the tens of ppbv to parts per million by volume (ppmv) range. This system utilized the reaction between gas-phase hydrochloric acid (HCl) and $NaNO_2$ powder to generate gas phase HONO, as described in Reaction (R2):

$$\mathbf{NaNO_{2(s)} + HCl_{(g)} \rightarrow HONO_{(g)} + NaCl_{(s)}} \qquad \mathbf{(R2)}$$

However, this calibration source requires a gas-tight vessel of HCl solution contained in a thermostatic bath that presents considerable difficulty for many field measurement applications. Adaptations include immersing thin-wall Teflon tubing in concentrated HCl, high-concentration HCl cylinders, and HCl permeation devices. Gaseous HCl generated by these methods then mixes with loose $NaNO_2$ crystals in a stirred reactor (Stutz et al., 2000), dispersed using 3 mm glass beads packed in PFA tubing to increase porosity (Roberts et al., 2010), or pieces of PFA tubing (McGrath et al., 2019; VandenBoer et al., 2015; Zhou et al., 2018). These adapted approaches have been used to calibrate many atmospheric HONO instruments (Crilley et al., 2019; Heland et al., 2001; Ren et al., 2010; Roberts et al., 2010; Stutz et al., 2000; VandenBoer et al., 2013, 2015; Wang and Zhang, 2000; Young et al., 2012). An alternative approach that utilized dilute H_2SO_4 for the acid displacement reaction with aqueous $NaNO_2$ was outlined by Taira and Kanda (1990). While this approach was shown to generate a stable and tunable HONO output at hundreds of ppbv, it has not been widely adapted, likely due to the need for complex custom glassware and liquid flow control in the calibration apparatus and significant dilution to reach single-digit ppbv mixing ratios (Kleffmann et al., 2004).

While widely used, the method described by Febo et al. (1995) presents several practical challenges. The typically high HONO mixing ratios generated by this approach (up to 20 ppmv) are challenging to dilute to atmospherically relevant mixing ratios. The high quantities also lead to autodissociation of HONO (R3), resulting in the production of nitrogen oxide impurities of NO and NO_2 (Febo et al., 1995; Neuman et al., 2016), and ClNO in the presence of HCl at ppmv levels (Gingerysty and Osthoff, 2020).

$$\mathbf{HONO_{(g)} + HONO_{(ads)} \rightarrow NO_{(g)} + NO_{2(g)} + H_2O} \quad \textbf{(R3)}$$

Further, to reduce the variability in HONO output over time, the powdered $NaNO_2$ bed requires continuous mixing to maintain equilibrium between the adsorbed HONO and carrier gas flowing over the salt bed to minimize the production of NO_x by Reaction (R3), as well as a Teflon filter to prevent loss of $NaNO_2$ powder by entrainment in the gas flow. The degradation of the powdered $NaNO_2$ structure can limit the lifetime of the source and results in unstable HONO production rates (Febo et al., 1995; Gingerysty and Osthoff, 2020). Other systems using dispersed $NaNO_2$ suffer from sensitivity to vibration, causing changes in HONO output and limiting calibration accuracy (Zhou et al., 2018). Once operational, the original or modified methods require up to a day to stabilize, and these systems must be kept continuously operating and stationary to preserve the HONO output stability.

One solution for producing gaseous HCl for acid displacement is to use a temperature-controlled permeation device (PD). A permeation oven is a simple instrument that can be used for the preparation of low mixing ratios of gases from ppbv to ppmv levels (Veres et al., 2010a; Washenfelder et al., 2003). This approach has been used to generate a consistent quantity of gaseous analytes for over 400 compounds because it is low cost, portable, and robust (Mitchell, 2000). Permeation devices are typically made of inert polymer tube of known permeability filled with a (semi)volatile liquid. Both ends of the device are sealed either with caps or permeable plugs, and the emission is determined by the surface area and thickness of permeable polymer, the concentration of the contained solution, and the temperature (O'Keeffe and Ortman, 1966; Susaya et al., 2012).

The aim of the current work was to make a portable and easy to assemble HONO calibration instrument compatible with HONO-measuring instruments commonly used within the atmospheric research community. We developed coated devices to facilitate reactions of sodium

nitrite ($NaNO_2$) which release HONO when exposed to water vapor and HCl (Reaction R2). Herein we demonstrate that the $NaNO_2$-coated reaction devices produce a stable and continuous supply of high-purity gaseous HONO. The output of this HONO calibration source spans the range of environmentally relevant mixing ratios, up to tens of ppbv. The emission quantities, mass balance, and purity of gaseous HONO were determined through a series of control tests with various instruments. We present evidence of its robustness, reproducibility, and stability in HONO output. Finally, we evaluated methods to control the mixing ratio output of the calibration source and provide several approaches and recommendations on its use.

2.2 Experimental methods

2.2.1 Coated $NaNO_2$ reaction devices

Reactions of $NaNO_2$ on humidified surfaces produce HONO. A large and consistent surface area is required to reproducibly produce HONO at the desired levels.

A $NaNO_2$ (EMSURE®; ACS Reag. Ph Eur, Germany) coating solution was made as a 20 g L^{-1} $NaNO_2$ solution. The coating solution solvent was composed of equal volumes of methanol (HPLC grade; Fisher Chemicals, Ottawa, ON) and 18.2 M MΩ·cm deionized water with 1.0 g L^{-1} glycerol (Sigma Chemical Company, St. Louis, MO, USA) to facilitate a uniform salt coating. The solution was made by dissolving the $NaNO_2$ in the water first, followed by the addition of the glycerol and then methanol. The coating solution was stored in an HDPE bottle wrapped in aluminum foil at 4 °C until needed and remade every 3 months. To coat a reaction device, 3 mL of coating solution was first transferred into a heat-straightened 1/2 in. (1.27 cm) PFA tube with a length of 14.4 cm and surface area of 86.2 cm^2. Rubber stoppers with centered 4.5 mm holes were inserted into both ends of the PFA tube to reduce solution loss while evaporating the solvent. The PFA reaction device was repeatedly inverted and rotated while covering both stopper holes to coat the inner surface completely. The reaction device was then dried by insertion into an 8 in. (20 cm) length of aluminum pipe (1–1/4 in./3.18 cm i.d.) and placed onto heated stainless-steel rollers to evenly coat the PFA reaction device surface as the solution evaporates over a few hours (Nostalgia Electrics, RHD800 Retro Series; or Great Northern Popcorn Company, 4078 GNP Hotdog 7 Roller Machine). Until their experimental use, prepared $NaNO_2$ PFA reaction devices were sealed with Parafilm or vinyl end caps (McMaster-Carr; part no. 40005K14) and kept in a dark box at room temperature.

Teflon-coated aluminum annular denuders (URG-2000- 30x150-3CSS, URG Corporation, Chapel Hill, NC) were also used in some experiments in place of the $NaNO_2$ device (Fig. 2-1). To coat these denuders, 3.0 mL of the $NaNO_2$ coating solution was transferred to the device, followed by capping, inversion, rotation, and shaking to ensure all concentric etched glass surfaces were coated. The excess $NaNO_2$ coating was decanted and the denuder dried with zero air at a flow of 1.0 standard liter per minute (SLPM) for about 10 min at room temperature.

2.2.2 Gas flows

The calibration source, which uses a permeation oven and $NaNO_2$ reaction device to generate HONO, was designed to be cost-effective, lightweight, and robust for use with dry compressed air as the carrier gas (Fig. 2-1). Full technical details of the design rationale and assembly of the custom-built permeation oven can be found in Appendix A (Sects. 2.S1– 2.S2, Figs. 2-S1–2-S5), with only a brief description given below. A NO_x analyzer was used to characterize the output from the HONO source. A single cylinder or zero air generator provided the separate carrier gas flows required for the PD, a humidifier, and a dilution flow.

Carrier gas flow through the permeation oven was provided by a compressed cylinder of zero air or nitrogen (Praxair; Air Ultra Zero, 99.999 %, AI 0.0UZ-K; high-purity nitrogen, 99.998 %, NI 4.8, Toronto, ON), but an in situ zero air generator could also be used (e.g., Aadco Instruments model 747-10, Cleves, OH; used only for dilution flows here), providing 20 psi of pressure to control the flow entering a four-way 1/4 in. (64 mm) Swagelok cross fitting. The zero air flows through two critical orifices setting flows of ~50 sccm (sccm: standard cubic centimeters per minute; Lenox Laser, Glen Arm, MD; SS-4-VCR-2-50) and a mass flow controller (MFC; MKS Instruments, Inc.; M100B00814CS1BV, 10 SLPM, gas; AIR, Kanata, Canada) set to deliver a dilution flow of 1.0 SLPM. A proportional-integral-differential (PID) temperature controller (Omega™; CN 7823, Saint-Eustache, QC, Canada) was used to regulate the temperature of a machined aluminum (Al) block. The first critical orifice connects to the HCl PD channel within the heated Al block, and the second connects to a 25 mL glass impinger (EMD Millipore Corporation, Billerica, MA, USA) containing deionized water at room temperature. The flows are combined and mixed to a resultant relative humidity (RH) of 50 %, which then enters the coated $NaNO_2$ reaction device in the temperature-controlled Al block. The HCl drives the acid displacement reaction in the $NaNO_2$-coated PFA device, releasing HONO into the gas phase. The

flow exits the oven into the dilution flow being delivered to an instrument or experimental system. If operating in cold environments, care should be taken to ensure the 50 % RH exiting the calibration system does not generate condensation in the lines.

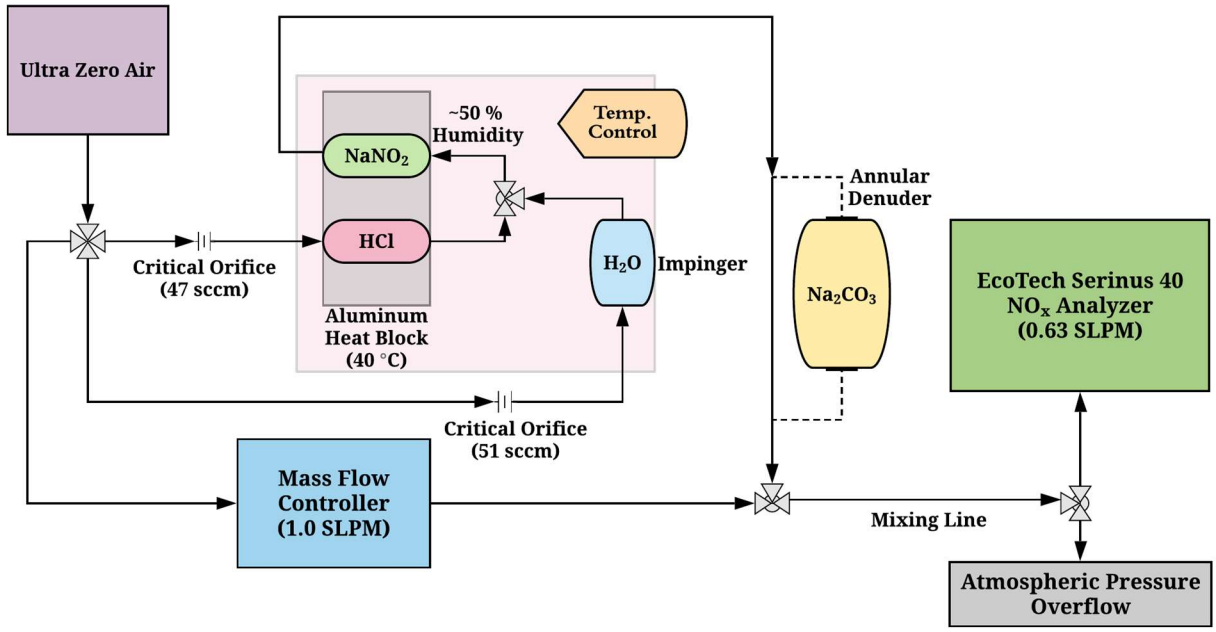

Figure 2-1. Flow and component schematic of the HONO calibration system (pink shaded region) interfaced with a NO_x analyzer (green), dilution mass flow controller (blue), and an exchangeable Na_2CO_3 annular denuder (yellow). Lines with black arrows denote the direction of gas flow through system components. Tee and cross fittings are denoted by arrays of grey triangles.

2.2.3 Custom-built HCl permeation devices (PDs)

Although PDs are available from commercial suppliers, they are custom-made here to reduce costs, as described in detail in Appendix A (Sect. 2.S2, Fig. 2-S5). Briefly, custom PDs are made from PFA tubing (3.2 mm i.d. with 5 mm o.d., part no. 5733K73; McMaster-Carr, Aurora, OH) fitted with PTFE plugs (3.2 mm diameter, part no. 84935K64; McMaster-Carr). A series of HCl PDs were made as aqueous solutions to obtain PDs containing 1.2 and 6 M HCl solutions (OmniTrace®; 34 %–37 %, HX0607-1, Sigma-Aldrich, Oakville, ON; Table 2-1). During operation the HCl PD is placed within the 1/2 in. tubing in the heating block, through which the carrier gas is flushed.

2.2.4 NO_x analyzer for HONO detection

The output from the HONO calibration source was monitored using a commercial chemiluminescent NO_x analyzer fitted with a Mo catalytic converter, set to 325 °C (Serinus 40, American Ecotech, Warren, RI). The conversion efficiency of NO_2 to NO was calculated by combining known concentrations of NO from a standard cylinder (Praxair; NI NO5MC-A3, 4.88 (± 5 %) ppmv, Toronto, ON) and O_3 using a gas calibration instrument (Gascal 1100TS, American Ecotech, Warren, RI). The conversion efficiency was determined according to the manufacturer specifications at 98.84 (± 0.38 %) for NO_2 mixing ratios delivered to the system spanning 100 to 400 ppbv. While the Mo catalyst is meant to convert NO_2 to NO for detection by the analyzer, it is well known that HONO is also quantitatively converted to NO (Febo et al., 1995), and the conversion efficiency was determined experimentally (Sect. 2.2.6). A NO_x analyzer was preferred to other independent calibration methods such as ion chromatography with conductivity detection (IC-CD), as it is capable of continuous real-time measurement of HONO, allowing rapid frequent checks on the calibration source output stability.

During experiments, ~100 sccm from the HONO source was diluted into an additional 1.0 SLPM of zero air from which the NO_x instrument sampled 0.63 SLPM (Fig. 2-1). The NO_x analyzer measured NO on either the NO or NO_x channels for an averaging period of 1 min with the Kalman filter set to 60 or 300 s. To correct for instrument drift or NO_x contamination in the zero air, the analyzer was flushed for at least 15 min at the beginning and end of each experiment. An annular denuder coated with 20 g L^{-1} sodium carbonate in 50:50 methanol and water solution (Na_2CO_3; ACS reagent > 99.7%; Sigma-Aldrich, St. Louis, MO) – similar to that used here for $NaNO_2$ – was inserted during some experiments to scrub HONO from the experimental flow (Fig. 2-1). The denuder was prepared by transferring 10 mL of Na_2CO_3-coating solution, capping, and then inverting and rotating to distribute the solution evenly. The remainder of the coating solution was decanted and the denuder surfaces dried under a flow of 1.0 SLPM of zero air until completely dry (~10 min). The denuder was inserted into experimental flows for at least 1 h as a second check on sources of background NO and NO_2 as impurities being emitted from the calibration source or carrier gas. A Na_2CO_3 denuder can also be used as a robust alternative to provide the NO_x analyzer inlet overflow instead of a cylinder of zero air. This enables corrections of HONO measurements or calibrations for NO_x present in the sample air or calibration source carrier gas, respectively.

2.2.5 Conversion efficiency of the NO_x analyzer Mo catalyst for HONO

A Mo catalyst at 325 °C will reduce HONO to NO, though reports have shown that this conversion may vary between NO_x analyzers (McGrath et al., 2019; Zhou et al., 2018). We measured the HONO generated by the calibration source with the NO_x analyzer and then directed the HONO to a scrubbing solution of 1 mM NaOH in two glass impingers connected in series for several hours to days to collect NO_2^- to a level that could be quantified by IC-CD. The second bubbler was used to determine the extent that HONO was quantitatively collected in the first bubbler (i.e., to capture any breakthrough). The HONO generated by the calibration source and quantified by IC was compared to the NO_x analyzer measurement, using the introduction of a Na_2CO_3 annular denuder to perform background correction. The HONO conversion efficiency determined by comparison to the IC was found to be 104 ± 4 % (n = 3), confirming unit conversion efficiency, with the associated error set by the 4 % accuracy of the IC-CD method for NO_2^- ($R^2 > 0.999$) when employing our previously developed separation method (Place et al., 2018). The IC precision near the analyzed concentrations for NO_2^- was measured to be 3 %. All data presented in this paper therefore use a conversion efficiency of unity for the Mo catalyst.

2.2.6 Supporting instrumentation

In our mass balance experiments for the production mechanisms governing HONO generation in the calibration system, we used two additional tools to monitor experimental gas flows. Mixing ratios of HCl were measured at 0.5 Hz using a cavity ring-down spectrometer (CRDS) (G2108 HCl gas concentration analyzer, Picarro, Santa Clara, CA) with a 5 pptv detection limit for 1 min averaged data. Further details on the performance of this instrumentation can be found in Dawe et al. (2019). Measurements of HCl and HONO to investigate acid displacement efficiency of the calibration system were performed at 2 Hz using a quadrupole chemical ionization mass spectrometer (CIMS, THS Instruments LLC, Atlanta, GA) using acetate reagent ions to facilitate proton transfer and detection of negative ions at m/z 35 and 46, respectively. Observed ions were normalized to the detected quantity of the acetate reagent ion and multiplied by 8×10^5, resulting in signal units of normalized counts, as we have previously reported for the detection of these analytes (VandenBoer et al., 2013). The signal from the CIMS was averaged to a 1 min time base to compare to other measurements.

In our purity and stability experiments, additional instrumentation was used to detect HONO, NO_y, and other reactive gases. A time-of-flight (ToF) chemical ionization mass spectrometer utilizing iodide adduct reagent ions (I^- ToF CIMS; Aerodyne Research Inc., Billerica, MA) was used to measure HONO and detect a wide array of other analytes (e.g., $ClNO_2$, HNO_3, N_2O_5, etc.) in experimental gas flows. Specific operational details of the I^- ToF CIMS for these atmospheric species are presented elsewhere (Neuman et al., 2016; Veres et al., 2020). A broadband cavity-enhanced absorption spectrometer (ACES) was used to measure HONO and NO_2 (Min et al., 2016), and a single-photon laserinduced fluorescence (LIF) instrument was used to measure NO (Rollins et al., 2020). A high-sensitivity chemiluminescent NO instrument fitted with a gold catalyst (NO_yO_3) was used to quantify NO and NO_y (Fahey et al., 1985; Fontijn et al., 1970; Ridley and Grahek, 1990; Ridley and Howlett, 1974; Ryerson et al., 1999).

2.3 HONO calibration source characterization

2.3.1 $NaNO_2$-coated reaction device

Previous calibration methods required a 1–2 g bed of loose crystalline $NaNO_2$ to generate high mixing ratios of HONO but only consumed a minimal amount of $NaNO_2$ from the total supply before being thrown away (Febo et al., 1995; Roberts et al., 2010). At maximum, our $NaNO_2$-coated PFA reaction devices could contain up to 60 mg of $NaNO_2$ (3.0 mL × 20 g L^{-1} $NaNO_2$ coating solution) or 40 mg of NO_2^- if there was 100 % coating efficiency. Due to the hydrophobic nature of PFA and the loss of liquid solution from the drying procedure, however, the reaction device retained only a fraction of the applied $NaNO_2$. The amount of NO_2^- present after coating the PFA devices (n = 3) was determined by rinsing with deionized water and analysis by IC-CD. An average mass of 0.53 ± 0.27 mg NO_2^- was deposited on the surface of the PFA device – 1.3 % of the total NO_2^- applied. The quantity coated on the PFA devices was sufficient to generate stable, low mixing ratios of HONO for extended periods. To efficiently use most of the salt, we calculated how long the $NaNO_2$ coating could provide a specific calibration mixing ratio of HONO (Eq. 1). Thus, we designed and operated our coated devices based on their calculated capacity to generate a specific mixing ratio of HONO (C_{HONO}) continuously over time based on the number of moles of $NaNO_2$ deposited in the coating (n_{NaNO2}) and the total dilution flow in moles of air for that same duration (F_{air}).

$$C_{HONO} = n_{NaNO2} / F_{air} \quad (1)$$

To generate higher mixing ratios of HONO, more $NaNO_2$ mass and/or coated surface area are required. The higher surface area of a coated glass annular denuder housed in Teflon-coated aluminum tubing was explored for use as an alternative to PFA tubing. To test this, three annular denuders were prepared using the same volume of coating solution. An average mass of 7.26 ± 1.80 mg of $NaNO_2$ on the denuder surface was determined – 18 % of the total applied. Thus, the coated annular denuder resulted in about 18 times more deposited $NaNO_2$ than the PFA devices, due to the higher available surface area of pattern-etched glass. Unfortunately, these devices proved unstable, as discussed below, and are expensive. The HONO output from other tubing materials was also tested (Sect. 2.3.7.2).

The lifetime of the $NaNO_2$ devices can be approximated using Eq. (1), under the assumption that a stable output of HONO is generated from the start of the experiment. At standard room temperature and pressure, a device generating 2 ppbv of HONO and containing the average 0.53 mg of NO_2^- observed for the PFA device could last for up to 88 d. In practice, we observed a PFA device generating approximately 2 ppbv min^{-1} of HONO to be reliable for over 4 weeks during experiments performed to test the stability and reproducibility of the PFA devices (Sect. 2.3.5, 2.3.6). The lifetime of the device is expected to decrease proportionally if a higher output of HONO for a given mass of $NaNO_2$ coating is required. Decreasing HONO mixing ratios on the order of a hundred pptv on hourly timescales (for an initial few ppbv of output) was used as a metric to indicate that coated reaction devices were depleted since their output was no longer stable.

2.3.2 HONO generation with water vapor

Prior calibration sources have exclusively reported HONO production via the acid displacement mechanism. In the mass balance experiments reported below, where we employ this mechanism, it was discovered that water vapor alone was responsible for a measurable amount of the generated HONO in the ppbv regime. Mixing ratios of HONO produced using our coated PFA reaction devices exposed to water vapor were too low to accurately measure using our NO_x analyzer (≤ 0.6 ppbv). To explore the influence of water vapor (i.e., humid air) on HONO output, we performed a series of experiments at different RH using an $NaNO_2$-coated annular denuder. The denuder generated higher HONO mixing ratios, on the order of several ppbv in 1.1 SLPM. Prior to the experiments, the calibration source unit was flushed with zero air for at least 12 h. The absence of HCl (< 5 pptv) was confirmed with the CRDS. When the RH passing through the denuder was 0

% we observed no HONO, with signal near the detection limit of the NO_x analyzer (0.50 ± 0.48 ppbv, n = 43). When we increased the RH of the carrier gas, we observed the production of HONO, but the variation was not monotonic. At a RH of 25 % HONO output increased to 11.73 ± 0.39 ppbv (n = 35) followed by a decrease at an RH of 50 % to 8.60 ± 0.63 ppbv (n = 38). This trend is likely due to the effective Henry law constant of HONO in the aqueous film on the surface of the $NaNO_2$ device, due to the weak acid nature of HONO (pKa = 3.4). When the humidity is higher, less HONO may be released from the surface due to the increased presence of water in which a larger equilibrium concentration of aqueous nitrite can be sustained. This contrasts with HCl (pK_a of -8), which completely dissociates in aqueous solution on the surface of the $NaNO_2$ device and facilitates the acid displacement mechanism (Reaction R2).

This is the first observation of water-vapor-produced HONO. Prior calibration sources typically generated very high HONO mixing ratios from 100 ppbv up to tens of ppmv in the displacement vessel, resulting in the contribution from humid air being undetected (Febo et al., 1995; Gingerysty and Osthoff, 2020; McGrath et al., 2019; Roberts et al., 2010; VandenBoer et al., 2015; Zhou et al., 2018). The observed HONO mixing ratios from this mechanism in our experiments would likely be within the error of the mass balance calculations or indistinguishable from noise in the analytical instrumentation in prior reports. Our results suggest that the use of water vapor passed over a $NaNO_2$-coated PFA reaction device produces sub-ppbv mixing ratios of HONO for calibration of instruments making ambient observations in remote environments. Using water vapor alone, the only way to increase the HONO mixing ratios from the calibration system is to increase the available amount of $NaNO_2$, which is challenging (Sect. 2.3.1 and 2.3.7.2). A more controlled approach to reach higher mixing ratios is through the acid displacement technique.

2.3.3 HCl emissions from custom-built PDs

To generate stable HONO mixing ratios using an $NaNO_2$ reaction device on the order of a few to tens of ppbv, a stable source of HCl is required. The HCl generated from custom-made PDs was therefore evaluated as a function of solution concentration contained (1.2–6 M), temperature (30–60 °C), and stability by CRDS (Table 2-1, Fig. 2-S6). Custom-made PDs of different concentration and lengths were tested for their ability to produce a range of HONO mixing ratios. Custom-made PDs have been previously demonstrated in our work to provide a stable emission source of HCl (MacInnis et al., 2016). The HCl output was found to be temperature dependent and increased

exponentially with temperature, as expected from theory (Sect. 2.S2). However, as the PD was ramped to higher temperatures (>50 °C) the permeation rate became more unstable, with a resulting settling time of about 1 h as the materials from the permeation oven apparatus re-equilibrated (Fig. 2.S7). Since the HCl PDs were observed to be most stable at 30 and 40 °C, these temperatures were considered optimal to generate the stable HONO mixing ratios. Note that the HONO mixing ratios in the 100 sccm flow exiting the reaction device range from 9.7 to 72 ppbv (Table 2-1), which are much lower than all prior calibration sources, enabling easy dilution to reach environmentally relevant HONO mixing ratios for instrument calibration or experimental applications.

Table 2-1. Description of custom-made HCl permeation devices used to generate HONO. Zero air-corrected mixing ratios of emitted HCl and generated HONO using a single $NaNO_2$-coated PFA reaction device were measured with the heated Al-block at 40 °C in 1.1. SLPM. The variability reported for each observation represents one standard deviation from the mean (n = 30 to 60 using 1-minute averaged data).

PD	HCl (M)	Date of Manufacture (YYYY/MM)	PFA Device (cm)	PTFE Plug (cm)	HCl (ppbv)	HONO (ppbv)	Measured Date (YYYY/MM)
PD-1	1.2	2017/04	9.92	0.60	0.58 ± 0.01	0.95 ± 0.51	2019/10
PD-6a	6	2017/04	9.41	0.70	0.21 ± 0.01	0.88 ± 0.4	2019/10
PD-6b	6	2019/04	9.11	0.75	2.0 ± 0.01	2.8 ± 0.4	2019/11
PD-6c	6	2019/04	9.65	0.70	5.0 ± 0.3	6.2 ± 0.5	2019/11

Two newly made 6 M HCl PDs (PD-6b and PD-6c) were found to emit different, yet highly stable (e.g., ± 0.01 ppbv), mixing ratios at identical oven temperatures (Fig. 2.S6). This demonstrates potential variability with each new device due to inconsistent results during custom fabrication compared to commercial PDs. The most likely source of such differences in output is variability in our sealing of the PTFE plugs resulting in increased emission rates. In any case, the PDs remain stable with less than 10 % relative standard deviation. In comparison, commercial-device emission rates are often certified within ± 30 %. The emission rates of commercial PDs are certified through measurement by gravimetric weight loss over time (ng min^{-1}). A commercial 1/4 in. (64 mm) Teflon HCl PDs of 6.55 M, certified to emit 1905 ± 520 ppbv in 100 sccm flow at 40 °C (relative standard deviation, RSD = 27.3 %; VICI Metronics, Inc.; Poulsbo, WA), has this output variance due to the coemission of water and propagated measurement uncertainties. A lower variance in the

emitted HCl was observed from our custom-made PDs when we quantified HCl directly by either CRDS or IC-CD. Custom-built PDs were therefore chosen over commercial PDs due to their demonstrated stability and low cost. It was found that HCl outputs of the custom-PDs slowly diminished over time, which emphasizes the need for regular calibrations. For example, the HCl output from 2-year-old PD-6a emitted 0.21 ± 0.01 ppbv in 1.1 SLPM in comparison to 2.0 ± 0.01 ppbv when it was newly made, which decreased the resulting HONO generation in the reaction device. Similar results have been observed in calibrations with PDs of aqueous NH_3 and HNO_3 solutions decreasing by ~30 % during 2 years of storage, as well as for carbonyl sulfide (Fried et al., 1998; Neuman et al., 2003). Despite the decreasing HCl output over a year or more of use, HCl PDs act as a stable acid source on the order of weeks, producing consistent HCl output to subsequently generate stable HONO, even when removed from the permeation oven or stored for up to 2 months. Overall, it is difficult to replicate PD emission rates using the same HCl concentration and material dimensions for a custom-made PD. The custom-built PD seals can be altered by replacing the PTFE plug by crimping the ends of heated-to-pliability PFA tubing to form welded polymer ends (Sect. 2.S2). Such an approach is expected to improve the reproducibility of the custom-device emission rates but is beyond the scope of this work to explore in more detail.

2.3.4 Acid displacement to generate HONO

Two techniques were used to assess the reaction completion between HCl and $NaNO_2$ in the calibration system. We applied a mass balance approach that combined the CRDS measurement of HCl, our NO_x analyzer HONO measurement, and IC-CD quantitation of these acids scrubbed into 1 mM NaOH. The displacement efficiency was further confirmed by simultaneous observation of HCl and HONO by acetate quadrupole CIMS.

2.3.4.1 Mass balance of HONO generated

Experiments were conducted to confirm that HONO can be generated by introducing only humid air (50 % RH) within the $NaNO_2$ devices without the presence of HCl. In humid air, we observed HONO levels above the detection limit (DL) of the NO_x analyzer. A single PFA device exposed to humid air (50 % RH) released up to 0.61 ppbv of HONO – equivalent to 77 % of the total HONO generated when coupled with an HCl PD (Table 2-2). The reaction of the humidified $NaNO_2$-coated device, resulting in the release of HONO, implies formation of NaOH. Further speculation

on the reaction mechanism is beyond the scope of this work. Given the existing challenge in producing low mixing ratios of HONO in the pptv range, it appears that these can be reached most easily without the use of an HCl PD in our calibration system, while higher mixing ratios necessitate the addition of HCl (Sect. 2.3.7). The NO_x analyzer signal was indistinguishable from zero when the $NaNO_2$ reaction device was absent, but all other conditions were matched. This demonstrates that HONO was generated only within the $NaNO_2$ reaction device.

The total flow for all mass balance experiments was 1.1 SLPM (Fig. 2-1) with zero air flows replacing those typically carrying reagents when they were removed. We observed that the HONO output from the reaction devices was greater than the HCl input from the PDs, confirming that another chemical reaction was generating the remaining HONO (Table 2-2). Mass balance could only be achieved when accounting for the HONO generated by the $NaNO_2$ exposed to humid air (~ 50 % RH). No other acidic or ionic contaminants were present in $NaNO_2$ reaction devices or the HCl PDs when scrubbed solutions were analyzed by IC-CD. Therefore, other NO_y species that could have biased the NO_x analyzer measurement high were judged to be absent, and pure HONO was generated (i.e., only NO_2^- was enhanced in calibration system flows scrubbed into 1 mM NaOH). Further investigation of the system HONO purity is presented in Sect. 2.3.7.3, which further supports this conclusion. The remainder of the HONO output from $NaNO_2$ devices quantitatively matched the HCl input to the reaction device in dry air after accounting for the water vapor production route. No HCl was observed to exit the devices, indicating unit acid displacement efficiency and reaching mass balance.

Table 2-2. Mass balance of measured mixing ratios of HCl entering and HONO exiting the calibration source to determine acid displacement efficiency (ADE) at 50 % RH and 40 °C. Uncertainties represent 1σ standard deviation from the mean for ≥30 minutes of measurements and 1σ propagated error for calculated values.

PD	HCl_{IN} (ppbv)	HONO from HCl+H_2O (ppbv)	HONO from H_2O (ppbv)	HONO from H_2O (%)	ADE (%)
PD-6a	0.08 ± 0.002	0.31 ± 0.15	0.24 ± 0.14	77 ± 45	>99
PD-6b	2.2 ± 0.011	2.78 ± 0.41	0.61 ± 0.44	22 ± 16	>99

2.3.4.2 CIMS measurement

Confirmation of these observations with the quadrupole CIMS provided higher time resolution observations of HONO and HCl simultaneously. The ions monitored were m/z 35 (Cl^-) for HCl and 46 (NO_2^-) for HONO (Fig. 2-2). The instrumental sensitivity to these two analytes is similar under this ionization scheme (VandenBoer et al., 2013). The HONO calibration source was stabilized for 2 h before the gas stream was introduced to the CIMS. Zero measurements were taken for 15 min before and after the measurements to correct for background drift in the m/z 46 signal. Upon sampling the output of the HONO calibration source the signal at m/z 46 rapidly increased (Fig. 2-2). The signal of Cl^- at m/z 35 was below the detection limit throughout this period, confirming again that the HCl from the PD was entirely consumed by the $NaNO_2$ reaction device throughout the measurement period, consistent with the experiments presented above where no HCl was measured by the CRDS. Overall, the results from these assessments indicate that the HONO calibration source is generating HONO with a one-to one displacement efficiency by HCl, consistent with this observation from other HONO calibration sources using higher quantities of HCl in a salt bed (Febo et al., 1995; Roberts et al., 2010), and the remainder originating from the water vapor reaction.

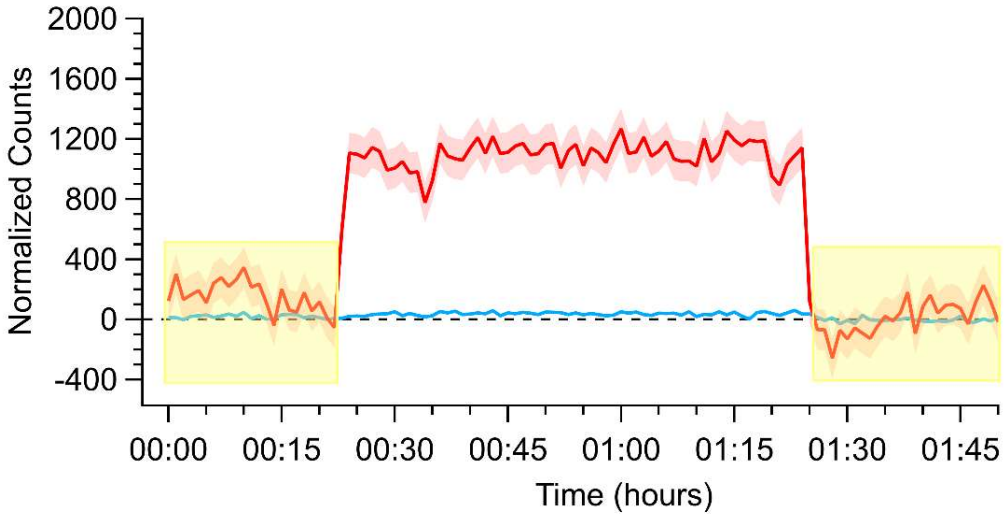

Figure 2-2. Conversion efficiency of HCl (blue) to HONO (red) via the acid displacement reaction on a $NaNO_2$ reaction device. The HCl PD-6a and one coated PFA device were used and measured following two hours of stabilization. The acids were observed by acetate quadrupole CIMS with time resolution of 0.50 s and averaged to 60 s. Yellow shaded regions indicate the addition of zero air to the instrument inlet for background correction, while red and blue shaded regions correspond to 1σ variance in the observations.

2.3.5 Stability of HONO production

The time required to achieve stable HONO signals was tested by inserting HCl PD-6a and the new $NaNO_2$ PFA reaction device into the calibration system, followed by flow start-up. Stable HONO signals were observed within 7 h of powering on the HONO calibration system. This is 5 h longer than required to reach stable mixing ratios for a previously stabilized $NaNO_2$ device. Three trials using newly coated $NaNO_2$ reaction devices and PD-6a, once stabilized, generated an average HONO output of 2.28 ± 0.58 ppbv, which corresponds to an RSD of 24 % between runs and a relative standard error (RSE) of 3 % (n = 2367; Fig. 2-3). The noise observed in the stabilized HONO output in Fig. 2-3 can be primarily attributed to the noise associated with the NO_x analyzer detector (18 of the 24 %; DL = 0.4 ppbv; 1 min average). This conclusion is supported by the lower noise in ~2.5 ppbv HONO mixing ratios observed by the CIMS (Fig. 2-2, RSD of 8.1 %), ACES (RSD 8.2 %), and NO_yO_3 (RSD 1.9 %). In these added observations with higher sensitivity instrumentation, the stability was equal to instrumental precision. This represents a major improvement over our previously reported calibration sources with potential for 30 % variability at a minimum (VandenBoer et al., 2013; Zhou et al., 2018).

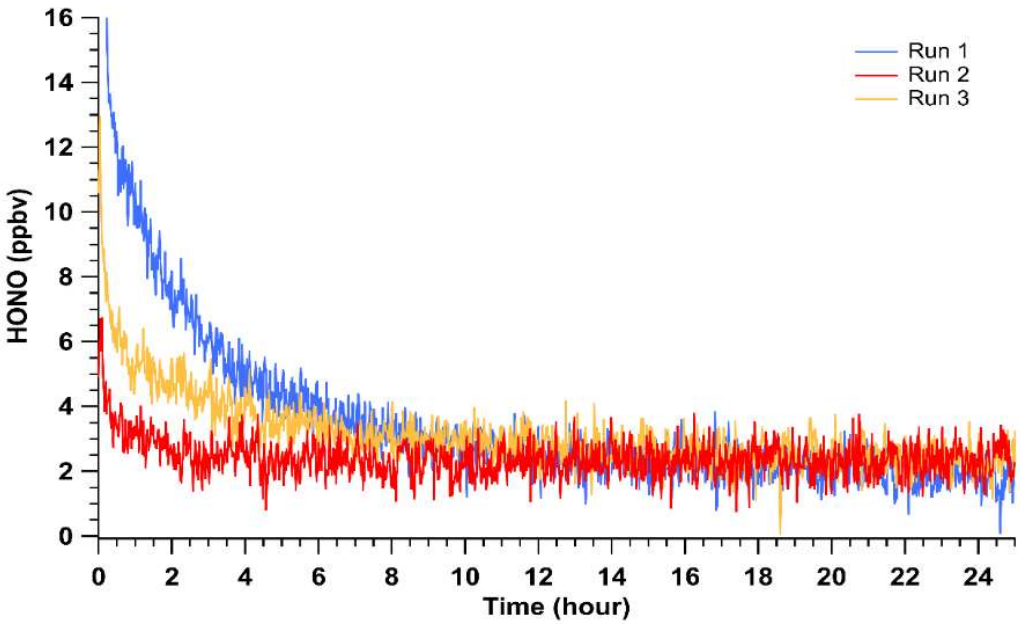

Figure 2-3. Mixing ratios of HONO observed using HCl PD-6a and three different, but freshly coated, $NaNO_2$ PFA reaction devices. Time zero indicates the start of HONO production in the calibration unit where no prior flow through the calibration unit existed, but all temperatures were stable at 40 °C. Reported measurements are one-minute average data with a 30 s Kalman filter on the NO_x analyzer.

However, when the HCl output from PDs is unstable, this can interfere with the stability of the HONO generated because it is dependent on acid displacement. A common characteristic of our custom-made PDs monitored by real-time CRDS measurements is short-duration increases in output over minutes up to 1 h, due to reduced emission of H_2O and increased emission of HCl, resulting in transient pulses from the device (Fig. 2-4a). The anticorrelation between HCl and H_2O is expected for a constant mass emission to result from the contained aqueous solution. A corresponding rapid increase in HONO production results from such occurrences (Fig. 2-4b).

Commercial PD manufacturers evaluate average mass emission rates by gravimetric weight loss over several weeks at 40 °C for certification, which could include such short-term events. The HONO output from a newly made custom-made HCl PD (PD-6c) over four consecutive observation periods upon insertion of a new $NaNO_2$ reaction device (Runs 1–4) at constant temperature (40 °C) shows that the new custom-made PD requires about 1 week of operation before its output is stable (Fig. 2-4b–c). Therefore, careful preparation of PDs and $NaNO_2$ reaction devices in advance of extensive use will yield a HONO calibration source with the fastest stabilization times possible for continuous operation over a period of months. Note again that the HONO measurements for Fig. 2-4b–c were performed several months before the HCl emission rates for PD-6c presented in Table 2-1 were obtained, resulting in high HONO mixing ratios produced in these experiments.

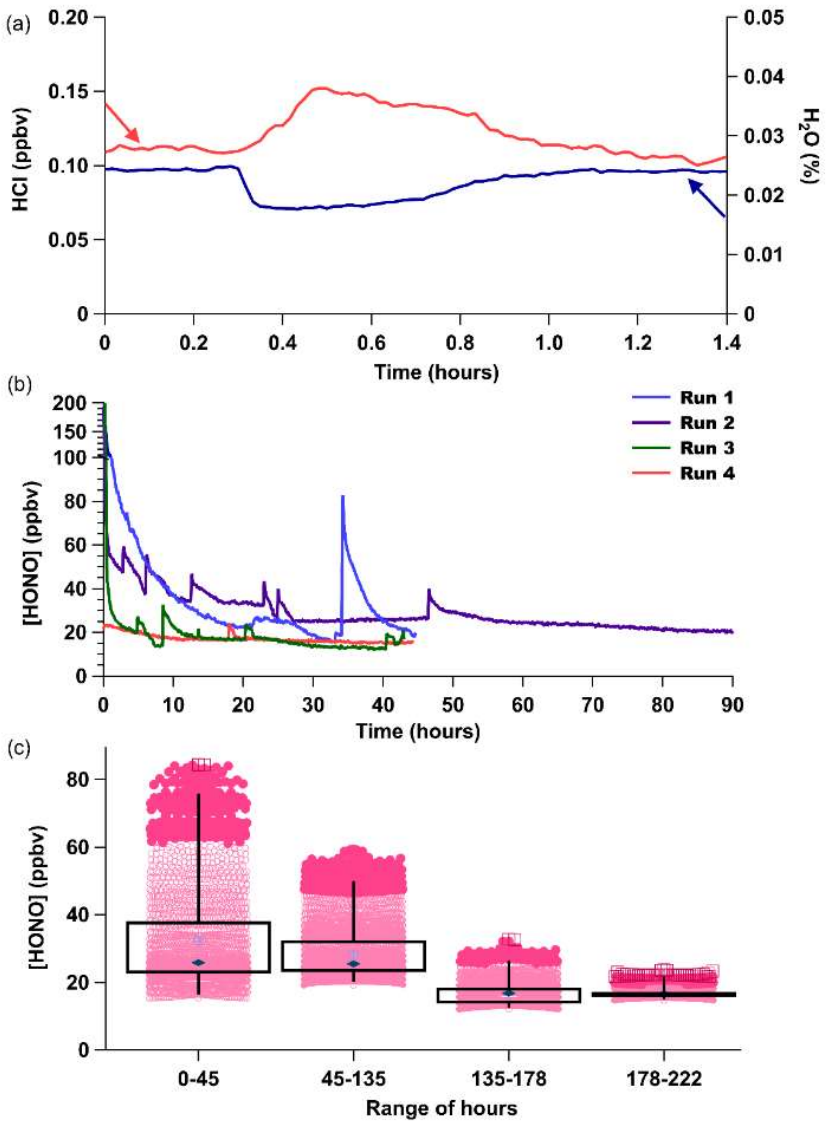

Figure 2-4. (a) CRDS high-resolution observation an HCl emission *burp* (red) and H_2O decrease (blue) from PD-6a resulting in 50 % increase of the HCl mixing ratio emitted. (b) Time series of four consecutive measurement periods of HONO production, using only PD-6c and a new $NaNO_2$ coated reaction device in each run. (c) Box (1st and 3rd quartile) and whiskers (3σ from the mean) of HONO mixing ratios observed for the four runs are binned by duration of use for each new reaction device in hours. Mean values are indicated with a filled dark blue diamond marker, median values by the light blue crossed box marker, dark pink circles are 2σ outliers and dark red squares 3σ outliers.

2.3.6 Reproducibility and robustness

The HONO calibration system was designed to not only be stable, but also reproducible in its output of HONO for a given PD and any $NaNO_2$ reaction device, resulting in robust portability. We tested the reproducibility, and therefore robustness, of the HONO calibration system by putting

it through a series of experiments designed to simulate transport to, and use in, the field. Further assessments of its reproducibility by measuring the output with different $NaNO_2$ reaction devices and HCl PDs were also made.

2.3.6.1 Field transport simulations

Simulations of field transportation subjected the system to full disassembly and reassembly of the acid displacement and permeation oven setup. In addition, for some experiments the calibration unit was transported on a lab cart over very rough flooring to simulate vibrations experienced for real use when transported using rolling carts, mobile labs, or aircraft. For the first eight simulations PD-6a and one $NaNO_2$-coated reaction device were used over several weeks (see Table 2-S1 for further detail). Following reassembly after the field transport simulations, the HONO calibration source was restarted, the system was equilibrated for 2 h, and then its output was measured by the NO_x analyzer (Fig. 2-5). An Na_2CO_3-coated annular denuder was incorporated into the middle of five of the eight trial experiments for 1 h to determine whether any NO_x was being generated between restarts and its associated variability (FS1–FS5; Table 2-S1). No measurable NO_x was detected in any of these experiments.

The average HONO mixing ratio within the eight field transport simulations (FS) ranged from 1.68 to 2.51 ppbv. The HONO output across all eight field simulations had an average of 2.07 ± 0.48 ppbv (RSD = 24 %; RSE = 2 %, n = 218). These measurements used a single $NaNO_2$ reaction device over 5 weeks of continuous operation, after which the depletion of $NaNO_2$ resulted in a decline of HONO mixing ratios. These HONO mixing ratios are similar to the average HONO output of 2.28 ± 0.58 ppbv (RSD of 24 %, RSE of 3 %, n = 2367) from the previous measurements with PD6a (Fig. 2-3), which were not subject to field simulations but did use freshly coated $NaNO_2$ reaction devices. The generated HONO mixing ratios varied most between our early experiments (FS1–FS4; RSD ≥ 24 %), when first gaining experience in ensuring gas-tight connections throughout the calibration system, with improvement clearly emerging over time (FS4–FS8; RSD ≤ 10 %). The RSE values of field transport simulations had a lower RSE of 1 % compared to 3 % for the experiments that were stationary (Fig. 2-5), likely due to the reuse of the same $NaNO_2$ reaction device. This demonstrates that the HONO calibration source can robustly generate a reproducible mixing ratio output within 25 % of the mean during each system reconstruction if the same HCl PD is used. It is worth noting here again that most of the variance observed in HONO

mixing ratio output within any of the presented trials derives from the precision of our NO_x analyzer detector (Sect. 2.3.5).

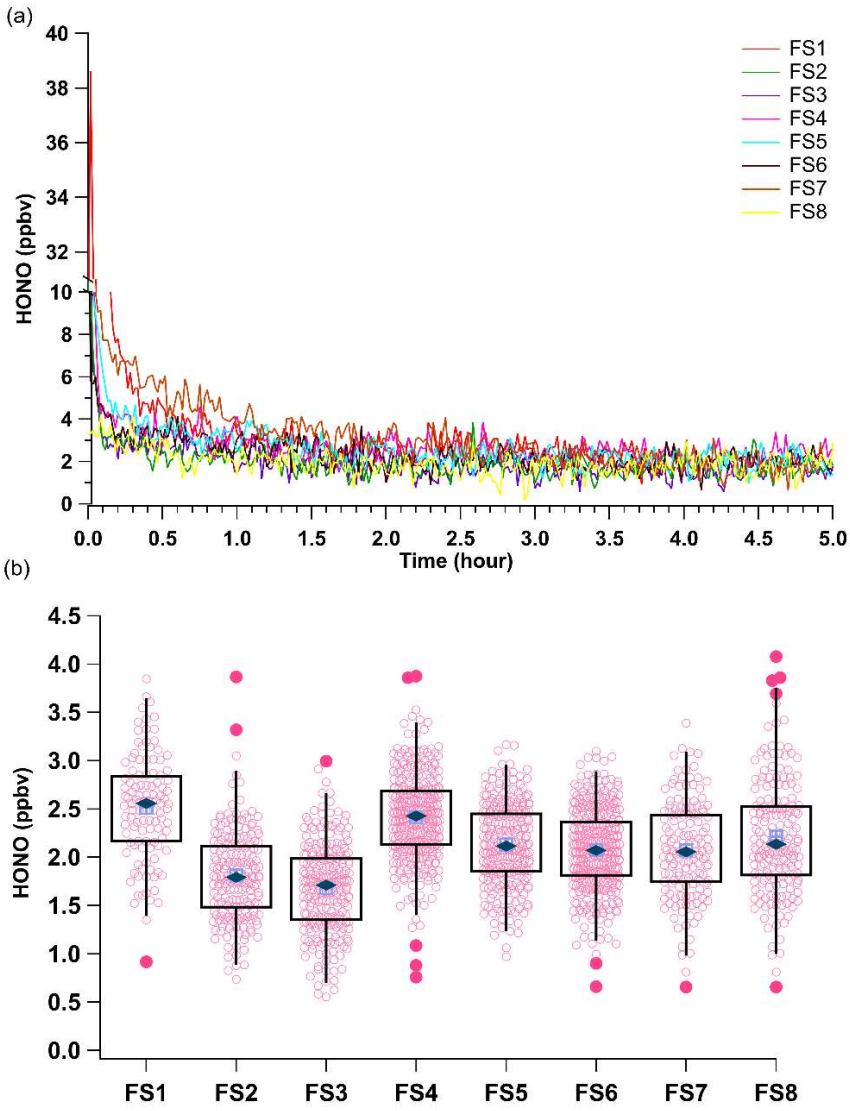

Figure 2-5. (a) Mixing ratios of HONO for the eight field transport simulations (Table 2-S1). All observations were background corrected by linear interpolation across the experiments using zero air before and after HONO observations and an Na_2CO_3 coated annular during (Fig. 2-S4). (b) Box and whiskers plot of the HONO output using measurements collected after two hours of calibration source stabilization. The light blue crossed box represents the median, the dark blue diamond the mean, light pink circles the data points, dark pink circles the 3σ outliers, and the black box the 1st and 3rd quartiles of observed HONO mixing ratios. The whiskers denote the 3σ standard deviation.

2.3.6.2 Factors acting reproducibility of HCl input

As shown in Table 1, PDs made with the same HCl concentration (6 M) and similar dimensions did not lead to the same HONO output, due to variability in the HCl emission rates. While it is possible for custom-made PDs to have similar HCl emissions and therefore HONO output (when using the same $NaNO_2$ device), it is difficult to achieve in practice. When making a new PD as per the methods described in Sect. 2.S2, it can be difficult to replicate because the emission rate depends on the effectiveness of the plug seal. For this reason, one cannot simply make a HCl PD with plugs using the same concentration and material dimensions and necessarily expect the same output. We present an alternative Teflon welding method to overcome this limitation in Sect. 2.S2, which has been successfully used for generation of VOC PDs. Regardless, the output of new HCl PDs should be quantified prior to use and not subject to extreme conditions to ensure the polymer permeability is retained.

The reproducibility of HONO output using a stable HCl PD is shown in Fig. 2-5. The observed HONO output ranged from 1.68 to 2.51 ppbv (n = 8, RSD = 24 %). We next tested the reproducibility for newly made HCl PDs. Two experiments used PD-6b, containing 6 M HCl (Fig. 2-S10). After a period of stabilization, the two experiments generated similar HONO mixing ratios (2.58 ± 0.43 ppbv after 25 h, RSD = 16.5 %, RSE = 1.43 %, n = 792). The spikes in HONO output at 15 and 21 h in the second experiment (green trace, Fig. 2-S10) were likely due to pulses of HCl, which we commonly observed with new PDs (e.g., Fig. 2-4a–b). This emphasizes our recommendation that new custom-made HCl PDs should be used for an extended period prior to use for acid displacement to ensure the emission rate has stabilized.

We made another PD with 1.2 M HCl, as it emits less HCl in comparison to a PD made with 6 M HCl (Table 2-1), to determine the reproducibility in HONO output at lower mixing ratios. Across three experiments using a previously stabilized $NaNO_2$ device, an output of 0.69–1.12 ppbv (RSD = 53.7 %, RSE = 4.52 %, n = 143) was observed (Fig. 2-S11). The high RSD is due to instrument noise as the HONO output approached the detection limit of the NO_x analyzer (0.4 ppbv). Nonetheless, a stable output of HONO was achieved within 2 h after starting the calibration system, similar to our previous results (Fig. 2-5). As long as a new custom-made HCl PD has been allowed adequate time to stabilize under a gas flow at constant temperature (ideally 7 d), a stable HONO output can be easily replicated within 2 h of starting the resulting HONO calibration

system. We recommend quantifying the HCl emissions prior to use if the PD has been stored for a long period or been subjected to extreme conditions.

2.3.7 Adjusting and controlling HONO mixing ratios

Increasing the mixing ratio of HCl and the type and quantity of $NaNO_2$ reaction devices connected in series were explored as methods to adjust the HONO mixing ratio exiting the calibration system.

2.3.7.1 Temperature control

The HONO calibration system was designed to be tunable by adjusting the oven temperature. HCl emissions increased with increasing temperatures (30–60 °C, Fig. 2-S6). The HONO mixing ratios increased exponentially with increasing oven temperatures (Table 2-3 and Fig. 2-S12). Very low levels of HCl exited the $NaNO_2$ device (≤ 3 % of HCl input), which demonstrated that there was continued near-unity acid displacement efficiency. With increasing temperature of the $NaNO_2$ reaction device in the presence of water vapor, a similar increase in HONO mixing ratio was observed, roughly doubling for every increase of 10 °C. Thus, the HONO mixing ratio output can be adjusted by changing the temperature of the Al block with either water vapor alone or in combination with an HCl PD. Part of the observed variability in HONO emissions at 50 °C was contributed by the increasingly unstable emissions of HCl at this temperature (e.g., see Fig. 2-S6). The use of multiple HCl permeation tubes in a single oven, in series, or in parallel are additional options to control the HONO mixing ratio generated in the calibration system. as the PFA devices (Sect. 2.2.1) to see if there was an improvement in output stability or increased emissions of HONO. The materials used were all cylindrical tubing with 1/2 in. (1.27 cm) inner diameters and were of similar lengths and surface area. The different materials that were tested showed similar HONO outputs (within variability), except for quartz (Table 4). The quartz tubing gave a notably lower HONO output compared to other materials. This may have been due to a poor coating efficiency on the surface, as observed visually when making this device. This is an unexpected outcome given that quartz is more hydrophilic than PFA. That we observed similar HONO outputs for the other materials could be due to the devices having the same internal surface area coated with $NaNO_2$, implying that HONO output is proportional to surface-available $NaNO_2$. The inside of a PFA device was etched manually every few millimeters in concentric circles in an attempt to increase the surface availability of $NaNO_2$, but no change in HONO output was observed compared to the unetched device

Table 2-3. Average mixing ratios of HCl input (PD-6a), and HONO emitted from reaction with water vapor and with both reagents as function of temperature. Uncertainty denotes 1σ standard deviation from the mean of measured values.

Temperature (°C)	HCl (ppbv)	HONO from H_2O (ppbv)	Total HONO (ppbv)
30	0.230 ± 0.003	0.3	0.5 ± 0.4
40	0.330 ± 0.007	0.7	1.0 ± 0.5
50	0.660 ± 0.037	1.3	2.0 ± 0.5

2.3.7.2 HONO output with different types of $NaNO_2$-coated devices

The produced HONO mixing ratios were tested using different materials coated with $NaNO_2$ via the same methodology as the PFA devices (Sect. 2.2.1) to see if there was an improvement in output stability or increased emissions of HONO. The materials used were all cylindrical tubing with 1/2 in. (1.27 cm) inner diameters and were of similar lengths and surface area. The different materials that were tested showed similar HONO outputs (within variability), except for quartz (Table 2-4). The quartz tubing gave a notably lower HONO output compared to other materials. This may have been due to a poor coating efficiency on the surface, as observed visually when making this device. This is an unexpected outcome given that quartz is more hydrophilic than PFA. That we observed similar HONO outputs for the other materials could be due to the devices having the same internal surface area coated with $NaNO_2$, implying that HONO output is proportional to surface-available $NaNO_2$. The inside of a PFA device was etched manually every few millimeters in concentric circles in an attempt to increase the surface availability of $NaNO_2$, but no change in HONO output was observed compared to the unetched device.

Two additional methods were tested to increase the available surface area in the $NaNO_2$ device: increasing the number of coated PFA reaction devices in series and using an annular denuder. The HONO output with two PFA devices connected in series increased when using either 2.0 ppbv (PD6b) or 5.0 ppbv of HCl (PD-6c) at 40 °C and 50 % RH. We did not observe HCl breakthrough at the exit of the first PFA device, indicating that the increased HONO mixing ratio is the result of the water vapor reaction. We observed variability in the amount of HONO produced between the four PFA devices, ranging from 0.8 to 1.3 ppbv per device.

More HONO can be generated using the same PDs in conjunction with an annular denuder, which has a larger internal surface area of 3063 cm^2 compared to 388 cm^2 for the PFA device. HONO

emissions using PD-6c and an annular denuder produced a factor-of-4 higher mixing ratio of 24.5 ± 1.0 ppbv compared to 6.2 ± 0.5 ppbv with a single PFA device, but it required 45 h to stabilize. Again, the increase is due to promotion of the water vapor reaction. The major drawback of using an annular denuder is that the output drifted to lower mixing ratios continuously at a rate of a few parts per billion by volume per hour (ppbv h^{-1}), which was not a feature of the PFA devices (Fig. 2-6). The HONO output over any 4 h period was reasonably stable (within 0.5 ppbv) following the first 24 h of stabilization time, which suggests that a $NaNO_2$-coated annular denuder could be viable for short duration HONO calibrations if a secondary quantitative method is available to confirm its output (e.g., a NO_x analyzer with a quantified HONO conversion efficiency). Overall, using a $NaNO_2$-coated annular denuder can provide higher HONO outputs than using PFA devices but requires at least daily independent verification.

2.3.7.3 Purity of the HONO output

Previous work has demonstrated that there can be a notable NO_x impurity when generating HONO via the acid displacement method (Febo et al., 1995). To test the purity of the calibration source, the HONO output was analyzed by additional reactive nitrogen, NO_x, and NO_y instrumentation. For these experiments, we used a 6 M HCl PD and two PFA devices in series in a 40 ◦C calibration system, which was determined to have an output of 770 pptv of HONO. First, the output was analyzed by an I^- ToF CIMS and found no evidence for any detectable amounts of other nitrogen-containing species (e.g., $ClNO_2$, ClNO, HNO_3; Fig. 2-S13) except for HONO (Neuman et al., 2016; Veres et al., 2020). The I^- ToF CIMS is not sensitive to NO or NO_2, so further measurements were made with our Mo catalyst NO_x analyzer, a cavity-enhanced absorption spectrometer (Min et al., 2016), and a gold-catalyst NO_y instrument (Fahey et al., 1985; Fontijn et al., 1970; Ridley and Grahek, 1990; Ridley and Howlett, 1974; Ryerson et al., 1999), which determined that NO_2 impurities were at or below 10 % of the generated HONO based on the detection precisions of the latter two instruments. Finally, we quantified NO impurities using a single-photon LIF instrument, which is sensitive to subpptv levels of NO (Rollins et al., 2020). We observed NO at 5.5 % of the measured HONO signal (42 versus 770 pptv). Examination of our modified NO_x analyzer experiments using the same calibration system configuration revealed 6 % NO on average compared to the observed HONO (ca. 6–9 ppbv), consistent with the LIF measurements. In contrast, when using a $NaNO_2$-coated annular denuder with the same HCl PD, our modified NO_x analyzer observed NO/HONO to decrease to 2 %.

Recent work, using an analogous HONO calibration system, has found high production of NO, NO_2, and ClNO (> 10 %) when HCl input to loose NaNO2 was > 4 ppmv (Gingerysty and Osthoff, 2020). We observed similarly high output of NO when the HCl input was increased to 2.4 ppmv through the $NaNO_2$-coated devices. Under these conditions, the impurity may be due to self-reactions of HONO at high mixing ratios, as seen in other packed or stirred $NaNO_2$ salt beds (Febo et al., 1995). NO impurities at HONO mixing ratios below 100 ppbv in the salt bed may result from other heterogeneous processes generating NO in the lower HONO production regime. It may be that such small absolute quantities of NO have been produced in all prior calibration sources but, as the mixing ratio of HONO produced has been reduced in our calibration system, that this impurity increases in a relative sense. The purity of the calibration source when generating < 100 ppbv in the salt bed is ≥ 90 % HONO, with the remainder accounted for as NO and/or NO_2.

2.3.8 Context and application

The RSE of our stable HONO output is < 2.5 % and less than previous HCl acid displacement calibration source adaptations (VandenBoer et al., 2013; Zhou et al., 2018). Potential reasons for the improved stability in HONO output are the stable production of HCl from custom-made PDs and that the calibration system presented in the current work eliminated the need for solid $NaNO_2$ powder, which is prone to disturbance of equilibrated emissions through vibrations that can result in changes of up to a factor of 2 in mixing ratio output (VandenBoer et al., 2013; Zhou et al., 2018). The RSD values at the low HONO mixing ratios in this work are larger than reported by Febo et al. (1995), who generated much larger mixing ratios but did not specify the measurement details of their NO_x analyzer to facilitate true comparison. The greatest accuracy possible for this calibration source requires quantitation of the HONO output by a separate analytical method (e.g., IC-CD) and should not rely on the assumption that the HONO generated is equivalent to the HCl delivered into the reaction device due to the additional production mechanism driven by water vapor. While the output of this system is demonstrated to be highly reproducible with a given HCl PD, we recommend regular calibration.

2.4 Conclusion

We present a cost-effective, portable, stable, tunable, and robust gas-phase HONO calibration source. We utilized both a water vapor only, as well as its combination with the acid displacement reaction of HCl, with sodium nitrite ($NaNO_2$) coated on the inner wall of a short length of PFA

tubing within a machined Al-block permeation oven to produce a stable and continuous supply of high-purity gaseous HONO. We demonstrated for the first time that HONO was produced by humid air in the $NaNO_2$ reaction device, such that the HONO output was consistently higher than the HCl input. If a HONO calibration source in the pptv range was desired, it could be achieved easily by using only humid air flowing through an $NaNO_2$-coated reaction device. The output of this HONO calibration source spans the range of environmentally relevant mixing ratios – from pptv levels to tens of ppbv. This will allow instruments to be calibrated and/or intercompared using their standard atmospheric sampling parameters, without the need for excessive – or impossible – dilution or additional pumps, valves, and mass flow controllers.

We demonstrated that our HONO calibration system mixing ratio was tunable by adjusting the temperature of the permeation oven to control the water vapor reaction, as well as HCl emission rates from PDs. The HONO calibration source was designed to facilitate multiple calibrant concentrations, as the four holes in the aluminum heating block (Fig. 2-S3) allows for the operation of parallel HONO sources if desired. The most stable HONO output was achieved using $NaNO_2$-coated PFA devices at 40 °C, with HONO mixing ratios of 2.28 ± 0.58 ppbv (RSD of 24 % and RSE of 3 %, n = 8) that were reliably reproduced following complete assembly of the system. From our wide range of instrumental observations, the output of the source appears to be constant within ± 10 % or better. The purity of HONO source was determined to be > 90%, and while lower than previous work (99.5 %; Febo et al., 1995) this may be a consequence of previously unseen side reactions of increasing importance at the low HONO mixing ratios generated. We consider this an acceptable trade-off for a robust field-deployable HONO source unit. The resulting system can be disassembled, transported, and reassembled to produce the same HONO mixing ratios reproducibly, without the need for regular maintenance – where the same PD is retained between rebuilds. Custom-made HCl PDs are prone to variability in emission rates, both between similarly made PDs and over time, and therefore require regular characterization but can provide a stable output over the order of weeks. While higher HONO outputs were possible to generate using an $NaNO_2$-coated annular denuder for any given HCl PD, the outputs were unstable over time.

This HONO calibration instrument provides a universal solution to gas-phase HONO calibrations suitable for the full range of atmospheric instrumentation used for outdoor or indoor field measurements or laboratory experiments. This calibration unit could be used to intercompare the

responses/measurements between HONO instruments to investigate and validate accuracy and precision of their ambient measurements in addition to identifying and isolating potential interferences (Crilley et al., 2019). We anticipate it will also find utility in the generation of isotopically labeled HONO for the emerging exploration of stable-isotopic composition of HONO and its relation to the wide variety of suspected atmospheric HONO sources (Chai et al., 2019).

2.5 Acknowledgements

The authors thank Elizabeth Gaona-Colmán for help in collecting the CIMS data, as well as John Liggio and Jeremy Wentzell for enabling the use of and training on the quadrupole CIMS. Melodie Lao acknowledges research support from an NSERC Undergraduate Student Research Award and travel support through a York University Fieldwork Cost Fund award. Leyla Salehpoor acknowledges research support from the Harold I. Schiff graduate award in Atmospheric Chemistry. Leigh R. Crilley and Trevor C. VandenBoer acknowledge travel support from the York University Faculty of Science Junior Faculty Fund. Cora J. Young acknowledges support for this project through an NSERC Discovery Grant. Trevor C. VandenBoer and Cora J. Young acknowledge funding for the instrumentation developed and used in this work provided by the Alfred P. Sloan Foundation Chemistry of Indoor Environments program.

2.6 References

Braman, R. S. and de la Cantera, M. A.: Sublimation Sources for Nitrous Acid and Other Nitrogen Compounds in Air, Anal. Chem., 58(7), 1533–1537, doi:10.1021/ac00298a059, 1986.

Chai, J., Miller, D. J., Scheuer, E., Dibb, J., Selimovic, V., Yokelson, R., Zarzana, K. J., Brown, S. S., Koss, A. R., Warneke, C. and Hastings, M.: Isotopic characterization of nitrogen oxides (NO_x), nitrous acid (HONO), and nitrate (pNO_3^-) from laboratory biomass burning during FIREX, Atmos. Meas. Tech., (12), 1–32, doi:10.5194/amt-2019-229, 2019.

Cheng, P., Cheng, Y., Lu, K., Su, H., Yang, Q., Zou, Y., Zhao, Y., Dong, H., Zeng, L. and Zhang, Y.: An online monitoring system for atmospheric nitrous acid (HONO) based on stripping coil and ion chromatography, J. Environ. Sci. (China), 25(5), 895–907, doi:10.1016/S1001-0742(12)60251-4, 2013.

Collins, D. B., Hems, R. F., Zhou, S., Wang, C., Grignon, E., Alavy, M., Siegel, J. A. and Abbatt, J. P. D.: Evidence for Gas-Surface Equilibrium Control of Indoor Nitrous Acid, Environ. Sci. Technol., 52(21), 12419–12427, doi:10.1021/acs.est.8b04512, 2018.

Crilley, L. R., Kramer, L., Pope, F. D., Whalley, L. K., Cryer, D. R., Heard, D. E., Lee, J. D., Reed, C. and Bloss, W. J.: On the interpretation of in situ HONO observations via photochemical steady state, Faraday Discuss., 189, 191–212, doi:10.1039/c5fd00224a, 2016.

Crilley, L. R., Kramer, L. J., Ouyang, B., Duan, J., Zhang, W., Tong, S., Ge, M., Tang, K., Qin, M., Xie, P., Shaw, M. D., Lewis, A. C., Mehra, A., Bannan, T. J., Worrall, S. D., Priestley, M., Bacak, A., Coe, H., Allan, J., Percival, C. J., Popoola, O. A. M., Jones, R. L. and Bloss, W. J.: Intercomparison of nitrous acid (HONO) measurement techniques in a megacity (Beijing), Atmos. Meas. Tech., 12(12), 6449–6463, doi:10.5194/amt-12-6449-2019, 2019.

Dawe, K. E. R., Furlani, T. C., Kowal, S. F., Kahan, T. F., VandenBoer, T. C. and Young, C. J.: Formation and emission of hydrogen chloride in indoor air, Indoor Air, 29(1), doi:10.1111/ina.12509, 2019.

Fahey, D. W., Eubank, C. S., Hübler, G. and Fehsenfeld, F. C.: Evaluation of a catalytic reduction technique for the measurement of total reactive odd-nitrogen NO_y in the atmosphere, J. Atmos. Chem., 3(4), 435–468, doi:10.1007/BF00053871, 1985.

Febo, A., Perrino, C., Gherardi, M. and Sparapani, R.: Evaluation of a High-Purity and High-Stability Continuous Generation System for Nitrous Acid, Environ. Sci. Technol., 29(9), 2390–2395, doi:10.1021/es00009a035, 1995.

Fontijn, A., Sabadell, A. J. and Ronco, R. J.: Homogeneous Chemiluminescent Measurement of Nitric Oxide with Ozone Implications for Continuous Selective Monitoring of Gaseous Air Pollutants, Anal. Chem., 42(6), 575–579, doi:10.1021/ac60288a034, 1970.

Fried, A., Henry, B. and Sewell, S.: Potential calibration errors in carbonyl sulfide permeation devices: Implications for atmospheric studies, J. Geophys. Res. Atmos., 103(D15), 18895–18906, doi:10.1029/98JD00620, 1998.

Gall, E. T., Griffin, R. J., Steiner, A. L., Dibb, J., Scheuer, E., Gong, L., Rutter, A. P., Cevik, B. K., Kim, S., Lefer, B. and Flynn, J.: Evaluation of nitrous acid sources and sinks in urban outflow, Atmos. Environ., 127(January 2016), 272–282, doi:10.1016/j.atmosenv.2015.12.044, 2016.

Gingerysty, N. J. and Osthoff, H. D.: A compact , high-purity source of HONO validated by Fourier Transform Infrared and Thermal Dissociation Cavity Ring-down Spectroscopy, Atmos. Meas. Tech. Discuss., (March), 1–20, doi:10.5194/amt-2020-92, 2020.

Gligorovski, S.: Nitrous acid (HONO): An emerging indoor pollutant, J. Photochem. Photobiol. A Chem., 314, 1–5, doi:10.1016/j.jphotochem.2015.06.008, 2016.

Gómez Alvarez, E., Wortham, H., Strekowski, R., Zetzsch, C. and Gligorovski, S.: Atmospheric photosensitized heterogeneous and multiphase reactions: From outdoors to indoors, Environ. Sci. Technol., 46(4), 1955–1963, doi:10.1021/es2019675, 2012.

Heland, J., Kleffmann, J., Kurtenbach, R. and Wiesen, P.: A new instrument to measure gaseous nitrous acid (HONO) in the atmosphere, Environ. Sci. Technol., 35(15), 3207–3212, doi:10.1021/es000303t, 2001.

Honrath, R. E., Lu, Y., Peterson, M. C., Dibb, J. E., Arsenault, M. A., Cullen, N. J. and Steffen, K.: Vertical fluxes of NO_x, HONO, and HNO_3 above the snowpack at Summit, Greenland, Atmos. Environ., 36(15–16), 2629–2640, doi:10.1016/S1352-2310(02)00132-2, 2002.

Kasibhatla, P., Sherwen, T., Evans, M. J., Carpenter, L. J., Reed, C., Alexander, B., Chen, Q., Sulprizio, M. P., Lee, J. D., Read, K. A., Bloss, W., Crilley, L. R., Keene, W. C., Pszenny, A. A. P. and Hodzic, A.: Global impact of nitrate photolysis in sea-salt aerosol on NO_x, OH, and O_3 in the marine boundary layer, Atmos. Chem. Phys., 18(15), 11185–11203, doi:10.5194/acp-18-11185-2018, 2018.

Kim, S., VandenBoer, T. C., Young, C. J., Riedel, T. P., Thornton, J. A., Swarthout, B., Sive, B., Lerner, B., Gilman, J. B., Warneke, C., Roberts, J. M., Guenther, A., Wagner, N. L., Dubé, W. P., Williams, E. and Brown, S. S.: The primary and recyling source of OH during the NACHTT-2011 campaign: HONO as an important OH primary source in the wintertime, J. Geophys. Res. Atmos., 119, 6886–6896, doi:10.1002/2013JD021186, 2014.

Kleffmann, J.: Daytime sources of nitrous acid (HONO) in the atmospheric boundary layer, ChemPhysChem, 8(8), 1137–1144, doi:10.1002/cphc.200700016, 2007.

Kleffmann, J. and Wiesen, P.: Technical Note: Quantification of interferences of wet chemical HONO LOPAP measurements under simulated polar conditions, Atmos. Chem. Phys., 8(22), 6813–6822, doi:10.5194/acp-8-6813-2008, 2008.

Kleffmann, J., Lörzer, J. C., Wiesen, P., Kern, C., Trick, S., Volkamer, R., Rodenas, M. and Wirtz, K.: Intercomparison of the DOAS and LOPAP techniques for the detection of nitrous acid (HONO), Atmos. Environ., 40(20), 3640–3652, doi:10.1016/j.atmosenv.2006.03.027, 2006.

Lee, B. H., Wood, E. C., Herndon, S. C., Lefer, B. L., Luke, W. T., Brune, W. H., Nelson, D. D., Zahniser, M. S. and Munger, J. W.: Urban measurements of atmospheric nitrous acid: A caveat on the interpretation of the HONO photostationary state, J. Geophys. Res. Atmos., 118(21), 12274–12281, doi:10.1002/2013JD020341, 2013.

Lee, J. D., Whalley, L. K., Heard, D. E., Stone, D., Dunmore, R. E., Hamilton, J. F., Young, D. E., Allan, J. D., Laufs, S. and Kleffmann, J.: Detailed budget analysis of HONO in central London reveals a missing daytime source, Atmos. Chem. Phys., 16(5), 2747–2764, doi:10.5194/acp-16-2747-2016, 2016.

Liu, J., Li, S., Zeng, J., Mekic, M., Yu, Z., Zhou, W., Loisel, G., Gandolfo, A., Song, W., Wang, X., Zhou, Z., Herrmann, H., Li, X. and Gligorovski, S.: Assessing indoor gas phase oxidation capacity through real-time measurements of HONO and NO x in Guangzhou, China , Environ. Sci. Process. Impacts, 21(8), 1393–1402, doi:10.1039/c9em00194h, 2019.

MacInnis, J. J., VandenBoer, T. C. and Young, C. J.: Development of a gas phase source for perfluoroalkyl acids to examine atmospheric sampling methods, Analyst, 141(12), doi:10.1039/c6an00313c, 2016.

McGrath, D. T., Ryan, M. D., Macinnis, J. J., Vandenboer, T. C., Young, C. J. and Katz, M. J.: Selective decontamination of the reactive air pollutant nitrous acid: Via node-linker cooperativity in a metal-organic framework, Chem. Sci., 10(21), 5576–5581, doi:10.1039/c9sc01357a, 2019.

Min, K. E., Washenfelder, R. A., Dubé, W. P., Langford, A. O., Edwards, P. M., Zarzana, K. J., Stutz, J., Lu, K., Rohrer, F., Zhang, Y. and Brown, S. S.: A broadband cavity enhanced absorption spectrometer for aircraft measurements of glyoxal, methylglyoxal, nitrous acid, nitrogen dioxide, and water vapor, Atmos. Meas. Tech., 9(2), 423–440, doi:10.5194/amt-9-423-2016, 2016.

Mitchell, G. D.: A review of permeation tubes and permeators, Sep. Purif. Methods, 29(1), 119–128, doi:10.1081/SPM-100100005, 2000.

Mushinski, R. M., Phillips, R. P., Payne, Z. C., Abney, R. B., Jo, I., Fei, S., Pusede, S. E., White, J. R., Rusch, D. B. and Raff, J. D.: Microbial mechanisms and ecosystem flux estimation for aerobic NO_y emissions from deciduous forest soils, Proc. Natl. Acad. Sci. U. S. A., 116(6), 2138–2145, doi:10.1073/pnas.1814632116, 2019.

Neuman, J. A., Ryerson, T. B., Huey, L. G., Jakoubek, R., Nowak, J. B., Simons, C. and Fehsenfeld, F. C.: Calibration and evaluation of nitric acid and ammonia permeation tubes by UV optical absorption, Environ. Sci. Technol., 37(13), 2975–2981, doi:10.1021/es026422l, 2003.

Neuman, J. A., Trainer, M., Brown, S. S., Min, K. E., Nowak, J. B., Parrish, D. D., Peischl, J., Pollack, I. B., Roberts, J. M., Ryerson, T. B. and Veres, P. R.: HONO emission and production determined from airborne measurements over the Southeast U.S., J. Geophys. Res., 121(15), 9237–9250, doi:10.1002/2016JD025197, 2016.

O'Keeffe, A. E. and Ortman, G. C.: Primary Standards for Trace Gas Analysis, Anal. Chem., 38(6), 760–763, doi:10.1021/ac60238a022, 1966.

Oswald, R., Behrendt, T., Ermel, M., Wu, D., Su, H., Cheng, Y., Breuninger, C., Moravek, A., Mougin, E., Delon, C., Loubet, B., Pommerening-Röser, A., Sörgel, M., Pöschl, U., Hoffmann, T., Andreae, M. O., Meixner, F. X. and Trebs, I.: HONO emissions from soil bacteria as a major source of atmospheric reactive nitrogen, Science (80-.)., 341(6151), 1233–1235, doi:10.1126/science.1242266, 2013.

Pinto, J. P., Dibb, J., Lee, B. H., Rappenglück, B., Wood, E. C., Levy, M., Zhang, R. Y., Lefer, B., Ren, X. R., Stutz, J., Tsai, C., Ackermann, L., Golovko, J., Herndon, S. C., Oakes, M., Meng, Q. Y., Munger, J. W., Zahniser, M. and Zheng, J.: Intercomparison of field measurements of nitrous acid (HONO) during the SHARP campaign, J. Geophys. Res., 119(9), 5583–5601, doi:10.1002/2013JD020287, 2014.

Place, B. K., Young, C. J., Ziegler, S. E., Edwards, K. A., Salehpoor, L. and VandenBoer, T. C.: Passive sampling capabilities for ultra-trace quantitation of atmospheric nitric acid (HNO_3) in remote environments, Atmos. Environ., 191, 360–369, doi:10.1016/j.atmosenv.2018.08.030, 2018.

Pusede, S. E., VandenBoer, T. C., Murphy, J. G., Markovic, M. Z., Young, C. J., Veres, P. R., Roberts, J. M., Washenfelder, R. A., Brown, S. S., Ren, X., Tsai, C., Stutz, J., Brune, W. H., Browne, E. C., Wooldridge, P. J., Graham, A. R., Weber, R., Goldstein, A. H., Dusanter, S., Griffith, S. M., Stevens, P. S., Lefer, B. L. and Cohen, R. C.: An Atmospheric Constraint on the NO2 Dependence of Daytime Near-Surface Nitrous Acid (HONO), Environ. Sci. Technol., 49(21), 12774–12781, doi:10.1021/acs.est.5b02511, 2015.

Reed, C., Evans, M. J., Crilley, L. R., Bloss, W. J., Sherwen, T., Read, K. A., Lee, J. D. and Carpenter, L. J.: Evidence for renoxification in the tropical marine boundary layer, Atmos. Chem. Phys., 17(6), 4081–4092, doi:10.5194/acp-17-4081-2017, 2017.

Ren, X., Gao, H., Zhou, X., Crounse, J. D., Wennberg, P. O., Browne, E. C., LaFranchi, B. W., Cohen, R. C., McKay, M., Goldstein, A. H. and Mao, J.: Measurement of atmospheric nitrous acid at Bodgett forest during BEARPEX2007, Atmos. Chem. Phys., 10(13), 6283–6294, doi:10.5194/acp-10-6283-2010, 2010.

Ridley, B. A. and Grahek, F. E.: A small, low flow, high sensitivity reaction vessel for NO chemiluminescence detectors, J. Am. Meteorol. Soc., 7, 307–311, 1990.

Ridley, B. A. and Howlett, L. C.: An instrument for nitric oxide measurements in the stratosphere, Rev. Sci. Instrum., 45(6), 742–746, 1974.

Roberts, J. M., Veres, P., Warneke, C., Neuman, J. A., Washenfelder, R. A., Brown, S. S., Baasandorj, M., Burkholder, J. B., Burling, I. R., Johnson, T. J., Yokelson, R. J. and De Gouw, J.: Measurement of HONO, HNCO, and other inorganic acids by negative-ion proton-transfer chemical-ionization mass spectrometry (NI-PT-CIMS): Application to biomass burning emissions, Atmos. Meas. Tech., 3(4), 981–990, doi:10.5194/amt-3-981-2010, 2010.

Rollins, A. W., Rickly, P. S., Gao, R.-S., Ryerson, T. B., Brown, S. S., Peischl, J. and Bourgeois, I.: Single-photon laser-induced fluorescence detection of nitric oxide at sub-parts per trillion mixing ratios, Atmos. Meas. Tech., 13, 2425–2439, doi:10.5194/amt-13-2425-2020, 2020.

Rubio, M. A., Lissi, E., Villena, G., Elshorbany, Y. F., Kleffmann, J., Kurtenbach, R., and Wiesen, P.: Simultaneous measurements of formaldehyde and nitrous acid in dews and gas phase in the atmosphere of Santiago, Chile, Atmos. Environ., 43, 6106–6109, https://doi.org/10.1016/j.atmosenv.2009.09.017, 2009.

Ryerson, T. B., Huey, L. G., Knapp, K., Neuman, J. A., Parrish, D. D., Sueper, D. T. and Fehsenfeld, F. C.: Design and initial characterization of an inlet for gas-phase NO_y measurements from aircraft, J. Geophys. Res., 104(D5), 5483–5492, 1999.

Sörgel, M., Trebs, I., Serafimovich, A., Moravek, A., Held, A. and Zetzsch, C.: Simultaneous HONO measurements in and above a forest canopy: Influence of turbulent exchange on mixing ratio differences, Atmos. Chem. Phys., 11(2), 841–855, doi:10.5194/acp-11-841-2011, 2011.

Sörgel, M., Trebs, I., Wu, D. and Held, A.: A comparison of measured HONO uptake and release with calculated source strengths in a heterogeneous forest environment, Atmos. Chem. Phys., 15(16), 9237–9251, doi:10.5194/acp-15-9237-2015, 2015.

Spataro, F. and Ianniello, A.: Sources of atmospheric nitrous acid: State of the science, current research needs, and future prospects, J. Air Waste Manag. Assoc., 64(11), 1232–1250, doi:10.1080/10962247.2014.952846, 2014.

Stutz, J., Kim, E. S., Platt, U., Bruno, P., Perrino, C. and Febo, A.: UV-visible absorption cross sections of nitrous acid, J. Geophys. Res. Atmos., 105(D11), 14585–14592, doi:10.1029/2000JD900003, 2000.

Stutz, J., Oh, H. J., Whitlow, S. I., Anderson, C., Dibb, J. E., Flynn, J. H., Rappenglück, B. and Lefer, B.: Simultaneous DOAS and mist-chamber IC measurements of HONO in Houston, TX, Atmos. Environ., 44(33), 4090–4098, doi:10.1016/j.atmosenv.2009.02.003, 2010.

Susaya, J., Kim, K. H., Cho, J. and Parker, D.: The controlling effect of temperature in the application of permeation tube devices in standard gas generation, J. Chromatogr. A, 1225, 8–16, doi:10.1016/j.chroma.2011.12.066, 2012.

Taira, M. and Kanda, Y.: Continuous Generation System for Low-Concentration Gaseous Nitrous Acid, Anal. Chem., 62(6), 630–633, doi:10.1021/ac00205a018, 1990.

Tong, S., Hou, S., Zhang, Y., Chu, B., Liu, Y., He, H., Zhao, P. and Ge, M.: Exploring the nitrous acid (HONO) formation mechanism in winter Beijing: Direct emissions and heterogeneous production in urban and suburban areas, Faraday Discuss., 189, 213–230, doi:10.1039/c5fd00163c, 2016.

Tsai, C., Spolaor, M., Fedele Colosimo, S., Pikelnaya, O., Cheung, R., Williams, E., Gilman, J. B., Lerner, B. M., Zamora, R. J., Warneke, C., Roberts, J. M., Ahmadov, R., De Gouw, J., Bates, T., Quinn, P. K. and Stutz, J.: Nitrous acid formation in a snow-free wintertime polluted rural area, Atmos. Chem. Phys., 18(3), 1977–1996, doi:10.5194/acp-18-1977-2018, 2018.

VandenBoer, T. C., Brown, S. S., Murphy, J. G., Keene, W. C., Young, C. J., Pszenny, A. A. P., Kim, S., Warneke, C., De Gouw, J. A., Maben, J. R., Wagner, N. L., Riedel, T. P., Thornton, J. A., Wolfe, D. E., Dubé, W. P., Öztürk, F., Brock, C. A., Grossberg, N., Lefer, B., Lerner, B., Middlebrook, A. M. and Roberts, J. M.: Understanding the role of the ground surface in HONO vertical structure: High resolution vertical profiles during NACHTT-11, J. Geophys. Res. Atmos., 118(17), doi:10.1002/jgrd.50721, 2013.

VandenBoer, T. C., Markovic, M. Z., Sanders, J. E., Ren, X., Pusede, S. E., Browne, E. C., Cohen, R. C., Zhang, L., Thomas, J., Brune, W. H. and Murphy, J. G.: Evidence for a nitrous acid (HONO) reservoir at the ground surface in Bakersfield, CA, during CalNex 2010, J. Geophys. Res. Atmos., 119, 1–14, doi:10.1002/2013JD020971, 2014.

VandenBoer, T. C., Young, C. J., Talukdar, R. K., Markovic, M. Z., Brown, S. S., Roberts, J. M. and Murphy, J. G.: Nocturnal loss and daytime source of nitrous acid through reactive uptake and displacement, Nat. Geosci., 8(1), 55–60, doi:10.1038/ngeo2298, 2015.

Večeřa, Z., Dasgupta, P. K. and Večeřa, Z.: Measurement of Ambient Nitrous Acid and a Reliable Calibration Source for Gaseous Nitrous Acid, Environ. Sci. Technol., 25(2), 255–260, doi:10.1021/es00014a006, 1991.

Veres, P., Gilman, J. B., Roberts, J. M., Kuster, W. C., Warneke, C., Burling, I. R. and De Gouw, J.: Development and validation of a portable gas phase standard generation and calibration system for volatile organic compounds, Atmos. Meas. Tech., 3(3), 683–691, doi:10.5194/amt-3-683-2010, 2010a.

Veres, P., Roberts, J. M., Burling, I. R., Warneke, C., De Gouw, J. and Yokelson, R. J.: Measurements of gas-phase inorganic and organic acids from biomass fires by negative-ion proton-transfer chemical-ionization mass spectrometry, J. Geophys. Res. Atmos., 115(23), 1–15, doi:10.1029/2010JD014033, 2010b.

Veres, P. R., Andrew Neuman, J., Bertram, T. H., Assaf, E., Wolfe, G. M., Williamson, C. J., Weinzierl, B., Tilmes, S., Thompson, C. R., Thames, A. B., Schroder, J. C., Saiz-Lopez, A., Rollins, A. W., Roberts, J. M., Price, D., Peischl, J., Nault, B. A., Møller, K. H., Miller, D. O., Meinardi, S., Li, Q., Lamarque, J. F., Kupc, A., Kjaergaard, H. G., Kinnison, D., Jimenez, J. L., Jernigan, C. M., Hornbrook, R. S., Hills, A., Dollner, M., Day, D. A., Cuevas, C. A., Campuzano-

Jost, P., Burkholder, J., Bui, T. P., Brune, W. H., Brown, S. S., Brock, C. A., Bourgeois, I., Blake, D. R., Apel, E. C. and Ryerson, T. B.: Global airborne sampling reveals a previously unobserved dimethyl sulfide oxidation mechanism in the marine atmosphere, Proc. Natl. Acad. Sci. U. S. A., 117(9), 4505–4510, doi:10.1073/pnas.1919344117, 2020.

Volkamer, R., Sheehy, P., Molina, L. T. and Molina, M. J.: Oxidative capacity of the Mexico City atmosphere-Part 1: A radical source perspective, Atmos. Chem. Phys., 10(14), 6969–6991, doi:10.5194/acp-10-6969-2010, 2010.

Wang, L. and Zhang, J.: Detection of nitrous acid by cavity ring-down spectroscopy, Environ. Sci. Technol., 34(19), 4221–4227, doi:10.1021/es0011055, 2000.

Washenfelder, R. A., Roehl, C. M., McKinney, K. A., Julian, R. R. and Wennberg, P. O.: A compact, lightweight gas standards generator for permeation tubes, Rev. Sci. Instrum., 74(6), 3151–3154, doi:10.1063/1.1570949, 2003.

Ye, C., Zhou, X., Pu, D., Stutz, J., Festa, J., Spolaor, M., Tsai, C., Cantrell, C., Mauldin, R. L., Campos, T., Weinheimer, A., Hornbrook, R. S., Apel, E. C., Guenther, A., Kaser, L., Yuan, B., Karl, T., Haggerty, J., Hall, S., Ullmann, K., Smith, J. N., Ortega, J. and Knote, C.: Rapid cycling of reactive nitrogen in the marine boundary layer, Nature, 532(7600), 489–491, doi:10.1038/nature17195, 2016.

Ye, C., Zhou, X., Pu, D., Stutz, J., Festa, J., Spolaor, M., Tsai, C., Cantrell, C., Mauldin III, R. L., Weinheimer, A., Hornbrook, R. S., Apel, E. C., Guenther, A., Kaser, L., Yuan, B., Karl, T., Haggerty, J., Hall, S., Ullmann, K., Smith, J. and Ortega, J.: Tropospheric HONO distribution and chemistry in the southeastern US, Atmos. Chem. Phys., 18, 9107–9120, doi:10.5194/acp-2018-105, 2018.

Young, C. J., Washenfelder, R. A., Roberts, J. M., Mielke, L. H., Osthoff, H. D., Tsai, C., Pikelnaya, O., Stutz, J., Veres, P. R., Cochran, A. K., Vandenboer, T. C., Flynn, J., Grossberg, N., Haman, C. L., Lefer, B., Stark, H., Graus, M., De Gouw, J., Gilman, J. B., Kuster, W. C. and Brown, S. S.: Vertically resolved measurements of nighttime radical reservoirs in Los Angeles and their contribution to the urban radical budget, Environ. Sci. Technol., 46(20), 10965–10973, doi:10.1021/es302206a, 2012.

Young, C. J., Zhou, S., Siegel, J. A. and Kahan, T. F.: Illuminating the dark side of indoor oxidants, Environ. Sci. Process. Impacts, 21(8), 1229–1239, doi:10.1039/c9em00111e, 2019.

Zhang, N., Zhou, X., Shepson, P. B., Gao, H., Alaghmand, M. and Stirm, B.: Aircraft measurement of HONO vertical profiles over a forested region, Geophys. Res. Lett., 36(15), doi:10.1029/2009GL038999, 2009.

Zhang, W., Tong, S., Ge, M., An, J., Shi, Z., Hou, S., Xia, K., Qu, Y., Zhang, H., Chu, B., Sun, Y. and He, H.: Variations and sources of nitrous acid (HONO) during a severe pollution episode in Beijing in winter 2016, Sci. Total Environ., 648, 253–262, doi:10.1016/j.scitotenv.2018.08.133, 2019.

Zhou, S., Young, C. J., Vandenboer, T. C., Kowal, S. F. and Kahan, T. F.: Time-Resolved Measurements of Nitric Oxide, Nitrogen Dioxide, and Nitrous Acid in an Occupied New York Home, Environ. Sci. Technol., 52(15), 8355–8364, doi:10.1021/acs.est.8b01792, 2018.

Zhou, X., He, Y., Huang, G., Thornberry, T. D., Carroll, M. A. and Bertman, S. B.: Photochemical production of nitrous acid on glass sample manifold surface, Geophys. Res. Lett., 29(14), 26-1-26–4, doi:10.1029/2002gl015080, 2002.

Chapter Three:

Design and validation of an automated nitrous acid (HONO) platform for indoor measurements

M. Lao[1], L.R. Crilley[1], and T.C. VandenBoer[1]

[1]Department of Chemistry, York University, Toronto, ON, Canada

Author Contributions:

TCV conceptualized the work and acquired the funding. TCV provided the resources to support this work. **ML** built the HONO platform and tN_r instrument with LC, following the design by TCV. **ML** performed all validation experiments and data analysis under the guidance of LC and TCV. **ML** prepared and TCV edited the manuscript.

Abstract

A new automated measurement platform was built to detect real-time changes in emerging indoor pollutants, NO_x and HONO. The platform is a subset of a total reactive nitrogen (tN_r) instrument that measures three fractions of nitrogenous species by exploiting their acidic, basic, or neutral molecular properties and is suitably designed for indoor air quality applications. This new instrument is safe, non-invasive, and user-friendly in comparison to cutting-edge instruments for research. In addition, it requires less space and generates minimal noise for ease of deployment in occupied residences. The automated platform utilizes an inlet with different sampling pathways to measure HONO by difference from NO_x in a given air sample by scrubbing it in a reactive base-coated annular denuder. A series of experiments were performed to characterize and validate the real-time detection, in which the NO_x and HONO response times were within 1 min. The denuder scrubbing efficiency for HONO was near 100 % and no bias in NO_x measured through the denuder and the rest of the sampling inlet was observed. This chapter describes the build and shows proof of function of the instrument for replication by other researchers to widely survey and improve our understanding of indoor chemistry of HONO.

3.1 Introduction

3.1.1 Indoor air chemistry

In recent years, buildings have evolved to become more energy efficient resulting in gastight indoor environments (Weschler and Carslaw, 2018). These result in increased exposure to elevated pollutant concentrations that are associated with adverse health effects, which is concerning because humans spend 90 % of their lives indoors (Klepeis et al., 2001; Leech et al., 2002). Indoor chemistry is complex, and the chemical transformations can be influenced by multiple factors including the use of household products and multiphase reactions on various surface materials ranging from furnishings to building materials. Everyday indoor activities can encourage direct pollutant emissions such as smoking, cleaning, and cooking, but these can vary based on human behavior. We have yet to understand how our indoor oxidative capacity is impacted from our daily lifestyles and how these pollutant levels impact our health.

3.1.2 An emerging indoor pollutant

Nitrous acid (HONO) is an important atmospheric pollutant and source of hydroxyl radical (OH), a principal daytime oxidant that can drive oxidation reactions (Spataro and Ianniello, 2014). Photolabile HONO can readily release OH under low light conditions ($\lambda \leq 400$ nm; R1) such as during early mornings in an outdoor environment (Kleffmann, 2007).

$$\mathbf{HONO_{(g)} + \mathit{hv}\ (\lambda \leq 40\ nm) \rightarrow OH + NO_{(g)}} \qquad \textbf{(R1)}$$

Studies have shown that light sources present in indoor environments are also of sufficient energy and intensity to promote HONO photodissociation including sunlight passing through windows (Gómez Alvarez et al., 2013) as well as artificial sources (i.e. light bulbs, fluorescent tube, incandescent, etc.) (Kowal et al., 2017; Zhou et al., 2018). Windows can attenuate photon wavelengths shorter than ~330 nm, but even with this cutoff the photons passed are of sufficient energy to initiate photochemistry of indoor pollutants like nitrogen dioxide (NO_2) and HONO (Kowal et al., 2017; Young et al., 2019). Both pollutants are important sources of oxidants that drive indoor oxidation chemistry, where HONO can form OH and NO_2 photolysis can result in O_3 formation (R2, R3) (Gandolfo et al., 2016; Gómez Alvarez et al., 2013; Kowal et al., 2017).

$$\mathbf{NO_2 + \mathit{hv}\ (\lambda < 398\ nm) \rightarrow NO + O} \qquad \textbf{(R2)}$$

$$\mathbf{O + O_2 \rightarrow O_3} \qquad \textbf{(R3)}$$

Outdoors, the primary precursor of OH is from ozone (O_3) photolysis, but recent residential studies have found indoor O_3 levels are relatively low (Liu et al., 2021; Zhou et al., 2018) unless an ozone-generating appliance is present (i.e. printers, air purifiers) (Britigan et al., 2006; Hubbard et al., 2005). Outdoor infiltration of O_3 can be facilitated by open doors and windows, but O_3 is quickly lost. It is titrated if NO is present, forming NO_2, in addition to O_3 being readily deposited onto surfaces (Liu et al., 2021; Weschler and Carslaw, 2018; Wisthaler and Weschler, 2010; Zhou et al., 2018). When O_3 levels are low indoors, OH may be the sole driver in indoor oxidation chemistry. However, the detection of OH is difficult indoors because of its short lifetime (<1 second, (s)), leading researchers to focus on and understand OH formation pathways for predictive analysis. Only recently has HONO attracted attention for its potential contributions as an oxidant precursor. As a result, increasing attention on HONO formation and loss processes can result in better estimation of the indoor OH budget and the role of oxidants in indoor air quality. Reports consistently show higher levels of HONO indoors than outdoors and these can range up to 100 parts per billion by volume (ppbv), often directly emitted from gas appliances and combustion processes when the highest quantities are observed (Collins et al., 2018; Mattila et al., 2020; Zhou et al., 2018). In comparison, outdoor levels of HONO are typically found to be below 1 ppbv (VandenBoer et al., 2014). Exposure to high levels of HONO may lead to adverse health effects such as a decrease in lung function (Beckett et al., 1995; Brauer et al., 1993; Jarvis et al., 2005; Rasmussen et al., 1995). The study by Beckett et al. observed an increase in respiratory and mucous membrane symptoms within their slightly asthmatic subjects when they were exposed to 650 ppb HONO for three hours. Another exposure risk includes the reaction products of HONO with amines (e.g. those emitted in thirdhand smoke and surface-deposited nicotine) which are carcinogenic nitrosamines (Sleiman et al., 2010). Past studies have focused on smoking as the indoor amine source of highest concern (Ge et al., 2011; Hems et al., 2019; Sleiman et al., 2010), but with a decline in smoking indoors other amine sources may be of emerging importance. Potential indoor amine sources may include household products that contain these organic compounds, for example in basic cleaning solutions and hair products. Currently, sources of amines are poorly characterized indoors and require more quantitative measurements, particularly because of their transformations with HONO. The second contributing source of HONO indoors is heterogeneous hydrolysis of NO_2 (R4) (Collins et al., 2018; Finlayson-Pitts et al., 2003; Spataro and Ianniello, 2014; Wang et al., 2020b). This reaction mechanism is complex and not well

understood under relevant atmospheric conditions. One well described mechanism of NO_2 hydrolysis has been presented by Finlayson-Pitts et al., (2003) which proposed dinitrogen tetroxide (N_2O_4) as a key intermediate. However, this can only occur when NO_2 concentrations are large enough to form N_2O_4 which is very small even in highly polluted atmospheres. There is limited exploration of the hydrolysis mechanism under atmospherically relevant conditions. Regardless, many studies have suggested and provided evidence that NO_2 can and does react with household surfaces (i.e., walls, ceilings, carpets, windows) to heterogeneously produce HONO (Gandolfo et al., 2017, 2020; Gómez Alvarez et al., 2014; Wainman et al., 2001).

$$\mathbf{2\ NO_{2(g)} + H_2O_{(ads)} \rightarrow HONO_{(g)} + HNO_{3(ads)}} \qquad \textbf{(R4)}$$

Various factors in indoor environments are thought to cause large variability in indoor HONO measurements including surface properties of building materials, and analytical methods for HONO that do not agree well with each other. When combined, these uncertainties complicate the interpretation of HONO chemistry (Crilley et al., 2019). Thus, there is a need for continual improvement in HONO-detecting instruments that mitigate bias and interferences to close the gap on reliable field measurements.

Indoor environments are vastly different than outdoors, and their unique properties can influence HONO formation. There are higher indoor surface-area-to-volume (SA:V) ratios typically ~3 m^{-1}, which is hundreds of times higher than outdoors and is on the order of 0.01 m^{-1} (Abbatt and Wang, 2020; Ault et al., 2020; Manuja et al., 2019; Wang et al., 2020a). Higher SA:V promotes heterogenous reactions, including the formation of HONO from NO_2. As mentioned above, indoor environments also have lower energy photons at lower fluxes, so HONO can significantly contribute to the indoor OH budget in sunlit areas. A classroom study in France reported HONO photolysis as being the primary source of OH and this generated 1.8 x 10^6 molecules per cubic centimeter (molec cm^{-3}) OH, which is similar to typical outdoor OH levels of ~10^6 molec cm^{-3} (Gómez Alvarez et al., 2013). Buildings with controlled heating ventilation and air conditioning (HVAC) units can play an additional role in facilitating chemical reactions. Commercial buildings, for example, have higher ventilation rates that increase indoor-outdoor air exchange in comparison to private residences, resulting in higher indoor levels of O_3 (Zhou et al., 2019). The increased O_3 can react with NO to form gas-phase NO_2, followed by NO_2 reacting on indoor surfaces to form

HONO. There are a few residential studies focused on HONO formation but fewer in a commercial environment for intercomparison (Collins et al., 2018; Wang et al., 2020b; Zhou et al., 2018). Household activities can directly influence HONO chemistry, acting as both sources and sinks. For example, a home cleaning study by Wang et al., (2020a) observed rapid decrease in HONO of 71 – 90 % when mopping the floor with bleach due to the release of reactive chlorinated species. Chlorinated species like hypochlorous acid were proposed to react with nitrite present on surfaces to form chlorine nitrite as a competing process against HONO formation, resulting in less gas-phase HONO (Mattila et al., 2020; Wang et al., 2020a). The use of acidic cleaning solutions (e.g. acetic acid) also increased the surface-gas HONO partitioning through acid displacement or changes in surface chemical properties, where both are currently thought to be potentially important factors regulating observed indoor HONO levels (Wang et al., 2020b). To understand the drivers of indoor HONO formation in all indoor environments, we require real-time and accurate measurements of both HONO and NO_2, along with other observations of indoor air and surface composition to constrain chemical production and loss pathways against air exchange.

There are limited studies that report simultaneous indoor measurements of NO, NO_2, and HONO together. Past outdoor studies have focused on NO and NO_2 because of their primary emissions from combustion engines and the related regulations due to their adverse effects on human health, which was translated to indoor studies (U.S EPA, 1993). Indoor levels of NO have been found to range up to 400 ppbv and NO_2 up to 300 ppbv when directly emitted from combustion processes using gas appliances or being transported indoors via outdoor air infiltration and HVAC (Zhou et al., 2018 and references therein). However, it is now recognized that most previous indoor studies measuring NO_2 would be biased high because HONO interferes quantitatively with both NO_2 passive samplers and NO_2 detection by Mo-catalyst chemiluminescence analyzers. As a result, we have a distorted picture of the amount and importance of NO_2 indoors, and no insight into the presence or variability of HONO. Passive samplers for NO_2 collection are coated with triethanolamine which also reacts readily with HONO (Spicer et al., 1994; Spicer et al., 2001), while Mo-catalysts in chemiluminescence analyzers convert HONO and some other NO_y species to NO as a measurement bias for NO_2 (Dunlea et al., 2007; Joseph and Spicer, 1978; Spicer et al., 1994; Villena et al., 2012) which we have exploited in the construction of our HONO calibration source (Lao et al., 2020). The indoor home study by Zhou et al. (2018) selectively observed that

HONO represented a significant fraction of the measurement that would typically be reported as NO_2 by the chemiluminescent technique. They concluded that previously reported indoor measurements of NO_2 could have been overestimated by a factor of three if these methods are all quantitatively detecting HONO. This recent discovery means that we require more measurements of in-situ indoor environments to accurately characterize the absolute and relative levels of NO, NO_2, and HONO, so that indoor chemical models can be improved for their representation of HONO, particularly allowing us to constrain its importance as an oxidant precursor.

3.1.3 The need for new instrumentation catered to indoor environments

The current suite of instrumentation to measure HONO was developed for outdoor research where these instruments are costly, immobile, and contain hazardous components like toxic dyes, acids, and radioactive ion sources. Examples of instruments used outdoors that cannot be easily used indoors include: the long path absorption photometer (LOPAP) (Heland et al., 2001; Reed et al., 2016; Ren et al., 2010), differential absorption optical spectroscopy (DOAS) (Perner and Platt, 1980; Wojtal et al., 2011) and chemical ionization mass spectroscopy (CIMS) (Collins et al., 2018; Roberts et al., 2010; Vandenboer et al., 2013; Wang et al., 2020a). While safer options are available like denuders or collection by scrubbing in to liquid, these methods are time consuming and labor intensive, requiring extraction and offline analysis by techniques like ion chromatography with conductivity detection, with the resulting data having low time resolution (Place et al., 2018; VandenBoer et al., 2014, 2015; Večeřa et al., 1991). Real-time detection is preferable because it provides the capacity to investigate the formation and fate of HONO at timescales on the order of minutes. This is impossible when relying on a collection medium which integrates observations over long collection periods and has the potential to become saturated. Consequently, new instrumentation that is compatible with the practical requirements of measuring indoors is needed to accurately identify direct emissions and chemical sources of HONO indoors, with safety paramount when working in occupied indoor environments like domestic residences with pets and children.

The new instrument developed in this work exploits a known observational strategy in obtaining accurate and precise data and can be programmed to facilitate easy data processing. The goal is to provide comfort to residents by constructing the instrument from safe and simple components, and therefore incentivize and improve understanding about their quality of indoor living environment.

The benefit of deploying this instrument for research purposes is that it is compact, safe, and quiet so that occupants can carry out their daily activities unobstructed. Measurements of NO, NO_2, and HONO are detected by chemiluminescence which does not require toxic reagent solutions or create any exposure concerns for other hazards. There is ideally no need for daily instrument inspection, maintenance, or removal of chemical waste. Smaller pumps are utilized to minimize waste heat production and they are soundproofed to decrease noise pollution. Electronic components are organized neatly and enclosed in a case for a high level of safety. The automated control of the instrument in particular reduces maintenance and supervision requirements, with a potential goal of being able to service and operate the instrument in full remotely. A user-friendly interface was designed to remove the requirements of a specialized operator, and the controls and measurements are automatically logged into a text file. Collected datasets can be uploaded into an integrated development environment with a custom-script to automate data processing and finalization for quick analysis and visualization. Lastly, the analytical platform is inexpensive, user-friendly, and mobile so that it can perform door-to-door measurements, in addition to being a subset to the total reactive nitrogen (tN_r) instrument that can measure three classes of nitrogenous species.

This new platform is built upon the time-resolved sampling method by Zhou et al. (2018) with an oscillating Teflon three way valve between two pathways to measure HONO using a difference technique and coupling this to a chemiluminescence analyzer. Two pathways contain a bypass channel inserted upstream of the analyzer and a gas denuder channel that scrubs acidic species like HONO and HNO_3 with a sodium carbonate (Na_2CO_3) coating. The chemiluminescence analyzer detects HONO as NO_2 because HONO decomposes on the 325 °C molybdenum (Mo) catalyst (Brauer et al., 1990; Spicer et al., 1994; Villena et al., 2012; Zhou et al., 2018). Our HONO platform integrates calibration quantities of HONO and the addition of a platinum catalyst in the tN_r instrument to provide a second quantitative method (Stockwell et al., 2018). The platinum catalyst allows the instrument to detect total reactive nitrogen by combusting all N-containing gases to NO, which can then be used to determine the fractions of NO, NO_2, and HONO to other fractions or the sum of all nitrogenous species present indoors. Quantifying the fractions of tN_r allows better overall assessment of indoor chemistry as it will limit the use of strategies that simply create secondary species, and directly improving our indoor air quality. Overall, this instrument is an upgraded method to previous works because it contains automated instrumental control,

operation, and datalogging, and the channels are optimized for several novel parameters that have not been attempted before. The instrument provides the best option to date to perform quick, routine analysis of reactive nitrogen chemistry in occupied indoor environments. Using this instrument to survey a large collection of indoor atmospheres, particularly in private homes, will help close the gap on understanding the controls and variability of indoor HONO chemistry. It may influence future new home regulations or provide advice on safer appliance practices to prevent poor indoor air quality.

The new automated HONO instrument was therefore constructed to provide real-time detection of gas-phase of NO, NO_2, and HONO. It was designed to be highly mobile so that it can be deployed in multiple residencies to survey the variability, formation, and fate of NO_x and HONO indoors. A series of experiments need to be performed to optimize the response time (95 – 0 %) by characterizing the inlet and minimizing potential interferences and biases for NO, NO_2, and HONO. These experiments will explore various factors known to promote nitrogen oxide heterogeneous chemistry including: the effects of sampling flow rates; variability in NO, NO_2, and HONO mixing ratios; and relative humidity changes governing surface water availability. Preliminary measurements in two different environments were performed to detect the air pollutants in an indoor laboratory and during a wildfire smoke event outdoors, which were used to identify limitations and allow improvements to the design before deployment in field campaigns (e.g. Chapter 4). The design and control of the instrument will be made open-sourced and widespread for the indoor atmospheric community to encourage more time-resolved measurements at various indoor facilities that have not been explored.

3.2 Method

3.2.1 Instrumental setup of the HONO instrument

The HONO instrument consists of three main components: the data acquisition (DAQ) control box, HONO calibration source, and a modified chemiluminescence detector (NO_x analyzer; Serinus 40, American Ecotech). The schematic overview of the HONO instrument (Figure 3-1) shows the flow pathways that are automated to selectively measure nitrogen oxides (NO_x = NO + NO_2) or HONO by chemiluminescence detection. Throughout this work, the NO_x* route is signified with an asterisk because the catalyst in the analyzer can generate NO from most species in the NO_y family (Dunlea et al., 2007; Joseph and Spicer, 1978). Similarly, NO_2* will represent

the sum of NO_2 and acidic species like HONO and HNO_3. It is important to note that the detected HONO may contain trace levels of HNO_3, but these are typically below the detection limit of the NO_x analyzer in indoor environments (Brauer et al., 1990; Fischer et al., 2003; Vichi et al., 2016) and is explained in more detail in Section 3.2.2.The multiple pathways of the tN_r instrument can be differentiated by two routes, NO_x* and tN_r. The NO_x* route includes both the NO_x/HONO pathway and HONO calibration.

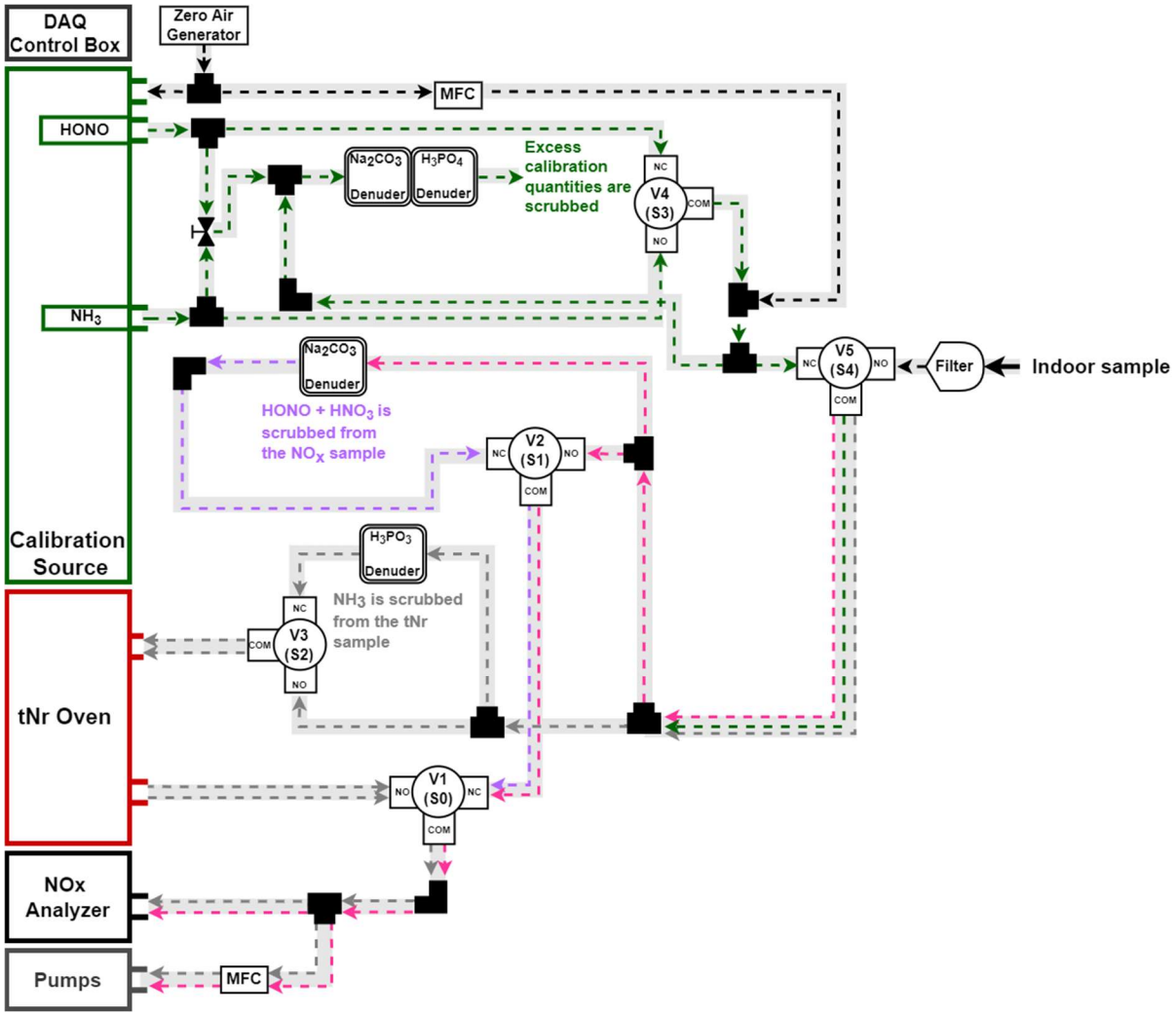

Figure 3-1. Flow schematic of the measurement pathways in the HONO instrument, a component of the tNr instrument. The tN_r instrument has five modules (top to bottom): DAQ control box, calibration source, tN_r oven, NO_x analyzer, and pumps. The solenoid valves are labelled with a "V" and a number. Each has three ports labelled as nominally open (NO), nominally closed (NC), and common (COM). The gas handling fittings are represented by the solid black objects (elbows, tees, and a manual valve for venting excess HONO from the calibration system. The measurement

of NO_x* + HONO (pink dashed lines) takes place in an unaltered transfer of indoor air to the Mo catalyst. The NO_x is measured after the air sample is scrubbed of acidic species (purple dashed lines) such as HONO and HNO_3 by travelling through the Na_2CO_3 denuder (black double-lined square). The on-demand calibration flow of HONO (green dashed lines) allows regular checks of system performance when mixed with a dilution flow of clean zero air (black dashed lines) supplied by an on-board zero air generator and regulated by a mass flow controller (MFC). Excess HONO from the calibration source is scrubbed and the remaining clean air released into the environment. The tN_r route (flows involving the tN_r oven and NH_3 calibration) is not a part of the HONO instrument and its pathways are denoted by the grey dashed arrows.

The frame of the tN_r instrument was constructe from T-slotted framing rails (5537T101, McMaster Carr, Aurora, OH, U.S.A) to form a standard 19-inch rack (length x width x height is 8 x 53 x 175 cm) to mount the five modules (Fig. 3-2). Three modules (DAQ control box, HONO calibration source, and tN_r oven) are enclosed in separate black 19" rack-mounted cases (RMCV190713BK1, Hammond Manufacturing, Geulph, ON, Canada). The instrument requires an electrical outlet capable of providing 110 V AC and 20 A, which is commonly used for indoor heavy-duty appliances and such outlets should be located in kitchens or laundry rooms. Two outlet strips are mounted vertically to the rack, one outlet strip has a NEMA 5-20 plug (71515K34, McMaster Carr, Aurora, OH, U.S.A) and the other has a NEMA 5-15 layout (7181K45, McMaster Carr, Aurora, OH, U.S.A).

Details of the electronics and wiring for the DAQ control box are provided in Appendix B, Fig. 3-S1. The components and construction of the HONO calibration source is provided in the Supplemental Information by Lao et al., (2020) (Appendix A, 2.S1). The zero-air generator provides gas flow through the HONO calibration source and also dilutes the generated HONO to adjust its calibration quantities based on the environment and expected range of measured HONO levels. The zero-air generator was custom-built, consisting of a small pump, water filter (¼" NPT, AFR-2000, SPK603, Thailand), membrane air dryer (IDG1-N02, Proax Technologies Ltd, Oakville, ON, Canada), and cartridges (400 cc, ¼" fitting, Indicating Moisture Trap, Chromatographic Specialties Inc.) filled with a mixture of molecular media (CP Blend, Purakol, Purafil Inc., Doraville, GA, U.S.A) to remove trace gases like NO_x, ammonia (NH_3), ozone (O3), water, and volatile organic compounds (VOCs). The mass flow controllers (MFC; MKS Instruments, Inc.) control the diluent zero air flow for HONO calibrations as well as the sample

flow out of the system via a pump to sample at a higher rate to improve the response time. To increase or decrease the flow rate of zero air for background/blank measurements in addition to diluting calibration gases, the flow through MFC1 was modified. The purpose of MFC2 is to allow an additional diaphragm vacuum pump to pull additional sample flow through the system and improve the response time of the system by minimizing the residence time of analytes in the inlet. This is particularly important for sticky compounds that adsorb readily onto surfaces like NH_3, which is a part of the tN_r pathway, but also for reducing NO2 heterogeneous hydrolysis to HONO on the inlet.

The sampling inlet consists of ¼" perfluoroalkoxy alkane (PFA) tubing (51805K72, McMaster Carr, Aurora, OH, U.S.A) and a polytetrafluoroethylene (PTFE) filter in a holder assembly (47 mm single-stage, ¼" x ¼" PFA Clamp, Savillex, Eden Prairie, MN, U.S.A) which is attached to the sample inlet to remove particles. Throughout the system, the minimized amount of PFA tubing is directed by ¼" PFA tees and elbows (PFA-420-3, PFA-420-9, Swagelok, Mississauga, ON, Canada). Gaseous compounds are diverted into different branches of the inlet as they enter the three-way ¼" solenoid valves (12V DC, Galtek®, Chaska, MN, U.S.A) by either the NO or NC port and exit through the COM port to reach the NO_x analyzer. Annular denuders (URG-2000-30x150-3CSS, URG Corporation, Carrboro, NC, U.S.A) selectively scrubs nitrogenous species based on its coating solution, as described below. Instrument noise is reduced by installing mufflers (4450K3, ¼" NPT Male Steel Fitting, McMaster Carr) on the pumps (GAST, Cole-Parmer Canada) and enclosing them in shelving lined with adhesive acoustic insulation (5692T26, 90 % Adhesive Backing Polyurethane foam, McMaster Carr, Aurora, OH, U.S.A) on top of custom-cut polycarbonate sheets (8707K134, McMaster Carr, Aurora, OH, U.S.A).

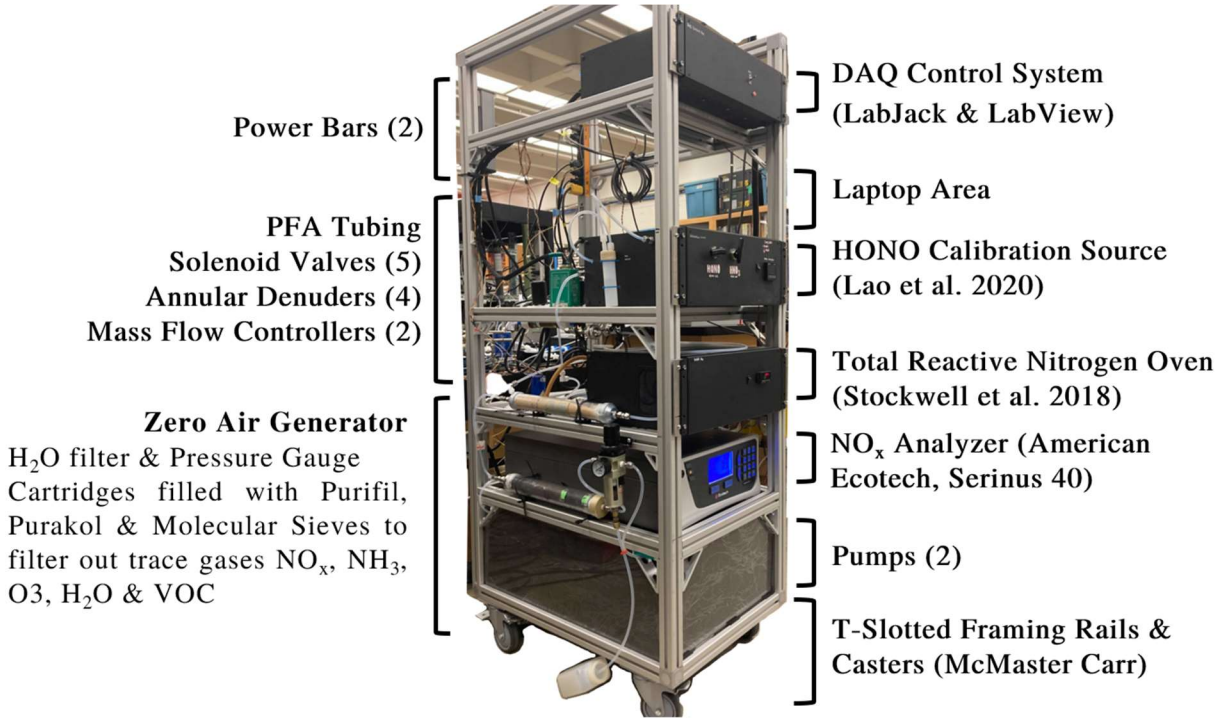

Figure 3-2. Diagram of the tN_r instrument. The T-slotted framing rails have continuous slots for additional fittings such as sensors, handles, and other accessories. The framing rails are buildable for future installation of additional instruments and casters were added for mobility.

3.2.2 Quantification of NO_x and HONO by differential measurement and chemiluminescence detection

The instrument relies on three important alternating pathways controlled by solenoid valves to selectively measure various nitrogenous species. First, the air sample is passed through the filter to remove particle-bound N_r and enters Valve 5 (V5, in Fig 3-1). Valve 5 can be switched to alternatively provide calibration measurements of HONO to the system. Valve 2 (V2 in Fig 3-1) switches between the measurements of NO_x + HONO or NO_x as a Na_2CO_3 denuder scrubs acidic N_r like HONO (R5) and HNO_3 (denoted as NO_x). The Na_2CO_3 denuder was prepared according to the EPA Compendium Method IO-4.2 (Winberry et al., 1999) to remove strong atmospheric acids by the reactive uptake of the basic coating. This scrubbing technique has been previously applied for indoor sampling and quantification of HONO (Brauer et al., 1990; Febo et al., 1993a; Zhou et al., 2018). Lastly, Valve 1 switches between the sample transported and processed by the NO_x route or tN_r route before reaching the NO_x analyzer for measurement of the gas composition.

$$\mathbf{2\ HONO_{(g)} + Na_2CO_{3(s)} \rightarrow 2\ NaNO_{2(s)} + H_2O_{(g)} + CO_{2(g)}} \qquad \mathbf{(R5)}$$

The commercially available NO_x analyzer provides continuous measurements of NO, NO_2*, and NO_x at a range of 0-20 parts per million by volume (ppmv) with a detection limit of 0.4 ppbv. This NO_x analyzer contains two alternating pathways to measure NO and NO_x, in which the NO_x pathway converts NO_2* to NO on a heated Mo catalytic converter (325 °C). We can utilize the NO_x pathway to measure HONO indirectly because the Mo catalyst can convert additional NO_y species to NO (HONO, NO_3, N_2O_5, HNO_3, HO_2NO_2, and organic nitrates, as observed from outdoor measurements) (Dunlea et al., 2007). Our previous work determined that this analyzer has a HONO conversion efficiency of 104 ± 4 % (Lao et al., 2020). The detection limit of HONO was determined by using Equation 1 (E1) which is the sum of squares error propagation of addition/subtraction (1). The detection of HONO relies on the NO_2 channel of the NO_x analyzer, in which the analyzer determines NO_2 by the difference of measured NO_x and NO. Blank measurements were performed using zero air to find the noise of both NO_x and NO, allowing calculation of the HONO detection limit for the NO_x analyzer. It was found to be 0.60 ppbv for 1 minute time resolution measurements.

$$\sigma_{HONO} = \sqrt{\sigma_{NOx}^2 + \sigma_{NO}^2} \quad \textbf{(E1)}$$

To quantify HONO, the measurements obtained from the alternating pathways of V2 can be calculated using E2. The NO_2* that passes through the Na_2CO_3 denuder (NO_2) will decrease proportionally to the amount of HONO scrubbed. Therefore, the HONO mixing ratio can be determined by difference when compared to the measurement of NO_2^* Although the Na_2CO_3 denuder can scrub HNO_3, it has been previously reported that negligible levels of HNO_3 are found indoors, likely due to rapid surface loss (Brauer et al., 1990; Fischer et al., 2003; Vichi et al., 2016). Vichi et al., (2016) observed HNO_3 of ~0.2 ppb in libraries, which is a factor of 25 times lower than average indoor measurements of ~5 ppb HONO (Collins et al., 2018; Zhou et al., 2018). These reported HNO_3 values indoors are less than the detection limit of the analyzer (0.60 ppb. This allows us to measure indoor HONO without the concern of interferences of other NO_y species because majority of them have insignificant levels indoors and consequently, HONO is one of the main species converted on the Mo converter.

$$\textbf{HONO} = \textbf{NO}_2\textbf{*} - \textbf{NO}_2 \quad \textbf{(E2)}$$

3.2.3 Calibrations checks of NO, NO_2 and HONO

A custom-built calibration source, described in detail by Lao et al. 2020 (Chapter 2) was installed in the instrument to perform routine calibration checks of measured HONO for drift. Briefly, the calibration source generates HONO mixing ratios in the low ppbv range by an acid displacement reaction. Gas-phase HONO is generated by passing zero air over a hydrochloric acid (HCl) permeation device (PD) to combine with humid air which enters a sodium nitrite ($NaNO_2$) reaction device at a total flow of ~110 cubic centimeters per minute (ccm) (R6). The calibration source has a high purity of 90-99 % HONO, with impurities being at most 10 % NO and/or NO_2. In this work, HONO mixing ratios of up to 20 ppbv were generated by inserting a custom-made HCl PD (12 M HCl in ¼" OD tubing) and two $NaNO_2$ reaction devices in an oven at 40 °C. The HONO mixing ratio output can be adjusted by adding a diluent flow of zero air. Typically, the minimum dilution flow was at least 1.0 liters per minute (LPM).

$$\mathbf{HCl_{(g)} + NaNO_{2(s)} \rightarrow HONO_{(g)} + NaCl_{(s)}} \qquad \mathbf{(R6)}$$

The NO_x analyzer is calibrated every 6 months and before a field campaign to ensure the detection and response of NO_x does not drift after prolong instrument use in its operating range (manufacturer specifications range of 0 – 20 ppm). A gas-calibration instrument (Gascal 1100TS, American Ecotech, Warren, RI, USA) is used to perform multi-point calibration checks of NO and NO_2 from 0 – 80 ppb by using a standard gas cylinder of NO (NI NO5MC-A3, NI NO2.85MZ2NAS, Praxair) to conduct gas titrations to generate NO_2 by reacting with O_3. Zero checks are performed by flushing the analyzer with zero air at 3000 sccm to perform a blank measurement to identify any bias or leaks are present in the system. The NO_2 to NO converter efficiency of the instrument is always calculated to ensure its response is linear in changes of NO and NO_2 mixing ratio and meet the specifications of the manufacturer within 96 %.

3.2.4 DAQ control, operation, and data processing

The DAQ device (T7 and PS12DC, LabJack, Lakewood, CO, USA) allows automated control of the solenoid valves and mass flow controllers when paired with additional power supplies. The DAQ device acts as an interface between a custom graphical computer program (LabVIEW, National Instruments, Austin, TX, USA) and acts as an analog-to-digital converter. The electronic layout and wiring diagram of the DAQ control system is presented in detail in Appendix B, Fig.

3-S1. A custom LabVIEW script was written to implement supervisory control and data acquisition on this instrument. The program automatically logs: the date and time; switching of solenoid valves according to timed intervals; analog output of the measurements from the NO_x analyzer; and MFC flow rates into a single text file. The design of the user interface (Fig. 3-3) allows the manual modification of each valve state and MFC. The timed intervals for switching the valve states can be adjusted in minutes to increase or decrease the time resolution of each sampling pathway, and the overall time resolution of the tNr instrument. The MFC control is independent of the valve controls. There are two MFCs operated by the software (Fig. 3-3). The software and data collection was designed to be user-friendly and discussed further in Section 3.3.1.1 All data and timeseries were processed using the software, IGOR Pro 8.04 (WaveMetrics Inc., Portland, OR, USA). The first 5 points of data (12 s averages) are rejected after each valve change to ensure accuracy and precision.

3.2.5 Instrument characterization experiments

3.2.5.1 Response time

To build an accurate real-time gas detection instrument, the instrument response time to changes between flow rate, analyte concentration, and sampling channel under conditions relevant to those commonly found in indoor environments must be characterized. All experiments are carried out by first overflowing the instrument inlet with zero air to observe any initial offset. The nitrogenous species of interest (NO, NO_2, and HONO) at known mixing ratios ranging from ~17 – 20 ppbv are introduced into the inlet with a PTFE three-way ball valve. Once the calibration source outputs a stable quantity of the target compound, it is turned off to initiate a decay to zero. These experiments were repeated at different inlet flow rates ranging from 630 – 2000 ccm to observe if the response time is quicker when decreasing the residence time of the target compound in the inlet. The NO_x analyzer requires a sample flow rate of 630 ccm, so to obtain experimental inlet flow rates >630 ccm a second MFC was utilized to allow higher flow through the inlet. The response time of HONO at concentrations ranging from 2 – 20 ppbv were tested at 630 ccm to observe if the analyte increases in residence time when the concentration increases. Lastly, the response time between two sampling channels of NO_x* and NO_x were determined by observing how long the Na_2CO_3 denuder scrubs HONO. All response times (95 – 0 %) were determined by exponential fit from

the stable initial mixing ratio via its decay to background levels or zero as shown in E3 (Moravek et al., 2019).

$$\boldsymbol{f(t) = y_0 + A_1 \cdot exp\left(\frac{-(t-t_0)}{\tau_1}\right) + A_2 \cdot exp\left(\frac{-(t-t_0)}{\tau_2}\right)} \quad \textbf{(E3)}$$

Where y_0 represents the offset from zero, A_1 and A_2 are the proportionality coefficients for the physical processes of sample volume exchange in the inlet and reaction cell, and wall interactions, respectively. The time response of the two processes is represented by tau (τ) and the start time of the addition of zero air is represented by t_0. In addition, the relative importance of each process can be described as D in E4 (Ellis et al., 2010).

$$\boldsymbol{D = \left(\frac{A_2}{A_1 + A_2}\right)} \quad \textbf{(E4)}$$

When determining the response time for NO, NO_2, and HONO, the wall interactions were found to be insignificant, and a single exponential fit was used. This was confirmed by calculation of D using E4 which was compared with the calculated time responses by double exponential fit. All time responses were multiplied by 4 (i.e. 4τ) to determine the 98 – 0% decay (Pape et al., 2009).

3.2.5.2 Testing the efficacy and bias of Na_2CO_3 denuders

Scrubbing efficacy of HONO by the Na_2CO_3 denuder was determined by delivering a mixture of zero air and HONO from the calibration source to achieve a stable output of 3.8 ppbv and 14.4 ppbv into the sampling inlet. The HONO mixture bypasses the denuder (NO_x* pathway) to determine the calibration source output. The valve is then switched using the software to direct the flow through the Na_2CO_3 denuder to quantify the fraction of HONO lost due to reaction on the carbonate coating. The experiment was repeated with standard NO of 17.88 ppbv (4.88 ppmv, NI NO5MC-A3, Praxair, Toronto ON, CA) and 17.29 ppbv NO_2 to determine any losses or transformations of these gases when interacting with the denuder. The NO_2 mixing ratio was generated by a standardized amount NO reacting with excess O_3 generated in a gas calibration instrument (Gascal 1100TD, American Ecotech, Warren, RI).

The sampling inlet was also investigated for positive biases such as HONO formation via the surface hydrolysis reaction of NO_2. The sampling inlet was supplied with a diluted mixture of standardized NO_2 (5.9 ppmv, NI NX5MC-A3, Lynde Canada Inc., Toronto, ON, CA) in zero air

(flow of 0.5 LPM). Humidified air to acheive 40 – 50 % relative humidity (RH, flow of 0.5 LPM) was mixed with the diluted NO_2 as a representative indoor range for RH. The flow of standardized NO_2 was adjusted to increase or decrease its mixing ratios across the range from 25 – 300 ppb to capture any concentration dependencies. The humidified air and NO_2 mixture was measured for at least 15 min before sending it through the Na_2CO_3-coated denuder to quantify any inlet-derived HONO produced.

3.2.6 Setup and location for preliminary measurements

3.2.6.1 Indoor measurements in a chemistry laboratory

Indoor laboratory measurements were performed to test if the tN_r instrument was satisfactorily operational for future deployment. The chemistry laboratory is located in a university building in Toronto, Ontario, Canada. Researchers typically come and go into this workspace from 8:00 – 18:00 conducting their individual experiments. The size of the laboratory was approximately 15 m x 8 m x 2.5 m with a fume hood near the position of the instrument. The instrument was positioned close to the center of the room. Indoor measurements were logged on a weeknight from September 23, 2020, to September 24, 2020. The intervals of the valve states were set to change every 20 min between the NO_x* and tN_r pathway with 5 min modulations between paths with no denuder or denuder.

3.2.6.2 Outdoor plume measurements from a chemistry laboratory

The tN_r instrument was deployed at a university building in Toronto, Ontario, Canada to measure transported biomass burning plumes from northern Ontario fires on the night of July 20th, 2021. The tN_r instrument was deployed in a laboratory with connection to outdoor air via a sampling port. The outdoor port was a long high flow tube tunnel with 20.3 cfm sample flow governed by a blower fan (Fig. 3-S2). The sample inlet of the tN_r instrument was attached to a sampling plenum on the high flow tubing. The sampling plenum consisted of an array of stainless steel and brass Swagelok fittings. The sampling plenum has not been utilized for an extended period of time and measurements were initiated shortly after turning on the blower fan. The instrument was programed to measure each inlet flow pathway for 5 minutes (10 min intervals between NO_x* and tN_r, and 5 min cycling with denuders).

3.3 Results and Discussion

3.3.1 Instrument operation

3.3.1.1 Rationale for the design of the user interface

The graphical user interface of the tN_r instrument was designed to be user-friendly and provide an open-sourced script of the supervisory control and data acquisition modules. The current interface (left to right, Fig. 3-3) has panels for calibration and diagnostics, valve states, NO, NO_2, and NO_x measurements, and MFC. The calibration and diagnostics panel is for future use after automating calibration quantities of $HONO/NH_3$ and adding another solenoid valve into the current setup. In this work, the calibration quantities were controlled by a manual valve due to time constraints and a limited number of available solenoids. The purpose of the diagnostics is to alert the user of any technical errors in the program execution. The middle panel for valve states displays the time interval (min) for modulating the three solenoid valves. Labels for each measurement pathway is adjacent to show which nitrogenous species are detected. The valve loops and total running time of the program are displayed to allow visual confirmation of the instrument setup prior to operation, and to confirm the impact of any changes. The amplitude versus time graph shows the state of each solenoid change during real-time monitoring. The program logs the valve state of the initial position as "0" and when it switches as "1" for easy flagging and automation of data processing. Our instrument relies on detecting nitrogenous species via these valve controls, so these visualizations gives us confirmation that instrument is operating according to specifications. The right panel displays the real-time measurements of nitrogenous species from the NO_x analyzer and the flowrates being regulated by the two MFCs. The MFC max flow (ccm) is entered first, then the setpoint is designated, in order to accurately control the flow rates of the inlet and calibration lines.

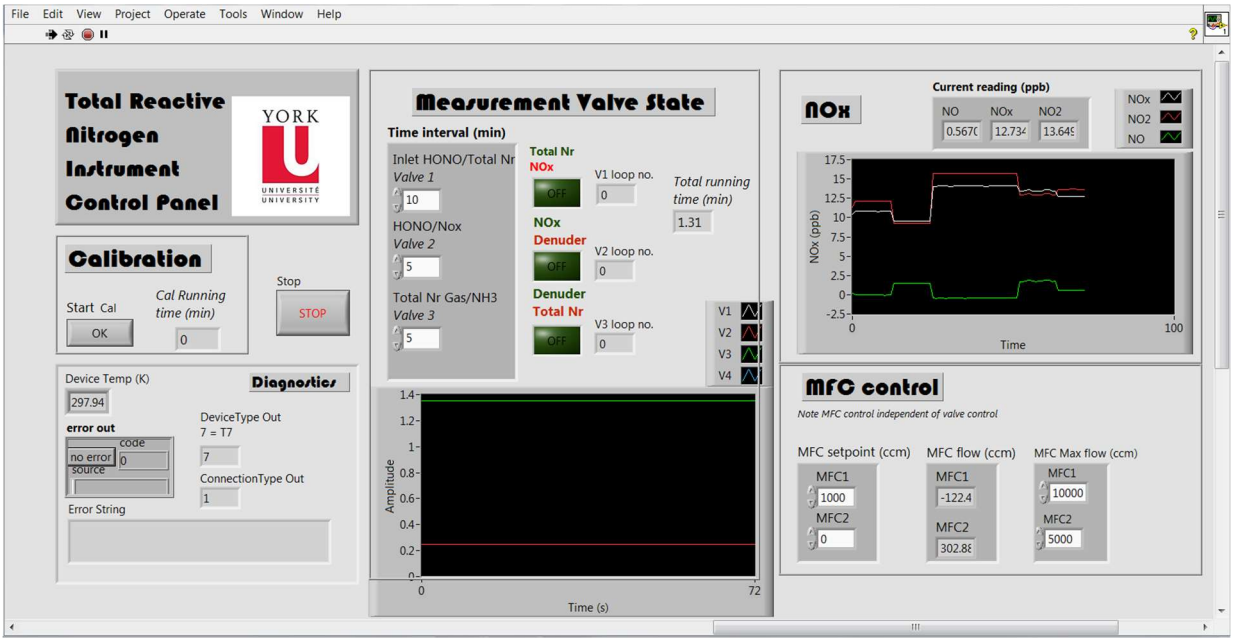

Figure 3-3. The front window of the custom-LabVIEW program to set automation controls over the various inlet channels of the tN_r instrument.

3.3.2 Instrument characterization

All measurements in this section are averaged from 1 s measurements of the analog voltage output from the NOx analyzer, which was then converted to mixing ratio in ppbv and averaged to a 12 s timebase.

3.3.2.1 Time Response Experiments of NO, NO_2, and HONO

The response times for NO, NO_2, and HONO were found to be similar at approximately 1 min when sampling with the baseline instrument flow of 630 ccm (Table 3-1). The response times calculated from these experiments used a single exponential fit (98 – 0 %). A comparison of single and double exponential fits was also made (Table 3-S1), but this analysis found that both tau values were similar. Investigation of this result determined that the D (%) value representing the wall interactions of NO, NO_2, and HONO were all similar, indicating that they undergo indistinguishable and minimal physical interactions with the inlet surfaces in the instrument.

Table 3-1. Time response (98-0 %) of the HONO instrument at a flow of 630 ccm and calculated by a single exponential fit for NO, NO_2, and HONO

Nr species	$\tau_{98\text{-}0\ \%}$ (min) (n=3)	Input mixing ratios (ppbv)
NO	1.09 ± 0.09	17.88 ± 0.81
NO_2	0.54 ± 0.06	17.60 ± 1.05
HONO	0.99 ± 0.11	20.23 ± 1.06

The response time experiments were repeated at different flow rates for NO, NO_2, and HONO and found to be independent of the instrument flow rate from 630-2000 ccm (Fig 3-4a). The linear trend of NO and NO_2 had slopes of -2.99×10^{-4} ppbv and 4.67×10^{-5} ppbv. For HONO the time response was also independent of instrument flow rate and mixing ratio (Fig 3-4bc), displaying no linear trends as all calculated regression slopes were within a value of zero when considering the uncertainties ($-3.79 \times 10^{-4} \pm 5.93 \times 10^{-4}$ ppbv). All three compounds demonstrating the same ≤1 min response times indicated that the instrument was likely limited by the inlet air exchange as well as that of the NO_x analyzer, inclusive of the instrument response time. The increased sample flow had no effect on NO, NO_2, and HONO response rates, indicating that these species do not readily adsorb onto the PFA inlet surfaces (VandenBoer et al., 2013). Similarly, increased mixing ratios of HONO did not affect the response time, demonstrating that there was no buildup of HONO (-0.007 ± 0.026 ppbv) on surfaces by adsorption on the sampling lines, making the response independent of HONO mixing ratio.

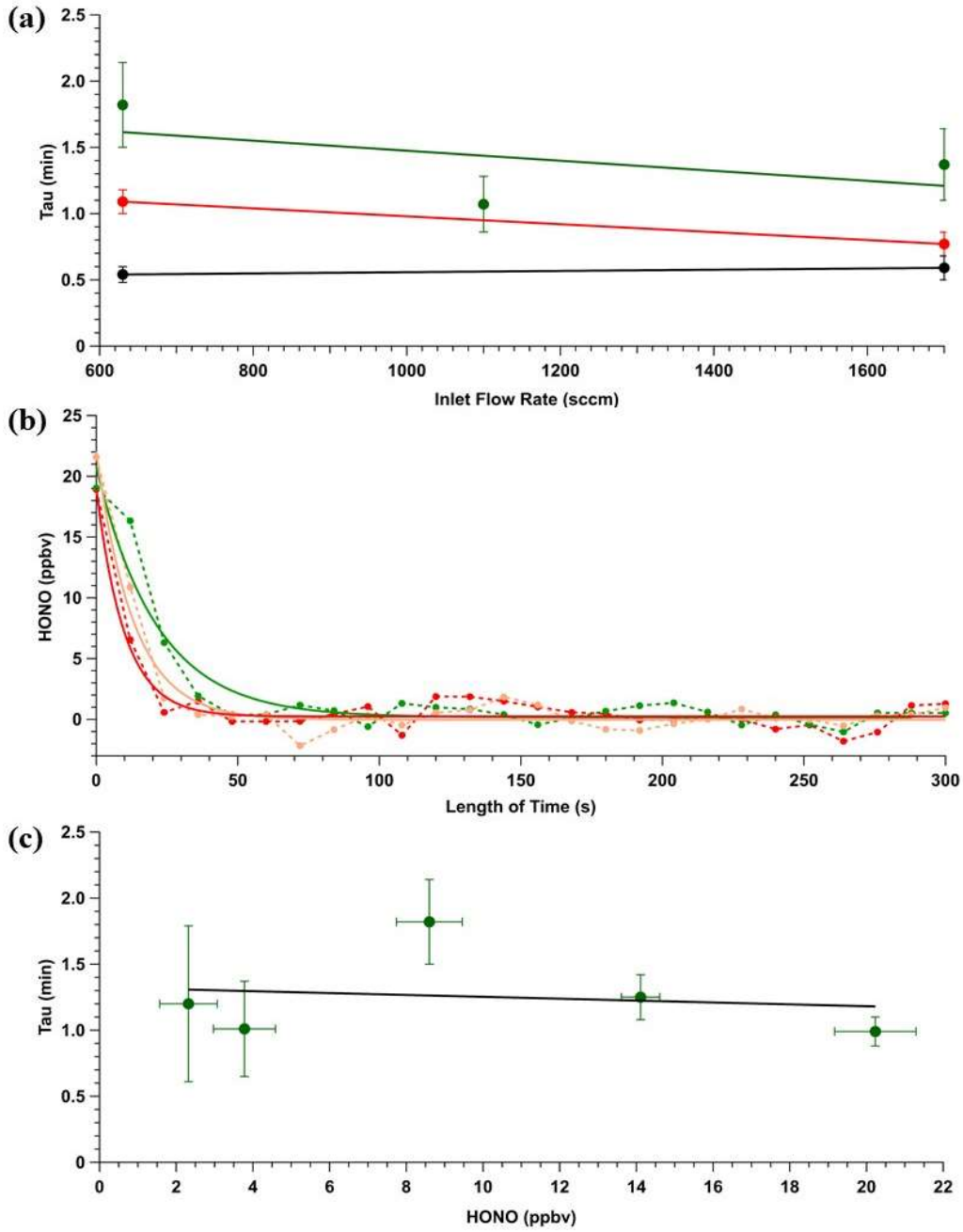

Figure 3-4. (a) Response time experiments at various flow rates for NO (red), NO_2 (black), and HONO (green) with their linear trends **(b)** Response time plot of HONO to zero at 630 ccm (12 s averages). The circles represent HONO measurements and their exponential decay (95 – 0 %). Each colored circle and line represents a response time experiment **(c)** Response time plot of averaged experiments (n=3) against various HONO mixing ratios at 630 ccm. The green circles represent the averaged HONO output ranging from ~2-20 ppbv. The weighted line of best fit (black) suggests the response time of HONO lies within 1 min regardless of a change in HONO mixing ratio sampled (slope = -0.007 ± 0.026 ppbv).

3.3.2.2 Response time and efficacy of Na_2CO_3 annular denuders

The response time and efficacy for the Na_2CO_3 denuder to scrub HONO were determined experimentally and are summarized in Table 3-2. The response time to scrub HONO by the denuder was calculated to be 1 min. Like the instrument response time for NO, NO_2, and HONO, the denuder response time is limited by the response of the inlet air exchange and NO_x analyzer. The scrubbing efficiencies of HONO were tested at two atmospherically relevant mixing ratios for indoor air: 14.4 ppbv and 3.8 ppbv. The fraction captured was observed to be greater than 99.6 % (Fig. 3-5). A stable mixture of NO and NO_2 (17.88 ± 0.81 ppbv and 17.29 ± 1.06 ppbv, respectively) was sent through the denuder (Fig. 3-S3 and Fig. 3-S4) to ensure that no significant adsorption or chemical loss of NO_x occurs on the surfaces of the denuder or its coating. The stable mixing ratio of NO was inserted into the sampling inlet and its flow switched between the two pathways with no denuder (NO_x*) and with the denuder (NO_x) to observe any decrease in the mixing ratio (flow paths denoted by pink and purple arrows, respectively, in Fig. 3-1). There was no decrease in NO when it transited the denuder and a slope of zero was observed in the timeseries that included this modulation ($-7.66 \times 10^{-5} \pm 7.52 \times 10^{-5}$ ppbv). The data of NO bypassing and entering the denuder were compiled into two datasets to apply a two-tailed t-test to confirm that the NO mixing ratios were not statistically different with a p-value of 0.02 (less than 0.05). The same experiment was carried out with the 17.29 ± 1.06 ppbv of NO_2 to observe similar results, but with a small 2 % decrease of NO_2 (16.96 ± 1.2 ppbv), likely due to chemical loss to the coating and/or surface of the denuder. The 2 % loss of NO_2 to the denuder will be considered when quantifying the mixing ratio of HONO. Previous studies have observed loss of NO_2 to carbonate denuders (Monge et al., 2010; Zhou et al., 2018). Zhou et al. (2018) reported an averaged decrease of 2.6 % NO_2 after flowing 13 – 270 ppbv into the denuder, which was similar to our findings. Like NO, the data of NO_2 bypassing and entering the denuder were compiled into two datasets to apply a two-tailed t-test to find a p-value of 0.13, which was greater than 0.05. This means that the there was a small significant loss of NO_2 when passing through the denuder, which can be easily corrected by implementing into the data processing code in the future. These measurements lends confidence that the instrument measurements are capable of quantifying the true value of indoor NO, NO_2, and HONO.

Table 3-2. Time response and efficacy of Na_2CO_3 annular denuders in scrubbing HONO and testing the percent loss of NO and NO_2 to Na_2CO_3 denuders at 630 ccm. N/A = means not applicable and n = number of experiments.

Species	Response time (min)	Input mixing ratio (ppbv)	After denuder (ppbv)	% Decrease
NO (n=3)	N/A	17.88 ± 0.81	17.88 ± 0.95	0.0
NO_2 (n=3)	N/A	17.29 ± 1.06	16.96 ± 1.20	2.0
HONO (n=3)	1.02 ± 0.16	14.38 ± 0.95	0.06 ± 0.71	99.6
HONO (n=4)	1.01 ± 0.36	3.78 ± 0.78	-0.62 ± 0.61	99.8

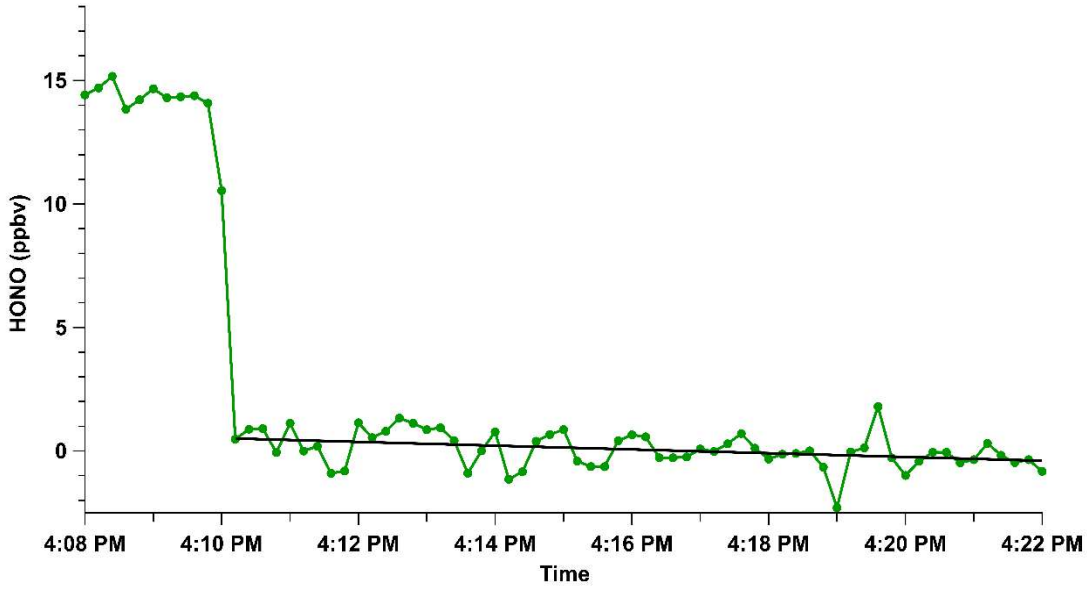

Figure 3-5. Delivery of HONO at 14.4 ppbv into the Na_2CO_3 denuder showing the rate of its decrease to zero and a slope of $-1.27 \times 10^{-3} \pm 4.32 \times 10^{-4}$ ppbv.

3.3.2.3 Testing for a positive bias in the sampling inlet

Table 3-3 demonstrates a very small positive bias of HONO formed in the sampling line when exposed to a mixture of humid air and NO_2, with the conversion ranging from 0.9-2.9 %, which is less than the instrument precision at 5 %. The range of RH tested in these experiments from 42 - 50.0% are representative of typical indoor RH. Mixing ratios of NO_2 up to 300 ppb were representative of NO_2 observed to be emitted indoors from combustion processes like cooking with a gas stove (Mullen et al., 2016; Park et al., 2008; Singer et al., 2017; Zhou et al., 2018). The

percent HONO formed was calculated by measuring the NO_2 signal difference between the input mixture and after it was scrubbed by a Na_2CO_3 denuder. A PTFE filter, PFA valves and tubing are positioned upstream of the denuder, representing about 33 % of the geometric surface area of the inlet, while the NO_x analyzer and a larger fraction of PFA valves and inlets are positioned downstream. PFA material was chosen because it is one of the most chemically insert materials in comparison to others, such as glass inlets that can result in the strong production of positive artifacts (Zhou et al., 2002). The small loss of 2.9 % of NO_2 to the Na_2CO_3 coating The small loss of 2.9 % of NO_2 to the Na_2CO_3 coating is likely resulted from the heterogenous HONO formation by NO_2 hydrolysis on the sampling lines upstream of the denuder when 24.0 ± 0.6 ppb NO_2 is mixed with humid air inserted into the instrument sampling inlet. Similarly, experiments in Section 3.3.2.2 displayed a 2 % loss of NO_2 at 17.29 ± 1.06 ppb, which can potentially result in a total of 5 % positive bias in our HONO measurements. This positive bias was not corrected in our proof-of-concept work presented in Section 3.3.3 as the artefact is within the precision of the instrument. However, this simple correction will be applied in future work. Overall, a total of 5 % of NO_2 can potentially be lost within the sampling line by the surface reaction of NO_2 under typical RH conditions for indoor air, and the 5 % decreases in NO_2 observed were just as probable to have been driven by instrument drift and/or noise.

Table 3-3. Percent difference of the mixture of NO_2 and humid air scrubbed by the Na_2CO_3 denuder at 630 ccm

NO_2 (ppbv)	**RH (%)**	**Input NO_2 and humid air mixture (ppbv)**	**After denuder (ppbv)**	**% Difference**
25	50.0	24.0 ± 0.6	23.3 ± 0.6	2.9
50	49.5	51.9 ± 0.8	50.1 ± 0.8	1.0
100	41.5	107.1 ± 1.2	105.3 ± 1.3	1.6
200	50.0	206.4 ± 1.4	204.6 ± 1.9	0.9
300	49.5	305.2 ± 1.8	301.6 ± 2.1	1.2

3.3.3 Preliminary instrument operation

In this section, preliminary measurements were performed to test the operation and identify the practical limitations of the instrument. The goal was to observe any technical, operational, or logical errors in using the instrument and to fix these problems before deploying if for a 3-week indoor campaign (see Chapter 4 of this thesis).

3.3.3.1 System checks and start up tests

Technical and operational tests were performed to conclude that the instrument was ready for use. The first check was to confirm the input and output communication between the DAQ control box and user interface was functional. This was done by using a custom-script to control each valve state manually as these controls are necessary for quantifying NO_2*, NO_2, and HONO. The solenoid will make an audible sound when switching positions to redirect a flow. The closed valves were confirmed to have a flow rate of zero. A flowmeter (Gilian Gilibrator-2 Calibrator, Sensidyne LP, St. Petersbury, FL, USA) confirmed that the flowrate of the MFC setpoint was within 5 % of the desired output. The design of the calibration pathway (green arrows on Fig. 3-1) allows the release of excess calibration gas flow through an exhaust port to prevent pressure buildup or leaks. Before deployment, a blank measurement is always performed with zero air to ensure there are no interferences when performing calibrations or measurements. These blank measurements can also be used to identify system leaks or contamination if the measurements are not zero. A second indicator to confirm that the instrument has no leaks is performed by using the flowmeter to measure that the sample inlet pulls 0.63 LPM when only sampling with the NO_x analyzer and confirming this by modulating the sample flow through each pathway. The HONO calibration source requires ~3 hours to warm up and generate a stable output for calibrating the instrument (Lao et al., 2020). The HONO calibration gas is sent to the Na_2CO_3 denuder to confirm its scrubbing efficacy is quantitative. Instrument operations were tested by measuring continuously for up to 7 days to see if the software crashes, electronics overheat, or if there are unexpected shutdowns. The instrument and LabView program ran successfully without crashing. Data collected from the automated inlet and instrument operation was graphed to confirm that the valve states changed within the specified time intervals for each pathway.

Both positive and negative control experiments were performed to determine how fast the instrument measurements reflected the switch between different pathways, so data processing

methodologies could be determined. In the positive control experiment (Fig. 3-4a) a known mixing ratio of NO (45.5 ± 1.2 ppbv) was introduced into the sample inlet, modulating a solenoid, and then observing the time required to obtain the initial mixing ratio measurement from the instrument within deviation (45.2 ± 0.8 ppbv). The results from actuating all of the solenoid values showed the NO signal remaining stable throughout the various valve changes and tubing where each valve state in Fig. 3-4a show similar mixing ratios within an error of one standard deviation (pink 46.48 ± 1.19 ppbv, green 46.84 ± 1.33 ppbv, blue 46.10 ± 0.65 ppbv, switched back to green 45.83 ± 0.90 ppbv and purple 45.04 ± 0.98 ppbv). Each valve change was compared to the initial input of NO (pink region) to confirm that the NO mixing ratio is statistically identical after NO enters a different pathway with all p-values less than 0.05. The stability of the NO confirms i) there are no leaks within the system and ii) the valves are reliable for continuous measurements as the instrument signal was unperturbed. The time to switch between the NO_x* and tN_r pathway was therefore set to only discard 1 minute of measurements (i.e. a single measurement) because the instrument control and flow redirection was found to be faster than the inlet time response for the analytes. In the negative control experiment the time for the instrument to reach zero in the NO_x* pathway was determined (Fig 3-4b). A mixing ratio of 45.0 ppbv of NO was added to the sample inlet, allowed to establish a stable signal, and then flushed with zero air. The instrument was found to reach a reading equivalent to zero within 3 minutes. The same experiment was conducted with NO passed through the Na_2CO_3 denuder and observing the same instrument response of 3 min. At this time, we were limited to 1 minute time resolution of the data generated from the American Ecotech software, Airodis. These experiments provided the insight that the instrument response time might actually be better than what was measured and convinced us to characterize the sample inlet further as it would be advantageous to seek faster measurements. Improvements to instrument time resolution were achieved by integrating the analog output of the photodetector from the NO_x analyzer directly into our LabVIEW script, yielding 1 second measurements. The analog input of the NO_x analyzer was connected to the DAQ control board, where our LabVIEW script logs the voltage output, corrects for a zero offset of 0.25 V, and converts the voltages to mixing ratios in ppbv using an appropriate transfer function. The integration of the date, time, and mixing ratio measurements of the NO_x analyzer improved in response time from 3 min to 1 min, which is discussed further in Section 3.3.3.2.

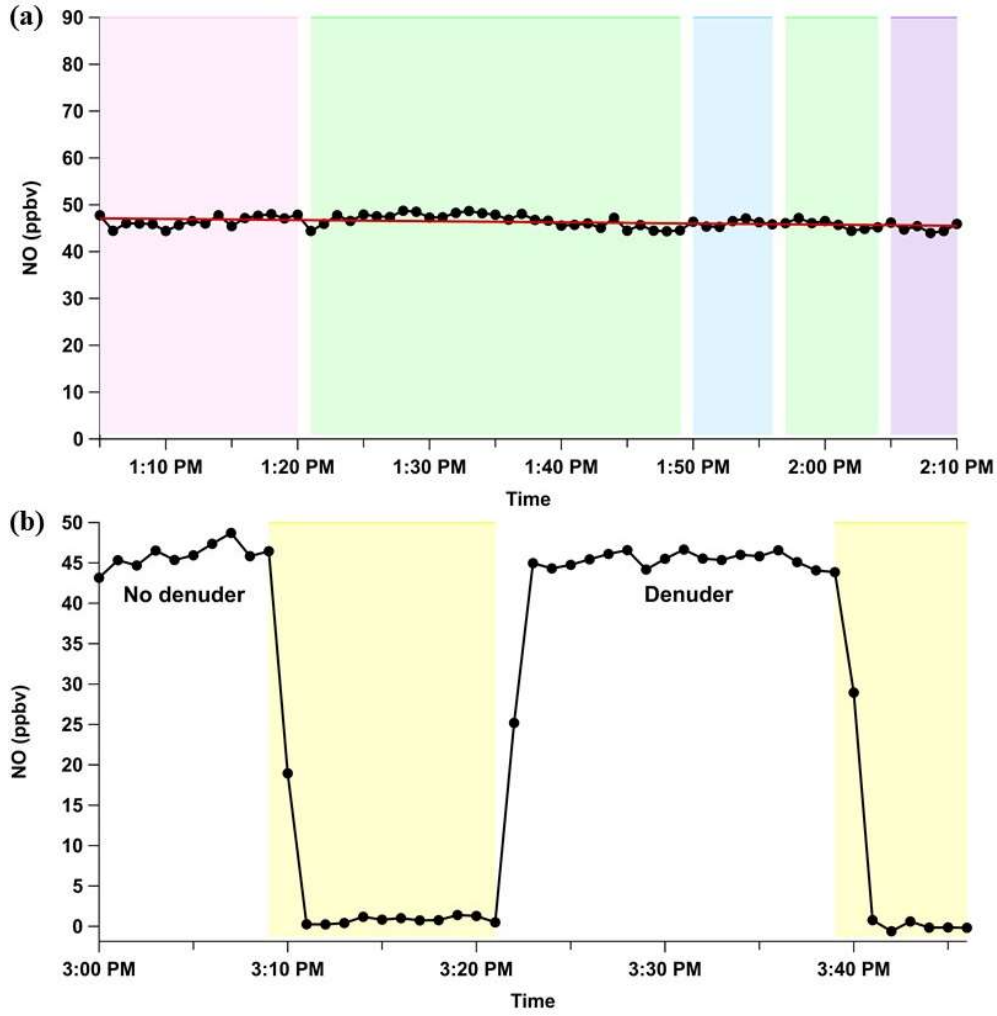

Figure 3-6. (a) A positive control experiment of flushing the sampling inlet with 46.5 ppb NO to observe any losses that occurred when NO was travelling through inlet different pathways. The mixture of NO traveled through the tN_r pathway (shaded pink region), NO_x* pathway (green), Na_2CO_3 denuder (blue), and H_3PO_3 denuder (purple). The calibration quantities of NO remain stable throughout each pathway displaying a very small negative slope of $4.1 \times 10^{-4} \pm 1.3 \times 10^{-4}$ ppbv. **(b)** Negative control experiment where the instrument reaches zero signal within 3 minutes when toggling the delivery of zero air into the inlet for the NO_x* pathway with and without the NO passing through the denuder.

3.3.3.2 Nighttime laboratory measurements

Nighttime measurements were performed to test the overall performance and automation of the tN_r instrument to observe if the instrument can run smoothly in a laboratory. The instrument operated as programmed, and raw measurements of the tN_r species were graphed (Appendix B, Fig. 3-S5). Five-minute averages of these species are presented in Fig. 3-7 to observe the mixing

ratios of NO_x and tN_r slowly increasing throughout the night. Levels of NO_2 were the highest fraction of tNr in the laboratory with an average of 18.42 ± 7.81 ppbv and 42 %. Nighttime levels of NO_2 likely originated from outdoors, followed by transportation indoors since the laboratory does not have any active combustion processes in it at night, and we measured that it has a high air exchange rate of 15 – 25 h^{-1}. The NO levels were near zero from 16:00 to 6:00 with an average of 0.83 ± 0.85 ppbv. Since the laboratory has a high air exchange rate (mostly driven by an equipped fume hood), there is an increase in the outdoor to indoor transport of air pollutants, such as O_3. Low levels of NO existed throughout the night because there are lower sources of NO outdoors and excess O_3 can rapidly react with NO to form NO_2, contributing as a source of NO_2 in the laboratory. Peak levels of NO_x and tN_r in the morning (8:00) suggest emissions from a nearby outdoor combustion source (vehicle exhaust from traffic or regional power plant like the YorkU Chimney Stack power plant) were circulated throughout the building, including the laboratory. An outdoor air quality monitoring station (Toronto North Ambient Air Monitoring Site, Environment and Climate Change Canada, Air Quality Ontario, 3.27 km away from the laboratory building) confirms the morning traffic with peak NO_2^* levels of 46.3 ppbv (1 h averages) which is also measured with a chemiluminescence analyzer. Levels of HONO were stable with an average of 1.67 ± 1.20 ppbv and likely sourced from heterogenous processes and transport of outdoor HONO indoors. After 6:00, HONO levels are slightly higher at 2.24 ± 0.60 ppbv, probably from the increased outdoor emissions of NO_2 transported indoors, that may have then deposited onto indoor surfaces to heterogeneously form HONO. Residential studies in North America have reported an average of ~4 – 5 ppbv HONO indoors and those values are ~2.7 times larger than our measured values of 1.67 ppbv HONO (Collins et al., 2018; Leaderer et al., 1999; Lee et al., 2002; Zhou et al., 2018). The lower background levels of HONO in the laboratory could be due to the high exchange rate of 15-25 h^{-1} from the fume hood, and the well-ventilated laboratory may result in a smaller HONO surface reservoir from less nitrite buildup on surfaces. The surface properties of the lab surfaces could also result in a smaller HONO reservoir. Residences typically have lower exchange rates than commercial buildings, with the median air exchange rate reported to be ~0.5 h^{-1} in previous residential studies in North America (Collins et al., 2018; Leaderer et al., 1999; Lee et al., 2002; Murray and Burmaster, 1995; Zhou et al., 2018). One residential study in Korea reported an average of 1.4 ppbv HONO, which is similar to our reported average of 1.7 ppbv HONO (Park and Cho, 2010). However, the in-situ formation of HONO from heterogenous

processes and HONO surface partitioning is not understood well enough, with supporting measurements, to make a detailed comparison between our proof-of-concept measurements and these prior studies. Future studies should investigate the chemistry of surface-gas interactions of nitrite and HONO that act as sources of in-situ HONO. Studies should also report building and surface materials present in indoors, as they may be a driving factor in building HONO reservoirs.

Preliminary measurements of HONO were calculated as NO_2 subtracted from NO_2*, using the 5-minute time resolution data. This method was not ideal because we assumed levels of NO_2* and NO_2 did not change significantly over the full inlet cycle period of 20 min that the instrument needs to complete all of its measurements through the tN_r pathway. This observation strategy in indoor environments has the potential to miss rapid changes in NO_x and HONO from human activities such as cooking. Based on these practical findings, we determined that the time intervals between measurements from the NO_x* and tN_r pathways needed to be decreased to 10 min, with a time resolution of 5 min within each pathway to accurately capture changes of moderately-lived chemical emission or transformation events (~10-30 min). These preliminary measurements were also collected using two timebases, one aligned with the measurements of the NO_x analyzer and the other with the PC operating the DAQ controls of the valve state and MFC. It was time consuming to merge both timebases due to the internal data processing of the NO_x analyzer and Airodis software. As a result, we integrated the analog output of the NO_x analyzer with DAQ system to collect all the measurements on the same timebase and this was applied moving forward.

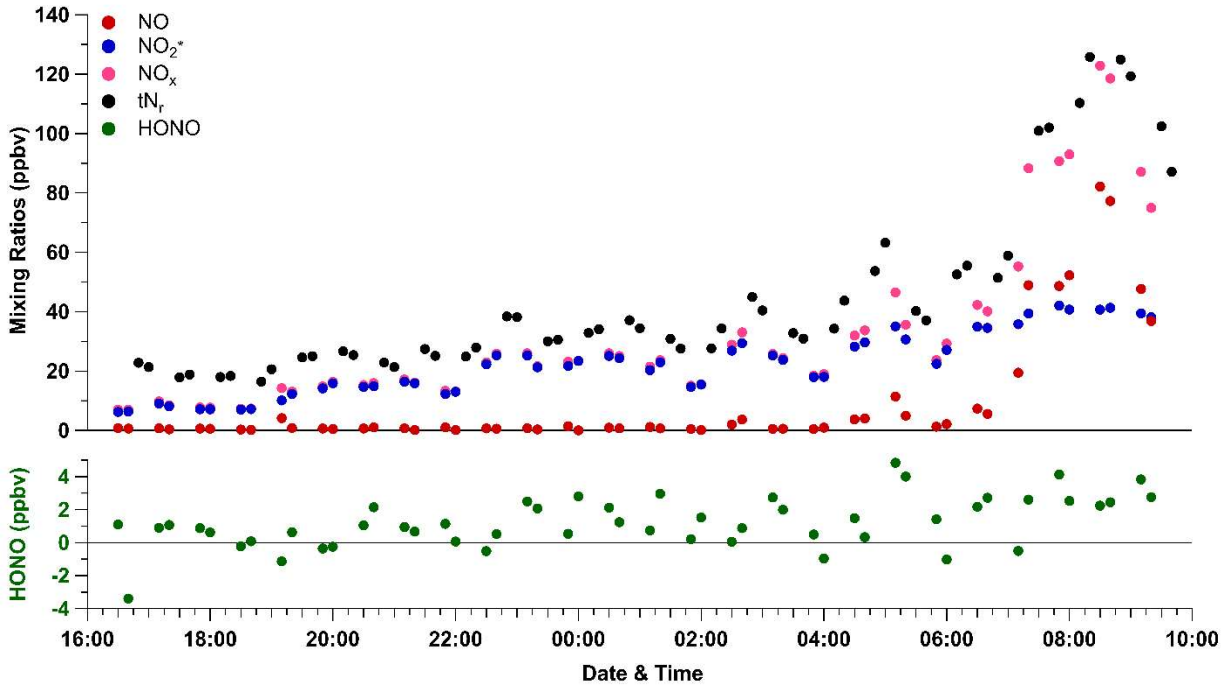

Figure 3-7. Extracted 5 min averages of nitrogenous species from the test measurements performed in a laboratory on the night of September 23-24, 2020. The top panel displays the 5 min averages of NO (red dots), NO_2 (blue dots), NO_x (pink dots) and tN_r (black dots). The mixing ratios of HONO (green dots in the bottom panel) were stable throughout the night at 1.68 ± 1.20 ppbv.

3.3.3.2 Outdoor fire plume measurements

Wildfires are important sources of atmospheric N_r, and the composition varies based on age, location, and pyrolysis temperature (Lindaas et al., 2021; Roberts et al., 2020). The number and total area of northwestern Ontario forest fires were record-breaking in 2021. A special air quality statement to Toronto was issued as biomass burning plumes were transported south, resulting in elevated particulate matter (PM) from the aging smoke in July. The tN_r instrument was deployed on the evening of July 20th, 2021 in an attempt to capture some of these aged smoke plumes and to test what the instrument could detect in terms of the gaseous N_r outdoors. Unfortunately, the instrument was deployed too late (20:00) to capture the most intense intrusion of the aged plumes when daytime $PM_{2.5}$ levels reached up to 43 $\mu g/m^3$ (hourly average) in the early morning and afternoon decreasing to < 10 $\mu g/m^3$ at 19:00 according to the nearby air quality monitoring station (Toronto North Ambient Air Monitoring Site, Environment and Climate Change Canada, Air Quality Ontario). Common nitrogen species observed in fires include NO, NO_2, HONO, HNO_3,

hydrogen cyanide (HCN), isocyanic acid (HNCO), NH_3, organic nitrates, and nitrogen-containing VOCs (Juncosa Calahorrano et al., 2021; Roberts et al., 2020). Outdoor levels of NO_2* detected by the tN_r instrument were compared to two NO_x analyzers at different locations (Fig. 3-8). The tN_r instrument sampled smoke plumes from an outdoor port situated on the southeast side of a university building. The other set of NO_2* data (1 min averages) was obtained from a NO_x analyzer measuring outdoor samples from a rooftop laboratory in the same building facing east, and the last set (1 h averages) came from a NO_X analyzer at a nearby air monitoring station 3.27 km away (Toronto North Ambient Air Monitoring Site, Environment and Climate Change Canada, Air Quality Ontario). All three datasets of NO_2* (Fig. 3-8a) display similar trends in NO_2*, with the tN_r instrument and air monitoring station being the most similar. The NO_2* measurements show higher levels of up to 23 ppbv than other detectors likely because of contaminants coming off of the outdoor sampling port. The outdoor sampling tube has been used for previous experiments, but has remained dormant for an unknown period of time, which could have resulted in contamination of the surfaces over time before air was sampled again. The NO_2* detected by the tN_r instrument went up to 23 ppbv while the rooftop NO_2* displayed a consistent trend of ~7 ppbv. The air quality station recorded the lowest NO_2* levels by 4-5 times, suggesting the smoke plumes were more detectable nearby the university building. Levels of NO_2* (tN_r instrument) are a factor of 5 times higher than NO_2 at ~21:00, which is expected from detecting NO_y species in a polluted urban airshed, with potential mixed-in aged smoke plumes. Levels of HONO cannot be directly inferred using the differential method because HNO_3 and peroxyacetyl nitrate (PAN) are positive interferences and that are also scrubbed in the Na_2CO_3 denuder, thus our approach is unable to quantify species within this acidic fraction of outdoor reactive nitrogen accurately (Bai and Wen, 2000; Fitz, 2002). However, the tN_r instrument can detect the sum of the acidic and basic fractions in the outdoor atmosphere, which may be useful in outdoor atmospheric research.

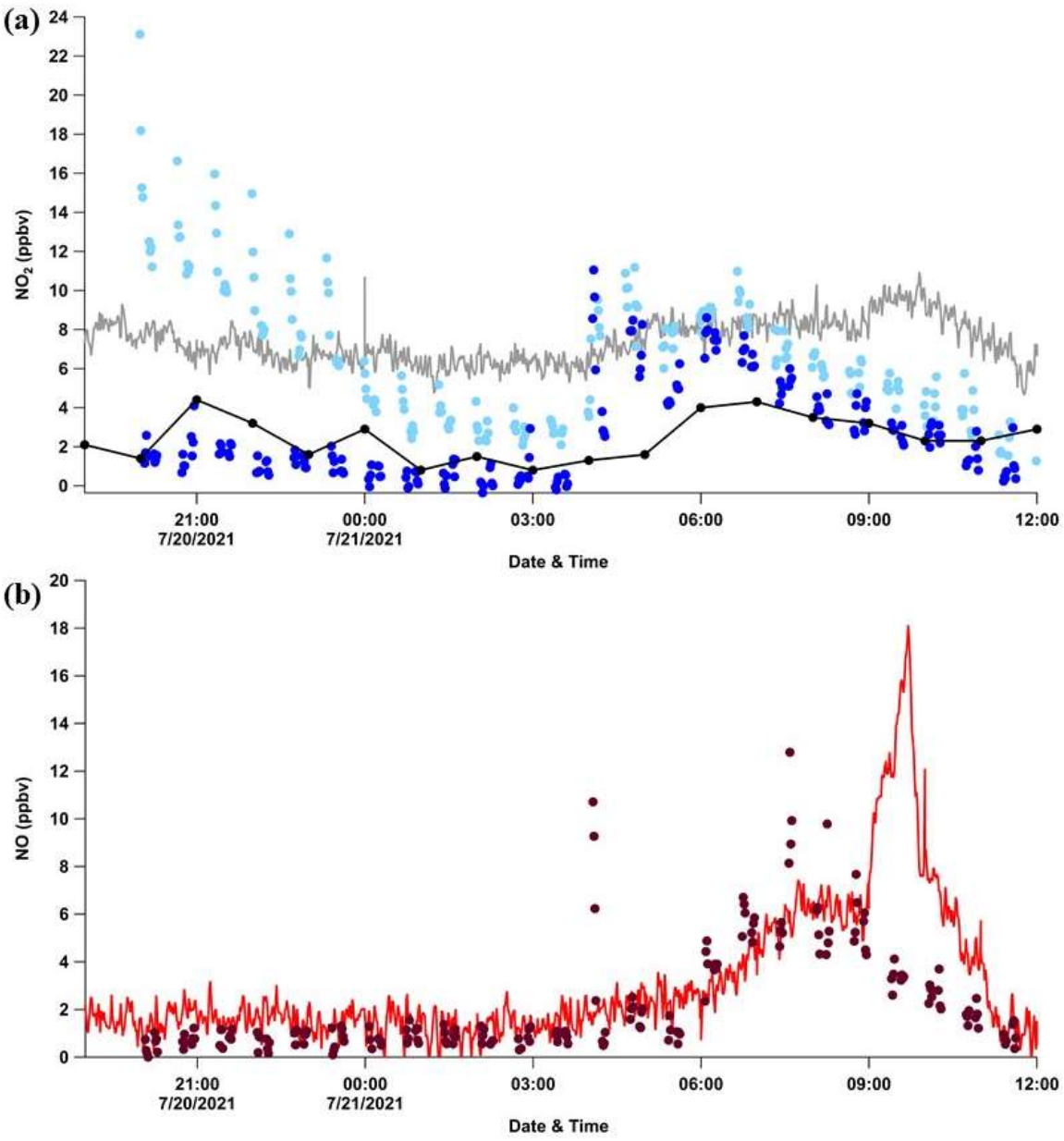

Figure 3-8. (a) Preliminary outdoor measurements (1 min averages) to capture aged wildfire plumes on the night of July 20th, 2021. Measurements of NO_2* (light blue circles) and NO_2 (blue circles) are collected from the tN_r instrument (1 min averages). These values are compared to nearby NO_2* measurements from two NO_x analyzers at different locations on a rooftop of the same building (grey line) and an air quality monitoring site 3.27 km away (black dots and line). **(b)** Comparison of outdoor NO measurements from the tN_r instrument (dark red circles) and rooftop NO_x analyzer (red line) are comparable in their general trends with slight variability due to sampling of local sources.

Unfortunately, the N_r fraction coming off the sampling pipe was found to have also contaminated the instrument solenoid valves and sampling lines after the campaign when flushing the instrument with humid air (zero air bubbled through 18.2 M MΩ·cm deionized water, then diluted with zero air). When using pure N_2 to perform zero measurements on the instrument inlet, the system seemed relatively clean (Fig. 3-9a). However, when sampling humid air (50 % RH), unknown species (25-30 ppbv) was observed to desorb off of the surfaces of the inlet and solenoid lines (Fig. 3-9b) and it was concluded to be some component of the acidic N_r pool because when it was passed through the Na_2CO_3 denuder it was quantitatively scrubbed. The contaminants were eventually removed by cleaning the valves and sampling lines with acetone and isopropyl alcohol six times. Heat was applied onto the tubing and solenoid valves to desorb any remaining contaminants and if present, the gas fittings were rinsed again with acetone and isopropyl alcohol. The acidic contaminant is suggested to contain HNO_3, known to adsorb onto surfaces rapidly. Previous studies have observed Teflon adsorbing HNO_3 with reported loss of 30 – 40 % of HNO_3 sampled (Febo et al., 1993b; Grosjean, 1985; Pang et al., 2002). The current setup of the tN_r is not designed to transfer high levels of HNO_3, but this could be mitigated by applying heating tape to the sampling inlet and valves to limit surface adsorption. The addition of a sodium chloride coated denuder to the inlet could also enable selective quantification of HNO_3 separate from HONO. An additional solenoid should be incorporated in Fig. 3-1 to provide a new pathway to scrub HNO_3, before entering Valve 2 (V2). This instrument is not the best option for speciated outdoor sampling compared to established outdoor methods. Rather, its design makes it able to detect bulk fractions of reactive nitrogen (acidic, basic, and neutral) by conversion in the tN_r oven and modulation of the denuders in the various inlet channels. While this outdoor test emphasized this fact, overall the instrument demonstrated that it was reliable for sampling of indoor and ambient air with many common practical considerations required in setting it up as one would have with any advanced atmospheric chemistry instrument, including the unexpected contaminants in complex air samples through an inlet of unknown usage history.

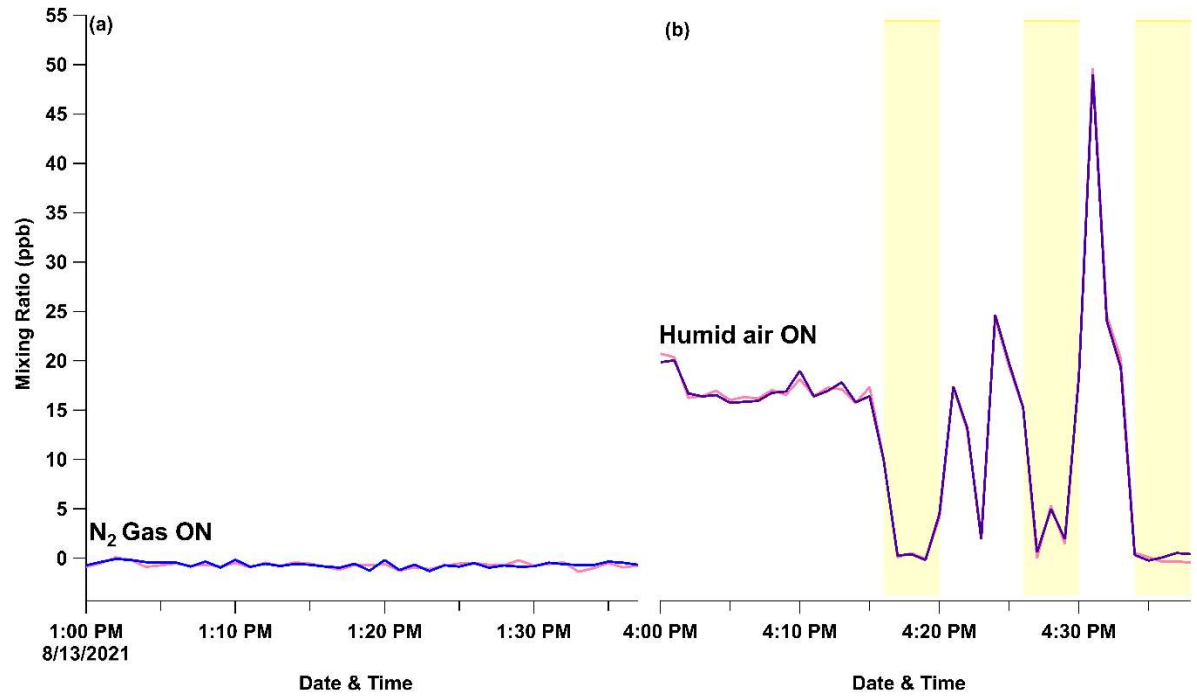

Figure 3-9. (a) Zero measurements of dry N_2 entering the sampling inlet through the NO_x* pathway. The blue lines represents the mixing ratios of NO_2* and pink is NO_x*. **(b)** Humid air inserted into the NO_x* pathway to observe the presence of contamination from measuring biomass plumes. The yellow shaded regions represents when the humid air mixture travels through the Na_2CO_3 denuder. The contaminant decreases to zero when scrubbed by the denuder, suggesting it is an acidic specie.

3.4 Conclusion and future improvements

Our instrument utilizes a total of two small pumps and detected multiple nitrogenous species with a chemiluminescence analyzer. The instrument controls and supervision are automated by a microcontroller and its user-friendly interface removes the requirements of a specialized operator for routine indoor air surveys. The HONO instrument is an upgraded method compared to the prior collaboration of this group with Zhou et al. (2018). Our instrument integrated a new and stable HONO calibration source with higher accuracy in HONO conversion efficiency achieved with the Mo catalyst of 104 ± 4 % compared to their reported 83.5 ± 3 %. We further characterized the sampling inlet, determining the instrument response time for detecting NO, NO_2, and HONO was within 1 min and limited by the response of the NO_x analyzer. The scrubbing efficiency of HONO by the Na_2CO_3 denuder was > 99.6 %. No losses of NO to the denuder was observed and NO_2 had a small loss of 2 % which has been previously reported when using this differential technique for

HONO. A positive bias of up to 2.9 % of HONO formation by NO_2 hydrolysis was identified to potentially form on the PFA sample inlet surfaces upstream of the denuder. Our findings show the decrease in NO_2 up to 5 % from characterizing the sampling lines can lead to a positive bias in our HONO measurements, which can be easily corrected in our future HONO measurements and integrated into our data processing code. The LOD of HONO is 0.6 ppb with 1 min time resolutions, which is acceptable for relevant indoor mixing ratios of HONO that have reported average background levels of ~5 ppbv (Collins et al., 2018; Wang et al., 2020b; Zhou et al., 2018). The modulation of two channels were successfully ran with the entire setup of the tN_r pathway through preliminary deployment in detecting indoor and outdoor air. Preliminary measurements of HONO in the chemical laboratory show a small HONO reservoir is present at night of 1.68 ± 1.20 ppbv, likely from lower NO_2 surface uptake or competing processes that may decrease nitrite buildup from other projects involving reactive chemicals. The tN_r instrument can detect the total sum of acidic and basic species in outdoor air but cannot quantify key fractions due to the presence of NO_y species. Overall, the HONO instrument in the tN_r instrument can perform time-resolved measurements of key indoor pollutants NO, NO_2, NO_x and HONO.

General instrument maintenance requires replacing the inlet filter, denuder coating, and scrubbing media in the zero-air generator to ensure optimized efficiency of quantifying fractions of the nitrogenous species. The maintenance time depends on the type of indoor environment and the number of chemical activities (e.g., cooking and cleaning). This study did not quantify the lifetime for the deactivation of the carbonate denuders. Zhou et al. (2018) recoated their denuder daily to minimize potential denuder deactivation when measuring in an urban residential house. The longevity of the zero-air generator relies on the membrane air dryer, which prevents moisture from adsorbing on to the scrubbing media. Without the attachment of the membrane air dryer, water saturated the scrubbing media resulting in N_r contaminants with mixing ratios equivalent to 2 - 4 ppbv of NO entering the system. These contaminants were suspected to be a mixture of N_r species. The voltage output of the NO_x analyzer drifts after long periods of use, so a calibration of the voltage output against known mixing ratios of NO, NO_2, and NO_x should be performed at least every 3 months and at the start/end of any field campaign. In the future, the automated control of the instrument should be upgraded by adding more solenoid valves to allow automation of the calibration quantities of HONO and NH_3 delivered to the system, along with their dilution by the

MFC. The manual two-way waste valve should also be automated. The next step following on this construction, characterization, and validation work was to deploy the tN_r instrument in a three-week indoor air quality campaign to measure pollutants in a commercial kitchen (Chapter 4). Planned future field measurements at various indoor facilities will allow detailed investigations of the total reactive nitrogen budget and give specific insight on the HONO chemistry of indoor air. Experience gained from surveying different indoor environments and continually undertaking practical developments of the instrument will result in easy and accurate real-time detection of NO, NO_2, and HONO.

3.5 References

Abbatt, J. P. D. and Wang, C.: The atmospheric chemistry of indoor environments, Environ. Sci. Process. Impacts, 22(1), 25–48, doi:10.1039/c9em00386j, 2020.

Ault, A. P., Grassian, V. H., Carslaw, N., Collins, D. B., Destaillats, H., Donaldson, D. J., Farmer, D. K., Jimenez, J. L., McNeill, V. F., Morrison, G. C., O'Brien, R. E., Shiraiwa, M., Vance, M. E., Wells, J. R. and Xiong, W.: Indoor Surface Chemistry: Developing a Molecular Picture of Reactions on Indoor Interfaces, Chem, 6, 1–16, doi:10.1016/j.chempr.2020.08.023, 2020.

Bai, H. and Wen, H. Y.: Performance of the Annular Denuder System with Different Arrangement for HNO3 and HNO2 Measurements in Taiwan, J. Air Waste Manag. Assoc., 50(1), 125–130, doi:10.1080/10473289.2000.10463991, 2000.

Beckett, W. S., Russi, M. B., Haber, A. D., Rivkin, R. M., Sullivan, J. R., Tameroglu, Z., Mohsenin, V. and Leaderer, B. P.: Effect of nitrous acid on lung function in asthmatics: A chamber study, Environ. Health Perspect., 103(4), 372–375, doi:10.1289/ehp.95103372, 1995.

Brauer, M., Ryan, P. B., Suh, H. H., Koutrakls, P. and Spengler, J. D.: Measurements of Nitrous Acid inside Two Research Houses, Environ. Sci. Technol., 24(10), 1521–1527, doi:10.1021/es00080a011, 1990.

Brauer, M., Rasmussen, T. R., Kjærgaard, S. K. and Spengler, J. D.: Nitrous Acid Formation in an Experimental Exposure Chamber, Indoor Air, 3(2), 94–105, doi:10.1111/j.1600-0668.1993.t01-2-00004.x, 1993.

Britigan, N., Alshawa, A. and Nizkorodov, S. A.: Quantification of ozone levels in indoor environments generated by ionization and ozonolysis air purifiers, J. Air Waste Manag. Assoc., 56(5), 601–610, doi:10.1080/10473289.2006.10464467, 2006.

Collins, D. B., Hems, R. F., Zhou, S., Wang, C., Grignon, E., Alavy, M., Siegel, J. A. and Abbatt, J. P. D.: Evidence for Gas-Surface Equilibrium Control of Indoor Nitrous Acid, Environ. Sci. Technol., 52(21), 12419–12427, doi:10.1021/acs.est.8b04512, 2018.

Crilley, L. R., Kramer, L. J., Ouyang, B., Duan, J., Zhang, W., Tong, S., Ge, M., Tang, K., Qin, M., Xe, P., Shaw, M. D., Lewis, A. C., Mehra, A., Bannan, T. J., Worrall, S. D., Priestley, M., Bacak, A., Coe, H., Allan, J., Percival, C. J., Popoola, O. A. M., Jones, R. L. and Bloss, W. J.: Intercomparison of nitrous acid (HONO) measurement techniques in a megacity (Beijing), Atmos. Meas. Tech. Discuss., (May), 1–31, doi:10.5194/amt-2019-139, 2019.

Dunlea, E. J., Herndon, S. C., Nelson, D. D., Volkamer, R. M., San Martini, F., Sheehy, P. M., Zahniser, M. S., Shorter, J. H., Wormhoudt, J. C., Lamb, B. K., Allwine, E. J., Gaffney, J. S., Marley, N. A., Grutter, M., Marquez, C., Blanco, S., Cardenas, B., Retama, A., Yillegas, C. R. R., Kolb, C. E., Molina, L. T. and Molina, M. J.: Evaluation of nitrogen dioxide chemiluminescence monitors in a polluted urban environment, Atmos. Chem. Phys., 7(10), 2691–2704, doi:10.5194/acp-7-2691-2007, 2007.

Febo, A., Perrino, C. and Cortiello, M.: A denuder technique for the measurement of nitrous acid in urban atmospheres, Atmos. Environ. Part A, Gen. Top., 27(11), 1721–1728, doi:10.1016/0960-1686(93)90235-Q, 1993a.

Febo, A., Perrino, C. and Allegrini, I.: Field intercomparison exercise on nitric acid and nitrate measurement (Rome, 1988): A critical approach to the evaluation of the results, Sci. Total Environ., 133(1–2), 39–71, doi:10.1016/0048-9697(93)90112-J, 1993b.

Finlayson-Pitts, B. J., Wingen, L. M., Sumner, A. L., Syomin, D. and Ramazan, K. A.: The heterogeneous hydrolysis of NO2 in laboratory systems and in outdoor and indoor atmospheres: An integrated mechanism, Phys. Chem. Chem. Phys., 5(2), 223–242, doi:10.1039/b208564j, 2003.

Fischer, M. L., Littlejohn, D., Lunden, M. M. and Brown, N. J.: Automated Measurements of Ammonia and Nitric Acid in Indoor and Outdoor Air, Environ. Sci. Technol., 37(10), 2114–2119, doi:10.1021/es026133x, 2003.

Fitz, D. R.: Evalulation of Diffusion Denuder Coatings for Removing Acid Gases from Ambient Air, Washington, D.C., 2002.

Gandolfo, A., Gligorovski, V., Bartolomei, V., Tlili, S., Gómez Alvarez, E., Wortham, H., Kleffmann, J. and Gligorovski, S.: Spectrally resolved actinic flux and photolysis frequencies of key species within an indoor environment, Build. Environ., 109(April 2018), 50–57, doi:10.1016/j.buildenv.2016.08.026, 2016.

Gandolfo, A., Rouyer, L., Wortham, H. and Gligorovski, S.: The influence of wall temperature on NO2 removal and HONO levels released by indoor photocatalytic paints, Appl. Catal. B Environ., doi:10.1016/j.apcatb.2017.03.021, 2017.

Gandolfo, A., Bartolomei, V., Truffier-Boutry, D., Temime-Roussel, B., Brochard, G., Bergé, V., Wortham, H. and Gligorovski, S.: The impact of photocatalytic paint porosity on indoor NOx and HONO levels, Phys. Chem. Chem. Phys., doi:10.1039/c9cp05477d, 2020.

Ge, X., Wexler, A. S. and Clegg, S. L.: Atmospheric amines - Part I. A review, Atmos. Environ., 45(3), 524–546, doi:10.1016/j.atmosenv.2010.10.012, 2011.

Gómez Alvarez, E., Amedro, D., Afif, C., Gligorovski, S., Schoemaecker, C., Fittschen, C., Doussin, J.-F. and Wortham, H.: Unexpectedly high indoor hydroxyl radical concentrations associated with nitrous acid, Proc. Natl. Acad. Sci., 110(33), 13294–13299, doi:10.1073/pnas.1309171110, 2013.

Gómez Alvarez, E., Sörgel, M., Gligorovski, S., Bassil, S., Bartolomei, V., Coulomb, B., Zetzsch, C. and Wortham, H.: Light-induced nitrous acid (HONO) production from NO2 heterogeneous reactions on household chemicals, Atmos. Environ., doi:10.1016/j.atmosenv.2014.06.034, 2014.

Grosjean, D.: Wall Loss of Gaseous Pollutants in Outdoor Teflon Chambers, Environ. Sci. Technol., 19(11), 1059–1065, doi:10.1021/es00141a006, 1985.

Heland, J., Kleffmann, J., Kurtenbach, R. and Wiesen, P.: A new instrument to measure gaseous nitrous acid (HONO) in the atmosphere, Environ. Sci. Technol., 35(15), 3207–3212, doi:10.1021/es000303t, 2001.

Hems, R. F., Wang, C., Collins, D. B., Zhou, S., Borduas-Dedekind, N., Siegel, J. A. and Abbatt, J. P. D.: Sources of isocyanic acid (HNCO) indoors: A focus on cigarette smoke, Environ. Sci. Process. Impacts, 21(8), 1334–1341, doi:10.1039/c9em00107g, 2019.

Hubbard, H. F., Coleman, B. K., Sarwar, G. and Corsi, R. L.: Effects of an ozone-generating air purifier on indoor secondary particles in three residential dwellings, Indoor Air, 15(6), 432–444, doi:10.1111/j.1600-0668.2005.00388.x, 2005.

Jarvis, D. L., Leaderer, B. P., Chinn, S. and Burney, P. G.: Indoor nitrous acid and respiratory symptoms and lung function in adults, Thorax, 60(6), 474–479, doi:10.1136/thx.2004.032177, 2005.

Joseph, D. W. and Spicer, C. W.: Chemiluminescence Method for Atmospheric Monitoring of Nitric Acid and Nitrogen Oxides, Anal. Chem., 50(9), 1400–1403, doi:10.1021/ac50031a054, 1978.

Juncosa Calahorrano, J. F., Lindaas, J., O'Dell, K., Palm, B. B., Peng, Q., Flocke, F., Pollack, I. B., Garofalo, L. A., Farmer, D. K., Pierce, J. R., Collett, J. L., Weinheimer, A., Campos, T., Hornbrook, R. S., Hall, S. R., Ullmann, K., Pothier, M. A., Apel, E. C., Permar, W., Hu, L., Hills, A. J., Montzka, D., Tyndall, G., Thornton, J. A. and Fischer, E. V.: Daytime Oxidized Reactive Nitrogen Partitioning in Western U.S. Wildfire Smoke Plumes, J. Geophys. Res. Atmos., 126(4), 1–22, doi:10.1029/2020JD033484, 2021.

Kleffmann, J.: Daytime sources of nitrous acid (HONO) in the atmospheric boundary layer, ChemPhysChem, 8(8), 1137–1144, doi:10.1002/cphc.200700016, 2007.

Klepeis, N. E., Nelson, W. C., Ott, W. R., Robinson, J. P., Tsang, A. M., Switzer, P., Behar, J. V., Hern, S. C. and Engelmann, W. H.: The National Human Activity Pattern Survey (NHAPS): A resource for assessing exposure to environmental pollutants, J. Expo. Anal. Environ. Epidemiol., 11(3), 231–252, doi:10.1038/sj.jea.7500165, 2001.

Kowal, S. F., Allen, S. R. and Kahan, T. F.: Wavelength-Resolved Photon Fluxes of Indoor Light Sources: Implications for HOx Production, Environ. Sci. Technol., 51(18), 10423–10430, doi:10.1021/acs.est.7b02015, 2017.

Lao, M., Crilley, L., Salehpoor, L., Furlani, T., Bourgeois, I., Neuman, J. A., Rollins, A., Veres, P., Washenfelder, R., Womack, C., Young, C. and VandenBoer, T.: A portable, robust, stable and tunable calibration source for gas-phase nitrous acid (HONO), Atmos. Meas. Tech. Discuss., 1–31, doi:10.5194/amt-2020-209, 2020.

Leaderer, B. P., Naeher, L., Jankun, T., Balenger, K., Holford, T. R., Toth, C., Sullivan, J., Wolfson, J. M., Koutrakis, P., Environmental, S., Perspectives, H., Mar, N., Leaderer, B. P., Naeher, L., Jankun, T., Balenger, K., Holford, T. R., Toth, C., Wolfson, J. M. and Koutrakis, P.: Indoor, Outdoor, and Regional Summer and Winter Concentrations of PM10, PM2.5, SO4, 2-, H+, NH4+, NO3-, NH3, and Nitroud Acid in Homes with and without Kerosene Space Heaters, Environ. Health Perspect., 107(3), 223–231 [online] Available from: https://www.jstor.org/stable/3434513, 1999.

Lee, K., Xue, J., Geyh, A. S., Özkaynak, H., Leaderer, B. P., Weschler, C. J. and Spengler, J. D.: Nitrous acid, nitrogen dioxide, and ozone concentrations in residential environments, Environ. Health Perspect., 110(2), 145–149, doi:10.1289/ehp.02110145, 2002.

Leech, J. A., Nelson, W. C., Burnett, R. T., Aaron, S. and Raizenne, M. E.: It's about time: A comparison of Canadian and American time-activity patterns, J. Expo. Anal. Environ. Epidemiol., 12(6), 427–432, doi:10.1038/sj.jea.7500244, 2002.

Liu, Y., Misztal, P. K., Arata, C., Weschler, C. J., Nazaroff, W. W. and Goldstein, A. H.: Observing ozone chemistry in an occupied residence, Proc. Natl. Acad. Sci. U. S. A., 118(6), doi:10.1073/pnas.2018140118, 2021.

Manuja, A., Ritchie, J., Buch, K., Wu, Y., Eichler, C. M. A., Little, J. C. and Marr, L. C.: Total surface area in indoor environments, Environ. Sci. Process. Impacts, 21(8), 1384–1392, doi:10.1039/c9em00157c, 2019.

Mattila, J. M., Lakey, P. S. J., Shiraiwa, M., Wang, C., Abbatt, J. P. D., Arata, C., Goldstein, A. H., Ampollini, L., Katz, E. F., Decarlo, P. F., Zhou, S., Kahan, T. F., Cardoso-Saldaña, F. J., Ruiz, L. H., Abeleira, A., Boedicker, E. K., Vance, M. E. and Farmer, D. K.: Multiphase Chemistry Controls Inorganic Chlorinated and Nitrogenated Compounds in Indoor Air during Bleach Cleaning, Environ. Sci. Technol., 54(3), 1730–1739, doi:10.1021/acs.est.9b05767, 2020.

Monge, M. E., D'Anna, B. and George, C.: Nitrogen dioxide removal and nitrous acid formation on titanium oxide surfaces-an air quality remediation process?, Phys. Chem. Chem. Phys., 12(31), 8991–8998, doi:10.1039/b925785c, 2010.

Moravek, A., Singh, S., Pattey, E., Pelletier, L. and Murphy, J. G.: Measurements and quality control of ammonia eddy covariance fluxes: A new strategy for high-frequency attenuation correction, Atmos. Meas. Tech., 12(11), 6059–6078, doi:10.5194/amt-12-6059-2019, 2019.

Mullen, N. A., Li, J., Russell, M. L., Spears, M., Less, B. D. and Singer, B. C.: Results of the California Healthy Homes Indoor Air Quality Study of 2011-2013: Impact of natural gas appliances on air pollutant concentrations, Indoor Air, 26(2), 231–245, doi:10.1111/ina.12190, 2016.

Murray, D. M. and Burmaster, D. E.: Residential Air Exchange Rates in the United States: Empirical and Estimated Parametric Distributions by Season and Climatic Region, Risk Anal., 15(4), 459–465, doi:10.1111/j.1539-6924.1995.tb00338.x, 1995.

Nazaroff, W. W. and Weschler, C. J.: Indoor ozone: Concentrations and influencing factors, Indoor Air, 32(1), 1–21, doi:10.1111/ina.12942, 2022.

Pang, Y., Eatough, N. L. and Eatough, D. J.: Evaluation of the performance of annular denuder samplers, Aerosol Sci. Technol., 36(6), 790–798, doi:10.1080/02786820290038465, 2002.

Pape, L., Ammann, C., Nyfeler-Brunner, A., Spirig, C., Hens, K. and Meixner, F. X.: An automated dynamic chamber system for surface exchange measurement of non-reactive and reactive trace gases of grassland ecosystems, Biogeosciences, 6(3), 405–429, doi:10.5194/bg-6-405-2009, 2009.

Park, S. S. and Cho, S. Y.: Performance evaluation of an in situ nitrous acid measurement system and continuous measurement of nitrous acid in an indoor environment, J. Air Waste Manag. Assoc., 60(12), 1434–1442, doi:10.3155/1047-3289.60.12.1434, 2010.

Park, S. S., Hong, J. H., Lee, J. H., Kim, Y. J., Cho, S. Y. and Kim, S. J.: Investigation of nitrous acid concentration in an indoor environment using an in-situ monitoring system, Atmos. Environ., doi:10.1016/j.atmosenv.2008.05.023, 2008.

Perner, D. and Platt, U.: Detection of nitrous acid in the atmosphere by differential optical absorption, Geophys. Res. Lett., 6(12), 917–920, doi:10.1029/GL006i012p00917, 1980.

Place, B. K., Young, C. J., Ziegler, S. E., Edwards, K. A., Salehpoor, L. and VandenBoer, T. C.: Passive sampling capabilities for ultra-trace quantitation of atmospheric nitric acid (HNO 3) in remote environments, Atmos. Environ., 191(November 2017), 360–369, doi:10.1016/j.atmosenv.2018.08.030, 2018.

Rasmussen, T. R., Brauer, M. and Kjærgaard, S.: Effects of nitrous acid exposure on human mucous membranes, Am. J. Respir. Crit. Care Med., 151(5), doi:10.1164/ajrccm.151.5.7735607, 1995.

Reed, C., Brumby, C. A., Crilley, L. R., Kramer, L. J., Bloss, W. J., Seakins, P. W., Lee, J. D. and Carpenter, L. J.: HONO measurement by differential photolysis, Atmos. Meas. Tech., 9(6), 2483–2495, doi:10.5194/amt-9-2483-2016, 2016.

Ren, X., Gao, H., Zhou, X., Crounse, J. D., Wennberg, P. O., Browne, E. C., LaFranchi, B. W., Cohen, R. C., McKay, M., Goldstein, A. H. and Mao, J.: Measurement of atmospheric nitrous acid at Bodgett forest during BEARPEX2007, Atmos. Chem. Phys., 10(13), 6283–6294, doi:10.5194/acp-10-6283-2010, 2010.

Roberts, J., Stockwell, C., Yokelson, R., Gouw, J. de, Liu, Y., Selimovic, V., Koss, A., Sekimoto, K., Coggon, M., Yuan, B., Zarzana, K., Brown, S., Santin, C., Doerr, S. and Warneke, C.: The nitrogen budget of laboratory-simulated western U.S. wildfires during the FIREX 2016 FireLab study, Atmos. Chem. Phys. Discuss., (2), 1–34, doi:10.5194/acp-2020-66, 2020.

Roberts, J. M., Veres, P., Warneke, C., Neuman, J. A., Washenfelder, R. A., Brown, S. S., Baasandorj, M., Burkholder, J. B., Burling, I. R., Johnson, T. J., Yokelson, R. J. and De Gouw, J.: Measurement of HONO, HNCO, and other inorganic acids by negative-ion proton-transfer chemical-ionization mass spectrometry (NI-PT-CIMS): Application to biomass burning emissions, Atmos. Meas. Tech., 3(4), 981–990, doi:10.5194/amt-3-981-2010, 2010.

Singer, B. C., Pass, R. Z., Delp, W. W., Lorenzetti, D. M. and Maddalena, R. L.: Pollutant concentrations and emission rates from natural gas cooking burners without and with range hood exhaust in nine California homes, Build. Environ., 122(2), 215–229, doi:10.1016/j.buildenv.2017.06.021, 2017.

Sleiman, M., Gundel, L. A., Pankow, J. F., Jacob, P., Singer, B. C. and Destaillats, H.: Formation of carcinogens indoors by surface-mediated reactions of nicotine with nitrous acid, leading to potential thirdhand smokehazards, Proc. Natl. Acad. Sci. U. S. A., doi:10.1073/pnas.0912820107, 2010.

Spataro, F. and Ianniello, A.: Sources of atmospheric nitrous acid: State of the science, current research needs, and future prospects, J. Air Waste Manag. Assoc., 64(11), 1232–1250, doi:10.1080/10962247.2014.952846, 2014.

Spicer, C. W., Kenny, D. V., Ward, G. F., Billick, I. H. and Leslie, N. P.: Evaluation of NO2 Measurement Methods for Indoor Air Quality Applications, Air Waste, 44(2), 163–168, doi:10.1080/1073161X.1994.10467245, 1994.

Spicer, C. W., Billick, I. H. and Yanagisawa, Y.: Nitrous Acid Interference with Passive NO2 Measurement Methods and the Impact on Indoor NO2 Data, Indoor Air, 11(3), 156–161, doi:10.1034/j.1600-0668.2001.011003156.x, 2001.

Stockwell, C. E., Kupc, A., Witkowski, B., Talukdar, R. K., Liu, Y., Selimovic, V., Zarzana, K. J., Sekimoto, K., Warneke, C., Washenfelder, R. A., Yokelson, R. J., Middlebrook, A. M. and Roberts, J. M.: Characterization of a catalyst-based total nitrogen and carbon conversion technique to calibrate particle mass measurement instrumentation, Atmos. Meas. Tech. Discuss., 1–38, doi:10.5194/amt-2017-419, 2018.

U.S. EPA. Air Quality Criteria for Oxides of Nitrogen (Final Report, 1993). U.S. Environmental Protection Agency, Washington, D.C., EPA/600/8-91/049aF-cF, 1993.

Vandenboer, T. C., Brown, S. S., Murphy, J. G., Keene, W. C., Young, C. J., Pszenny, A. A. P., Kim, S., Warneke, C., De Gouw, J. A., Maben, J. R., Wagner, N. L., Riedel, T. P., Thornton, J. A., Wolfe, D. E., Dubé, W. P., Öztürk, F., Brock, C. A., Grossberg, N., Lefer, B., Lerner, B., Middlebrook, A. M. and Roberts, J. M.: Understanding the role of the ground surface in HONO vertical structure: High resolution vertical profiles during NACHTT-11, J. Geophys. Res. Atmos., 118(17), 10155–10171, doi:10.1002/jgrd.50721, 2013.

VandenBoer, T. C., Markovic, M. Z., Sanders, J. E., Ren, X., Pusede, Browne, E. C., Cohen, R. C., Zhang, L., Thomas, J., Brune, W. H. and Murphy, J. G.: Evidence for a nitrous acid (HONO) reservoir at the ground surface in Bakersfield, CA, during CalNex 2010, J. Geophys. Res. Atmos., 119, 9093–9106, doi:10.1002/ 2013JD020971, 2014.

VandenBoer, T. C., Young, C. J., Talukdar, R. K., Markovic, M. Z., Brown, S. S., Roberts, J. M. and Murphy, J. G.: Nocturnal loss and daytime source of nitrous acid through reactive uptake and displacement, Nat. Geosci., 8(1), 55–60, doi:10.1038/ngeo2298, 2015.

Večeřa, Z., Dasgupta, P. K. and Večeřa, Z.: Measurement of Ambient Nitrous Acid and a Reliable Calibration Source for Gaseous Nitrous Acid, Environ. Sci. Technol., 25(2), 255–260, doi:10.1021/es00014a006, 1991.

Vichi, F., Mašková, L., Frattoni, M., Imperiali, A. and Smolík, J.: Simultaneous measurement of nitrous acid, nitric acid, and nitrogen dioxide by means of a novel multipollutant diffusive sampler in libraries and archives, Herit. Sci., 4(1), 1–8, doi:10.1186/s40494-016-0074-5, 2016.

Villena, G., Bejan, I., Kurtenbach, R., Wiesen, P. and Kleffmann, J.: Interferences of commercial NO2 instruments in the urban atmosphere and in a smog chamber, Atmos. Meas. Tech., 5(1), 149–159, doi:10.5194/amt-5-149-2012, 2012.

Wainman, T., Weschler, C. J., Lioy, P. J. and Zhang, J.: Effects of surface type and relative humidity on the production and concentration of nitrous acid in a model indoor environment, Environ. Sci. Technol., 35(11), 2200–2206, doi:10.1021/es000879i, 2001.

Wang, C., Bottorff, B., Reidy, E., Rosales, C. M. F., Collins, D. B., Novoselac, A., Farmer, D. K., Vance, M. E., Stevens, P. S. and Abbatt, J. P. D.: Cooking, Bleach Cleaning, and Air Conditioning Strongly Impact Levels of HONO in a House, Environ. Sci. Technol., 54(21), 13488–13497, doi:10.1021/acs.est.0c05356, 2020a.

Wang, C., Collins, D. B., Arata, C., Goldstein, A. H., Mattila, J. M., Farmer, D. K., Ampollini, L., DeCarlo, P. F., Novoselac, A., Vance, M. E., Nazaroff, W. W. and Abbatt, J. P. D.: Surface reservoirs dominate dynamic gas-surface partitioning of many indoor air constituents, Sci. Adv., 6(8), 1–12, doi:10.1126/sciadv.aay8973, 2020b.

Weschler, C. J. and Carslaw, N.: Indoor Chemistry, Environ. Sci. Technol., 52(5), 2419–2428, doi:10.1021/acs.est.7b06387, 2018.

Winberry, W. T., Ellestad, T. and Stevens, B.: Compendium of Methods for the Determination of Inorganic Compounds in Compendium of Methods for the determination of Inorganic Compounds in Ambient Air, Compendium Method IO-4.2: Determination of Reactive Acidic and Basic Gases and Strong Acidity of Atmos., 1999.

Wisthaler, A. and Weschler, C. J.: Reactions of ozone with human skin lipids: Sources of carbonyls, dicarbonyls, and hydroxycarbonyls in indoor air, Proc. Natl. Acad. Sci. U. S. A., 107(15), 6568–6575, doi:10.1073/pnas.0904498106, 2010.

Wojtal, P., Halla, J. D. and McLaren, R.: Pseudo steady states of HONO measured in the nocturnal marine boundary layer: A conceptual model for HONO formation on aqueous surfaces, Atmos. Chem. Phys., 11(7), 3243–3261, doi:10.5194/acp-11-3243-2011, 2011.

Young, C. J., Zhou, S., Siegel, J. A. and Kahan, T. F.: Illuminating the dark side of indoor oxidants, Environ. Sci. Process. Impacts, 21(8), 1229–1239, doi:10.1039/c9em00111e, 2019.

Zhou, S., Young, C. J., VandenBoer, T. C., Kowal, S. F. and Kahan, T. F.: Time-Resolved Measurements of Nitric Oxide, Nitrogen Dioxide, and Nitrous Acid in an Occupied New York Home, Environ. Sci. Technol., 52(15), 8355–8364, doi:10.1021/acs.est.8b01792, 2018.

Zhou, S., Young, C. J., VandenBoer, T. C. and Kahan, T. F.: Role of location, season, occupant activity, and chemistry in indoor ozone and nitrogen oxide mixing ratios, Environ. Sci. Process. Impacts, 21, 1374–1383, doi:10.1039/c9em00129h, 2019.

Zhou, X., He, Y., Huang, G., Thornberry, T. D., Carroll, M. A. and Bertman, S. B.: Photochemical production of nitrous acid on glass sample manifold surface, Geophys. Res. Lett., 29(14), 5–8, doi:10.1029/2002gl015080, 2002.

Chapter Four:

Nitrous acid (HONO) surface reservoir chemistry in a commercial kitchen during the KOCENA (Kitchen Organic Carbon, Emissions, Nitrogen, and Aerosol) Campaign

M. Lao[1], L.R. Crilley[1], J.C. Ditto[2,3], Zilin Zhou[2], C.J. Young[1], Jonathan P.D. Abbatt[2], Arthur W. H. Chan[3], and T.C. VandenBoer[1]

[1]Department of Chemistry, York University, Toronto, ON, Canada

[2]Department of Chemistry, University of Toronto, Toronto, ON, Canada

[3]Department of Chemical Engineering and Applied Chemistry, University of Toronto, Toronto, ON, Canada

Author Contributions:

ML and LC setup, operated, and calibrated instruments during the campaign. LC and TCV organized the campaign. JD provided the exhaust fan measurements in rotations per minute and ZZ provided spectral irradiance measurements. TCV, CJY, JPDA, and AWHC provided the supervision, concept, guidance, and supported this project. **ML** collected, processed, and analyzed the data presented in this work. **ML** wrote and TCV edited this work.

Abstract

The KOCENA (Kitchen Organic Carbon, Emissions, Nitrogen, and Aerosol) campaign was a collaborative project to detect the emissions and chemical transformations of indoor pollutants present in a commercial kitchen. Measurements of nitrogen oxides ($NO_x = NO + NO_2$) and nitrous acid (HONO) were detected using a newly built total reactive nitrogen (tN_r) instrument that can perform modulated quantification of nitrogenous species like NO_x, HONO, and ammonia (NH_3). Nitrogen oxides and HONO are important indoor pollutants that can participate in oxidant formation, with mixing ratios typically higher indoors than outdoors especially when from direct combustion emissions by cooking with gas appliances. The commercial kitchen had a sensor-controlled ventilation system to control an optimal exhaust rate to rapidly removed pollutants from the kitchen during high volumes of cooking activities. As a result, most HONO directly emitted from cooking emissions were lost during data processing because the tN_r instrument could not reliably capture rapid cooking emissions with high ventilation that spanned less than 20 minutes. The direct emissions of HONO were found to be unimportant because it is efficiently removed by the high air exchange rate in the commercial kitchen. Measurements during the day (5:00 – 22:00) and night (22:00 – 5:00) were compared based on the initiation of the ventilation and kitchen operation hours. Transportation of NO_x and HONO from outdoors contributed to high indoor levels in the early morning suspected to come from nearby combustion sources. Stable nighttime levels of NO_2 and HONO were also contributed by outdoor transportation. Heterogenous processes played a crucial role in dictating the temporal behaviours of HONO (total average of 2.41 ± 2.05 ppb, daytime average 2.48 ± 2.07 ppb, and nighttime average 2.36 ± 1.29 ppb). Predicted levels of HONO were calculated by determining the concentration of HONO produced from NO_2 surface uptake and its loss by photolysis to quantify the relative importance of these processes toward generating the observed levels. Our results show that equilibrium partitioning of HONO on surfaces is evident in sustaining levels of HONO in the absence of direct cooking emissions. This HONO reservoir is likely located on indoor surfaces with deposited nitrite that can desorb as HONO, which is supported by previous indoor home studies (Collins et al., 2018; Wainman et al., 2001; Wang et al., 2020b). Calculations of the production rate of OH by HONO photolysis confirms that the kitchen acts as a persistent OH source (average of 9.72×10^{-5} molecules cm^{-3} s^{-1}, $J_{HONO} = 1.66 \times 10^{-5}$ s^{-1} at average HONO concentrations of $5.85 \times 10^{10} \pm 4.95 \times 10^{10}$ molec cm^{-3}). The 24-hour lighting indicates that consistent production of

OH by HONO photolysis may be an important driver in indoor oxidation chemistry in commercial environments.

4.1 Introduction

In recent years, the construction of indoor facilities has become increasingly airtight to improve energy efficiency (Weschler, 2009). Indoor air quality has simultaneously decreased due to increased concentration of indoor pollutants, leading to higher exposure as we spend > 90 % of our lives indoors (Klepeis et al., 2001; Leech et al., 2002). Established societal regulations and research have focused on the mitigation of poor outdoor air quality to protect human health, yet we do not fully understand the chemistry of indoor air and its oxidative capacity. Indoor air pollutants can undergo multiphase chemistry to be produced, removed, or transformed by many indoor processes including direct emissions, indoor-outdoor air exchange, and surface deposition (Abbatt and Wang, 2020). Nitrogen oxides (NO_x = NO + NO_2) and nitrous acid (HONO) are well known and emerging pollutants indoors respectively, with reported mixing ratios higher indoors than outdoors. Direct emissions of NO_x can range up to 400 parts per billion (ppb) and HONO up to 100 ppb from high-temperature combustion processes such as cooking with gas appliances, lighting candles, and open fireplaces (Bartolomei et al., 2015; Collins et al., 2018; Dennekamp et al., 2001; Lee et al., 2002; Mullen et al., 2016; Zhou et al., 2018). Transportation of NO_x indoors from outside can be facilitated by open windows, doors, ventilated air, or infiltration through the building envelope. Nitrogen oxides play an essential role in oxidant cycling as both sources and sinks, especially in sunlit areas where NO_2 photolysis can contribute to O_3 formation (Kowal et al., 2017). In the presence of O_3, NO will rapidly react to form NO_2. The reactive uptake of NO_2 to indoor surfaces is another important sink in areas where photon levels are low and away from sunlit areas (Finlayson-Pitts et al., 2003; Kowal et al., 2017). The surface uptake of NO_2 can heterogeneously form HONO, however its exact mechanism is unclear. One well-described heterogenous mechanism is NO_2 hydrolysis, where gaseous NO_2 interacts with a thin film of water on surfaces, forming gas-phase HONO and adsorbed nitric acid (HNO_3) (R1) (Finlayson-Pitts et al., 2003).

$$\mathbf{2\ NO_2 + H_2O \xrightarrow{surface} HONO + HNO_3} \qquad \mathbf{(R1)}$$

Laboratory studies have proposed that heterogenous HONO formation is first order in NO_2, and water is crucial in the NO_2 to HONO conversion process (Finlayson-Pitts et al., 2003; Pitts et al., 1984; Sakamaki et al., 1983; Svensson et al., 1987). Finlayson-Pitts et al., (2003) observed that the NO_2 hydrolysis is relatively linear in water vapour concentrations below ~65 % relative humidity (RH). Unlike outdoor HONO chemistry, its indoor levels are not entirely reliant on NO_2 surface uptake. Previous studies have observed steady state levels of HONO in the dark (Stutz et al., 2004; Vandenboer et al., 2013) which also suggested HONO deposition onto surfaces is a potential loss process (Collins et al., 2018; Lee et al., 2002; Spicer et al., 1993). Taken together, established observations imply that dynamic production and exchange of HONO on surfaces should be a widespread phenomenon. Indoors, Wainman et al., (2001) suggested that an effective Henry's Law equilibrium explains the codependence of RH and slow emissions of gaseous HONO various surfaces. Gaseous HONO observations have since supported such equilibrium with interior surfaces (R2 and R3), which have been able to reasonable explain the typical average background levels of ~5 ppb observed in the absence of direct cooking emissions (Brauer et al., 1990; Collins et al., 2018; Gómez Alvarez et al., 2013; Jarvis et al., 2005; Lee et al., 2002; Zhou et al., 2018). Interior surfaces can readily sorb water to make them reactive to NO_2 and then act as a reservoir for HONO including a prolonged release of HONO even after NO_2 has been removed from the indoor air (Wainman et al., 2001). Other lab studies have found gas-phase HONO readily formed and partitioned from acidic surfaces (R4) (Collins et al., 2018; Finlayson-pitts, 2009; Finlayson-Pitts et al., 2003; Spicer et al., 1993; Wainman et al., 2001; Wang et al., 2020b). To demonstrate the presence and capacity of the HONO surface reservoir, Collins et al., (2018) performed perturbation experiments by ventilating a home after ensuring substantial HONO deposition to surfaces by exposure to elevated levels of HONO from cooking with gas appliances. They observed a rapid decrease in HONO mixing ratio after opening windows and doors due to indoor-outdoor air exchange diluting the indoor air. Once the dilution by ventilation was halted, stable levels of HONO immediately returned, and the authors hypothesize that these background levels were sustained by partitioning of nitrite from surface reservoirs (Collins et al., 2018).

$$\mathbf{HONO_{(g)} \rightarrow HONO_{(surface)}} \quad \textbf{(R2)}$$

$$\mathbf{HONO_{(surface)} \rightarrow HONO_{(g)}} \quad \textbf{(R3)}$$

$$\mathbf{HONO_{(surface)} \leftrightharpoons HONO_{(g)}} \quad \textbf{(R4)}$$

A recent study by Wang et al., (2020) performed additional enhanced ventilation experiments and measured that surface nitrite was present on deployed glass plates in the home. These observations support the potential for equilibrium control of gaseous HONO from a large surface reservoir. The materials capable of this chemistry include those in studies that have identified heterogenous HONO formation such as concrete, glass, soil, mineral dust, and indoor wall materials coated with photocatalytic paint (Ammann et al., 1998; Finlayson-Pitts et al., 2003; Gandolfo et al., 2020; Grosjean, 1985; Kirchstetter et al., 1996; Schwartz-Narbonne et al., 2019; Stemmler et al., 2006; Wainman et al., 2001). The parameters controlling the conversion of NO_2 to HONO include: the type of surfaces, chemical composition, RH, and temperature (Finlayson-Pitts et al., 2003; Jacob, 2000; Pitts et al., 1984; Wainman et al., 2001). Other studies of heterogenous HONO formation include surface photochemistry on solid organic films (George et al., 2005; Stemmler et al., 2006) and indoor surfaces (Gómez Alvarez et al., 2014; Schwartz-Narbonne et al., 2019). Investigating these production processes is essential because HONO directly impacts indoor air quality as a source of hydroxyl radical (OH) by photolysis (≤ 405 nm) (R5), even at the low light levels and photon energies in these spaces (Kowal et al., 2017; Schwartz-Narbonne et al., 2019). The hydroxyl radical (OH) is a driver of indoor oxidative capacity and can react with volatile organic compounds (VOC) to form secondary species.

$$\mathbf{HONO_{(g)} \xrightarrow{h\nu} OH + NO_{(g)}} \qquad \mathbf{(R5)}$$

There are limited measurements of NO_2 and HONO detected simultaneously in residencies (Brauer et al., 1990; Collins et al., 2018; Jarvis et al., 2005; Lee et al., 2002; Zhou et al., 2018) and fewer measurements in a commercial setting (Allen and Miguel, 1995; Khoder, 2002). Previously reported values of NO_2 in residencies with gas appliances may be positively biased with HONO interference in both real-time and passive sampling approaches, potentially overestimated by a factor of 3 (Spicer et al., 2001; Zhou et al., 2018). More time-resolved measurements of NO_2 and HONO are required in indoor environments to constrain the multiphase chemistry of HONO, its impact on the indoor oxidative capacity, and for improved modelling. Surface reservoir chemistry may play a key role in controlling indoor levels of HONO, and each indoor environment may vastly differ based on the frequency of activities (e.g., cooking and cleaning), lighting (sunlit areas or artificial lighting), ventilation, surface-area-to-volume ratio (SA:V), and building material. Recent advancements in indoor instrumentation make widespread measurements accessible for

deployment at different indoor facilities to understand how these factors can affect or drive indoor chemistry.

This study presents novel NO, NO_2, and HONO measurements in a commercial kitchen inside a university residence building for three weeks. The kitchen recently reopened after an extended closure (due to the COVID-19 pandemic), giving us a rare insight into capturing the increased emissions of pollutants as cooking activities increase from incoming/returning students. The custom-built instrument presented in Chapter 3 was deployed in the kitchen to provide modulated measurements of NO_x, HONO, and NH_x (NH_x = ammonia and amides), and the total gaseous reactive nitrogen indoors. Field observations of NO, NO_2, and HONO were targeted to provide a greater understanding of their chemical transformation and fate in a commercial setting with an on-demand ventilation system, varied cooking, and a high volume of known direct-emission activities like cooking and cleaning. In this work, we will investigate the processes of HONO formation present in a commercial kitchen, including the dynamic surface-gas partitioning of HONO. Time-resolved field measurements in the kitchen will be used to explore indoor processes that influence the formation of stable HONO during the day and night. There are four possible sources of HONO in the kitchen: transportation of outdoor HONO indoors, direct emissions from combustion cooking processes (these can also partition to surfaces), and heterogenous reaction of NO_2 on interior surfaces, and equilibrium partitioning of HONO generated on surfaces. The loss of HONO by photolysis is determined by measuring the photon flux via spectral irradiance in the kitchen. A simple model was used to calculate if these known processes can explain the observed levels of HONO in contrast to the role of gas-surface equilibrium. Environmental influences such as the air exchange rate (AER), temperature, NO_2 levels, lighting, and RH are investigated to understand their impact on the observed HONO budget.

4.2 Method

4.2.1 Sampling location and set up

Measurements of NO, NO_2, and HONO took place from August 27th to September 17th, 2021, at a commercial kitchen inside a university residence in Toronto, Ontario, Canada. These measurements were made by the HONO sub-unit in the tN_r instrument, which provides modulated measurements between two inlet pathways. One pathway bypasses and the other enters a Na_2CO_3-coated denuder, followed by analyte detection by a chemiluminescence analyzer (NO_x analyzer).

The first pathway detects NO_x* (NO + NO_2*), which includes interfering gas-phase NO_y species like HONO and HNO_3. The second sample flow pathway enters the carbonate denuder to scrub gaseous acidic species, which is primarily HONO because HNO_3 levels are negligible indoors (Brauer et al., 1990; Fischer et al., 2003; Vichi et al., 2016). The second pathway allows us to detect accurate levels of NO_2 by removing interfering HONO from the NO_2* measurement. This is a common interference in indoor NO_x measurements with these instruments (Spicer et al., 1994; Zhou et al., 2018). Thus, levels of HONO are determined by the difference calculated between NO_2* and NO_2 measurements. The tN_r instrument was set to change sample flow between four inlet pathways (NO_x*, NO_x, gas-phase tN_r, and tN_r scrubbing NH_x) every 5 minutes (min) with a total cycle time of 20 min at a chemiluminescent detector time resolution of 1 second (s). The sampling flow rate of the NO_x analyzer was 630 cubic centimeters per minute (ccm). The NO_x analyzer was calibrated to ensure precision in its response across its operating range (manufacturer specifications of 0 – 20 parts per million; ppm) before the campaign by a gas-calibration instrument (Gascal 1100TS, American Ecotech, Warren, RI, USA) using a standard gas cylinder of NO (Praxair, NI NO5MC-A3, 4.88 (± 5 %) ppm, Toronto, ON, CA) and conducts gas titrations to produce NO_2 by reaction with ozone (O_3). Prior to the start of the campaign, the HONO output from the HONO calibration source (Lao et al., 2020) was tested to ensure the calibration quantities were in an acceptable range (up to 20 ppb) that was suitable in detecting high HONO mixing ratios in a commercial kitchen, which was expected to increase up to 100 ppb from cooking with gas appliances. Calibration and quality checks were performed regularly (every 1-2 days) during the campaign using a custom-built zero-air generator and HONO calibration source during low cooking and cleaning activities in the kitchen. Zero air was also sent into the sample inlet of the tN_r instrument to measure backgrounds and to assess an inlet contamination. Calibration quantities of HONO were also sent through the carbonate denuders to confirm its scrubbing efficacy. Denuders were replaced with freshly coated Na_2CO_3 denuders every two days and tested to confirm their effectiveness of >95 %.

The tN_r and supporting instruments were housed in an air-conditioned office nearby the main kitchen area (Figure 4-1). All instruments shared the same sampling line (51805K72, 1/4" OD PFA tubing, McMaster-Carr, Aurora, OH, USA) as a shared inlet, which was fitted with a polytetrafluoroethylene (PTFE) filter (47 mm single stage, ¼" x ¼" PFA Clamp, Savillex, Eden Prairie, MN, U.S.A) to remove particles. The inlet operated a total sampling flow rate of 3.5 LPM.

Outside the main kitchen is a serving area for customers, operating from 8:00 to 21:00 every day and includes cooking stations for stir-frying and grilling. Multiple hood vents located throughout the kitchen are combined into one exhaust pathway. A microcontroller (Arduino Uno R3, Arduino, Italy) logged the rotations per minute (RPM) from the kitchen exhaust fan panel to determine the AER from August 27th to September 17th, 2021. The exhaust fan controller and panel was located outside of the kitchen in a mechanical room near the roof of the residence building. The cooking ventilation in the main kitchen is controlled by on-demand exhaust hoods (ECOAZUR®, Laser Heating & Air Conditioning, Brampton, Ontario, Canada), which optimizes the airflow rate (up to a maximum of 25 000 cubic feet per min; CFM) based on the temperature and detection of steam and particulate matter with a light-scattering sensor. The ventilation system includes remote monitoring of the kitchen temperature and has nine temperature sensors co-located with the exhaust hoods. The average of all temperature sensors (15 min resolution) was calculated to obtain a representative temperature for model calculations from August 27th to September 17th, 2021. The kitchen contains no windows, and the lights are always on. The lighting intensity was typical for an indoor environment at 3.2 W m^{-2} which was measured using a spectral radiometer (Black Comet, C-50, StellarNut, Inc., Tampa, FL, USA). Continuous measurements of NO_x* were collected from a second chemiluminescence analyzer (EC9841, American Ecotech, Warren, RI, USA) and deployed from September 3rd to September 17th, 2021. Continuous measurements of O_3 by an O_3 analyzer (Serinus 10, American Ecotech, Warren, RI, USA) was deployed from August 27th to September 17th, 2021. The RH was logged every minute using a simple sensor (BME680, Adafruit, New York City, USA) connected to a microcontroller (Raspberry Pi 0w, Raspberry Pi Foundation, UK) from September 3rd to September 17th, 2021. This was placed in the main kitchen adjacent to the office housing the instruments. The kitchen outer surface area (e.g. walls, floors, ceiling) is 656.6 m^2. The furniture and kitchen appliances were not measured separately to determine the total surface area in the kitchen. Instead, the value was multiplied by three to approximate the additional surface area within the space to obtain a lower limit estimate of 1970 m^3. The kitchen volume is 617.3 m^3, and the resulting SA:V is 3.2 m^{-1}. The dimensions of the kitchen are presented in detail in Appendix C, Fig. 4-S1.

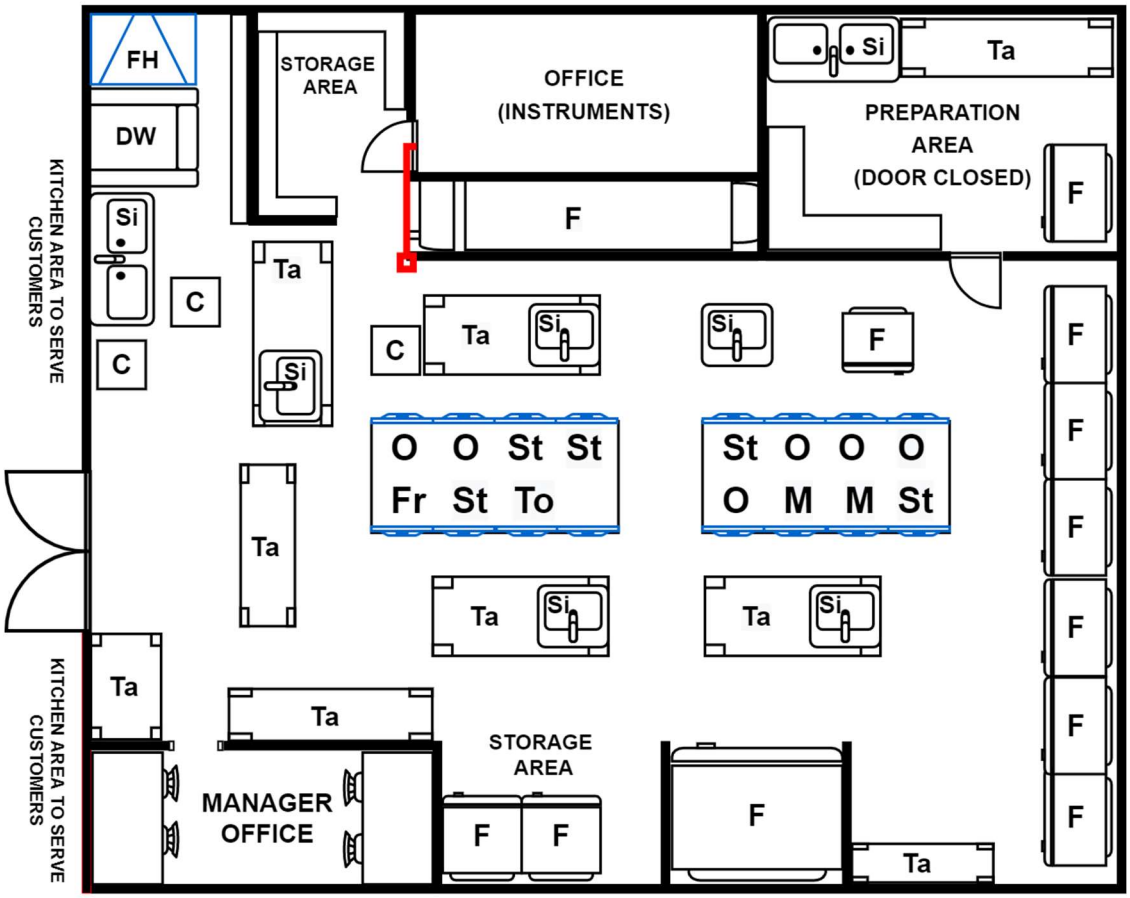

Figure 4-1. Floor plan of the commercial kitchen. The red line represents the instrument sampling line to detect kitchen emissions and the blue symbols represents the exhaust vents. Labels of the furniture/appliances are fume hood (FH), dishwasher (DW), sink (Si), table (Ta), fridge and/or freezer (F), steamer and/or stove top (St), fryer (Fr), O oven (O), mixer (M), and toaster (Ts). The quarter circles represent doors, and the solid black lines are walls. The unlabeled L-shape represents shelves. Note: the floor plan does not depict all furniture and appliances present in the kitchen.

4.2.2. Calculations

4.2.2.1 Kitchen air exchange rate

The kitchen AER was calculated using data logged from the exhaust fan. The exhaust fan panel sends an analog output of 4 milliamperes (mA) at 0 RPM (minimum speed) and 20 mA at 1750 RPM (maximum speed). A 250-ohm resistor was attached to the Arduino device to convert the current outputs to voltage values ranging from 1-5 V for logging, and these were then converted back to RPM. All negative values in RPM were corrected to 0 and the accuracy of the fan signal output is ± 10 % (specifications by the manufacturer). The maximum rotation rate of the exhaust

fan is 1750 RPM which translates to 25 000 CFM ventilation flow. The total kitchen volume is 617 m^3. These three values were used to calculate the kitchen air exchange per unit time (AER; h^{-1}) with the measured exhaust fan rotation rate (x RPM; E1).

$$\mathbf{AER\ (h^{-1}) = \frac{x\ RPM}{1750\ RPM} \times \frac{25000\ CFM}{total\ room\ volume\ m^3} \times \frac{60\ min}{h} \times \frac{m^3}{35.31\ ft^3}} \quad \mathbf{(E1)}$$

The kitchen AER can be separated into two periods: daytime (5:00 – 22:00) when kitchen ventilation is operating, and nighttime (22:00 – 5:00) when this exhaust fan controlling the kitchen ventilation is off is low and/or near zero.

4.2.2.2 Estimating the production rate of HONO from NO_2

The surface uptake coefficient of NO_2 (γ_{NO2}) is the probability of gaseous NO_2 colliding onto an indoor surface to produce HONO (E2). The equation, E2 has been described for the indoor environment where γ_{NO2} is directly affected by the high SA:V and AER from the removal rate of NO_2 by the reactive uptake to indoor surfaces ($k_{rem,NO2}$) (Collins et al., 2018; Mendez et al., 2017). In outdoor environments, γ_{NO2} corresponds to the geometric surface area and does not include AER. Briefly, the $k_{rem,NO2}$ is based on the loss of NO_2 to the surfaces to undergo reaction to form gas-phase HONO and combined with the indoor AER. Where V is the room volume (m^3), ωNO_2 is the thermal velocity of NO_2 at the average indoor temperature over the campaign (28.0 °C; m s^{-1}), S is the indoor surface area (m^2), and $k_{rem,NO2}$ is the removal rate of gaseous NO_2 to surface (s^{-1}). Continuous measurements of NO_2* from the second chemiluminescence analyzer were used to determine the daytime average $k_{rem,NO2}$ of $8.03 \times 10^{-3} \pm 6.03 \times 10^{-3}$ s^{-1} (28.88 ± 21.73 h^{-1}) (individual values can be found in Table 4-S1) from a total of 23 events. An exponential fit (Fig. 4-S3) was applied to peak levels of NO_2 prior to their clear loss to find the decay time constant (τ) and removal rate ($k_{rem,NO2} = 1/\tau$). Daytime NO_2* is removed by the kitchen exhaust vent. No peaks of NO_2 were present during the night since the kitchen was closed with no cooking-related emissions. Therefore, the averaged nighttime AER of 2.85×10^{-5} s^{-1} (0.10 h^{-1}) is the average nighttime $k_{rem,NO2}$. The averaged nighttime AER was calculated by averaging the kitchen AER per night (total of 21 nights) from 22:00 – 5:00 using E1. The calculated daytime and nighttime γ_{NO2} in the kitchen are compared to previous indoor studies in Section 4.3.4.

$$\mathbf{\gamma_{NO2} = \frac{4k_{rem,NO2}V}{\omega_{NO2}S}} \quad \mathbf{(E2)}$$

The HONO production (P_{HONO}) by heterogenous NO_2 uptake to surfaces was calculated using E3, where 0.5 represents the moles of HONO produced from NO_2 and measured number density of NO_2 in molecules per cubic centimeter ([NO_2]; molec cm^{-3}). In E3, $k_{rem,NO2}$ represents the deposition velocity driving the rate of HONO production and concentration of gaseous NO_2 (Abbatt and Wang, 2020; Collins et al., 2018). Values of P_{HONO} calculated with this approach represents the upper limit of HONO formation from NO_2 uptake (Collins et al., 2018).

$$\mathbf{P_{HONO} = 0.5 \times k_{rem,NO2} \times [NO_2]} \quad \textbf{(E3)}$$

4.2.2.2 Photolysis rates of HONO

The spectral radiometer measured the spectral irradiance as a function of wavelength (W m^{-2} nm^{-1}) at roughly human head height since most chemical models simulate chemistry at this respiration region for exposure determinations. Photolysis rates of HONO were calculated to determine if it is an important sink in the kitchen via R5 and also the rate of OH production. Measurements of the spectral irradiance were converted to photon flux (F) (photons cm^{-2} nm^{-1} s^{-1}) (Fig. 4-S3). The photolysis rate constant of HONO (J_{HONO}) was calculated via E4 (Kowal et al., 2017) using the measured photon fluxes (F), the absorption cross-section (σ) (Kenner et al., 1986; Stutz et al., 2000) and photolysis quantum yields (ϕ) at a given wavelength (λ) in nm and integrated over the relevant range. Reported quantum yields for HONO photolysis are unity (Burkholder et al., 2020; Cox and Derwent, 1976).

$$\mathbf{J_{HONO}} = \int_{\lambda i}^{\lambda f} \boldsymbol{\sigma(\lambda)\phi(\lambda)F(\lambda)d\lambda} \quad \textbf{(E4)}$$

The rate of HONO photolysis (L_{HONO}) is then dependent on the photolysis rate in s^{-1} (J_{HONO}) and measured number density of HONO ([HONO]; molec cm^{-3}) (E5) (Kowal et al., 2017).

$$\mathbf{L_{HONO} = J_{HONO}[HONO]} \quad \textbf{(E5)}$$

4.2.3.3. Predicted HONO concentrations

Since the direct emissions of HONO were rapidly ventilated from the kitchen, to the extent that we could not quantify them with the time resolution of our instrument, it seemed unlikely that this was playing a major role in setting the observed HONO levels in the kitchen. A simple model was constructed using E6 to investigate if the well-known processes of NO_2 heterogenous reactions and photolysis are the main controllers on the temporal behavior of HONO observed in the kitchen.

Predicted concentrations of HONO (molec cm^{-3}) were therefore calculated by the difference between the produced HONO from heterogenous NO_2 reactions and HONO photolysis over the modeled time intervals (dt).

$$\mathbf{[HONO]_{predicted} = (P_{HONO} - L_{HONO})\ dt} \quad \textbf{(E6)}$$

4.3 Results and Discussion

4.3.1 Data processing of tNr measurements

The tN_r instrument has a user-friendly interface to control the flow rate, valving switching, and time resolution of each pathway. The datetime, valve switches, and measurements from the NO_x analyzer are logged into a text file. Text files are saved every 1-2 days to prevent data loss/corruption. These files are uploaded to an integrated development environment (RStudio, Boston, MA, USA) to apply a custom-written R script to quickly clean and process the data for further analysis and visualization. A summary of the data processing (focusing on NO_x*, NO_x, and HONO) in the R script (4.S4) includes:

1. Organizing tN_r datasets by each sampling pathway and the number of cycles through the inlet configuration
2. Separating each cycle number into multiple data frames and integrating it into a large list for each inlet configuration
3. Calculating an average at 1 min time-resolution for each data frame located in the list
4. Removing the first minute of each data frame to account for the time response of the tN_r instrument, which is limited by the NO_x analyzer
5. Concatenating each sampling pathway and sorting by datetime to have a total of four data frames per pathway (e.g., attached all measurements of NO_x* into one data frame)
6. Filling in missing datetimes and applying linear interpolation for each sampling pathway to estimate mixing ratios in missing gaps of 15 min
7. Calculating the difference of NO_2* and NO_2 to determine the mixing ratio of HONO
8. Generating scatter plots as a quick QA/QC visualization and then saving processed datasets into the assigned directory
9. Combining daily processed datasets into one large dataset for the entire campaign
10. Removing interpolated data when they do not make physical or chemical sense. For example, if NO_2 levels that are greater than NO_2*, and this would result in negative values for calculated HONO
11. Calculating the rate of change between measured data points of NO_2* and NO_2; if it is ±50 %, then flag for manual removal of interpolated values of NO_2*, NO_2, and calculated values of HONO. The rate change was calculated to determine the percent change in mixing ratio over

a period of time (1 min). This identifies emission events for measurements determined by difference (e.g. HONO) that have a duration shorter than the time resolution of the instrument inlet cycling time.

Linear interpolation was incorporated into the R script to fill in missing gaps of ~16 min from removed data points from Step 4 and modulated inlet pathways for each pollutant. This statistical method utilizes two measurement periods bracketing the gap and fills in missing data between the measured points with a straight line. The interpolated data could underestimate or overestimate the mixing ratio of pollutants, depending on the distribution of measured values and length of time gap (Junninen et al., 2004). This is because linear interpolation assumes the rate of change is uniform, which could be unrealistic in a commercial environment with activities that result in short duration emission spikes. In this commercial kitchen, high levels of NO_x and HONO are directly emitted from combustion cooking processes and could be missed in our data processing approach. The exhaust vent quickly removes these chemical emissions during the day because the kitchen has a high AER of 27.2 ±7.28 h^{-1}. High variability in the measured daytime AER is driven by the fact that the exhaust ventilation in the kitchen is regulated on-demand or by sensor feedbacks, and as a result the exhaust fan speed adjusts accordingly based on the sensed cooking temperature or smoke/steam transiting a light beam and causing scattering.

Interpolated points generated under such conditions are manually removed using analytical software (Igor Pro 8.04, Wavemetrics Inc., Portland, OR, USA) when cooking events shorter than our total instrument cycle time of 20 min were encountered. This prevents gross systematic bias in our final dataset. This removes the bias of assuming pollutants levels are stable when they are known to be rapidly increasing or decreasing, which was identified in this campaign by comparing the tN_r measurements (NO, NO_2*, and NO_x*) to those of the second chemiluminescence analyzer. Steps 10 and 11 in the R-script were written to speed up the data finalization process. Step 11 flags gaps between our measured data points with a rate change of ± 50 % for manual removal of interpolated data points. For example, the first data point measured from cycle 2 has increased/decreased in mixing ratio by 50 % compared to the last data point measured from cycle 1. This will be flagged to remove the interpolated points that was filled in between measured cycle 1 and cycle 2. Flagging the rate change of ± 50 % may work better in indoor facilities with stable or lower AER. This commercial kitchen has varying AER throughout the day, so rapid changes in mixing ratio may be less than 50 %. Therefore, requiring manual removal by visualization in the

graphed time-series to remove interpolated data when measuring pollutants rapidly change in mixing ratio between detection cycles. Measured data points (NO, NO_2, NO_x, NO_2*, and NO_x*) were retained during these rapid cooking events since they are real measurements. As a result, the majority of direct HONO emissions during the rapid cooking events were removed from the final dataset due to high uncertainty in their values from the short lifetimes of the plumes in the kitchen. Thus, the presented HONO levels in this work are lower-limit representations that do not fully capture the peak values resulting from direct combustion emissions. The final dataset that results from this processing is at 1 min time resolution with 4 minutes of data measured, and the remaining data points linearly interpolated or left unreported based on these interpretation and processing criteria.

4.3.2 Intercomparison of NO_x* measurements between NO_x analyzers

Linear regression was included in the comparison of the relationship of NO, NO_2*, and NO_x* measurements from the tN_r instrument (real measurements every 15 min) against the second chemiluminescence analyzer (measures continuously at 1 min resolution). Both analyzers were calibrated at the same time using the gas-calibration instrument prior to the campaign. The tN_r instrument is the independent variable, while the chemiluminescence analyzer is the dependent variable because it is the more reliable measure with its continuous detection. Table 4-1 displays the slope, coefficient of determination (R^2), and intercept for NO, NO_2*, and NO_x* measurements on September 17th, 2021. The slope of NO_2* and NO_x* show good comparability between the two analyzers and have similar mean changes in response. Both NO_2* and NO_x* have a positive linear relationship of R^2 (0.96), confirming that both analyzers are aligned in detection. Throughout the campaign, NO levels were highly variable temporally, and most of its levels were near the detection limit of 0.4 ppb. Levels of NO_2 were always above the instrument LOD of 0.6 ppb, which was why the comparison between both analyzers were good.

The uncertainty of measurements near the detection limit is ±50 %, which contributes to the lower correlation coefficient and linear relationship between both analyzers for NO ($R^2 = 0.30$). The poor comparison in NO measurements is also likely from the tN_r instrument underestimating NO levels because it cannot capture high NO emissions, unlike the second chemiluminescence analyzer with continuous measurements. When comparing a short period (30 min) of measured NO during cooking events with high levels (> 66 ppb), the linearity increased to an R^2 of 0.70 and a slope of

1.0. Overall, the tN_r instrument is reliable in measuring NO_2* and NO_x* with a low potential for error from the time averaging intervals and interpolation. Measurements of NO are reliable when levels are above the detection limit. The current data analysis in this work includes data below the LOD. Future implementation of tN_r data finalizing should reject data below the instrument LOD to improve accuracy and precision in detecting pollutants. The intercepts can be used to correct the datasets for finalizing the NO, NO_2*, and NO_x* measurements since they represent the mean value of the response variable when all predictor variables in the linear model are zero.

Table 4-1. Linear Regression of NO, NO_2*, and NO_x* measurements from tN_r instrument and chemiluminescence analyzer on September 17th, 2021

Pollutant	Slope	R^2	Intercept
NO	0.46	0.30	0.90
NO_2*	0.96	0.96	2.80
NO_x*	1.0	0.96	3.2

4.3.3 Kitchen measurements

Daily and hourly diurnal trends in AER, temperature, RH, HONO, NO, NO_2, and NO_x are presented in Fig. 4-2 and Fig. 4-3. Trends of AER (Fig. 4-2a, Fig. 4-3a) are correlated to cooking events because the on-demand ventilation is linked to their exhaust hoods. The ventilation system was designed to generate an optimal exhaust airflow when cooking to save energy (instead of continuously operating at maximum flow), resulting in varied AER throughout the campaign. Average daytime and nighttime AER are 27.22 ± 7.3 h^{-1} (range of 0 – 35 h^{-1}) and 0.10 ± 0.17 h^{-1} (0 – 0.46 h^{-1}). Monday was the least busy (Fig. 4-2a, Fig.4-3a) with fewer customers purchasing meals leading to less cooking. Monday had the highest variability in activity since the first Monday of the campaign was also a national holiday, and the kitchen was closed with a daytime AER of 0 h^{-1}. Weekdays from Tuesday through Thursday had AER up to 40 h^{-1} during the afternoon because it was the busiest with cooking events. The daytime average AER in the kitchen was 4.5 times greater than the recommended minimum of 6 – 8 h^{-1} for acceptable indoor air quality set by the American Society of Heating, Refrigerating and Air-Conditioning Engineers (ASHRAE) (ASHRAE 2019). This observation suggests the kitchen staff have low exposure to indoor pollutants from cooking emissions since they are quickly transferred out of the kitchen by the exhaust fan. Temperature and RH (Fig. 4-2b, Fig. 4-3b) were stable throughout the campaign at 28.0 ± 2.46 °C and 31.2 ± 3 %. Hourly temperature trends show a slow increase of ~4 °C from

26 °C starting from 6:00, reaching its max at 30 °C at noon. This is driven by outdoor air being transported into the kitchen. The response of the automated heating, ventilation, and air conditioning (HVAC) system to maintain cool temperatures indoors as outdoor summer temperatures peak in the early afternoon mutes the actual temperature changes of the outdoor air through energy exchange. The temperature slowly decreases back to 26 °C as outdoor temperatures fall and energy is exchanged into the air to maintain the indoor temperature. Trends of RH are inverse to temperature, where RH increases at night when the temperature is low and decreases when the temperature is high, as expected.

The tN_r instrument can capture nitrogen oxides directly emitted from cooking combustion processes. However, what is observed depends on its measurement cycle and whether cooking events last longer than its total cycle time of 20 min to provide the most reliable quantitative data. Hourly diurnal trends of NO and NO_2 (Fig-4-2c, Fig. 4-3c) are the highest during the day from 6:00 – 16:00. During this time, hourly averages of NO range from 4.21 – 19.65 ppb, NO_2 9.46 – 17.49 ppb, and NO_x 12.21 – 34.27 ppb. The reviewed kitchen cooking logs reported the most active cooking with gas appliances from 9:00 – 16:00, but high levels of NO_x initiate at 6:00. The morning increase in NO_x emissions is likely from outdoor air transported indoors. These are suspected to be from a nearby combustion point source or regional pollution (e.g., YorkU Chimney Stack power plant or commuter traffic). These increased emissions of NO_x indoors were also observed on the university campus when the tN_r instrument was deployed in a laboratory (Chapter 3, Section 3.3.6.1). Transportation of NO and NO_2 can raise indoor kitchen levels and occur by natural ventilation (open doors and windows), infiltration (outdoor air penetrating the building envelope through cracks and porous materials), and mechanical ventilation (e.g., HVAC). The high AER from 9:00 – 16:00 matches the known high emissions of NO and NO_2, originating from cooking with gas appliances, which are then efficiently transferred out of the kitchen by the on-demand air exchange. The high range and variability in NO and NO_2 throughout the day is affected by the type of cooking, cooking temperature, and AER. For example, the higher the combustion temperature, the higher the expected NO formation and emission from a gas stove burner (Dennekamp et al., 2001). When the kitchen is idle (i.e., low or zero cooking activities) or closed (17:00 – 5:00), levels of NO range from 2.09 – 3.94 ppb, NO_2 8.83 – 14.31 ppb, and NO_x 10.70 – 17.68 ppb. As expected, NO levels were much lower when the kitchen was idle than daytime NO (4.21 – 19.65 ppb) because there were no or little combustion processes from cooking

with gas appliances. The range of NO_2 when the kitchen was idle (8.83 – 14.31 ppb) and busy (9.46 – 17.49 ppb) were relatively similar in range, suggesting another source of NO_2 outside of cooking combustion processes. Nighttime kitchen hours (22:00 – 5:00) have less variable levels with averages of 3.32 ± 0.39 ppb NO, 13.12 ± 0.85 ppb NO_2, and 16.12 ± 1.02 ppb NO_x because of its low AER (0 – 0.46 h^{-1}) and no activities in a closed kitchen. The nighttime range of NO was much lower than daytime and often near the instrument detection limit of 0.4 ppb from the absence of cooking activities. The steady levels of NO_2 during the day and night suggests that outdoor transportation by mechanical ventilation plays a large source outside of direct combustion cooking emissions. Nighttime levels of NO_2 are expected to decrease from the lack of cooking activities, however the stable NO_2 levels at night suggests outdoor transportation of NO_2 is maintaining these levels.

The next important loss process of indoor NO_2, after removal by the exhaust system, is heterogenous surface uptake since indoor environments have high SA:V (Finlayson-Pitts et al., 2003; Gandolfo et al., 2017; Gómez Alvarez et al., 2014; Wainman et al., 2001). The γ_{NO2} was calculated to understand the probability of gaseous NO_2 undergoing reaction with the indoor surfaces of the kitchen during the daytime and nighttime periods of $k_{rem,NO2}$ had very different removal rates due to the operation of the HVAC system. A daytime γ_{NO2} of 4.27 x 10^{-5} was calculated using the average daytime $k_{rem,NO2}$ of 28.9 h^{-1} driven by the kitchen exhaust), which was similar to the average daytime AER of 27.2 h^{-1}. Daytime γ_{NO2} in the commercial kitchen was greater by 10 times to reported residential studies because our $k_{rem,NO2}$ was larger by ~27 times than has been reported for residential NO_2 removal rates of 0.5-1.5 h^{-1} (Collins et al., 2018; Spicer et al., 1989; Zhou et al., 2018). No comparisons of the NO_2 removal rate or γ_{NO2} can be made to other commercial settings due to lack of prior studies. Given the comparability between AER and $k_{rem,NO2}$ during the day, the nighttime γ_{NO2} of 1.52 x 10^{-7} was estimated using the average nighttime AER of 0.1 h^{-1} since no direct emissions of NO_2 were observed to calculate its removal rate. These findings suggest that surface uptake of NO_2 is more active during the day when high ventilation which promotes the constant delivery of outdoor NO_2 to interior surfaces, while nighttime surface uptake in contrast is slower by a factor of ~100.

Several papers have used E2 to calculate γ_{NO2} to determine the probability of NO_2 to surface uptake to form gas-phase HONO indoors (Collins et al., 2018; Mendez et al., 2017). This equation takes

into account the influence of the geometries of indoor surfaces and the combined loss rate of NO_2 to surface uptake and ventilation ($k_{rem,NO2}$) (Table 4-S1, Fig. 4-S2). Gas-phase NO_2 has been reported to have high deposition velocities (0 – 0.18 cm s^{-1}) for a large range of indoor materials but these can vary depending on the rate of uptake on different surfaces (Abbatt and Wang, 2020; Grøntoft and Raychaudhuri, 2004; Mendez et al., 2017). There are limitations in using E2 because there is limited information on the parameters of indoor environments from indoor modelling studies, which means that describing surface transformations with a value for γ_{NO2} no longer represents a reaction probability and the SA:V is always an estimate. This is because the term combines the reactive removal rate of NO_2 and its physical mixing and transport processes (e.g. AER and transport within the kitchen in this work; $k_{rem,NO2}$). However, past literature has not been clear on providing detailed explanation on how this representation of the removal loss of NO_2 indoors is representative of the heterogeneous formation of HONO, despite giving reasonable results when used, and requires further investigation.

The γ_{NO2} calculated in this work uses a geometrically-determined SA:V of 3.2 m^{-1} multiplied by a factor of three to scale the area to be inclusive of the large volume of furnishings and kitchen equipment, which is similar to the approach of previous indoor studies (Carslaw, 2007; Collins et al., 2018; Manuja et al., 2019). This approximated SA:V, therefore, comes with a factor three uncertainty because we do not know the absolute value of the kitchen surface area. Most indoor studies have multiplied their indoor surface area by a multiple of two to three times and this was considered as a lower limit to properly represent the true surface area from other room contents and not just the geometric area from the wall, ceiling, and floors. Taken together this approach to γ_{NO2} and SA:V currently limits our knowledge when modeling the reactive uptake of NO_2 to various surface materials, and further characterization of the different reactive surfaces and surface reservoirs are required to fully understand indoor chemistry. This work provides insight into a commercial setting by presenting time-resolved measurements and utilizes these equations from previous works to estimate the heterogenous processes of HONO for comparison purposes.

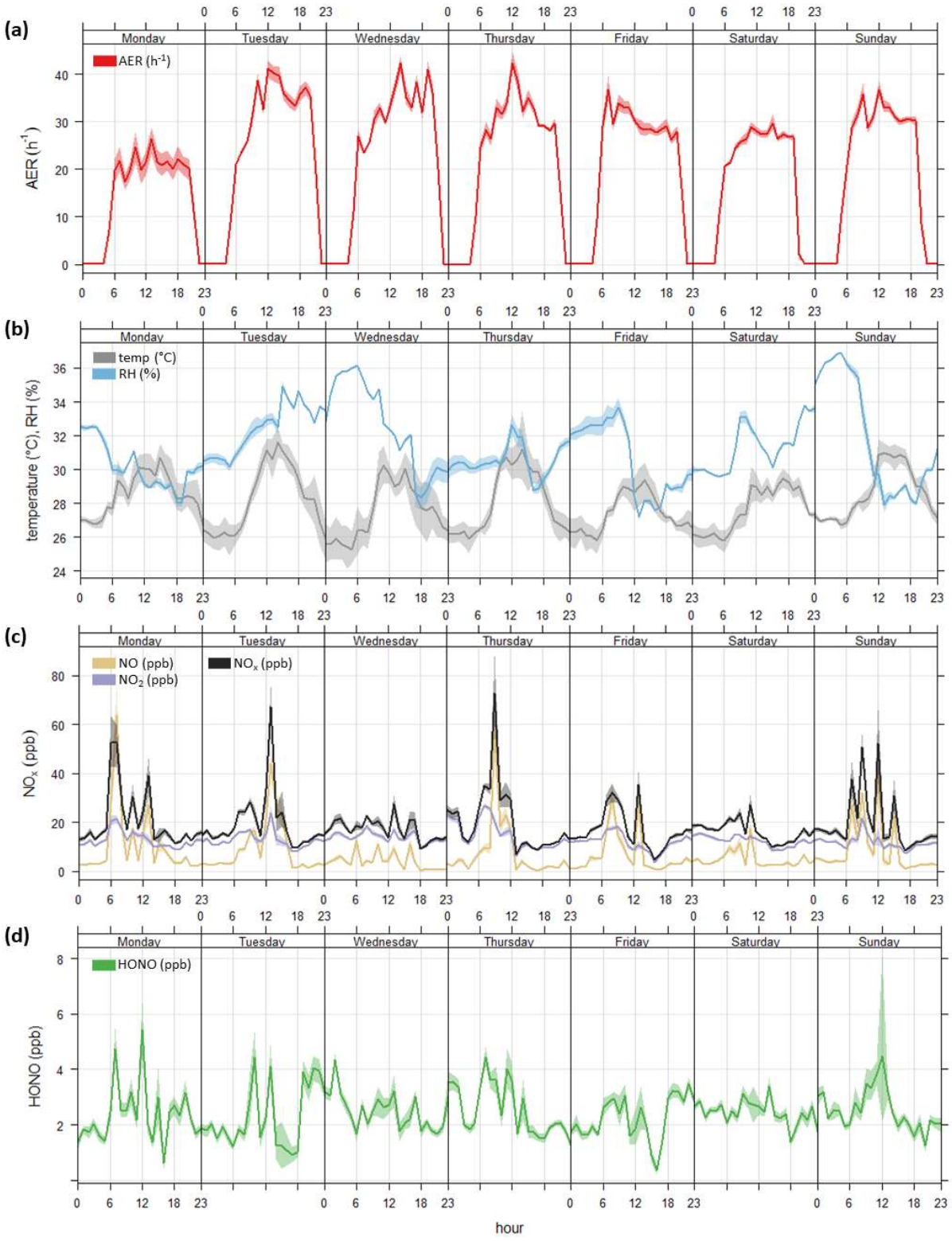

Figure 4-2. Daily diurnal trends of 21 days except for RH (14 day) for **(a)** AER (red), **(b)** temperature (grey) and RH (blue), **(c)** NO (tan), NO_2 (purple), and NO_x (black), and **(d)** HONO (green).

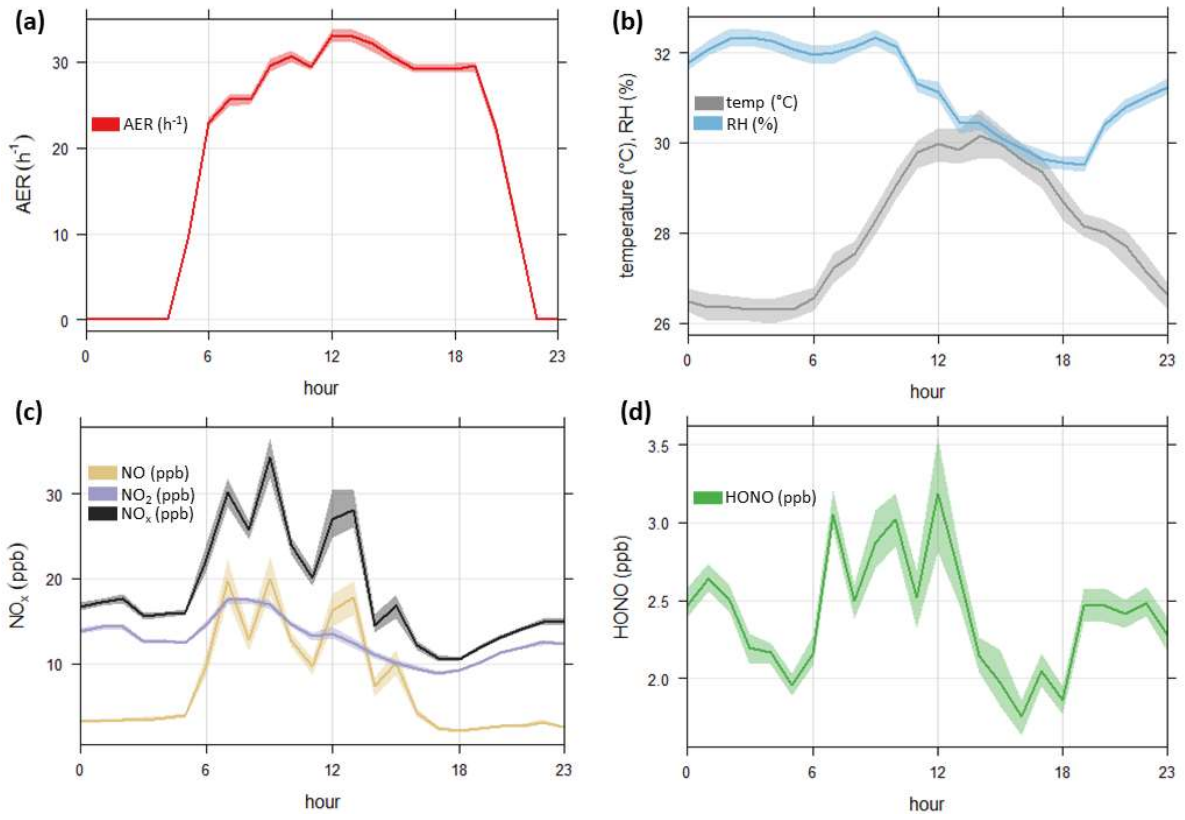

Figure 4-3. 24-Hour diurnal plots of 21 days except for RH (14 day) **(a)** AER (red), **(b)** temperature (grey) and RH (blue), **(c)** NO (tan), NO_2 (purple), and NO_x (black), and **(d)** HONO (green).

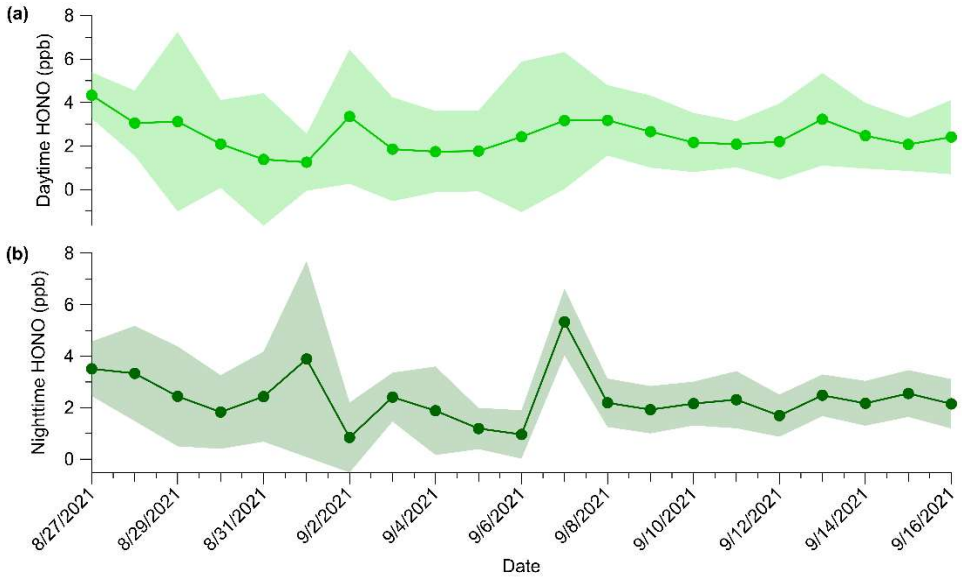

Figure 4-4. Comparison of **(a)** average HONO mixing ratios during the day (light green circles with line) ranging from 1.25 – 4.33 ppb and **(b)** average nighttime mixing ratios (dark green with circles) ranging from 0.96 – 5.33 ppb.

4.3.4 HONO chemistry

Mixing ratios of HONO (Fig. 4-2d, Fig. 4-3d) in the absence of direct emissions, had stable background levels throughout the campaign with an average of 2.41 ± 2.05 ppb. Average daytime and nighttime levels of HONO were similar at 2.48 ± 2.07 ppb and 2.36 ± 1.29 ppb (Fig. 4-4) regardless of the difference in AER during these two periods (daily day and night HONO averages presented in Appendix C, Table 4-S2). A two-tailed t-test was performed to determine that the average daytime and night values were statistically similar with a p-value of 0.05, which was equal to the significance level of 0.05. Daytime levels of HONO were thought to be higher from the direct combustion emissions from cooking with gas appliances. However, the time resolution of the instrument and effective ventilation system resulted in detecting the heterogenous HONO processes rather than the combination with direct HONO emissions. The stability between daytime and nighttime averages suggests that an HONO equilibrium is present in the kitchen, since the tN_r instrument captured the majority of HONO emissions outside of the direct cooking events that rapidly decayed in ≤ 20 min.

Previous work on the characterization of the automated HONO platform in the tN_r instrument (Chapter 3) has identified that a positive bias of HONO is present in the instrument sampling lines of up to 5 % from the combined production of HONO from NO2 on the inlet and loss of NO2 in the denuder. Here, this could translate into an additional 0.12 ppb of HONO reported in the average measurement of 2.41 ppb. This was not a significant bias and is less than out instrument precision/noise of 0.4 ppb, while this was not corrected in our measurements presented here, the minor corrections will be applied to the finalized dataset for this study. Like NO_x, high levels of HONO were emitted between 6:00 – 16:00, and outdoor HONO co-emitted from nearby combustion processes was transported indoors in the early morning. From 9:00 – 16:00, higher NO_2 levels emitted from increased cooking activities can react on surfaces (daytime γ_{NO2} of 4.27 x 10^{-5}) to undergo heterogenous HONO formation. Outdoor HONO can travel into the kitchen at night via HVAC, which can contribute to the measurements of nighttime HONO because typical outdoor levels are ≤ 1 ppb (Lee et al., 2002; VandenBoer et al., 2013). The stable levels of HONO observed at night are suggestive of HONO partitioning from an indoor surface reservoir with a nitrite precursor to sustain the observed levels in the absence of NO_2 reactions, which has been reported by recent indoor residential home studies (Collins et al., 2018; Wang et al., 2020b). Background levels of HONO observed in this commercial kitchen (2.41 ± 2.05 ppb) is only about

50 % of the average HONO observed in residencies (~5 ppb) (Brauer et al., 1990; Collins et al., 2018; Febo and Perrino, 1991; Lee et al., 2002; Zhou et al., 2018). The high AER in the kitchen may decrease the probability of surface uptake of NO_2 and HONO onto the kitchen surfaces, depleting the nitrite abundance and HONO reservoir.

A simple chemical model was constructed to investigate processes that influence the temporal behaviour of HONO in the kitchen (Fig. 4-5). The production of HONO by NO_2 surface uptake and HONO photolysis are, as a result of the prior analysis, the likely competing processes in changing the levels of HONO in this space. Concentrations of P_{HONO}*dt is dependent on $k_{rem,NO2}$ and AER, which both change significantly during the day (5:00 – 22:00, $k_{rem,NO2}$ = 28.9 h^{-1}) and night (22:00 – 5:00, $k_{rem,NO2}$ = 0.10 h^{-1}). Comparing P_{HONO}*dt and measured HONO confirms that daytime HONO is primarily produced from heterogenous surface uptake of NO_2 (Fig. 4-4a). High NO_2 mixing ratios (Fig. 4-5b) are present in the kitchen from a combination of combustion cooking processes and outdoor NO2 brought indoors that then deposit onto kitchen surfaces, followed by its conversion (γ_{NO2} of 4.27 x 10^{-5} and $k_{rem,NO2}$ of 28.9 h^{-1}). These uptake values are reasonably similar to those reported for many indoor and outdoor surfaces (1 x 10^{-5} – 1 x 10^{-7}) (Collins et al., 2018; Klosterköther et al., 2021; Kurtenbach et al., 2001; Liu et al., 2020; Mendez et al., 2017; Ren et al., 2020; Spicer et al., 1989, 1993; Vandenboer et al., 2013). The high AER in the kitchen could influence the background HONO level observed since the commercial kitchen has lower background levels by 50 % compared to residencies with an average AER of ~0.5 h^{-1} (Collins et al., 2018; Wang et al., 2020b; Zhou et al., 2018) and this may reduce the buildup of nitrite on kitchen surfaces. The NO_2 surface uptake occurs regardless of the high AER, but because it can increase up to 40 h^{-1} it will flush pollutants out of the kitchen that partition from surfaces as well. Generally, this also points towards a HONO equilibrium that is generated from a HONO surface reservoir. Our model shows that nighttime formation of HONO is likely originating from the conversion of NO_2 since it has a small nighttime γ_{NO2} and removal rate of 1.52 x 10^{-7} and 0.1 h^{-1}. As a result, nighttime levels of NO_2 react on surfaces with 100 times less effectiveness compared to daytime γ_{NO2}. Therefore, the major source of nighttime HONO is likely driven by equilibrium partitioning from a reservoir of nitrite on kitchen surfaces that readily releases gas-phase HONO. Building material with a thin layer of water can readily sorb nitrite. In the presence of abundant NH_3, the nitrite will become deprotonated and can result in delayed HONO partitioning from surfaces at night (Wainman et al., 2001). Collins et al., (2018) and Wang et al., (2020) have

measured large nitrite quantities (average surface concentrations of 10^{12} molecules cm^{-2}) on indoor surfaces that is further evidence in support HONO reservoirs on many indoor surfaces. Extractions of surface nitrite quantities on multiple kitchen surfaces during the day (after periods of cooking and cleaning) and night could be used to strengthen our analysis and proof of HONO reservoirs driving HONO chemistry in the kitchen. Zhou et al., (2018) observed that their reactive NO_2 removal rate of 0.74 ± 0.35 h^{-1} was larger than their mean AER of 0.5 h^{-1}, which could mean that the probability of NO_2 surface uptake is higher in the commercial kitchen at night by up to 50 %. The increased NO_2 surface uptake by 50 % with $k_{rem,NO2}$ of 0.75 h^{-1} results in an increase of 2 % in P_{HONO}*dt, which is not enough to replicate the measured HONO at night. Predicted concentrations of HONO (Fig. 4-5a) were calculated (E6) to see if the measured HONO in the kitchen can be reproduced by using the upper limits of HONO production via direct NO_2 surface uptake (P_{HONO}*dt) and loss of HONO by photolysis to form OH (L_{HONO}*dt) (Fig. 4-4a). The loss rate of HONO by photolysis is minor and do not significantly influence the predicted HONO concentrations, but it improves the accuracy towards reproducing measured concentrations of HONO during the day. Predicted HONO concentration does not replicate measured HONO at night because our model does not account for gas-phase HONO partitioning from a reservoir in dynamic equilibrium with deposited nitrite. Future field laboratory studies should aim to measure concentrations of nitrite sorbed onto different indoor material to understand HONO surface reservoir chemistry and homogeneity. The consistent loss of HONO by photolysis shows that HONO could play a key role as an OH formation pathway indoors, requiring further investigation on their importance on the HO_x budget.

Indoor photolysis of HONO is a loss process that can result in the formation of OH, which has been suggested to happen readily in indoor environments, especially in sunlit areas (Gómez Alvarez et al., 2013; Zhou et al., 2018). Spectral irradiance measurements of the kitchen lighting were performed to determine OH production (-L_{HONO}*dt) from HONO in Fig. 4-5c. The kitchen lighting uses standard fluorescent bulbs, and the lights are always on, so J_{HONO} of 1.66 x 10^{-5} s^{-1} is constant throughout the day and night. The production of OH by HONO photolysis is on the order of 10^5 – 10^6 molecules cm^{-3} s^{-1} when considering the average HONO levels of 2.41 ± 2.05 ppb (5.85 x 10^{10} ± 4.95 x 10^{10} molec cm^{-3}). The J_{HONO} measured in this commercial kitchen is lower compared to previously reported indoor light sources (i.e., uncovered office fluorescent, halogen, incandescent) (Kowal et al., 2017) likely from being measured at head height and covered

fluorescent lighting, and in sunlit areas of residential areas at 10^{-4} – 10^{-5} s^{-1}. (Gómez Alvarez et al., 2013; Kowal et al., 2017; Zhou et al., 2018). The OH production rate calculated is 10 times smaller than observed in a residential home with a sunlit area (near a glass door) of 8.3 x 10^{6} molecules cm^{-3} s^{-1} when considering background HONO levels of 4.3 ppb (Zhou et al., 2018).

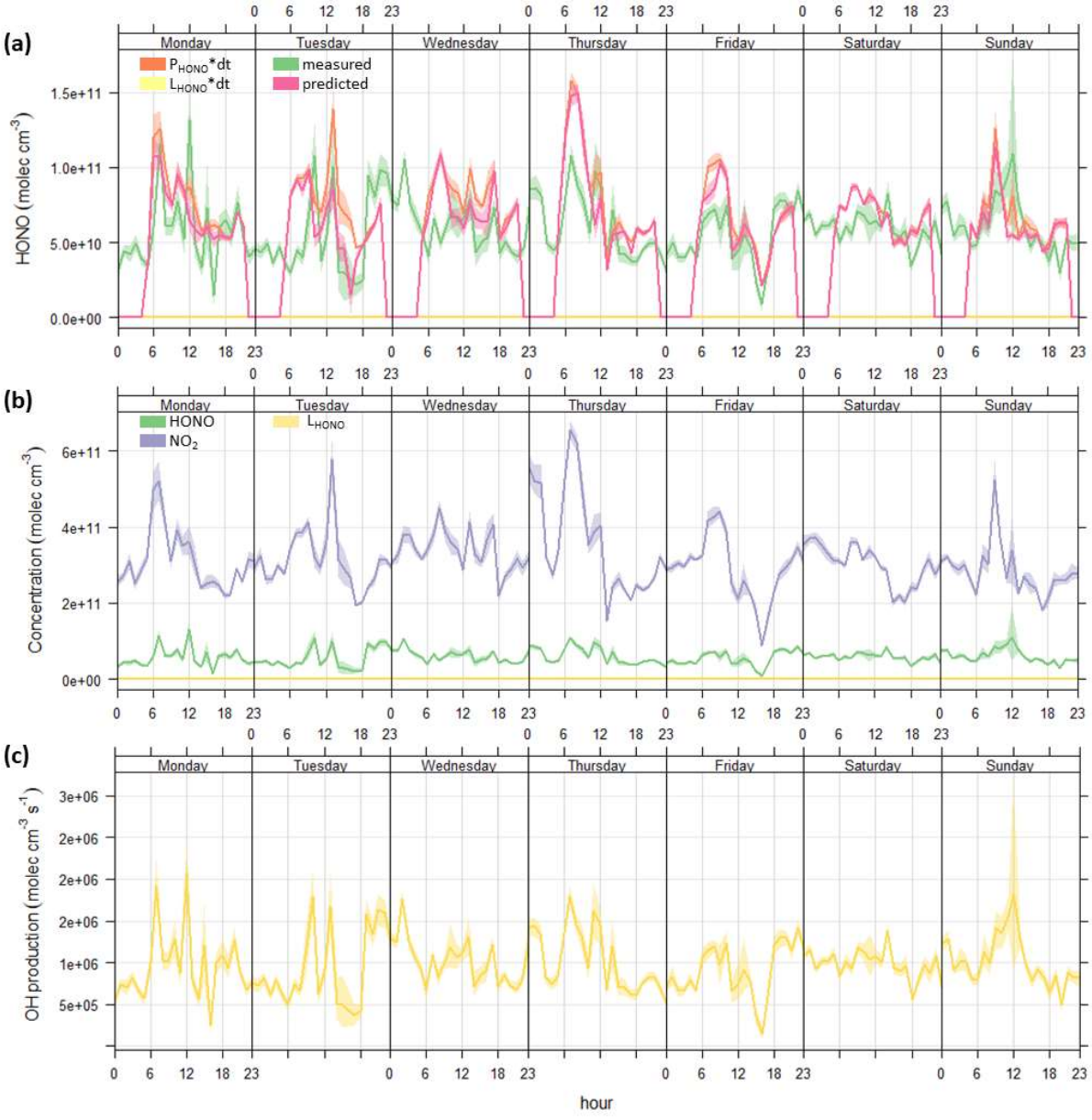

Figure 4-5. Workweek diurnal trends of **(a)** a constructed model to predict if the HONO concentrations (predicted, pink) generated by the source (P_{HONO}, orange) and loss (L_{HONO}, yellow) processes can replicate the measured HONO (green) in the kitchen; **(b)** comparison of measured HONO, NO_2 (purple), and L_{HONO}; **(c)** OH production rate (molecules cm^{-3} s^{-1}) by HONO photolysis.

The commercial kitchen has artificial lighting with lower photon levels than indoor environments with sunlight passing through windows, which has shorter wavelengths to promote HONO photolysis. Classrooms and university buildings have more sunlit areas with reported J_{HONO} values two times larger than our reported J_{HONO} (Gandolfo et al., 2016; Kowal et al., 2017). This study does not report steady state levels of OH in the kitchen because we would require VOC measurements to consider other potential sinks of OH, which is outside of the scope of this work. Future work may include this OH analysis with our collaborators who have performed VOC measurements during the campaign and are currently finalizing their datasets. The calculated OH production rates in the commercial kitchen shows that indoor environments in low light conditions can generate OH with artificial lighting. The commercial kitchen has a consistent source of OH production by HONO photolysis because the lights are on 24 hours a day, which is very different from prior reports (Gómez Alvarez et al., 2013; Zhou et al., 2018). Previous models have predicted OH concentrations to be ~10^5 molecules cm^{-3} indoors (Carslaw, 2007; Waring and Wells, 2015; Weschler and Shields, 1996; White et al., 2010), which greatly underestimates OH formation compared to recent indoor studies reporting OH concentrations up to 10^5 – 10^6 molec cm^{-3} in sunlight passing through windows (Gómez Alvarez et al., 2013; Kowal et al., 2017; Zhou et al., 2018). Our study shows that consistent production of OH (10^5 – 10^6 molecules cm^{-3} s^{-1}) is made with covered fluorescent lighting 24 hours a day. The OH production may be greater than expected in many indoor facilities because a typical house can generate up to 10^6 molec cm^{-1} for a few hours per day in sunlit areas and generate a lower amount under artificial lighting. The inclusion of all light sources should be incorporated into new OH models since HONO photolysis is a major contributor to the OH budget. Direct measurements of OH are difficult because of its short lifetime, therefore by improving models can result in better assessments of our indoor air quality and to limit secondary species production.

4.4 Conclusion and Future Work

Modulated measurements of NO, NO_2, NO_x, and HONO were performed in a commercial kitchen for three weeks using a new custom-built tN_r instrument that quantifies three key nitrogenous species of NO_x, HONO, and NH_3. Indoor factors like temperature, RH, and AER were measured to observe their influence on the temporal behavior of NO, NO_2, and HONO. The kitchen temperature and RH were stable throughout the campaign with averages of 28.0 ± 2.46 °C and

31.2 ± 3 %. The commercial kitchen has an on-demand ventilation system hooked to their exhaust hoods to generate an optimal exhaust flow rate and efficiently removes cooking-related emissions out of the kitchen. High daytime AER (average of 27.2 ±7.28 h^{-1}) is higher by 4.5 times than the minimal recommended AER in restaurants, indicating that the ventilation is optimal in maintaining acceptable indoor air quality. Nighttime AER is much lower (average of 0.10 ± 0.17 h^{-1}) than the daytime because there are no cooking activities after 22:00. The tN_r instrument could not capture high cooking emissions that lasted ≤ 20 min because it is less than its total cycle time and is set to detect four pathways every 5 minutes (NO_x*, NO_x, gas-phase tN_r, and tN_r scrubbing NH_x). The detection of HONO in this work presents in-situ HONO because direct HONO emissions from cooking were quickly ventilated out of the kitchen. Measurements of NO, NO_2* and NO_x* by the tN_r instrument were compared to a second chemiluminescence analyzer to confirm the reliability of the tN_r instrument, displaying positive linear relationships in NO (when above the instrument detection limit of 0.4 ppb $R^2 = 0.70$), NO_2* ($R^2 = 0.96$), and NO_x* ($R^2 = 0.96$). Emissions of NO_x were the highest from 6:00 – 16:00 from outdoor transport of nearby combustion processes in the early morning and higher volume of cooking activities (NO = 4.21 – 19.65 ppb, NO_2 = 9.46 – 17.49 ppb, and NO_x = 12.21 – 34.27 ppb). Levels of NO_2 were relatively steady throughout the day and night, with outdoor transportation via HVAC as the main source of nighttime NO_2 (22:00 – 5:00) at 13.12 ± 0.85 ppb. Nighttime NO (3.32 ± 0.39 ppb) was low because it is quickly titrated by O_3 to form NO_2 and no cooking events with gas appliances.

Stable levels of HONO were observed throughout the campaign with an average of 2.41 ± 2.05 ppb. Their average daytime and nighttime levels of 2.48 ± 2.07 ppb and 2.36 ± 1.29 ppb were statistically similar with a p-value of 0.05 with significant levels ≤ 0.05. Heterogenous NO_2 surface uptake is the dominant loss process of NO_2, with a high daytime γ_{NO2} of 4.27 x 10^{-5}. Daytime cooking emits NO_2 to rapidly uptake onto kitchen surfaces and undergo heterogenous formation to release gas-phase HONO, which our model supported. The model was poor in replicating nighttime HONO, suggesting that direct NO_2 surface uptake was not the source in nighttime HONO concentrations. Nighttime NO_2 has a lower probability of depositing onto surfaces with a small γ_{NO2} of 1.52 x 10^{-7}, pointing towards a HONO reservoir as the source in observing stable HONO at night. Our results are supported by recent residential studies in concluding that a large HONO surface reservoir was present to maintain stable HONO (Collins et al., 2018; Wang et al., 2020b). Direct evidence of nitrite depositing on indoor surfaces has been

reported (Collins et al., 2018; Wang et al., 2020b), and future laboratory work should include measuring sorbed nitrite concentrations on various interior surfaces. Various studies have probed the parameters of heterogenous NO_2 hydrolysis and provided evidence of this reaction on multiple surfaces (Finlayson-Pitts et al., 2003; Pitts et al., 1984; Ramazan et al., 2004; Sakamaki et al., 1983; Stutz et al., 2004; Svensson et al., 1987; Wang et al., 2020a) and the next step is to explore pre-existing nitrite films on surfaces to understand its sorption chemistry and mechanism. Calculations of HONO production via direct NO2 surface uptake were representative of our observed HONO in the kitchen and can be applied to indoor modelling for commercial or indoor facilities with high and varied AER. The proposed HONO reservoir is new and should be explored and incorporated into future models to understand indoor oxidative capacity. A better understanding of how indoor pollutants respond to perturbations from human activities (cooking, cleaning, use of commercial products, opening windows and doors for natural ventilation, or controlling their HVAC, etc.) and the change of chemical composition (pH, nitrite concentrations on surfaces) to improve indoor models of various indoor facilities and predict potential exposures and concentrations of pollutants indoors. The consistent production of OH (average of 9.72×10^{-5} molecules cm^{-3} s^{-1}, $J_{HONO} = 1.66 \times 10^{-5}$ s^{-1}) by HONO photolysis suggests that OH may be an essential driver in oxidation chemistry for indoor facilities that have lights on 24/7. The continuous OH production by HONO photolysis may contribute to other complex chemical interactions such as ozonolysis with cooking oil (Zhou et al., 2019). Future publications of this work will include a full report of our findings during the KOCENA campaign with collaborating scientists and shared on an open-sourced platform.

4.5 Reference

Abbatt, J. P. D. and Wang, C.: The atmospheric chemistry of indoor environments, Environ. Sci. Process. Impacts, 22(1), 25–48, doi:10.1039/c9em00386j, 2020.

Allen, A. G. and Miguel, A. H.: Indoor Organic and Inorganic Pollutants: In-situ Formation and Dry Deposition in Southeastern Brazil, Atmos. Environ., 29(23), 3519–3526, 1995.

Ammann, M., Kalberer, M., Jost, D. T., Tobler, L., Rössler, E., Piguet, D., Gäggeler, H. W. and Baltensperger, U.: Heterogeneous production of nitrous acid on soot in polluted air masses, Nature, 395(6698), 157–160, doi:10.1038/25965, 1998.

ASHRAE. 2019. ANSI/ASHRAE Standard 62.1-2019, Ventilation for Acceptable Indoor Air Quality. Atlanta: ASHRAE.

Bartolomei, V., Gomez Alvarez, E., Wittmer, J., Tlili, S., Strekowski, R., Temime-Roussel, B., Quivet, E., Wortham, H., Zetzsch, C., Kleffmann, J. and Gligorovski, S.: Combustion processes as a source of high levels of indoor hydroxyl radicals through the photolysis of nitrous acid, Environ. Sci. Technol., doi:10.1021/acs.est.5b01905, 2015.

Brauer, M., Ryan, P. B., Suh, H. H., Koutrakls, P. and Spengler, J. D.: Measurements of Nitrous Acid inside Two Research Houses, Environ. Sci. Technol., 24(10), 1521–1527, doi:10.1021/es00080a011, 1990.

Burkholder, J. B., Sander, S. P., Abbatt, J. P. D., Barker, J. R., Huie, R. E., Kolb, C. E., Kurylo, M. J., Orkin, V. L., Wilmouth, D. M. and Wine, P. H.: Chemical Kinetics and Photochemical Data for Use in Atmospheric Studies, Evaluation No. 19, JPL Publ. 19-5, 1–153 [online] Available from: http://jpldataeval.jpl.nasa.gov/, 2020.

Carslaw, N.: A new detailed chemical model for indoor air pollution, Atmos. Environ., 41(6), 1164–1179, doi:10.1016/j.atmosenv.2006.09.038, 2007.

Collins, D. B., Hems, R. F., Zhou, S., Wang, C., Grignon, E., Alavy, M., Siegel, J. A. and Abbatt, J. P. D.: Evidence for Gas-Surface Equilibrium Control of Indoor Nitrous Acid, Environ. Sci. Technol., 52(21), 12419–12427, doi:10.1021/acs.est.8b04512, 2018.

Cox, R. A. and Derwent, R. G.: The ultra-violet absorption spectrum of gaseous nitrous acid, J. Photochem., 6(1), 23–34, doi:10.1016/0047-2670(76)87004-9, 1976.

Dennekamp, M., Howarth, S., Dick, C. A. J., Cherrie, J. W., Donaldson, K. and Seaton, A.: Ultrafine particles and nitrogen oxides generated by gas and electric cooking, Occup. Environ. Med., 58(8), 511–516, doi:10.1136/oem.58.8.511, 2001.

Febo, A. and Perrino, C.: Prediction and experimental evidence for high air concentration of nitrous acid in indoor environments, Atmos. Environ. Part A, Gen. Top., 25(5–6), 1055–1061, doi:10.1016/0960-1686(91)90147-Y, 1991.

Finlayson-Pitts, B. J., Wingen, L. M., Sumner, A. L., Syomin, D. and Ramazan, K. A.: The heterogeneous hydrolysis of NO2 in laboratory systems and in outdoor and indoor atmospheres: An integrated mechanism, Phys. Chem. Chem. Phys., 5(2), 223–242, doi:10.1039/b208564j, 2003.

Fischer, M. L., Littlejohn, D., Lunden, M. M. and Brown, N. J.: Automated Measurements of Ammonia and Nitric Acid in Indoor and Outdoor Air, Environ. Sci. Technol., 37(10), 2114–2119, doi:10.1021/es026133x, 2003.

Gandolfo, A., Gligorovski, V., Bartolomei, V., Tlili, S., Gómez Alvarez, E., Wortham, H., Kleffmann, J. and Gligorovski, S.: Spectrally resolved actinic flux and photolysis frequencies of key species within an indoor environment, Build. Environ., 109(April 2018), 50–57, doi:10.1016/j.buildenv.2016.08.026, 2016.

Gandolfo, A., Rouyer, L., Wortham, H. and Gligorovski, S.: The influence of wall temperature on NO2 removal and HONO levels released by indoor photocatalytic paints, Appl. Catal. B Environ., doi:10.1016/j.apcatb.2017.03.021, 2017.

Gandolfo, A., Bartolomei, V., Truffier-Boutry, D., Temime-Roussel, B., Brochard, G., Bergé, V., Wortham, H. and Gligorovski, S.: The impact of photocatalytic paint porosity on indoor NOx and HONO levels, Phys. Chem. Chem. Phys., doi:10.1039/c9cp05477d, 2020.

George, C., Strekowski, R. S., Kleffmann, J., Stemmler, K. and Ammann, M.: Photoenhanced uptake of gaseous NO2 on solid organic compounds: A photochemical source of HONO?, in Faraday Discussions., 2005.

Gómez Alvarez, E., Amedro, D., Afif, C., Gligorovski, S., Schoemaecker, C., Fittschen, C., Doussin, J.-F. and Wortham, H.: Unexpectedly high indoor hydroxyl radical concentrations associated with nitrous acid, Proc. Natl. Acad. Sci., 110(33), 13294–13299, doi:10.1073/pnas.1309171110, 2013.

Gómez Alvarez, E., Sörgel, M., Gligorovski, S., Bassil, S., Bartolomei, V., Coulomb, B., Zetzsch, C. and Wortham, H.: Light-induced nitrous acid (HONO) production from NO2 heterogeneous reactions on household chemicals, Atmos. Environ., doi:10.1016/j.atmosenv.2014.06.034, 2014.

Grosjean, D.: Wall Loss of Gaseous Pollutants in Outdoor Teflon Chambers, Environ. Sci. Technol., 19(11), 1059–1065, doi:10.1021/es00141a006, 1985.

Jacob, D. J.: Heterogeneous chemistry and tropospheric ozone, Atmos. Environ., 34(12–14), 2131–2159, doi:10.1016/S1352-2310(99)00462-8, 2000.

Jarvis, D. L., Leaderer, B. P., Chinn, S. and Burney, P. G.: Indoor nitrous acid and respiratory symptoms and lung function in adults, Thorax, 60(6), 474–479, doi:10.1136/thx.2004.032177, 2005.

Kenner, R. D., Rohrer, F. and Stuhl, F.: OH(A) production in the 193-nm photolysis of HONO, J. Phys. Chem., 90(12), 2635–2639, doi:10.1021/j100403a015, 1986.

Khoder, M. I.: Nitrous acid concentrations in homes and offices in residential areas in Greater Cairo, J. Environ. Monit., 4(4), 573–578, doi:10.1039/b201818g, 2002.

Kirchstetter, T. W., Harley, R. A. and Littlejohn, D.: Measurement of nitrous acid in motor vehicle exhaust, Environ. Sci. Technol., 30(9), 2843–2849, doi:10.1021/es960135y, 1996.

Klepeis, N. E., Nelson, W. C., Ott, W. R., Robinson, J. P., Tsang, A. M., Switzer, P., Behar, J. V., Hern, S. C. and Engelmann, W. H.: The National Human Activity Pattern Survey (NHAPS): A resource for assessing exposure to environmental pollutants, J. Expo. Anal. Environ. Epidemiol., 11(3), 231–252, doi:10.1038/sj.jea.7500165, 2001.

Klosterköther, A., Kurtenbach, R., Wiesen, P. and Kleffmann, J.: Determination of the emission indices for NO, NO2, HONO, HCHO, CO, and particles emitted from candles, Indoor Air, 31(1), 116–127, doi:10.1111/ina.12714, 2021.

Kowal, S. F., Allen, S. R. and Kahan, T. F.: Wavelength-Resolved Photon Fluxes of Indoor Light Sources: Implications for HOx Production, Environ. Sci. Technol., 51(18), 10423–10430, doi:10.1021/acs.est.7b02015, 2017.

Kurtenbach, R., Becker, K. H., Gomes, J. A. G., Kleffmann, J., Lörzer, J. C., Spittler, M., Wiesen, P., Ackermann, R., Geyer, A. and Platt, U.: Investigations of emissions and heterogeneous formation of HONO in a road traffic tunnel, Atmos. Environ., 35(20), 3385–3394, doi:10.1016/S1352-2310(01)00138-8, 2001.

Lao, M., Crilley, L., Salehpoor, L., Furlani, T., Bourgeois, I., Neuman, J. A., Rollins, A., Veres, P., Washenfelder, R., Womack, C., Young, C. and VandenBoer, T.: A portable, robust, stable and tunable calibration source for gas-phase nitrous acid (HONO), Atmos. Meas. Tech. Discuss., 1–31, doi:10.5194/amt-2020-209, 2020.

Lee, K., Xue, J., Geyh, A. S., Özkaynak, H., Leaderer, B. P., Weschler, C. J. and Spengler, J. D.: Nitrous acid, nitrogen dioxide, and ozone concentrations in residential environments, Environ. Health Perspect., 110(2), 145–149, doi:10.1289/ehp.02110145, 2002.

Leech, J. A., Nelson, W. C., Burnett, R. T., Aaron, S. and Raizenne, M. E.: It's about time: A comparison of Canadian and American time-activity patterns, J. Expo. Anal. Environ. Epidemiol., 12(6), 427–432, doi:10.1038/sj.jea.7500244, 2002.

Liu, J., Deng, H., Lakey, P. S. J., Jiang, H., Mekic, M., Wang, X., Shiraiwa, M., Gligorovski, S. and Salthammer, T.: Unexpectedly High Indoor HONO Concentrations Associated with Photochemical NO2Transformation on Glass Windows, Environ. Sci. Technol., 54(24), 15680–15688, doi:10.1021/acs.est.0c05624, 2020.

Mendez, M., Blond, N., Amedro, D., Hauglustaine, D. A., Blondeau, P., Afif, C., Fittschen, C. and Schoemaecker, C.: Assessment of indoor HONO formation mechanisms based on in situ measurements and modeling, Indoor Air, 27(2), 443–451, doi:10.1111/ina.12320, 2017.

Mullen, N. A., Li, J., Russell, M. L., Spears, M., Less, B. D. and Singer, B. C.: Results of the California Healthy Homes Indoor Air Quality Study of 2011-2013: Impact of natural gas appliances on air pollutant concentrations, Indoor Air, 26(2), 231–245, doi:10.1111/ina.12190, 2016.

Pitts, J. N., Sanhueza, E., Atkinson, R., Carter, W. P. L., Winer, A. M., Harris, G. W. and Plum, C. N.: An investigation of the dark formation of nitrous acid in environmental chambers, Int. J. Chem. Kinet., 16(7), 919–939, doi:10.1002/kin.550160712, 1984.

Ramazan, K. A., Syomin, D. and Finlayson-Pitts, B. J.: The photochemical production of HONO during the heterogeneous hydrolysis of NO2, Phys. Chem. Chem. Phys., doi:10.1039/b402195a, 2004.

Ren, Y., Stieger, B., Spindler, G., Grosselin, B., Mellouki, A., Tuch, T., Wiedensohler, A. and Herrmann, H.: Role of the dew water on the ground surface in HONO distribution: A case measurement in Melpitz, Atmos. Chem. Phys., 20(21), 13069–13089, doi:10.5194/acp-20-13069-2020, 2020.

Sakamaki, F., Hatakeyama, S. and Akimoto, H.: Formation of nitrous acid and nitric oxide in the heterogeneous dark reaction of nitrogen dioxide and water vapor in a smog chamber, Int. J. Chem. Kinet., doi:10.1002/kin.550151006, 1983.

Schwartz-Narbonne, H., Jones, S. H. and Donaldson, D. J.: Indoor Lighting Releases Gas Phase Nitrogen Oxides from Indoor Painted Surfaces, Environ. Sci. Technol. Lett., 6(2), 92–97, doi:10.1021/acs.estlett.8b00685, 2019.

Spicer, C. W., Coutant, R. W., Ward, G. F., Joseph, D. W., Gaynor, A. J. and Billick, I. H.: Rates and mechanisms of NO2 removal from indoor air by residential materials, Environ. Int., 15(1–6), 643–654, doi:10.1016/0160-4120(89)90087-1, 1989.

Spicer, C. W., Kenny, D. V., Ward, G. F. and Billick, I. H.: Transformations, Lifetimes, and Sources of NO2, HONO, and HNO3 in Indoor Environments, J. Air Waste Manage. Assoc., 43(11), 1479–1485, doi:10.1080/1073161X.1993.10467221, 1993.

Spicer, C. W., Kenny, D. V., Ward, G. F., Billick, I. H. and Leslie, N. P.: Evaluation of NO2 Measurement Methods for Indoor Air Quality Applications, Air Waste, 44(2), 163–168, doi:10.1080/1073161X.1994.10467245, 1994.

Spicer, C. W., Billick, I. H. and Yanagisawa, Y.: Nitrous Acid Interference with Passive NO2 Measurement Methods and the Impact on Indoor NO2 Data, Indoor Air, 11(3), 156–161, doi:10.1034/j.1600-0668.2001.011003156.x, 2001.

Stemmler, K., Ammann, M., Donders, C., Kleffmann, J. and George, C.: Photosensitized reduction of nitrogen dioxide on humic acid as a source of nitrous acid, Nature, 440(7081), 195–198, doi:10.1038/nature04603, 2006.

Stutz, J., Kim, E. S., Platt, U., Bruno, P., Perrino, C. and Febo, A.: UV-visible absorption cross sections of nitrous acid, J. Geophys. Res. Atmos., 105(D11), 14585–14592, doi:10.1029/2000JD900003, 2000.

Stutz, J., Alicke, B., Ackerman, R., Geyer, A., Wang, S., White, A. B., Williams, E. J., Spicer, C. W. and Fast, J. D.: Relative humidity dependence of HONO chemistry in urban areas, J. Geophys. Res. Atmos., 109(3), doi:10.1029/2003jd004135, 2004.

Svensson, R., Ljungström, E. and Lindqvist, O.: Kinetics of the reaction between nitrogen dioxide and water vapour, Atmos. Environ., 21(7), 1529–1539, doi:10.1016/0004-6981(87)90315-5, 1987.

VandenBoer, T. C., Brown, S. S., Murphy, J. G., Keene, W. C., Young, C. J., Pszenny, A. A. P., Kim, S., Warneke, C., De Gouw, J. A., Maben, J. R., Wagner, N. L., Riedel, T. P., Thornton, J. A., Wolfe, D. E., Dubé, W. P., Öztürk, F., Brock, C. A., Grossberg, N., Lefer, B., Lerner, B., Middlebrook, A. M. and Roberts, J. M.: Understanding the role of the ground surface in HONO vertical structure: High resolution vertical profiles during NACHTT-11, J. Geophys. Res. Atmos., 118(17), 10155–10171, doi:10.1002/jgrd.50721, 2013.

Vandenboer, T. C. T. C., Brown, S. S. S. S., Murphy, J. G. J. G., Keene, W. C. W. C., Young, C. J. C. J., Pszenny, A. A. P. A. P., Kim, S., Warneke, C., De Gouw, J. A. J. A., Maben, J. R. J. R., Wagner, N. L. N. L., Riedel, T. P. T. P., Thornton, J. A. J. A., Wolfe, D. E. D. E., Dubé, W. P. W. P., Öztürk, F., Brock, C. A., Grossberg, N., Lefer, B., Lerner, B., Middlebrook, A. M. A. M. and Roberts, J. M.: Understanding the role of the ground surface in HONO vertical structure: High resolution vertical profiles during NACHTT-11, J. Geophys. Res. Atmos., 118(17), 10155–10171, doi:10.1002/jgrd.50721, 2013.

Vichi, F., Mašková, L., Frattoni, M., Imperiali, A. and Smolík, J.: Simultaneous measurement of nitrous acid, nitric acid, and nitrogen dioxide by means of a novel multipollutant diffusive sampler in libraries and archives, Herit. Sci., 4(1), 1–8, doi:10.1186/s40494-016-0074-5, 2016.

Wainman, T., Weschler, C. J., Lioy, P. J. and Zhang, J.: Effects of surface type and relative humidity on the production and concentration of nitrous acid in a model indoor environment, Environ. Sci. Technol., 35(11), 2200–2206, doi:10.1021/es000879i, 2001.

Wang, C., Bottorff, B., Reidy, E., Rosales, C. M. F., Collins, D. B., Novoselac, A., Farmer, D. K., Vance, M. E., Stevens, P. S. and Abbatt, J. P. D.: Cooking, Bleach Cleaning, and Air Conditioning Strongly Impact Levels of HONO in a House, Environ. Sci. Technol., 54(21), 13488–13497, doi:10.1021/acs.est.0c05356, 2020a.

Wang, C., Collins, D. B., Arata, C., Goldstein, A. H., Mattila, J. M., Farmer, D. K., Ampollini, L., DeCarlo, P. F., Novoselac, A., Vance, M. E., Nazaroff, W. W. and Abbatt, J. P. D.: Surface reservoirs dominate dynamic gas-surface partitioning of many indoor air constituents, Sci. Adv., 6(8), 1–12, doi:10.1126/sciadv.aay8973, 2020b.

Waring, M. S. and Wells, J. R.: Volatile organic compound conversion by ozone, hydroxyl radicals, and nitrate radicals in residential indoor air: Magnitudes and impact of oxidant sources, Atmos. Environ., 106, 382–391, doi:10.1016/j.atmosenv.2014.06.062., 2015.

Weschler, C. J.: Changes in indoor pollutants since the 1950s, Atmos. Environ., 43(1), 153–169, doi:10.1016/j.atmosenv.2008.09.044, 2009.

Weschler, C. J. and Shields, H. C.: Production of the hydroxyl radical in indoor air, Environ. Sci. Technol., 30(11), 3250–3258, doi:10.1021/es960032f, 1996.

White, I. R., Martin, D., Paz MuñOz, M., Petersson, F. K., Henshaw, S. J., Nickless, G., Lloyd-Jones, G. C., Clemitshaw, K. C. and Shallcross, D. E.: Use of reactive tracers to determine ambient OH radical concentrations: Application within the indoor environment, Environ. Sci. Technol., 44(16), 6269–6274, doi:10.1021/es901699a, 2010.

Zhou, S., Young, C. J., VandenBoer, T. C., Kowal, S. F. and Kahan, T. F.: Time-Resolved Measurements of Nitric Oxide, Nitrogen Dioxide, and Nitrous Acid in an Occupied New York Home, Environ. Sci. Technol., 52(15), 8355–8364, doi:10.1021/acs.est.8b01792, 2018.

Zhou, Z., Zhou, S. and Abbatt, J. P. D.: Kinetics and Condensed-Phase Products in Multiphase Ozonolysis of an Unsaturated Triglyceride, Environ. Sci. Technol., 53(21), 12467–12475, doi:10.1021/acs.est.9b04460, 2019.

CHAPTER FIVE: Conclusions and Future Work

5.1 Conclusions

This thesis provided the build and detailed operation of two new, cost-effective instruments to improve the accuracy and detection of HONO, and be used to better understand the dominant processes that control HONO indoors.

The following three thesis chapters provided detailed results and discussion to answer the research questions addressed in Chapter 1.

Chapter 2:

A new calibration source provides stable, tunable, and robust HONO calibration quantities of a few ppt to tens of ppb, which are environmentally relevant mixing ratios. The source generates stable HONO output using two methods: water vapor only and an acid displacement reaction of HCl and $NaNO_2$ coated PFA devices in a machined Al-block permeation oven. The source is tunable by adjusting the temperature of the permeation oven to control the water vapor reaction and the HCl emission rates from the permeation devices. The source is robust by generating reproducible HONO output regardless of being disassembled, transported, and reassembled. The $NaNO_2$ coated devices replaced the need for solid $NaNO_2$ powder, which was prone to changing HONO outputs when disturbed or vibrated. The source has a purity of > 90 % , which is lower than previous work (99.5 %; Febo et al., 1995) but is an acceptable trade-off for robust field deployment. The calibration source was compatible with the current state-of-the-art instrumentation, and the output of the source was constant within ± 10 %, proving to be a valid universal source. This calibration source could be used for intercomparison between responses and measurements of HONO-detecting instruments to validate the accuracy and precision of their ambient measurements.

Chapter 3:

The new automated HONO instrument was constructed from safe and simple components for quick routine indoor analysis in various facilities (e.g. private homes, schools, commercial spaces). It can be used to provide accurate and precise HONO measurements to improve our understanding of the processes of NO_x and HONO, and their contributions to the indoor oxidative capacity. This

instrument can detect NO_x and HONO using alternating Teflon three-way valves between two pathways to measure HONO using a differential technique coupled to a chemiluminescence analyzer (HONO LOD is 0.6 ppb). Its automated instrumental control, operation, and datalogging is an upgraded method to previous strategies and a subset of the tNr instrument that can also detect fractions of NH_x and total reactive nitrogen. The HONO calibration source is integrated into the instrument to decrease measurement uncertainty and to provide confidence in our HONO measurements during field campaigns. The instrument response time (95 – 0 %) was optimized to 1 min for NO, NO_2, and HONO and is limited by the response of the NO_x analyzer. The scrubbing efficiency of HONO by the Na_2CO_3 denuder was > 99.6 %. No significant NO losses were observed, and a 2% loss of NO_2 to the Na_2CO_3 denuder can be easily corrected in the data processing code. There was a small amount of heterogenous HONO formation when flushing the lines with a mixture of humid air and NO_2 with a conversion range of 0.9 – 2.9 %, which is insignificant because it is less than the instrument precision/noise of 5 %. Preliminary measurements were performed to test the overall performance and automation of the tN_r instrument in two different environments including an indoor laboratory and during a wildfire smoke event outdoors. The chemical laboratory showed a small HONO reservoir was present at night of 1.68 ± 1.20 ppbv, likely from lower NO_2 surface uptake or competing processes that may decrease nitrite buildup from other on-going projects on the interior surfaces. The outdoor wildfire measurements proved that the tN_r instrument could be used to detect the total sum of acidic and basic species in outdoor air but cannot quantify NO_x and HONO because of the presence of NO_y species. This new instrument can be used to survey various indoor atmospheres, to understand the control, processes, and variabilities of indoor HONO chemistry and its contributions to the OH budget.

Chapter 4:

The newly developed platform successfully detected NO, NO_2, NO_x, and HONO in a commercial kitchen for three weeks during the KOCENA campaign. The high AER in the kitchen strongly influenced the detection of these pollutants. The sensor-controlled ventilation system hooked to the kitchen exhaust hoods efficiently removed cooking-relative emissions out of the kitchen. The averaged ventilation during the day (5:00 – 22:00) was 27.2 ±7.28 h^{-1} and night (22:00 – 5:00) was 0.10 ± 0.17 h^{-1}. The instrument could not reliably capture the high cooking-related emissions that spanned less than 20 minutes from the high ventilation. As a result, most HONO directly emitted

from cooking combustion processes were removed from the data processing code and this work focused on the heterogenous processes of HONO in the kitchen. The kitchen temperature and RH were stable throughout the campaign with averages of 28.0 ± 2.46 °C and 31.2 ± 3 %. Measurements of NO_x in the kitchen were the highest during the day at 6:00 – 16:00 sourced from the outdoor transport of nearby combustion emissions in the early morning and cooking activities (NO = (4.21 – 19.65) ± 5.14 ppb, NO_2 = (9.46 – 17.49) ± 2.84 ppb, and NO_x = (12.21 – 34.27) ± 6.81 ppb). The levels of NO_2 were relatively steady throughout the day and night. The outdoor transport of NO_2 indoors by mechanical ventilation was the main source of nighttime NO_2 (22:00 – 5:00) at 13.12 ± 0.85 ppb. Nighttime NO was low at 3.32 ± 0.39 ppb because outdoor sources of NO are low, and NO is quickly titrated in the presence of O_3 to form NO_2. Stable levels of HONO were detected throughout the campaign with a total average of 2.41 ± 2.05 ppb. The daytime average of HONO was 2.48 ± 2.07 ppb and nighttime average was 2.36 ± 1.29 ppb, which were relatively similar. A simple model was constructed using these time-resolved measurements to calculate predicted concentrations of HONO. The model shows that equilibrium partitioning of HONO on surfaces is evident outside of direct cooking emissions, which agreed with previous residential studies (Collins et al., 2018; Wang et al., 2020b). This HONO reservoir is likely located on the kitchen surfaces with deposited nitrite that can desorb as gas-phase HONO. Calculations of the production rate of OH by HONO photolysis confirmed that the 24-hour lighting in the kitchen is a persistent OH source (average of 9.72 x 10^{-5} molecules cm^{-3} s^{-1}, J_{HONO} = 1.66 x 10^{-5} s^{-1} at average HONO concentrations of 5.85 x 10^{10} ± 4.95 x 10^{10} molec cm^{-3}), indicating HONO photolysis may be an important driver in indoor oxidation chemistry in a commercial environment.

5.2 Future work

The design and detailed operations of these two new instrumentations are/will be open source for the atmospheric science community to replicate and encourage scientists to detect HONO in various environments. Currently, the HONO calibration instrument has been built by other research groups proving as a universal solution, generating stable gas-phase HONO calibration quantities that is suitable for all atmospheric instrumentation for outdoor and indoor environments. Future improvements to the automated HONO platform include quantifying the lifetime for the deactivation of the carbonate denuders, its automated controls, and optimizing the data processing code for various environments to become more user-friendly. The automated control of the instrument will be upgraded by adding more solenoid valves to allow automation of the HONO

calibration quantities, and their dilution controlled by an MFC. The manual two-way waste valves will also be automated. A standard operating procedure with detailed instructions of its design and instrument programming in its automation of datalogging and data processing will be published online. Lastly, the automated HONO instrument can investigate indoor processes and give insight into the HONO chemistry in various environments. Future laboratory work should focus on measuring sorbed nitrite concentrations on various interior surfaces to better understand HONO reservoir chemistry and explore the pre-existing nitrite films on surfaces to understand its sorption mechanism. Recent indoor studies have reported that the chemical composition of indoor surfaces can influence HONO chemistry (Wang et al., 2020b, Wang et al., 2020a). The presence of NH_3 on indoor surfaces could deplete HONO reservoirs by deprotonating nitrite, which should also be further investigated. This work will also contribute to understanding other complex chemical interactions happening in the kitchen that is investigated by our KOCENA collaborators. The continuous OH production by HONO photolysis in the commercial kitchen with 24-hour lighting may contribute to other complex chemical interactions such as ozonolysis with cooking oil (Zhou et al., 2019). The OH budget can be estimated using measurements (data in progress) of ozone and volatile organic compounds to determine the production rate of OH by ozonolysis of alkenes.

5.3 References

Collins, D. B., Hems, R. F., Zhou, S., Wang, C., Grignon, E., Alavy, M., Siegel, J. A. and Abbatt, J. P. D.: Evidence for Gas-Surface Equilibrium Control of Indoor Nitrous Acid, Environ. Sci. Technol., 52(21), 12419–12427, doi:10.1021/acs.est.8b04512, 2018.

Febo, A., Perrino, C., Gherardi, M. and Sparapani, R.: Evaluation of a High-Purity and High-Stability Continuous Generation System for Nitrous Acid, Environ. Sci. Technol., 29(9), 2390–2395, doi:10.1021/es00009a035, 1995.

Wang, C., Bottorff, B., Reidy, E., Rosales, C. M. F., Collins, D. B., Novoselac, A., Farmer, D. K., Vance, M. E., Stevens, P. S. and Abbatt, J. P. D.: Cooking, Bleach Cleaning, and Air Conditioning Strongly Impact Levels of HONO in a House, Environ. Sci. Technol., 54(21), 13488–13497, doi:10.1021/acs.est.0c05356, 2020a.

Wang, C., Collins, D. B., Arata, C., Goldstein, A. H., Mattila, J. M., Farmer, D. K., Ampollini, L., DeCarlo, P. F., Novoselac, A., Vance, M. E., Nazaroff, W. W. and Abbatt, J. P. D.: Surface reservoirs dominate dynamic gas-surface partitioning of many indoor air constituents, Sci. Adv., 6(8), 1–12, doi:10.1126/sciadv.aay8973, 2020b.

Zhou, Z., Zhou, S. and Abbatt, J. P. D.: Kinetics and Condensed-Phase Products in Multiphase Ozonolysis of an Unsaturated Triglyceride, Environ. Sci. Technol., 53(21), 12467–12475, doi:10.1021/acs.est.9b04460, 2019.

Appendix A:

Supporting information for Chapter Two: A portable, robust, stable and tunable calibration source for gas-phase nitrous acid (HONO)

2.S1 Rationale for components selected for custom-built permeation oven

The custom-built permeation oven (Figs. 2-S1) is comprised of a bent aluminum bent plate (exact dimensions provided in Fig. 2-S2), temperature controller, solid state relay, custom-built four-channel aluminum heating block, cartridge heater with integrated thermocouple, and PFA tubing connected with Swagelok® fittings. The PFA tubing was interfaced with four 2-way stainless steel valves (SS-43GS6-LL, Swagelok®) to provide gas flow independently to each channel of the oven.

Gas flow to the system is provided by a source of dry compressed air, either from a cylinder or a zero-air generator at 20 psi (138 kPa). The flow can be turned on and off to each of the four permeation channels in the aluminum heating block (20.3 x 7.7 x 7.7 cm (8 x 3 x 3”); l x w x h, Fig 2-S2) using 2-way Swagelok® valves (Weston Valve & Fitting Ltd., Mississauga, ON). The flow through each channel is regulated by a 50-micron critical orifice (Lenox Laser, Glen Arm, MD; SS-4-VCR-2-50) housed in a ¼” Swagelok® VCR assembly (SS-4-VCR-1, SS-4-VCR-4, and SS-4-VCR-3-4TA) to ~50 sccm. The aluminum heating block (Al-block) houses four ½” PFA tubes to provide inert oven surfaces. Each are mounted within machined holes passing through the center of the short axis of the block. The machined holes are the exact size of the outer diameter of the ½” PFA tubes, resulting in firm contact between the polymer and Al. Permeation devices (PDs) can be placed inside the ½” PFA ovens to emit stable quantities of their chemical contents (Section 2.S2). From the input of the oven to all downstream applications, Swagelok® or Entegris PFA fittings were used to minimize sorption effects for generated gases.

The thermal system is composed of three critical components: a temperature controller, temperature sensor and a heat source. All components were purchase from either OmegaTM Environmental (St. Eustache, QC) or Allied Electronics, Inc. (Fort Worth, TX). The temperature controller regulates the temperature of the system by receiving an input signal (measurement) from the thermocouple to compare to its setpoint value. An output signal will be generated if the input value is below the temperature-control setpoint. The output signal is sent to a solid-state relay

which enables the heater function and increases the temperature. A proportional-integral-differential (PID) temperature controller (OmegaTM; CN 7823) monitors and sets the temperature of the Al block shown in Fig. 2-S4. Using PID mode regulates the temperature of the system automatically by using feedback from the thermocouple and associated heating element to compensate for any changes relative to the set point. The PID controller is programmed to match the appropriate thermocouple (Type K used here). The PID parameters are adjusted by using the auto tune function to give the precise control (±0.1 °C) without overshooting the set point. The solid-state relay (Allied; SSR, D1210, Crydom) switches the heating cycle by converting the 5 V DC output from the temperature controller to 120 V AC used to operate the heating element. To dissipate the energy required for switching, the SSR was mounted on an aluminum heat sink (Allied; HS172, Crydom) and protected by a Bussman rectifier fuse (OmegaTM; Tron, KAX-10 A) against excess current flow that could result from a latching failure. The fuse holder (OmegaTM; FB-1) allows easy replacement of a blown fuse in the circuit. A cartridge heater with an integrated K-type thermocouple housed in a high-temperature incoloy sheath (OmegaTM; CIR, 300 W, 120 V) is inserted into a 20.3 cm (8”) hole with a 3/8” internal diameter, on the long axis of the Al-block. The heater is a high watt density cartridge with maximum working temperature of 760 ºC and F-type leads with fiberglass insulation. The thermocouple measures temperature by the thermoelectric effect which results in a voltage. A K-type thermocouple consists of chromel (Ni-Cr) and alumel (Ni-Al) alloys that generates an accurate voltage in the temperature range of 0 to 1250 ºC. An upper limit on the temperature controller should be set at 150 °C to prevent thermal degradation of PFA tubing in the Al-block during use.

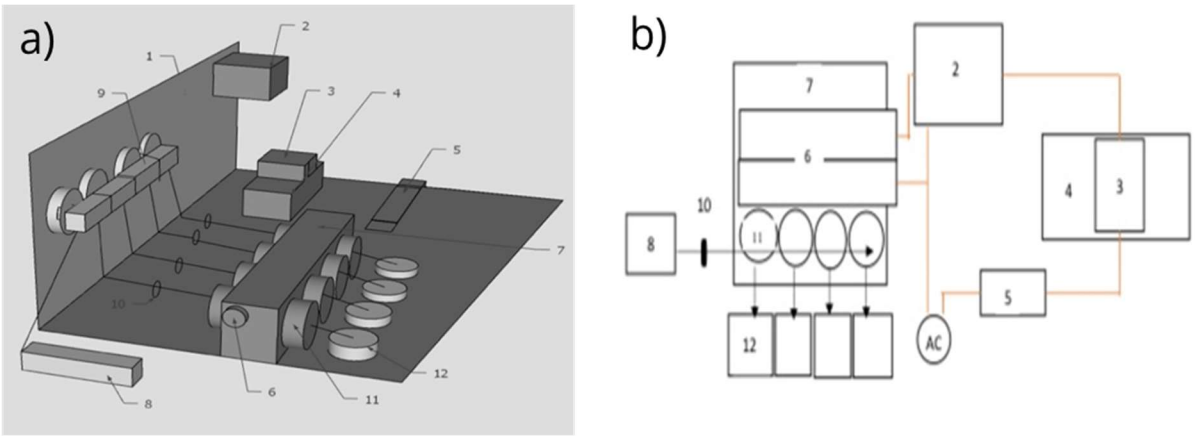

Figure 2-S1. Three (a) and two (b) dimension layout schematics of permeation-oven components on the bent aluminum plate (1), with mounted temperature controller (2), solid state relay (3) and its heat sink (4), electrical fuse (5), cartridge heater with integrated thermocouple (6), aluminum block (7), source of dry compressed air (8), 2-way gas valve (9), critical orifice (10), PFA oven (11), and gaseous output to external system. Black lines represent PFA lines guiding gas flows throughout the system.

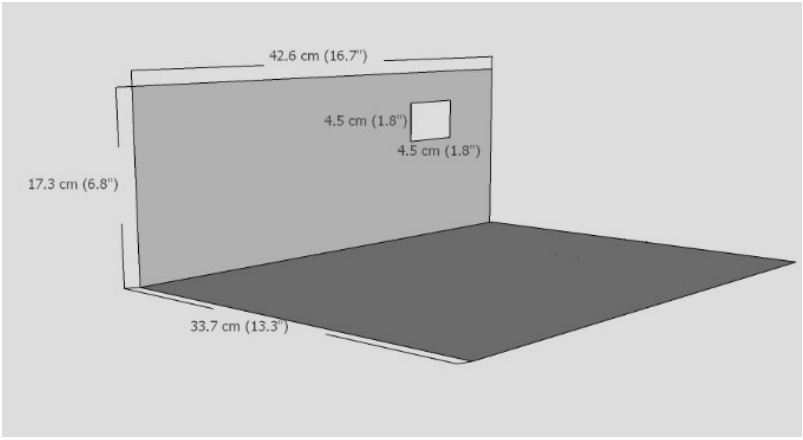

Figure 2-S2. Dimensions of bent aluminum plate and cut-out measurements to mount the temperature controller. Further holes for valves or a holder for the water impinger were created with an electric drill on an as-needed basis.

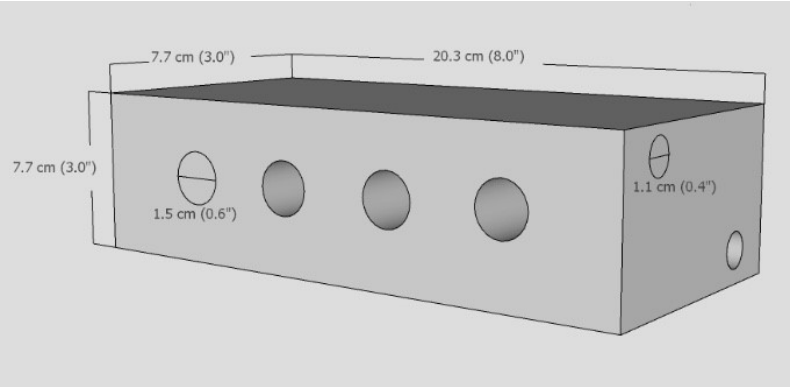

Figure 2-S3. Dimensions and machining specifications of aluminum block oven.

2.S1.2 Electrical connections for temperature control feedback

Power is supplied to the entire setup from 120 V AC outlet capable of providing up to 15 A of current (Fig. 2-S4). The temperature controller monitors the voltage signal from the thermocouple (here: yellow/+ and red/-; terminals 4 and 5, respectively; Fig. 2-S4). When the thermocouple signal falls below the control setpoint it sends a 5 V signal (terminals 1(-) and 2(+)) to the solid-state relay (3-32 V DC input D(-) and C(+)). The solid-state relay closes the switch to deliver current to the cartridge heater leads from the AC terminals (120 V AC output A(+) and B(-); Fig. 2-S4). The relay and cartridge heater are protected by a fuse. The entire case is grounded, with a ground wire of the power supply fixed to the bent aluminum plate.

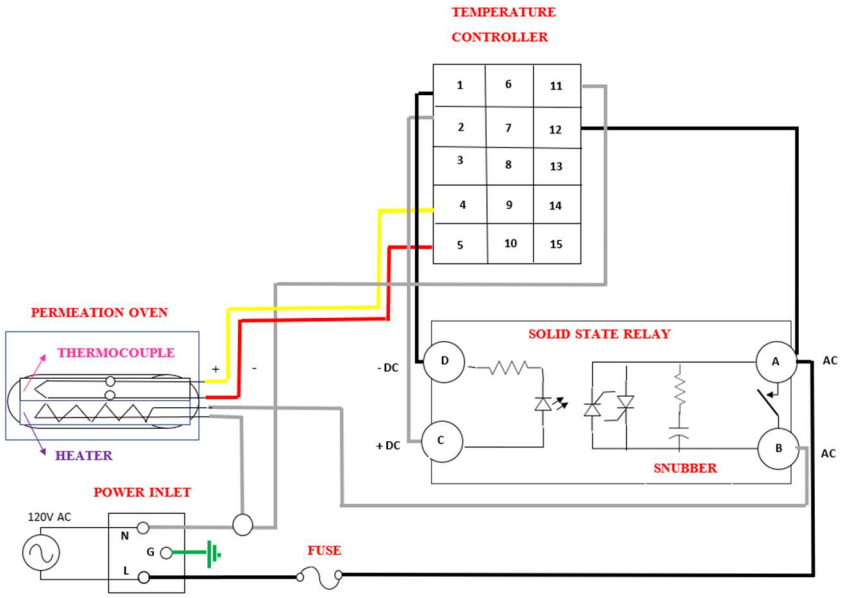

Figure 2-S4. Schematic of the wiring and connections of the custom-built permeation oven. The power supply is distributed from the power inlet into the system through different wires consisting of live wires (black), neutral wires (grey) and a ground wire (green). The temperature controller receives signals by inputs 4 and 5 (yellow and red) connected to the thermocouple. To control the function of the heater, the temperature controller sends a signal from output 1 and 2 to input C and D of the solid-state relay to reach the temperature setpoint.

2.S2 Rationale and construction of custom permeation devices (PDs)

The purpose of a permeation oven is to obtain a consistent quantity of gaseous analyte via a constant permeation rate, which results in a known mass per unit time delivered to an experimental system or an analytical instrument for calibration purposes. A permeation oven is typically coated or made with inert material to limit surface interactions experienced by the generated gas. The calibration gas permeates by diffusion through the porous polymer according to Fick's second law of diffusion (E1, $m^2\ s^{-1}$). If the analyte is in an aqueous solution it is emitted into the oven as a vapor based on its effective Henry's Law constant, which is the product of its acid dissociation constant and volatility (E2, Pa mol m^{-3}; R4) (Mitchell, 2000; Scaringelli et al., 1970). The product of these two properties combine into the overall permeability term (P, Pa mol $m^{-1}\ s^{-1}$; E3).

$$D = D_0 e^{-\frac{\Delta E_D}{RT}} \quad \text{(E1)}$$

$$S = S_0 e^{-\frac{\Delta H_S}{RT}} \quad \text{(E2)}$$

$$P = D \cdot S \quad \text{(E3)}$$

$$NO_2^-{}_{(aq)} + H^+{}_{(aq)} \rightleftharpoons HONO_{(aq)} \rightleftharpoons HONO_{(g)} \quad \text{(R4)}$$

Where, S_0, and D_0 are pre-exponential constants of solubility and diffusion. In Equations 1 and 2: E_D is the activation energy for diffusion (J mol^{-1}) and H_S is the enthalpy of solvation (J mol^{-1}), while T is temperature (K) and R is the ideal gas constant (J mol^{-1} K^{-1}). The permeation rate depends on temperature because both diffusion and vapor pressure are exponentially temperature dependent. Therefore, permeation ovens can provide a stable and pure emission rate that can be tuned by adjusting the temperature of the oven.

Clean air moves through the ½" PFA oven tubes, where the vapor emissions from PDs are accumulated, to carry them into the reaction devices, a scrubbing solution, or other instrumentation. High precision of a permeation rate can be obtained by regulating and maintaining constant temperature within ± 0.1 ºC because an increase of 1 ºC of operating temperature results in a 10 % change in sample permeation rate (Lucero, 1971). Adequate precision of our custom-built permeation oven was achieved by choosing the temperature controller, heater, and thermocouple with very strict tolerances. Long-term stability of the system can be ascertained from ion chromatography or real-time measurements (see main manuscript). Also, calibrating the permeation rate of a custom-PD can easily indicate the precision and stability of this custom-built permeation oven.

To construct a custom-PD, a length ¼" PFA tube is filled with analyte solution and the ends are plugged. One end of the tubing is initially made malleable with a heat-gun. Once the tube is sufficiently pliable, a rod of porous PTFE (0.125" diameter, P/N: 84935K64; McMaster-Carr) is carefully inserted with a twisting motion and cut to keep the tubing and rod flush. To ensure an effective seal the two materials are heated further, then compressed and rolled on a flat surface. The open-end of the PD is then filled with analyte solution until it is approximately ½" from the top. The PTFE plugging process is repeated to close the tube. Extra caution during this step should be taken to avoid having the solution boil over or undergoing spontaneous ignition during heating. It is worth noting that the length and quality of the seal around the porous PTFE rod can change the emission rate, where a longer plug may yield a more reliable emission rate. Generally, plugs one centimeter in length were used in this work. If the plug length is too short leakages may arise, resulting in rapid and unstable emission of the contained solution. An alternative that avoids PTFE plugs and associated leaks is to weld the tubing ends. This can be accomplished by heating the end

of the tubing with a heat-gun until it is malleable, followed by pinching it with a pair of pliers to create the weld.

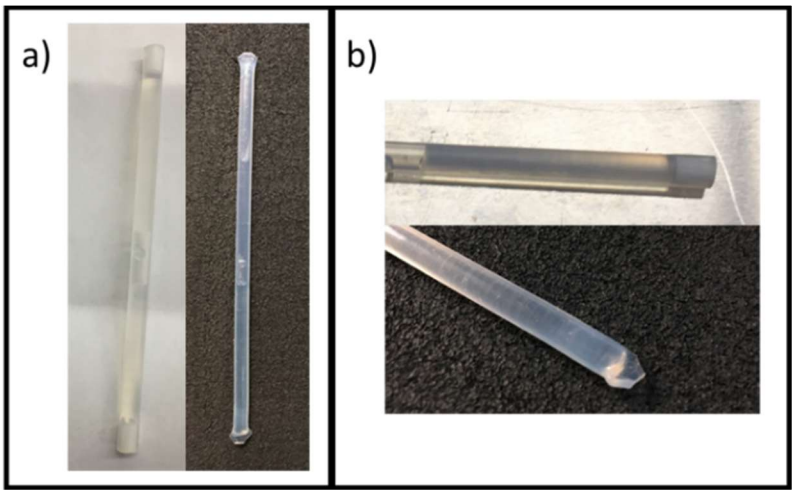

Figure 2-S5. a) Two PDs containing analyte solution fully sealed using the porous PTFE rod (left) and PFA weld (right) techniques. b) Close-up perspective of finished PD ends after sealing by the methods of PTFE rod (top) and PFA weld (bottom).

2.S3 Additional Supporting Figures and Tables

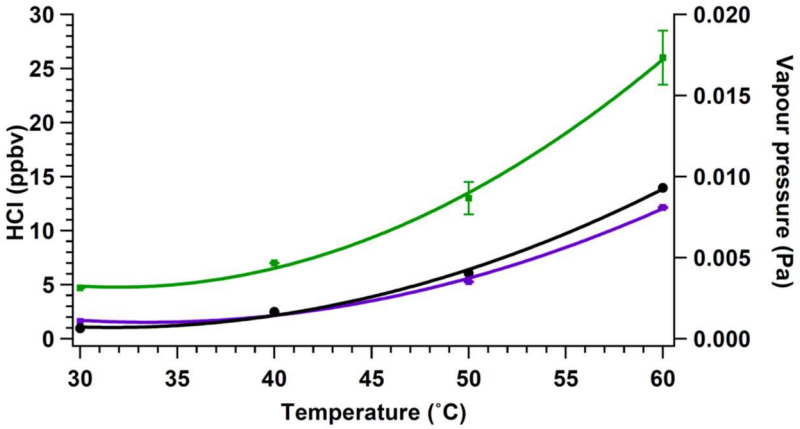

Figure 2-S6. Mixing ratio output of two 6 M HCl PDs as a function of temperature (PD-6b, blue; PD-6c, green). Calculated vapor pressure of 6 M HCl (black) solution using Henry's Law (Sander, 2015). Mean HCl mixing ratios measured for 30 minutes after stable signal was observed by CRDS (1-minute average, see Fig. 2-S7). Error bars denote 1σ standard deviation from the mean.

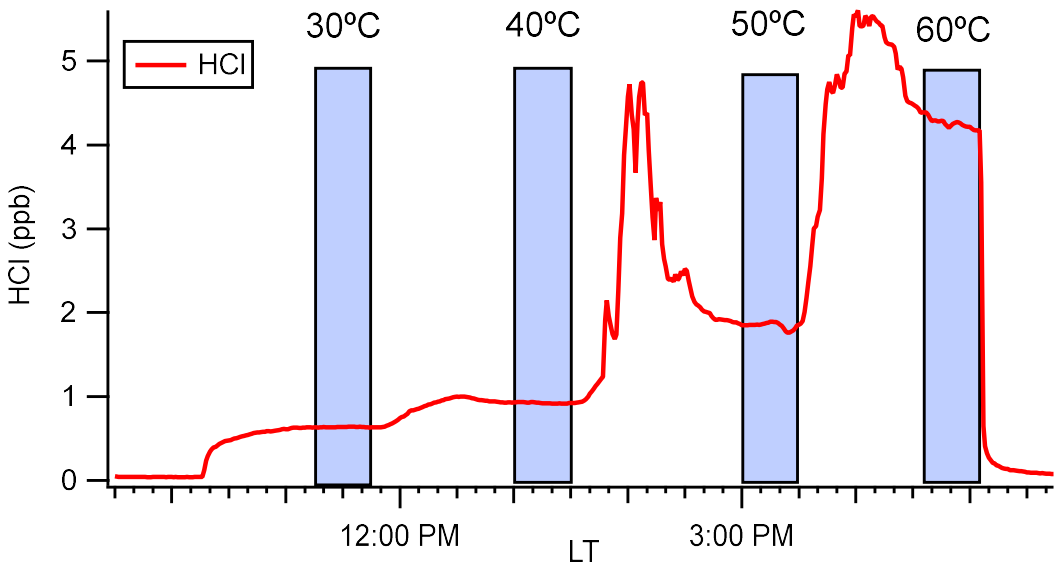

Figure 2-S7. Time series of the measured HCl output from PD-6b using CRDS. The blue-shaded bars indicate the region where HCl output was considered stable and this data was used to calculate the variance shown in Figure 2-S6.

Table 2-S1. The calculated average HONO (ppbv) output (AVG), standard deviation (SD), and standard error (SE) following the field transport simulations using HCl PD-6a and the same $NaNO_2$ coated device throughout all experiments. The AVG, RSD, and RSE were all calculated from data points collected after two hours of stabilization in each trial run. All experiments were background corrected by linear interpolation using zero air and five experiments had insertions of Na_2CO_3 denuder for further identification of NO_x impurities (*). The NO_x analyzer collected one-minute measurements using a 30 s Kalman filter.

ID	Description of Field Transport Simulation	AVG (ppbv)	SD (ppbv)	SE (ppbv)	Data Points	RSD (%)	RSE (%)
FS1*	Minor shaking for 10 min with the oven off and PD removed overnight	2.51	0.548	0.0537	112	26.6	2.13
FS2*	Transport by cart over rough surfaces for 10 min with the oven off and PD removed overnight	1.81	0.469	0.0342	188	25.9	1.89
FS3*	Transport by cart over rough surfaces for 10 min with the oven off and PD removed overnight	1.68	0.469	0.0308	231	27.8	1.83
FS4*	Minor shaking of stationary setup for 10 min with the oven off and PD removed overnight	2.43	0.447	0.0257	301	18.4	1.06

ID	Description of Field Transport Simulation	AVG (ppbv)	SD (ppbv)	SE (ppbv)	Data Points	RSD (%)	RSE (%)
FS5*	Minor shaking of stationary setup for 10 min with the oven off and PD removed overnight	2.13	0.429	0.0270	253	20.1	1.27
FS6	Oven turned off overnight and Pd kept inside permeation oven	2.04	0.417	0.0240	300	20.5	1.18
FS7	Oven turned off and PD removed overnight	1.73	0.467	0.0340	189	27.0	1.97
FS8	Oven turned off and PD removed overnight	2.21	0.604	0.0454	177	27.3	2.05

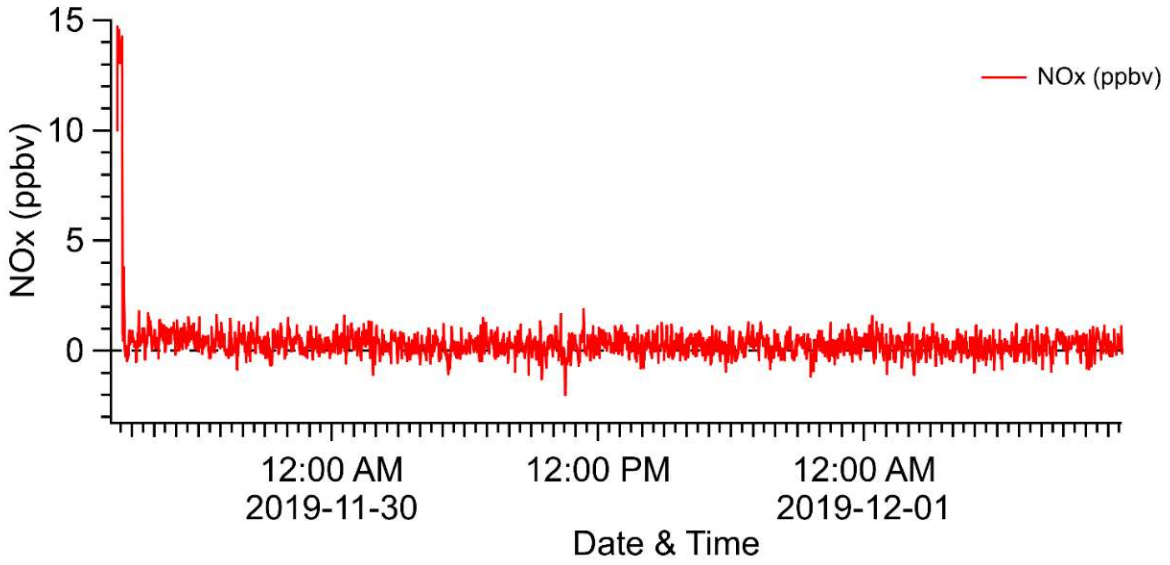

Figure 2-S8. An example of the suitability of nitrogen gas sampled by the NO_x analyzer used for background measurement and subsequent correction of observations.

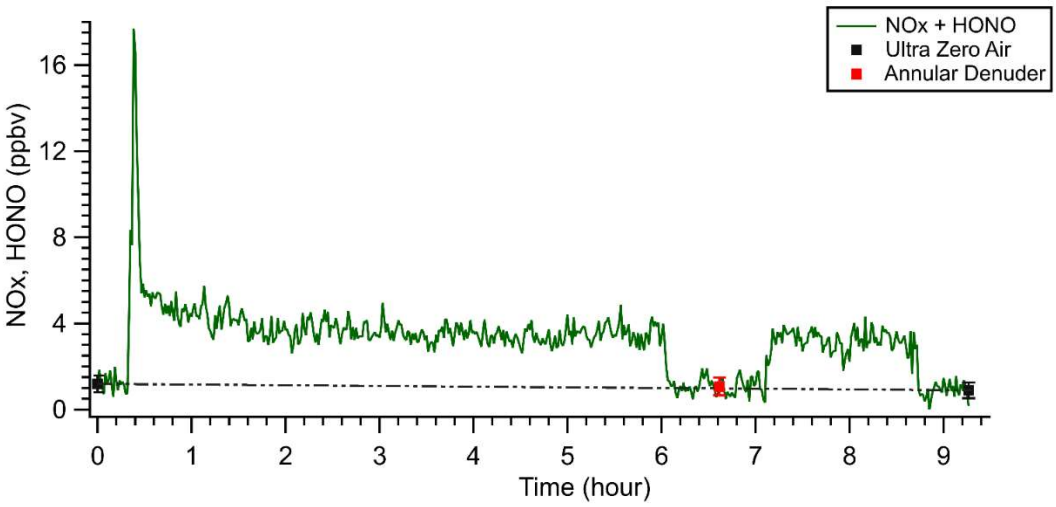

Figure 2-S9. Run FS4 of Table 2-S1 to demonstrate that measured signal from zero air (black square) and HONO passing through the Na_2CO_3 annular denuder (red square) are identical and therefore free of detectable NO_x. These negative controls were combined to create a linearly interpolated background correction over the course of experiments FS1-5 to quantify HONO.

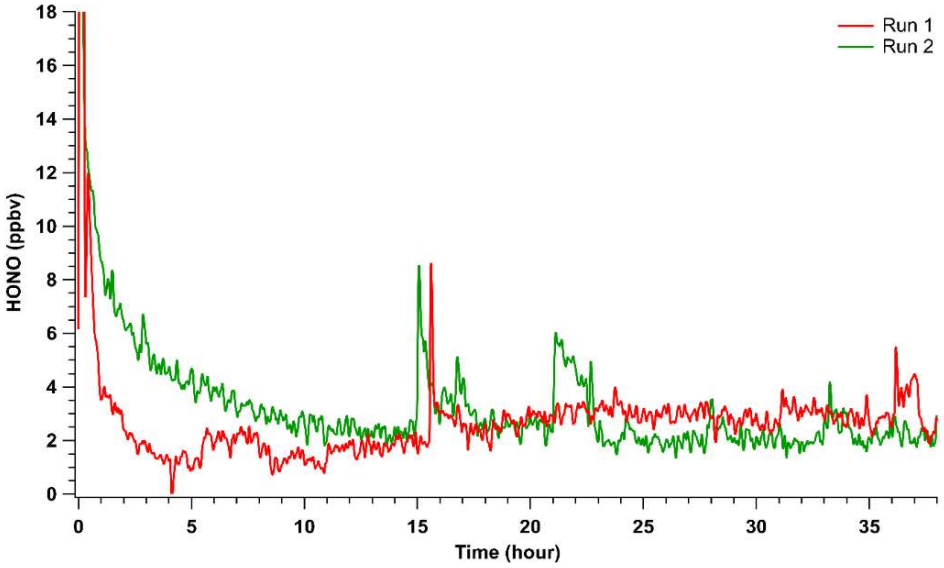

Figure 2-S10. Reproducibility in generating HONO using PD-6b and the same $NaNO_2$ coated device. The red line represents the first trial of using PD-6b followed by a second trial (green) 15 days later. In the intervening time other experiments were performed which involved shutting down and restarting the system with these components. The lag in the second trial results from keeping the PD in the oven while shut down between experiments, resulting in additional HCl that must be reacted in the calibration system before stability is reached. The NO_x analyzer mad one-minute measurements using a Kalman filter of 300 s.

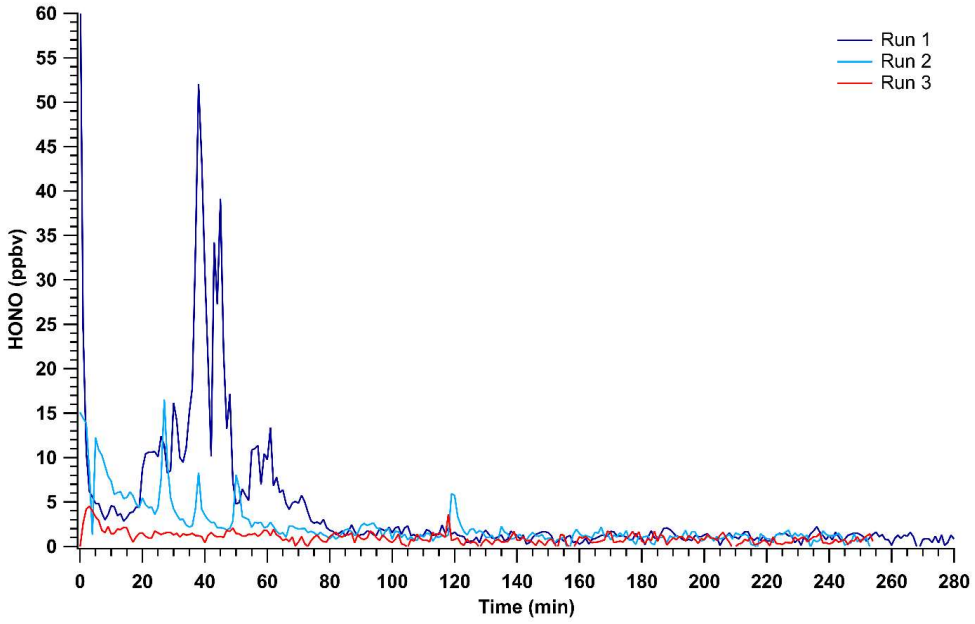

Figure 2-S11. Determining reproducibility in generating HONO (ppbv) against time (min) using PD-1a with a used $NaNO_2$ PFA device.

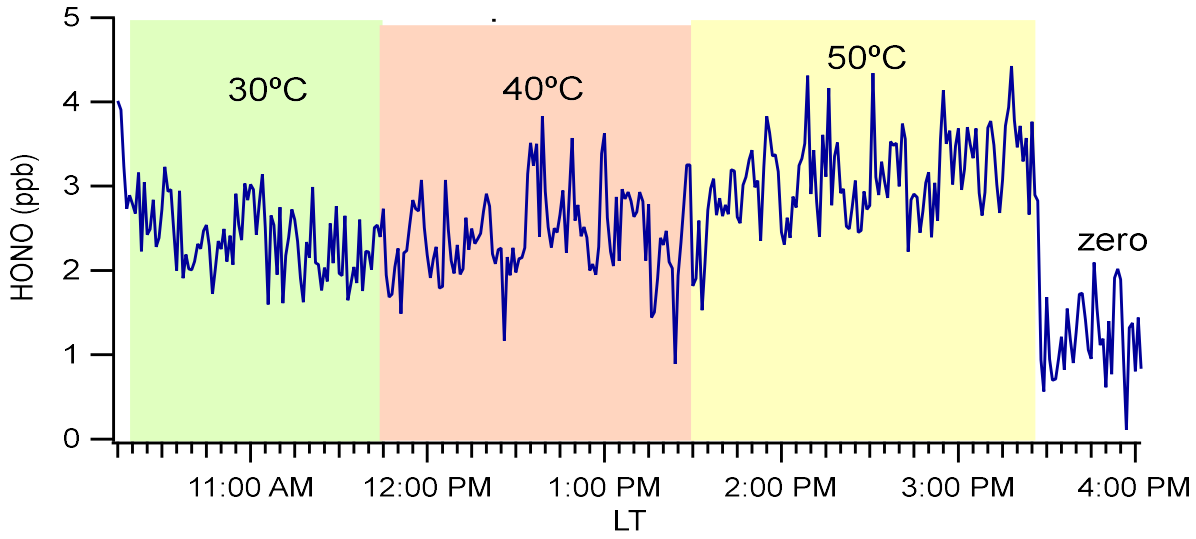

Figure 2-S12. Time series of measured HONO output (ppb) for three different temperatures using HCl PD-6b.

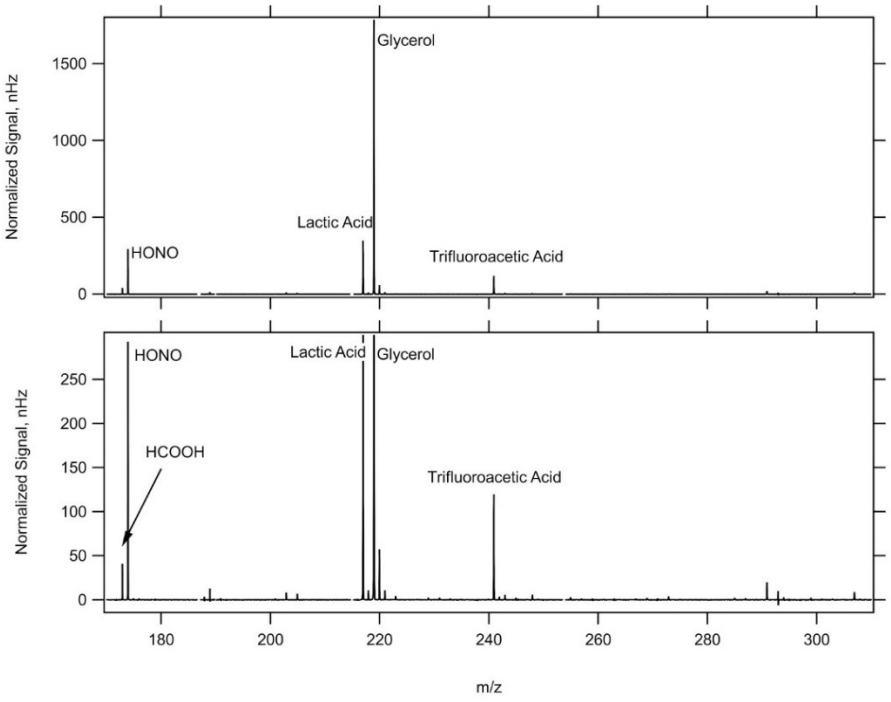

Figure 2-S13. Ion scan of the HONO calibration source output made with the I^--CIMS. Major ions observed in addition to HONO include glycerol from the coating solution, and lactic acid from skin contact with system components. Smaller quantities of formic and trifluoroacetic acids from the plastics used in the instrument assembly were also observed.

2.S4 References

Lucero, D. P.: Performance Characteristics of Permeation Tubes, Anal. Chem., 43(13), 1744–1749, doi:10.1021/ac60307a005, 1971.

Mitchell, G. D.: A review of permeation tubes and permeators, Sep. Purif. Methods, 29(1), 119–128, doi:10.1081/SPM-100100005, 2000.

Sander, R.: Compilation of Henry's law constants (version 4.0) for water as solvent, Atmos. Chem. Phys., 15(8), 4399–4981, doi:10.5194/acp-15-4399-2015, 2015.

Scaringelli, F. P., O'Keeffe, A. E., Rosenberg, E. and Bell, J. P.: Preparation of Known Concentrations of Gases and Vapors with Permeation Devices Calibrated Gravimetrically, Anal. Chem., 42(8), 871–876, doi:10.1021/ac60290a012, 1970.

Appendix B:

Supporting information for Chapter Three: Design and validation of an automated nitrous acid (HONO) platform for indoor measurements

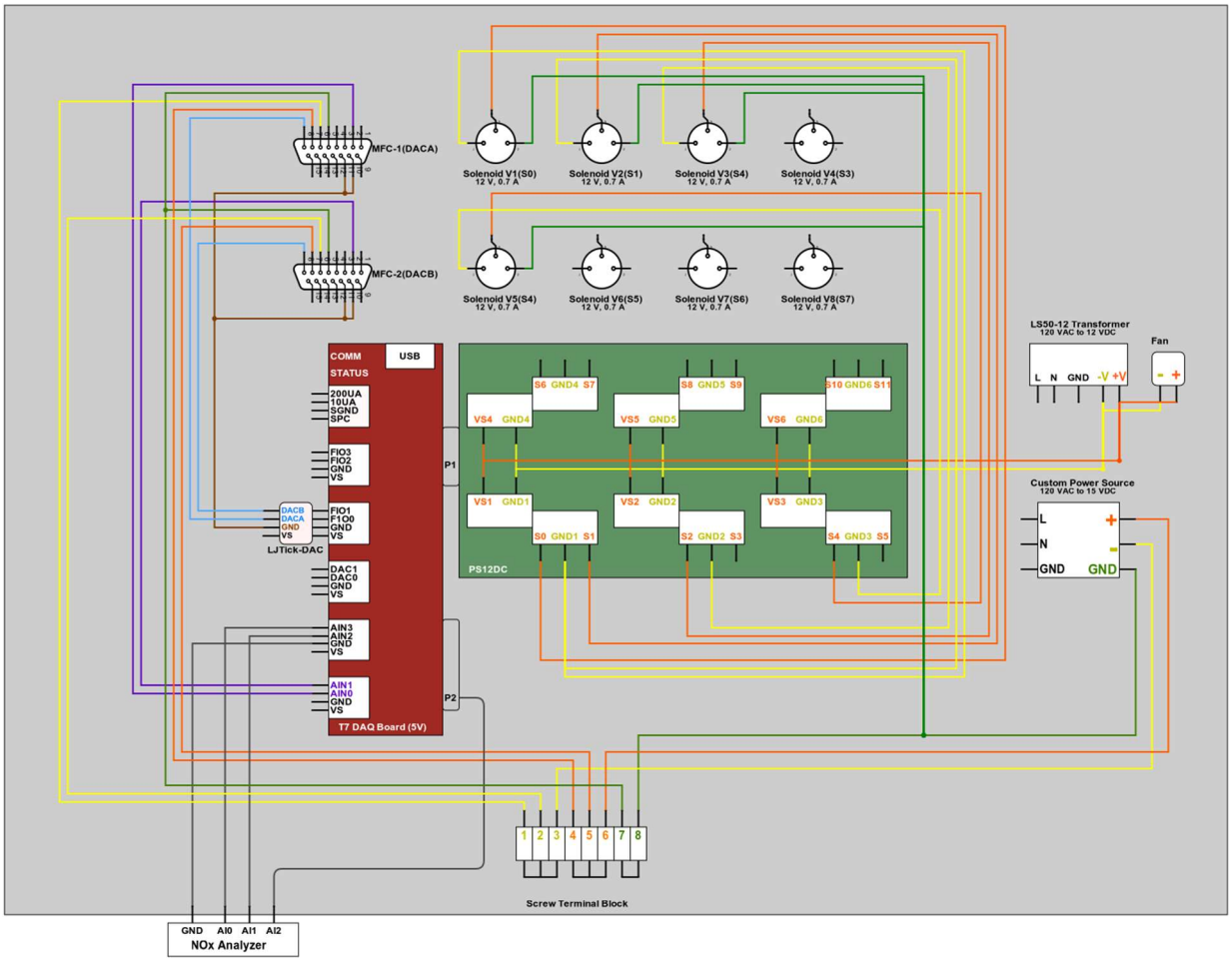

Figure 3-S1. Electronic diagram of the DAQ control box. The closed circles represent the junction of the wiring. Throughout the wiring scheme, the orange lines represents the positive wiring (+) , yellow is negative wiring (-), and green is ground (GND). A cooling fan (5 V DC) was inserted to provide temperature management of the electronics and it was powered by the 12 V DC transformer. The 12 V DC transformer also supplies power to the solenoid valves by converting a 120 V AC power source to a 12 V DC output. The power switching board (green square; PS12DC, LabJack, Lakewood, CO, U.S.A) was wired in parallel to distribute power to the solenoids and remove the need for multiple solid-state relays. The power switching board was attached to the red DAQ board (T7, LabJack, Lakewood, CO, U.S.A) through the DB15 connector (15 pin D-sub). An analog output expansion module (LJTick-DAC, LabJack, Lakewood, CO, U.S.A) was connected to the DAQ board to provide communication with the mass flow controllers (MFC). The custom 15 V DC power source supplies power to two MFCs and is organized through a screw terminal block for power distribution. The wiring of the MFC communication cables requires a 15 pin D-sub male and female assembly for connection of the cable to the case (DACA and DACM)

and the connections are numbered and configured as: 1. No Connection (NC); 2. Flow out (0-5 V, purple wire); 3-4. NC; 5. Ground (0 V, green wire); 6. Neutral (-15 V, yellow wire); 7. Live (+15 V, orange); 8. Flow rate set (0-5 V, blue wire); 9-10. NC; 11-12. Signal common (brown wire); and 13-15. NC. The grey lines show the analog input and ground connections between the DAQ board and the NOx analyzer to sync and log its measurements and datetime.

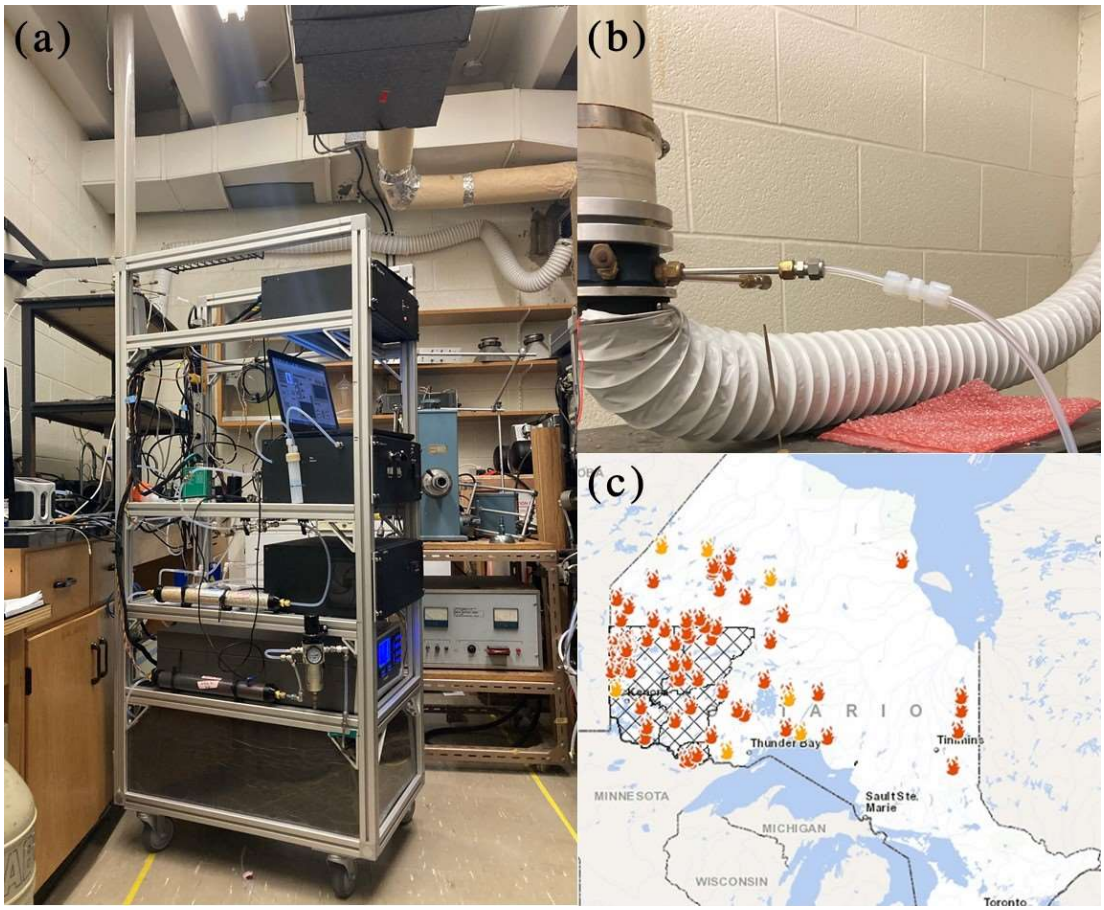

Figure S3-2. (a) Instrument setup in a chemistry laboratory with an outdoor port to measure the outdoor fire plumes on July 20th, 2021. **(b)** Closeup of the tN_r sampling port connected to the outdoor sampling assembly and manifold made of brass and stainless steel fittings. The outdoor sampling assembly has a blower fan between the pipe and a white flexible exhaust line, pulling the outdoor through the assembly. Excess outdoor air is removed through the white flexible exhaust line into an HVAC vent in the lab. **(c)** A map of Ontario showing the northern biomass burning events in July 2021.

Table 3-S1. Calculation of the time response of NO, NO_2, and HONO through the instrument at 630 ccm by double exponential fit.

Nr species	τ_1 (min)	τ_2 (min)	D (%)	Input mixing ratios (ppbv)
NO	1.10	1.07	46	17.88 ± 0.81
NO_2	0.19	1.54	39	17.60 ± 1.05
HONO	0.99	1.00	44	20.23 ± 1.06

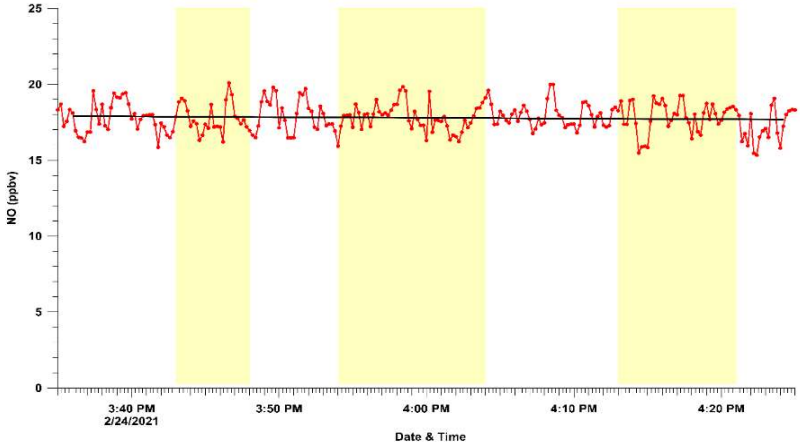

Figure 3-S3. Inputting a known mixing ratio of NO through the Na_2CO_3 denuder (yellow shaded regions) and observing a slope not significantly different from zero of -7.66 x 10^{-5} ± 7.52 x 10^{-5} ppbv, indicating no reaction loss of NO. A t-test was performed to confirm that mixing ratios of NO were not statistically different from bypassing and entering the denuder with a p-value of 0.02.

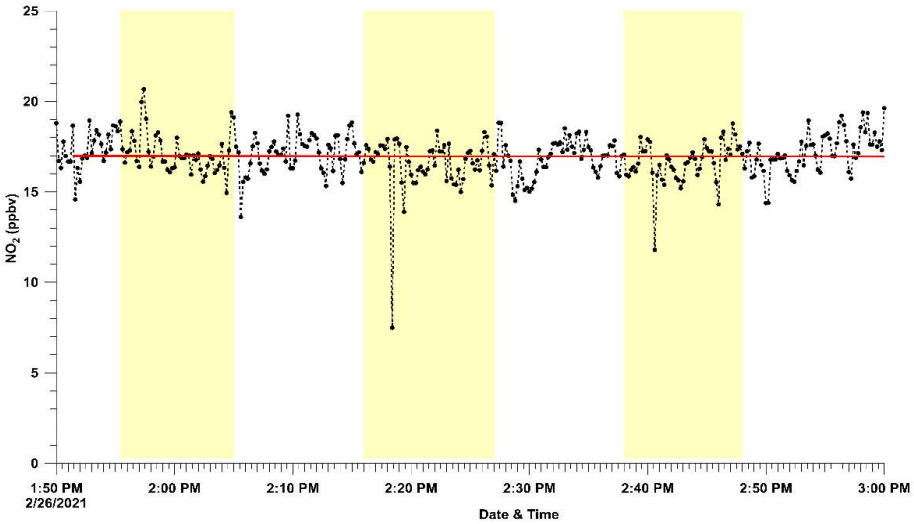

Figure 3-S4. Inputting a known mixing ratio of NO_2 through the Na_2CO_3 denuder (yellow shaded regions) and observing a slope of -3.42 x 10^{-6} ± 5.25 x 10^{-5} ppbv. The averaged mixing ratios of NO_2 bypassing the denuder (16.97 ± 1.06 ppbv) and entering the denuder (16.76 ± 1.32 ppbv) had a small significance difference between both routes likely due to small chemical loss to the coating

and/or surface of the denuder. A t-test was performed to confirm a small significant difference between the two routes with a p-value of 0.13.

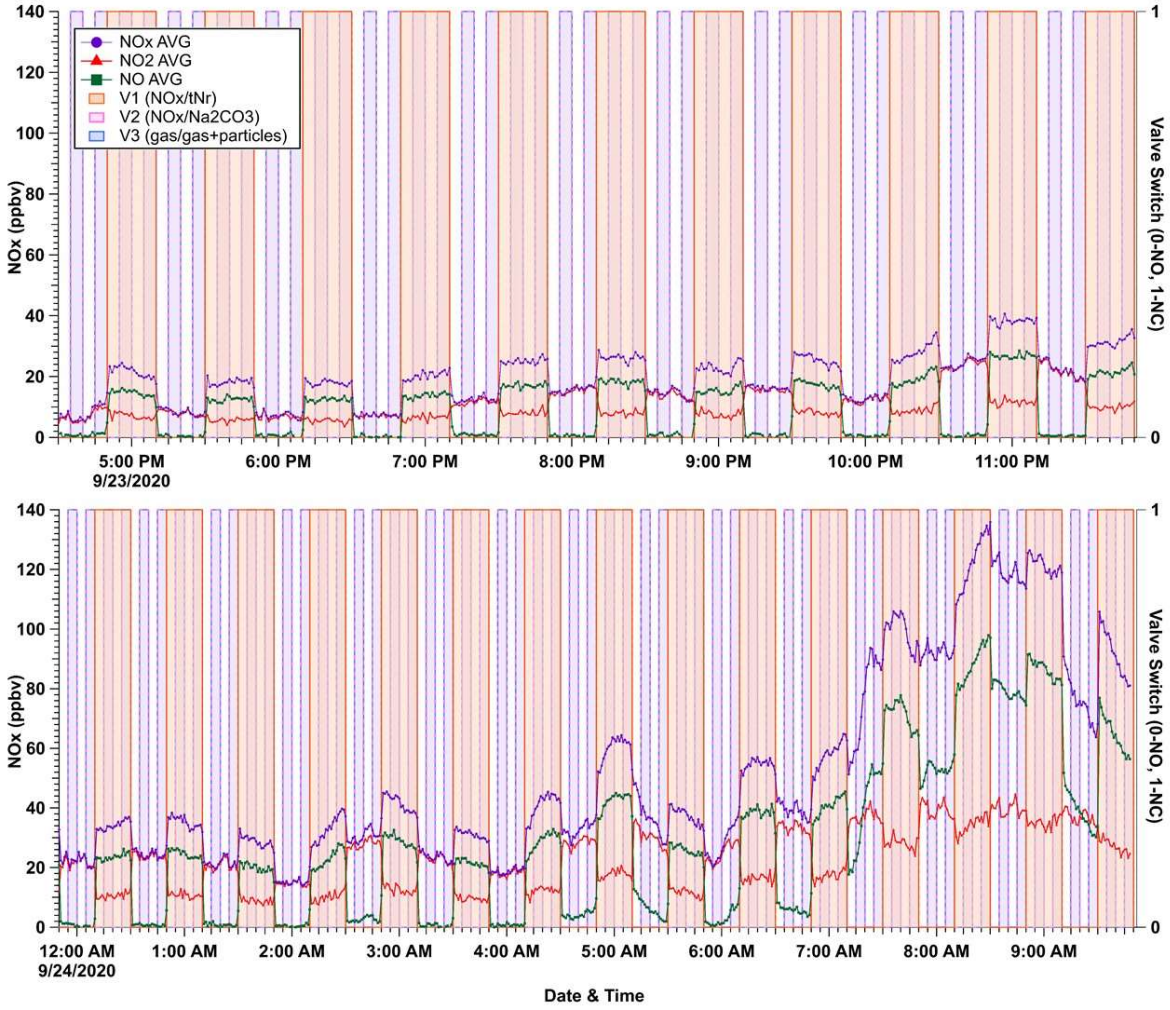

Figure 3-S5. Test measurements (1 min averages) inside a laboratory on the night of September 23-24, 2020 by the tN_r instrument. The raw data from each channel of the NO_x analyzer are presented here to demonstrate the changes in signal, combined with the valve switching logs to process the data into the various fractions of tNr. The valves were programmed to switch from nominally open (NO, 0) to nominally closed (NC, 1) using the schedule assigned in our custom LabView program. Each shaded bar represents when a valve is turned on (NC, 1). The orange bars represent when Valve 1 is switched on (NC, 1) to allow the indoor sample to flow through the tN_r pathway and when it is not shaded, it is switched towards the NO_x* pathway (NO, 1). Similarly, the purple bars represent Valve 2 and Valve 3 are switched on (NC, 1) to allow the sample to enter the denuders. When there are no purple bars, Valve 2 and Valve 3 are switched to NO, 0, in which the sample is bypassing denuders. The colored lines represent the raw measurements of reactive nitrogen detected by the NO_x analyzer that has not been quantified, where the purple line is NO_x*, the red line NO_2*, and the green line NO.

APPENDIX C:
Supporting information for Chapter Four: Nitrous acid (HONO) surface reservoir chemistry in a commercial kitchen during the KOCENA (Kitchen Organic Carbon, Emissions, Nitrogen, and Aerosol) Campaign

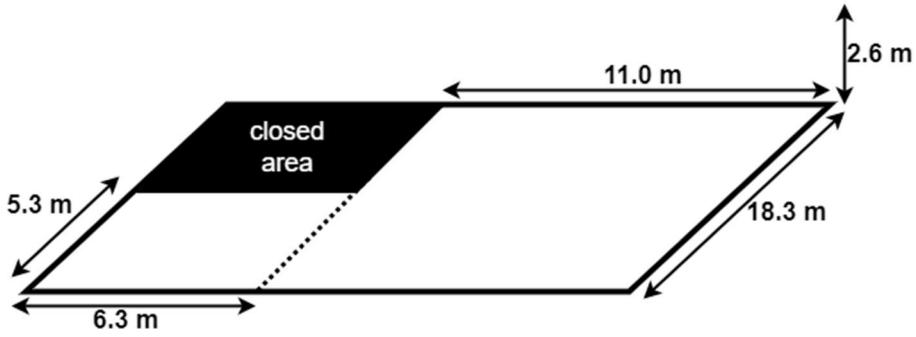

Figure 4-S1. Dimensions of the kitchen and the closed area (office with instruments and preparation area) were not included in calculating the surface area because the doors were closed, disconnecting them from the chemistry observed in the rest of the kitchen.

Table 4-S1. The removal rate of NO_2* from the kitchen hood exhaust and room ventilation during the day by exponential fit of all observed events. The time response (Tau) and standard deviation (SD) of the exponential decay were used to determine the removal rate in s^{-1} and h^{-1}.

Date	Time	Tau (s)	Tau SD (s)	Rate (s^{-1})	Rate (h^{-1})
9/4/2021	9:30	279	20	3.59×10^{-3}	12.92
9/7/2021	14:30	777	45.5	1.29×10^{-3}	4.63
9/8/2021	6:30	148	17.5	6.77×10^{-3}	24.36
9/8/2021	9:15	79.0	5.71	1.27×10^{-2}	45.56
9/9/2021	12:30	418	20	2.39×10^{-3}	8.61
9/10/2021	7:40	136	18	7.34×10^{-3}	26.42
9/10/2021	9:00	123	12.6	8.15×10^{-3}	29.35
9/12/2021	9:30	171	10.2	5.84×10^{-3}	21.02
9/12/2021	11:45	240	12.1	4.17×10^{-3}	15.00
9/12/2021	13:35	53.6	3.48	1.90×10^{-2}	68.45
9/12/2021	14:00	130	17.7	7.71×10^{-3}	27.77
9/12/2021	18:30	160	14.7	6.23×10^{-3}	22.43
9/13/2021	8:15	389	44	2.57×10^{-3}	9.26
9/13/2021	7:30	77.6	10.8	1.29×10^{-2}	46.40
9/13/2021	16:30	345	51.9	2.90×10^{-3}	10.43
9/14/2021	10:45	62.3	4.73	1.61×10^{-2}	57.82
9/14/2021	12:00	73.0	9.91	1.37×10^{-2}	49.31
9/14/2021	15:50	39.7	6.8	2.52×10^{-2}	90.80
9/15/2021	10:45	313	22.6	3.19×10^{-3}	11.49
9/15/2021	17:00	483	16.1	2.07×10^{-3}	7.45
9/16/2021	7:10	163	54.9	6.12×10^{-3}	22.05
9/16/2021	7:50	124	14.6	8.04×10^{-3}	28.93
9/16/2021	12:25	152	6.79	6.60×10^{-3}	23.74

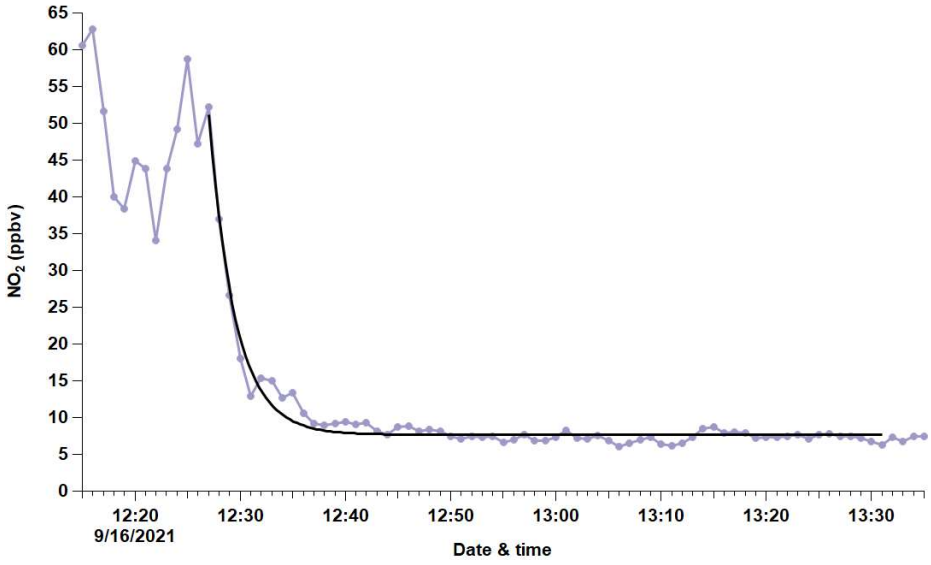

Figure 4-S2. Example of determining the exponential fit (black line) of measured NO_2 decay rate in the kitchen during the day (purple line with dots) to calculate $k_{rem,NO2}$. The exponential fit, $f(t) = y_0 + A \exp\left(\frac{-(t-t_0)}{\tau_1}\right)$ was only applied to periods when high levels of NO_2 were present (e.g. from cooking or outdoor transportation of NO_2 indoors) and decayed to stable or background levels. The equation f(t) is the indoor NO_2 after time (t), y_0 represents the background levels of NO_2 (ppb), A is the initial peak in NO_2 (ppb), and τ is the response time of the decay.

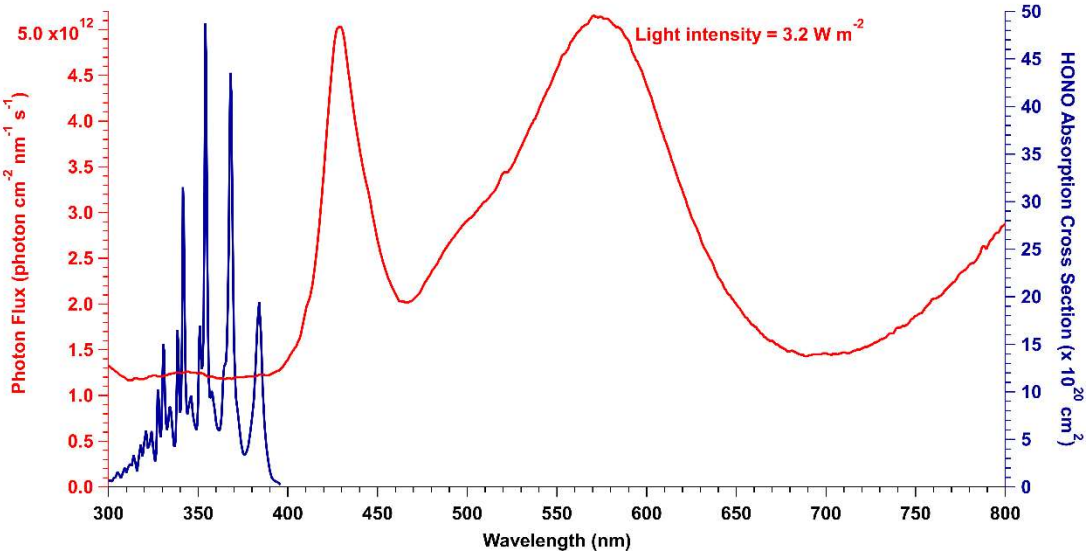

Figure 4-S3. Photon flux measurements of the kitchen (red line) and the HONO absorption cross section (blue line) (Burkholder et al., 2020). The integrated light intensity was 3.2 W m^{-2} and ranged in the visible region of 435 – 700 nm.

4.S4. R-script to finalize and process data from the tN_r instrument.

```
# AUTHORS
################################################################################
# Entire script is written by Melodie and Leigh 2021 from VDB Research Group
# R Script to process collected data from the tNr instrument to measure
nitrogenous species indoors
# 1. PROCESS
################################################################################
#PACKAGES
################################################################################
library(xts)
library(zoo)
library(data.table)
library(lubridate)
library(tidyverse)
library("padr")
rm(list=ls(all=TRUE)) #clear all previous variables in environment

#VARIABLES
################################################################################
# TD = tnr dataframe
# CL = combined list of removing 1 min data from beginning of each cycle and
averaged
# NL = no linear interpolation
# O = original measurements and datetimes
#PRELIM DATA
################################################################################
## Directory
################################################################################
#set directory to save your files
setwd("C:/Users/laome/OneDrive - York University/backup/research/HONO_tNr/R/R
data files")

## Choose File
################################################################################
infile<- file.choose() #choose the file you want to analyze
tnrdata <- read.csv(infile, sep = "\t")

## Modify Dataset
################################################################################
tnrdata <- tnrdata[ -c(5:6)] #removes columns of v4 and MFC2
tnrdata$date <- dmy_hms(tnrdata$datetime)
colnames(tnrdata) <- c("datetime",
                       "V1",
                       "V2",
                       "V3",
                       "NO",
                       "NO2",
                       "NOx",
                       "date")
tnrdata$Vt <- rowSums(tnrdata[2:4]) #add up valve total in new column
tnrdata <- tnrdata %>%
  mutate(tnr_cycle = case_when(
    Vt == 0 ~ "tNr",
    Vt == 2 ~ "NH3",
    Vt == 1 ~ "HONO",
```

```
    Vt == 3 ~ "NOx"))
#add a cycle count up column.
#cycle defined as a measurement mode, i.e. NOx, HONO, tNr or NH3
tnrdata$Vt<- rowSums(tnrdata[2:4])
foo<-rle(tnrdata$Vt) #creates cycle based on total valve change
foo$values <- 1:length(foo$values)
tnrdata$cycle <- inverse.rle(foo)
ncyc = max(tnrdata$cycle)

TD <- subset(tnrdata, select = c(8,9,5,6,7,10,11))
TD <- data.table(TD)
### *Voltage drift correction
#########################################################################
#calibration of NOx analyzer on 09-17-2021
#NOcorr = 1.0018[NO] - 0.8569
#NO2 corr = 1.0018[NO2] - 0.8459
#NOx corr = NOcorr + NO2corr
TD2 <- TD %>%
  mutate(TD, NOcorr = (1.0018*TD$NO) - 0.8569) %>%
  mutate(TD, NO2corr = (1.0018*TD$NO2) - 0.8469)

TD2 <- mutate(TD2, NOxcorr = TD2$NOcorr + TD2$NO2corr)

TD3 <- subset(TD2, select = c("date", "Vt", "NOcorr", "NO2corr", "NOxcorr",
"tnr_cycle", "cycle"))

#create new df of each cycle
for(i in unique(TD3$cycle)) {
  nam <- paste("TD", i, sep = "_")
  assign(nam, TD3[TD3$cycle == i, ])}

# *CYCLE 1
#########################################################################
#The length of cycle 1 is not divisible by 60, ruining the averaged start
time
#Remove the first rows by nth to make it divisible by 60
#Future steps = to make a loop to automatically remove or add in nth row as
NA by using a mod operator
TD_1 <- tail(TD_1, -5)

# CLEAN/AVG
#########################################################################
## Avg 1 min
#########################################################################
list_TD <- mget(ls(pattern = 'TD_'))  #makes a list of all df with cycles

#apply averaging of every 60 rows to list
AVG_list <- map(list_TD, ~ .x %>%
                group_by(date = cut(date, breaks = "60 sec")) %>%
                summarize(NO = mean(NOcorr),
                          NO2 = mean(NO2corr),
                          NOx = mean(NOxcorr),
                          Vt = mean(Vt),
                          cycle = mean(cycle)))
#NOTE: averaged times are different by seconds in cycle 1 to other cycles due
to uneven lengths, so we need to round the datetime
```

```
## Remove Rows
################################################################################
#Removes first row in this list because the response time of the NOx analyzer
is 1 min
AVG_list2 <- lapply(AVG_list, tail, -1)

## Combine Data
################################################################################
CL <- bind_rows(AVG_list2, .id = "column_label")
CL <- arrange(CL, cycle)

CLtot <- CL %>%
  mutate(tnr_cycle = case_when(
    Vt == 0 ~ "tNr",
    Vt == 2 ~ "NH3",
    Vt == 1 ~ "HONO",
    Vt == 3 ~ "NOx"))

for(i in unique(CLtot$tnr_cycle)) {
  nam1 <- paste("CL", i, sep = "_")
  assign(nam1, CLtot[CLtot$tnr_cycle == i, ])}

# CALCULATIONS
################################################################################
## Linear Interp
################################################################################
### HONO
################################################################################
CL_HONO[['date']] <- as.POSIXct(CL_HONO[['date']],
                                format = "%Y-%m-%d %H:%M:%S")
#aggregate if the time series don't match up (seconds skipped,etc)
#datetime variable contains missing values, they are left in place in the df
with thicken
CL_HONO2 <- thicken(CL_HONO, '1 min')
CL_HONO2 <- CL_HONO2[ -c(2)]

CL_HONO2[['date_min']] <- as.POSIXct(CL_HONO2[['date_min']],
                                format = "%Y-%m-%d %H:%M:%S")

LI_HONO <- CL_HONO2 %>%
  pad(group = 'tnr_cycle', interval = 'min') %>%   # Explicitly fill by 1 min
  fill_by_value(0)

LI_HONO_2 <- LI_HONO
LI_HONO_2$NO <- na.approx(LI_HONO$NO)
LI_HONO_2$NO2 <- na.approx(LI_HONO$NO2)
LI_HONO_2$NOx <- na.approx(LI_HONO$NOx)

### NOx
################################################################################
CL_NOx[['date']] <- as.POSIXct(CL_NOx[['date']],
                               format = "%Y-%m-%d %H:%M:%S")
CL_NOx2 <- thicken(CL_NOx, '1 min')
CL_NOx2 <- CL_NOx2[ -c(2)]
CL_NOx2[['date_min']] <- as.POSIXct(CL_NOx2[['date_min']],
                                    format = "%Y-%m-%d %H:%M:%S")
```

```
LI_NOX <- CL_NOx2 %>%
  pad(group = 'tnr_cycle', interval = 'min') %>%   # Explicitly fill by 1 min
  fill_by_value(0)

LI_NOX_2 <- LI_NOX
LI_NOX_2$NO <- na.approx(LI_NOX$NO)
LI_NOX_2$NO2 <- na.approx(LI_NOX$NO2)
LI_NOX_2$NOx <- na.approx(LI_NOX$NOx)

### NH3
################################################################################
CL_NH3[['date']] <- as.POSIXct(CL_NH3[['date']],
                               format = "%Y-%m-%d %H:%M:%S")

CL_NH3_2 <- thicken(CL_NH3, '1 min')
CL_NH3_2 <- CL_NH3_2[ -c(2)]

CL_NH3_2[['date_min']] <- as.POSIXct(CL_NH3_2[['date_min']],
                                     format = "%Y-%m-%d %H:%M:%S")

LI_NH3 <- CL_NH3_2 %>%
  pad(group = 'tnr_cycle', interval = 'min') %>%   # Explicitly fill by 1 min
  fill_by_value(0)

LI_NH3_2 <- LI_NH3
LI_NH3_2$NO <- na.approx(LI_NH3$NO)
LI_NH3_2$NO2 <- na.approx(LI_NH3$NO2)
LI_NH3_2$NOx <- na.approx(LI_NH3$NOx)

### tNr
################################################################################
CL_tNr[['date']] <- as.POSIXct(CL_tNr[['date']],
                               format = "%Y-%m-%d %H:%M:%S")
CL_tNr2 <- thicken(CL_tNr, '1 min')
CL_tNr2 <- CL_tNr2[ -c(2)]
CL_tNr2[['date_min']] <- as.POSIXct(CL_tNr2[['date_min']],
                                    format = "%Y-%m-%d %H:%M:%S")
LI_TNR <- CL_tNr2 %>%
  pad(group = 'tnr_cycle', interval = 'min') %>%   # Explicitly fill by 1 min
  fill_by_value(0)
LI_TNR_2 <- LI_TNR
LI_TNR_2$NO <- na.approx(LI_TNR$NO)
LI_TNR_2$NO2 <- na.approx(LI_TNR$NO2)
LI_TNR_2$NOx <- na.approx(LI_TNR$NOx)
## No Interpolation
################################################################################
NL_HONO <- merge(LI_HONO, LI_NOX, by = "date_min", all = TRUE)
NL_NH3 <- merge(LI_TNR, LI_NH3, by = "date_min", all = TRUE)
NL_Nr <- merge(NL_HONO, NL_NH3, by = "date_min", all = TRUE)

#merge columns again for vt and cycles
NL_Nr2 <- NL_Nr
NL_Nr2$vt = NL_Nr2$Vt.x.x
NL_Nr2$vt[!is.na(NL_Nr2$Vt.y.x)] = NL_Nr$Vt.y.x[!is.na(NL_Nr$Vt.y.x)]
NL_Nr2$vt[!is.na(NL_Nr2$Vt.x.y)] = NL_Nr$Vt.x.y[!is.na(NL_Nr$Vt.x.y)]
NL_Nr2$vt[!is.na(NL_Nr2$Vt.y.y)] = NL_Nr$Vt.y.y[!is.na(NL_Nr$Vt.y.y)]
```

```
NL_Nr2$cycle = NL_Nr2$cycle.x.x
NL_Nr2$cycle[!is.na(NL_Nr2$cycle.x.y)] =
NL_Nr$cycle.x.y[!is.na(NL_Nr$cycle.x.y)]
NL_Nr2$cycle[!is.na(NL_Nr2$cycle.y.x)] =
NL_Nr$cycle.y.x[!is.na(NL_Nr$cycle.y.x)]
NL_Nr2$cycle[!is.na(NL_Nr2$cycle.y.y)] =
NL_Nr$cycle.y.y[!is.na(NL_Nr$cycle.y.y)]

NL_Nr2 <- NL_Nr2[ -c(2,6:9,13:16,20:23, 27:29)]

colnames(NL_Nr2) <- c("date_min",
                      "HONO.NO",
                      "HONO.NO2",
                      "HONO.NOx",
                      "NOx.NO",
                      "NOx.NO2",
                      "NOx.NOx",
                      "tnr.NO",
                      "tnr.NO2",
                      "tnr.NOx",
                      "nh3.NO",
                      "nh3.NO2",
                      "nh3.NOx",
                      "vt",
                      'cycle')
#compile original data with accurate datetime averaged to 1 min
O_HONO <- merge(CL_HONO, CL_NOx, by = "date", all = TRUE)
O_NH3 <- merge(CL_tNr, CL_NH3, by = "date", all = TRUE)
O_Nr <- merge(O_HONO, O_NH3, by = "date", all = TRUE)

O_Nr2 <- O_Nr
O_Nr2$vt = O_Nr2$Vt.x.x
O_Nr2$vt[!is.na(O_Nr2$Vt.y.x)] = O_Nr$Vt.y.x[!is.na(O_Nr$Vt.y.x)]
O_Nr2$vt[!is.na(O_Nr2$Vt.x.y)] = O_Nr$Vt.x.y[!is.na(O_Nr$Vt.x.y)]
O_Nr2$vt[!is.na(O_Nr2$Vt.y.y)] = O_Nr$Vt.y.y[!is.na(O_Nr$Vt.y.y)]

O_Nr2$cycle = O_Nr2$cycle.x.x
O_Nr2$cycle[!is.na(O_Nr2$cycle.x.y)] = O_Nr$cycle.x.y[!is.na(O_Nr$cycle.x.y)]
O_Nr2$cycle[!is.na(O_Nr2$cycle.y.x)] = O_Nr$cycle.y.x[!is.na(O_Nr$cycle.y.x)]
O_Nr2$cycle[!is.na(O_Nr2$cycle.y.y)] = O_Nr$cycle.y.y[!is.na(O_Nr$cycle.y.y)]

O_Nr2 <- O_Nr2[ -c(2,6:9,13:16,20:23, 27:29)]
colnames(O_Nr2) <- c("date_min",
                     "HONO.NO",
                     "HONO.NO2",
                     "HONO.NOx",
                     "NOx.NO",
                     "NOx.NO2",
                     "NOx.NOx",
                     "tnr.NO",
                     "tnr.NO2",
                     "tnr.NOx",
                     "nh3.NO",
                     "nh3.NO2",
                     "nh3.NOx",
                     "vt",
                     'cycle')
```

```
## HONO-NO2
################################################################################
#here we take the avg data and calc HONO and NH3 by differnce using the
nearest points

#1st HONO calculation from NOx
#merge files based on base
F_HONO <- merge(LI_HONO_2, LI_NOX_2, by = "date_min", all = TRUE)
# .x columns are HONO pathway, .y columns are true NOx pathway

F_HONO$cycle = F_HONO$cycle.x
F_HONO$cycle[!is.na(F_HONO$cycle.y)] = F_HONO$cycle.y[!is.na(F_HONO$cycle.y)]
F_HONO <- F_HONO[ -c(2,6,7,9,13,14)]

#new df, subtract differences to form new column, HONO
G_HONO <- mutate(F_HONO, HONO = NO2.x-NO2.y)

hono <- subset(G_HONO, select = c("date_min", "HONO" , "NOx.x", "NO2.x",
"cycle"))
nox <- subset(F_HONO, select = c("date_min", "NOx.y", "NO2.y", "NO.y"))
colnames(hono) <- c("date_min", "HONO", "NOx.star", "NO2.star", "cycle")
colnames(nox) <- c("date_min", "NOx.true", "NO2.true", "NO")
tp1 <- full_join(nox, hono, by = "date_min")

## tNr-NH3
################################################################################
F_NH3 <- merge(LI_TNR_2, LI_NH3_2, by = "date_min", all = TRUE)
# .x columns are TNr pathway, .y columns are NH3 pathway

F_NH3$cycle = F_NH3$cycle.x
F_NH3$cycle[!is.na(F_NH3$cycle.y)] = F_NH3$cycle.y[!is.na(F_NH3$cycle.y)]

F_NH3 <- F_NH3[ -c(2,6,7,9,13,14)]

G_NH3 <- mutate(F_NH3, NH3 = NOx.x-NOx.y)

#NH3 calculated using NOx
nh3 <- subset(G_NH3, select = c("date_min", "NH3", "cycle"))
tnr <- subset(F_NH3, select = c("date_min", "NOx.x"))
colnames(tnr) <- c("date_min", "tnr")

tp2 <- full_join(tnr, nh3, by = "date_min")

#recombine four datasets(NOx, HONO, tNr, NH3)
all <- full_join(tp1, tp2, by = "date_min")
all <- arrange(all, date_min)
all$cycle = all$cycle.x
all$cycle[!is.na(all$cycle.y)] = all$cycle.y[!is.na(all$cycle.y)]
all <- all[-c(8,11)]

# NO2 as true NO2, NO2.star is NO2 + Nr...etc
all2 <- all %>%
  group_by(date = cut (date_min, breaks = "5 min")) %>%
  summarize(NOx.true = mean(NOx.true, na.rm = TRUE),
            NOx.star = mean(NOx.star, na.rm = TRUE),
            HONO = mean(HONO, na.rm = TRUE),
            NO2.true = mean(NO2.true, na.rm = TRUE),
```

```
            NO2.star = mean(NO2.star, na.rm = TRUE),
            NO = mean(NO, na.rm = TRUE),
            NH3 = mean(NH3, na.rm = TRUE),
            tnr = mean(tnr, na.rm = TRUE))

# GRAPHS
################################################################################
summary(all)
all %>%
  gather("key", "value", -date_min) %>%
  ggplot(aes (x = date_min,
              y = value,
              color = key)) +
  geom_point()

all2 %>%
  gather("key", "value", -date) %>%
  ggplot(aes (x = date,
              y = value,
              color = key)) +
  geom_point()

# FINAL DATA
################################################################################
#saves the final processed data csv file in your directory
#measured and interpolated data averaged to 1 min
outfile_final=(paste(sub('.csv', '',
infile),"_1min_processed_final_data.csv",sep=""))
print(outfile_final)
write.csv(all, outfile_final, row.names=F)

#the measured and interpolated data is averaged to 5 min
outfile_final2=(paste(sub('.csv', '',
infile),"_5min_processed_final_data.csv",sep=""))
print(outfile_final)
write.csv(all2, outfile_final2, row.names=F)

#measured data with no interpolation, with rounded datetimes per min
outfile_final3=(paste(sub('.csv', '',
infile),"_1min_measurements_no_lin_interp.csv",sep=""))
print(outfile_final)
write.csv(NL_Nr2, outfile_final3, row.names=F)

#measured data with no interpolation, with the exact averaged datetime in 1
min
outfile_final4=(paste(sub('.csv', '',
infile),"_1min_ORIGINAL_datetime_measurements.csv",sep=""))
print(outfile_final4)
write.csv(O_Nr2, outfile_final4, row.names=F)

#.##############################################################################
# 2. COMBINE
################################################################################
# BIND WEEKLY DF
################################################################################
#KOCENA tNR processing
# aim bind all processed tNr files (ML script) to one file.
```

```
# script in two halfs, 1 min and 5 min avg data
# Written by Leigh Crilley Dec 2021 and modified by Melodie Dec 2021
library(readr)
library(gridExtra)
library(ggpubr)
library(lmodel2)

# SET DIRECTORY
##############################################################################
setwd("C:/Users/laome/OneDrive - York University/backup/research/HONO_tNr/R/R
data files")

# 1 MIN BIND
##############################################################################
#first 1 min interpolated and measured data
data.path.1min="C:/Users/laome/OneDrive - York
University/backup/research/HONO_tNr/R/R data files/12-17-2021 processed 1min
and 5 min R tnr/1 min"

# load files into a list
filenames.1min=list.files(path=data.path.1min, pattern =
"Total*",full.names=TRUE)
d.1min <- rbindlist(lapply(filenames.1min, fread,
header=T,blank.lines.skip=TRUE))

d.1min$date.m <- ymd_hms(d.1min$date_min)

## Measured only 1 min data
##############################################################################
data.path.1min.m="C:/Users/laome/OneDrive - York
University/backup/research/HONO_tNr/R/R data files/12-17-2021 processed 1min
and 5 min R tnr/1 min/measured 1 min"

## Combine All
##############################################################################
filenames.1min.m=list.files(path=data.path.1min.m, pattern =
"Total*",full.names=TRUE)
d.1min.m <- rbindlist(lapply(filenames.1min.m, fread,
header=T,blank.lines.skip=TRUE))

d.1min.m$date <- ymd_hms(d.1min.m$date_min)

#select true NOx, NO2 star and tnr measurements

d.1min.meas <- select(d.1min.m, date, NOx.NO, NOx.NO2, NOx.NOx, HONO.NO2,
tnr.NOx, nh3.NOx, vt)
colnames(d.1min.meas) <- c("date", "NO.true.meas", "NO2.true.meas",
"NOx.true.meas", "NO2.star.meas", "tnr.meas", "tnr.nh3.meas", "Vt")

#combine 1 min files
tp1 <- cbind(d.1min.meas, d.1min)
all.1min <- select(tp1, -c("cycle"))

## Time Plot Check
##############################################################################
all.1min %>%
  gather("key", "value", -date) %>%
```

```
  ggplot(aes (x = date,
              y = value,
              color = key)) +
  geom_point()
ggplot() +
  geom_point(data = all.1min, aes(x=date, y=tnr, colour = group), colour =
"green")+
  geom_point(data = all.1min, aes(x=date, y=tnr.meas, colour = group), colour
= "gold")+
  geom_point(data = all.1min, aes(x=date, y=NH3, colour = group), colour =
"red")+
  geom_point(data = all.1min, aes(x=date, y=tnr.nh3.meas, colour = group),
colour = "purple")+
  theme(legend.position = "right")+
  theme_light()
write.csv(all.1min, "tNr processed week2 11-17 Sept 1 min.csv", row.names =
F)
#5 MIN WEEKLY
################################################################################
#5 min data interpolated and measured data
#Note no measure only file for 5 min data
data.path.5min="C:/Users/laome/OneDrive - York
University/backup/research/HONO_tNr/R/R data files/12-17-2021 processed 1min
and 5 min R tnr/5 min"

# FINAL CSV
################################################################################
filenames.5min=list.files(path=data.path.5min, pattern =
"Total*",full.names=TRUE)
d.5min <- rbindlist(lapply(filenames.5min, fread,
header=T,blank.lines.skip=TRUE))
d.5min$date <- ymd_hms(d.5min$date)

d.5min %>%
  gather("key", "value", -date) %>%
  ggplot(aes (x = date,
              y = value,
              color = key)) +
  geom_point()

write.csv(d.5min, "tNr processed week3 11-17 Sept 5 min.csv", row.names = F)

#.###############################################################################
# 3. FLAGGING (Optional)
# Written by ML 01/10/2022
library(tidyverse)
library(readxl)
library(xts)
library(zoo)
library(data.table)
library(lubridate)
setwd("C:/Users/laome/OneDrive - York University/backup/research/HONO_tNr/R/R
data files")
## Choose File
################################################################################
infile<- file.choose() #choose the file you want to analyze
tnrdata <- read_excel(infile, col_types = c("date", "numeric")
```

```
# Criteria
##############################################################################
# 1.NO2*/tNr measured data (vt = 0, Vt = 1)
# 2. flag interpolated data if NO2.star < NO2.true and remove

## Removing Negatives
#####################################################################
### HONO ########################

flag_hono <- subset(tnrdata, select = c(1:5, 8:14))
flag_hono2 <- subset(tnrdata, select = c("date", "NO2.true", "NO2.star",
"HONO"))
flag_hono3 <- flag_hono2 %>%
  mutate(bad_hono = case_when(
    NO2.true > NO2.star ~ "NO2.true greater than",
    NO2.true < NO2.star ~ "NO2.true less than"))

badhono <- flag_hono2 %>%
  filter(NO2.true > NO2.star, na.rm = TRUE)
meas_only <- subset(flag_hono, select = c(1:6))
honodata0 <- merge(meas_only,flag_hono3, by = "date", all = T)

goodhono <- honodata0 %>%
  select(date, HONO, bad_hono) %>%
  filter(str_detect(bad_hono, 'NO2.true less than') | HONO >= -1, na.rm =
TRUE)

colnames(goodhono) <- c("date", "noneg_HONO", "HONO_filteredconditions")
honodata <- merge(honodata0, goodhono, by = "date", all = T)

# 3. compare consecutive measured NO2.true vs NO2.star to see if HONO agrees
meas_no2 <- subset(honodata, select = c("date",
                                        "NO.true.meas",
                                        "NO2.true.meas",
                                        "NO2.star.meas",
                                        "NOx.true.meas",
                                        "NO2.true",
                                        "NO2.star",
                                        "noneg_HONO"))

vt <- subset(tnrdata, select = c("date", "Vt"))
meas <- merge(meas_no2, vt, by = "date", all = T)

#NO2.true ##########################################################
# %increase = increase/original number * 100
NO2.true <- subset(meas, select = c("date", "NO2.true.meas"))
NO2.true <- drop_na(NO2.true)

NO2.true <- NO2.true %>%
  mutate(Diff_NO2.true = (NO2.true.meas - lag(NO2.true.meas)))

NO2.true <- NO2.true %>%
  mutate(pINC_NO2.true = (Diff_NO2.true / lag(NO2.true.meas)*100))

#NO2.star ##########################################################
NO2.star <- subset(meas, select = c("date", "NO2.star.meas"))
```

```
NO2.star <- drop_na(NO2.star)
NO2.star <- NO2.star %>%
  mutate(Diff_NO2.star = (NO2.star.meas - lag(NO2.star.meas)))
NO2.star <- NO2.star %>%
  mutate(pINC_NO2.star = (Diff_NO2.star / lag(NO2.star.meas)*100))
all_NO2 <- merge(NO2.true, NO2.star, all = T)
filtered_data <- subset(meas, select = c("date","NO2.true", "NO2.star",
"noneg_HONO"))
comp_NO2 <- merge(all_NO2, filtered_data, group_by = "date", all = T)

#flags if the perecent increase of NO2.star | NO2.true is >= 100 %
comp_tot_NO2 <- comp_NO2 %>%
  mutate(low_high_NO2 = case_when(
    pINC_NO2.true >= 50 ~ "NO2.true inc. 50%",
    pINC_NO2.star >= 50 ~ "NO2.star inc. 50%",
    pINC_NO2.true <= -50 ~ "NO2.true dec. 50%",
    pINC_NO2.star <= -50 ~ "NO2.star dec. 50%" ))

### NH3 #####
flag_nh3 <- subset(tnrdata, select = c("date",
                                       "NO.true.meas",
                                       "NOx.true.meas",
                                       "tnr.meas",
                                       "tnr.nh3.meas",
                                       "NOx.true",
                                       "NOx.star",
                                       "tnr",
                                       "NH3"))

flag_nh3.2 <- subset(tnrdata, select = c("date", "NOx.true.meas", "tnr.meas",
"tnr.nh3.meas", "tnr", "NH3"))
meas_onlynh3 <- subset(flag_nh3, select = c(1:4))
goodnh3 <- flag_nh3.2 %>%
  select(date, NH3) %>%
  filter(NH3 >= -1, na.rm = TRUE)

colnames(goodnh3) <- c("date", "noneg_NH3")
nh3data <- merge(flag_nh3, goodnh3, by = "date", all = T)
meas_nh3 <- merge(nh3data, vt, by = "date", all = T)

#tnr.meas ##################################################
tnr.meas <- subset(meas_nh3, select = c("date", "tnr.meas"))
tnr.meas <- drop_na(tnr.meas)
tnr.meas <- tnr.meas %>%
  mutate(Diff_tnr.meas = (tnr.meas - lag(tnr.meas)))
tnr.meas <- tnr.meas %>%
  mutate(pINC_tnr.meas = (Diff_tnr.meas / lag(tnr.meas)*100))

#tnr.nh3.meas ##############################################
tnr.nh3.meas <- subset(meas_nh3, select = c("date", "tnr.nh3.meas"))
tnr.nh3.meas <- drop_na(tnr.nh3.meas)
tnr.nh3.meas <- tnr.nh3.meas %>%
  mutate(Diff_tnr.nh3.meas = (tnr.nh3.meas - lag(tnr.nh3.meas)))
tnr.nh3.meas <- tnr.nh3.meas %>%
  mutate(pINC_tnr.nh3.meas = (Diff_tnr.nh3.meas / lag(tnr.nh3.meas)*100))
all_nh3 <- merge(tnr.meas, tnr.nh3.meas, all = T)
comp_NH3 <- merge(all_nh3, nh3data, group_by = "date", all = T)
```

```
#flags if the perecent increase of NO2.star | NO2.true is >= 100 %
comp_tot_NH3 <- comp_NH3 %>%
  mutate(low_high_NH3 = case_when(
    pINC_tnr.meas >= 50 ~ "tnr.meas inc. 50%",
    pINC_tnr.nh3.meas >= 50 ~ "tnr.nh3 inc. 50%",
    pINC_tnr.meas <= -50 ~ "tnr.meas dec. 50%",
    pINC_tnr.nh3.meas <= -50 ~ "tnr.nh3  dec. 50%" ))

comp_all <- merge(comp_tot_NO2, comp_tot_NH3, group_by = "date", all = T)
write.csv(comp_all, "tNr processed data flagged 1 min.csv", row.names = F)
```

Table 4-S2. Average daytime and nighttime HONO (ppbv) in the kitchen, SD is standard deviation

Dates	Daytime HONO (ppb)	Daytime HONO SD (ppb)	Nighttime HONO (ppb)	Nighttime HONO SD (ppb)
8/27/2021	4.33	1.06	3.51	1.06
8/28/2021	3.05	1.50	3.33	1.85
8/29/2021	3.12	4.13	2.44	1.94
8/30/2021	2.09	2.02	1.83	1.43
8/31/2021	1.38	3.05	2.43	1.75
9/1/2021	1.25	1.31	3.89	3.81
9/2/2021	3.35	3.09	0.84	1.36
9/3/2021	1.85	2.39	2.41	0.95
9/4/2021	1.74	1.87	1.88	1.72
9/5/2021	1.77	1.86	1.19	0.80
9/6/2021	2.42	3.46	0.96	0.94
9/7/2021	3.17	3.15	5.33	1.30
9/8/2021	3.18	1.62	2.19	0.94
9/9/2021	2.66	1.66	1.92	0.92
9/10/2021	2.16	1.36	2.16	0.85
9/11/2021	2.08	1.06	2.31	1.11
9/12/2021	2.20	1.75	1.69	0.82
9/13/2021	3.23	2.13	2.48	0.81
9/14/2021	2.47	1.51	2.17	0.87
9/15/2021	2.07	1.22	2.55	0.91
9/16/2021	2.41	1.71	2.15	0.96
9/17/2021	3.00	1.66	3.51	1.06